Strål
säkerhets
myndigheten
Swedish Radiation Safety Authority

Author: Digby D. Macdonald
Samin Sharifi-Asl
George R. Engelhardt
Mirna Urquidi-Macdonald

Research

2012:11

Issues in the corrosion of copper in a Swedish high level nuclear waste repository

Report number: 2012:11 ISSN: 2000-0456
Available at www.stralsakerhetsmyndigheten.se

SSM perspective

Background

The KBS-3 repository concept developed by SKB for disposal of spent nuclear fuel is based on a multi barrier principle for isolation of the fuel and to delay any escaping radionuclides. The concept is based on three barriers; copper canister, bentonite buffer and granitic bedrock. The copper canister will in this respect work as a corrosion barrier and completely isolate the spent nuclear fuel from the surroundings until failure of the 5 cm thick copper canister by either corrosion or mechanical loads occurs.

In order to review the license application for spent nuclear fuel it is important that all corrosion mechanisms that can occur in the repository are understood in detail. The objectives for research by SSM are in this respect to maintain and develop knowledge at SSM and in the research community, in order to conduct a comprehensive and effective review of the license application for a spent nuclear fuel repository submitted by SKB.

This report covers research result obtained during 2011 in an ongoing research work planned to continue to end of 2013.

Objectives

The objective with this research project was to increase knowledge in the area of copper corrosion in the planned repository environment and obtain information on how copper corrosion evolves during the assessment period of 100 000 years.

Results

The equilibrium chemical composition of groundwater close to the canister as a function of temperature has been calculated by use of a thermodynamics code called GEMS. Based on the results, the following sulphide species (S^{2}-, HS-, H_2S, HS_2^{2}-, and S_2^{2}-) are predicted to be present in sufficient concentrations to cause copper corrosion in the repository environment. Among the sulphide species HS- is predicted to be in highest concentration. It must be emphasized that GEMS calculation cannot consider the influence of sulphate reducing microbes which can be an important source of sulphide concentration at repository depth. The most important variables that need to be included in defining how corrosion of copper will evolve during the assessment period are found to be temperature, pH, [HS-] and [H_2].

Within the research program a physico-electrochemical model for copper corrosion during the assessment period of 100 000 years has been developed. The model considers, transport through the saturated buffer, temperature variation and copper corrosion kinetics with HS-, O_2, H_2O_2 present naturally or produced by radiolysis of water by gamma radiation from the spent fuel. The output from this modeling work can be used to predict how redox potential, corrosion potential and corrosion damage

of copper develops during the assessment period. This output can for example be used to predict if copper could undergo general or localized corrosion during the repository evolution. In this report only preliminary modeling trails have been performed, mainly with the intention of testing the model. A lot of input data for the model is lacking but these data will be measured in the continuation of this work.

Need for further research

In order to accomplish the modeling work presented in this work, further development work on the model as well as experimental measurements of important input parameters for the model like kinetic parameters for the evolution of hydrogen on copper and calibration of the radiolysis model need to be conducted.

The modeling work in this report assumes a fully saturated buffer, for an unsaturated buffer, modeling work is considerably more complicated and has therefore not been included. In order to predict the influence atmospheric corrosion in the relevant repository environment more experimental work is needed.

Project information

Contact person SSM: Jan Linder
Reference: SSM 2011/733

Strål
säkerhets
myndigheten
Swedish Radiation Safety Authority

Authors: Digby D. Macdonald[1], Samin Sharifi-Asl[1], George R. Engelhardt[2] and Mirna Urquidi-Macdonald[3]

1. Center for Electrochemical Science and Technology,Department of Materials Science and Engineering College of Earth and Mineral Sciences,Pennsylvania State University,University Park, PA16802
2. OLI Systems, 108 American Rd. Morris Plains, NJ 07950
3. Department of Engineering Science and Mechanics, College of Engineering,Pennsylvania State University,University Park, PA16802

2012:11

Issues in the corrosion of copper in a Swedish high level nuclear waste repository

Date: March 2012
Report number: 2012:11 **ISSN:** 2000-0456
Available at www.stralsakerhetsmyndigheten.se

This report concerns a study which has been conducted for the Swedish Radiation Safety Authority, SSM. The conclusions and viewpoints presented in the report are those of the author/authors and do not necessarily coincide with those of the SSM.

Table of Contents

Executive Summary

This Phase II report continues to address a central issue of the KBS-2 and KBS-3 plans for the disposal of high level nuclear waste (HLNW) in Sweden; that although copper metal in pure water under anoxic conditions can exist in the thermodynamically-immune state, and hence will not corrode, the environment in the proposed repository is far from being pure water and contains species that activate copper toward corrosion. Thus, SKB recognizes that, in practical repository environments, such as that which exists at Forsmark, copper is no longer immune, because of the presence of sulphide ion, and that the metal will corrode at a rate that is controlled by the rate of transport of sulphide ion to the canister surface. This rate is estimated by SKB to be at a high of about 10 nm/year [1] (corresponding to an average corrosion current density of 4.3×10^{-8} A/cm^2), at least for a number of canisters in the envisaged repository, resulting in a loss of copper over a 100,000 year storage period of approximately 1 mm, which is well within the 5-cm corrosion allowance of the current canister design. However, it is important to note that native copper deposits have existed for geological time (presumeably, billions of years), which can only be explained if the metal has been thermodynamically more stable than any product that may form via the reaction of the metal with the environment over much of that period and it is of interest to speculate as to whether conditions within the near-field environment might be engineered to render copper thermodynamically immune and hence impossible to corrode. Such conditions would almost certainly require the absence of strongly activating species, such as sulphide ion, as well as the absence of oxygem. Nevertheless, even the assumption of immunity of copper in pure water under anoxic conditions has been recently questioned by Swedish scientists (Hultquistand Szakálos [2-4]), who report that copper corrodes in oxygen-free, pure water with the release of hydrogen. While this finding is controversial, it is not at odds with thermodynamics, provided that the concentration of Cu^+ and the partial pressure of hydrogen are suitably low, as we demonstrated in the Phase I report [5]. The fact that others are expereiencing difficulty in repeating these experiments may simply reflect that the initial values of $[Cu^+]$ and p_{H_2} in their experiments are so high that the quantity $P = [Cu^+]p_{H_2}^{1/2}$ is greater than the equilibrium value, P^e, as expressed in a Corrosion Domain Diagram (plots of P and P^e versus pH). Under these conditions, corrosion is thermodynamically impossible, and no hydrogen is released, because its occurrence would require a positive change in the Gibbs energy of the reaction. Under these conditions, copper is therefore said to be "thermodynamically immune". If, on the other hand, $P < P^e$ corrosion will proceed and the value of P will rise as Cu^+ and H_2 accumulate at the interface. It is postulated that this condition was met in the Hultquist and Szakálos [2-4] experiments, thereby leading to a successful result. Eventually, however, as the corrosion products build up in the system, P increases until $P = P^e$ and the rate of corrosion occurs under "quasi-equilibrium" conditions. Under these conditions, the reaction can occur no faster than the rate of transport of the corroding species (e.g., H^+ in the reaction $Cu + H^+ \rightarrow Cu^+ + 1/2H_2$) to, or corrosion products (Cu^+, H_2) from, the copper surface. These rates may be sufficiently low that the assumption of immunity is unnecessary to qualify copper as a suitable canister material. Thus, if the corrosion rate can be maintained at a value of less than 10^{-8} m/year (0.01 μm/year, i.e., 10 nm/year), the canister will lose only 1 mm of metal over a one hundred thousand year storage period, which is well within the designed corrosion allowance of 5-cm, as noted above.

Prior to beginning the extensive calculations of Phase II, it was recognized that the most deleterious species toward copper are sulphur-containing entities, such as sulphide, and various polysulphides, poly thiosulphates, and polythionates, particularly those species

that readily transfer atomic sulphur to a metal surface (e.g. $2Cu+S_2O_3^{2-} \rightarrow Cu_2S + SO_3^{2-}$). Accordingly, we performed a very thorough literature search in Phase I, which was continued into Phase II, and successfully located extensive thermodynamic data for sulphur-containing species, primarily from studies performed in Israel, that are not contained in established databases. Many of these data were incorporated into the database developed in Phase I, and were further used in Phase II to address the issues that were scheduled for that latter phase. The work reported here has resulted in a number of important conclusions that have a bearing on the behavior of copper in a Forsmark type repository. These conclusions are as follows:

Following our work in Phase I, the thermodynamic properties of copper were expressed in the form of corrosion domain diagrams as P^e versus pH, where P^e is the partial quotient of the reaction at equilibrium, as noted above. For any other value of the reaction quotient, P, where $P \neq P^e$, the system is not at equilibrium and, provided that $P < P^e$, corrosion will occur and the composition (as described by P) will change, such that $P \rightarrow P^e$. Thus, corrosion is spontaneous only for $P < P^e$. Cu is immune for $P > P^e$. Certain species commonly found in ground water, e.g. HS^-, polysulphides, and certain polysulphur oxyanions are deleterious by (thermodynamically) activating copper and hence denying the metal thermodynamic immunity. This activation process renders hydrogen evolution via the rewduction of protons (pH < 4) or water (pH > 4) to be viable cathodic reactions. The thermodynamic conditions for the corrosion of copper in water have been further defined in Phase II with emphasis on complexing systems. Species that form complexes with *Cu(I)* and *Cu(II)* can also activate copper thermodynamically. These species include the halides, ammonia, carbonate ion, and phosphates, amongst others. Some polythiosulphates, notably, $S_xO_3^{2-}$, x = 3 – 7, are found not to activate copper, for reasons that are not yet completely understood. These species tend to possess very negative volt equivalencies and to have low, positive average sulphur oxidation states, as emphasized in Phase I. All polysulphides are predicted to activate copper. Amongest all the complexing species, only ammonia was found not to activate the copper, by virtue of its low activity. In addition, some of the polythionate family lost the ability to activate the copper with increasing the temperature.

In order to explore the composition of granitic groundwater, we decided to employ a modern, sophisticated Gibbs energy minimization code to predict the composition of the repository environment as a function of temperature and redox conditions, with the latter being adjusted by changing the relative concentrations of hydrogen and oxygen in the input to the code, in order to simulate the initial oxic conditions and the eventual anoxic conditions that develop at longer storage times. After evaluating several codes, we chose GEMS, which was developed in Switzerland by Prof. Dmitri Kulik. This code is designed specifically to model geochemical systems, contains a large database of compounds, and is in general use in the geochemical community. Prior to using the code to model the repository, we upgraded the database by adding thermodynamic data for various polysulphur species (polysulphides, poly thiosulphates, and polythionates) that had been developed earlier in this program. However, the code became ill-behaved when the data for $S_xO_3^{2-}$, x = 3 – 7 were added. Consultation with the code developer, Prof. Dmitrii Kulik, at the Paul Scherer Institute in Switzerland, failed to identify and isolate the problem and, accordingly, it was necessary to remove those species from the database. The reader will recall that these are the very species that, anomalously, do not activate copper. With the code in its present form, we have modeled the repository under both oxic and anoxic conditions with the greatest emphasis being placed on the latter, because the great fraction of the storage time is under anoxic conditions. The most important finding to date is that the concentrations of many, but not all, polysulphur species (polysulphides, poly thiosulphates, and polythionates) under anoxic conditions are predicted to be very low, but it

is still not possible, because of the uncertainties in the calculations, to ascertain with certainty whether these species will activate copper in the repository. However, the point may be moot, because sulphide species and the lower polysulphides (S^{2-}, HS^-, H_2S, HS_2^{2-}, and S_2^{2-}) are predicted to be present in sufficient concentration to activate copper and cause the metal to corrode under simulated repository conditions. Among all of the available, activating sulphur species, bisulphide (HS^-) ion is predicted to have the highest concentration and to be able to activate copper. The activity of dissolved hydrogen gas in the simulated system is much lower than that reported by SKB and it could be concluded that the system is not in an equilibrium condition.

During Phase II, we also developed Mixed Potential Models (MPMs) for estimating the redox potential of the repository environment and for calculating the corrosion potential of the copper canister as the system evolves along the corrosion evolutionary path. While the model was being developed, we detected a conceptual problem with the use of the generalized Butler-Volmer equation for describing the kinetics of the cathodic reactions. As a result, the MPM became superceded by the Physico-Electrochemical Model (PEM) for canister corrosion and the work that had been performed on the former (the MPM) was rolled into the development of the latter (see below). Accordingly, further development of the MPM was discontinued soon after formulation of the mathematics. As originally envisioned, the MPM used the Generalized Butler-Volmer equation to describe the cathodic reactions, which is appropriate for a metal corroding in a bulk electrolyte environment, rather than solving the Nernst-Planck equations for the transport of species through the bentonite buffer. The Nernst-Planck equations provide a much more accurate description of the mass-transport limited movement of species to/from the canister surface.

We continued our work of defining the corrosion evolutionary path (CEP) in preparation for modeling the corrosion of the canisters. This task essentially involves predicting the redox potential (E_h), pH, and granitic groundwater composition as defined by the variation of temperature (note that the temperature decreases roughly exponentially due to radioactive decay of the short-lived isotopes), and then applying Gibbs energy minimization to predict speciation at selected times along the path. At each step, the CDD for copper is derived and the value of P is compared to P^e to ascertain whether copper is active or thermodynamically immune. Although the polysulphur species are predicted to be present at very low concentrations (e.g., HS_2^- and S_2^{2-}) or are predicted to be absent altogether (e.g., polysulphur oxyanions), the CDDs indicate that certain species need be present at only miniscule concentrations (10^{-44} M) for activation to occur, at least theoretically. Accordingly, the assumption that copper will not corrode during the anoxic storage period is untenable, despite the fact that native deposits of copper do occur in some granitic formations. Furthermore, the issue of corrosion rate is a matter of chemical kinetics, with the maximum rate being determined by transport of the sulphur-containing species through the buffer, as outlined below. Therefore, it is our view that the success of the KBS-3 program must rely upon the multiple barriers being sufficiently impervious that the corrosion rate can be reduced to an acceptable level. Thus, in performing the work in Phase II, we have addressed the most important issue related to the corrosion of copper; whether HS^- is the only significant sulphur species in the repository environment, or whether it is necessary to incorporate the polysulphur species in the model, particularly under anoxic conditions. Noting that the rate of supply of sulphur to the copper surface in the form of the polysulphur species $S_{x-1}SZ$ is $(x-1)J$, where J is the flux of the species through the buffer at the metal surface and $(x-1)$ is the number of sulphur atoms that can be donated to the surface to form Cu_2S, it is evident that the contribution that each species makes is determined by the concentration multiplied by $(x-1)$, because the Nernst-Planck equation is linear in concentration. Our analysis indicates that bisulphide (HS^-) is, overwhelmingly, the most

important species under anoxic conditions. Accordingly, only this species has been considered in developing the physico-electrochemical model for predicting corrosion damage to the canister.

A comprehensive physico-electrochemical model for canister corrosion over the repository horizon of 100,000 years has been developed. The model considered the three modes of specie transport (diffusion, migration, and convection), incorporates water radiolysis, evolving temperature from the decay of radionuclides in the waste, chemical reaction between HS^- and radiolysis products (O_2, H_2O_2), and electrochemical kinetics. The model is deterministic, because the predictions are constrained by the two relevant natural laws; the conservation of charge and Faraday's Law (equivalence of mass and charge). As noted above, the model also recognizes the reaction between water radiolysis products (O_2, H_2O_2) and bisulphide ion (HS^-), with HS^- being converted to another sulphur species that is non-activating (e.g. SO_3^{2-} or SO_4^{2-}). Using "guesstimates" of the various model parameters, it is shown that the model predicts specie concentrations, metal loss, and the corrosion potential values that are considered to be eminently reasonable, except for the concentration of hydrogen peroxide, which is considered to be too high. However, this issue is expected to be resolved once radiolytic aspects of the model are calibrated against the highly successful codes that we have previously developed for modeling the radiolysis of water in water-cooled nuclear reactors, particularly Boiling Water Reactors (BWRs), albeit at much lower dose rates [6]. We will also employ the extensive radiolysis data that have been obtained at the Radiation Laboratory at the University of Notre Dame in South Bend, Indiana. These activities are scheduled for Phase III. Despite the paucity of data for the model parameters, the predicted loss of metal from a canister is predicted to vary between 1.7 nm/y and 100 nm/y, depending upon the dose rate, when averaged over a two thousand-year period, with most of the loss occurring at short times, when oxic conditions prevail and when HS^- is available close to the canister surface.

It has known that the canister temperature will be high enough (around 100^{o}C) to evaporate adjacent groundwater and, hence, the canister is expected to be in contact with steam. If this condition exists, then the canister may suffer steam corrosion. In order to assess whether this scenario is likely, it will be necessary to estimate the pressure in the repository, which is located 500m below the surface. Unfortunately, there is a lack of information about steam corrosion of pure copper in the available literature and, therefore, some experimental work needs to be done, in order to address the corrosion mechanism and rate of copper canister corrosion in the earlist time possible.

Using "guesstimated" values for important model parameters, the physico-electrochemical model developed in this Phase II work was used to explore the impact of water radiolysis on the corrosion behavior of the canisters. Although a comprehensive and accurate set of model parameter values is not yet available, "scoping" calculations suggests that at an initial γ-dose rate of 1 Gy/h, radiolysis is not a significant factor in determining the corrosion behavior of the canisters. This same modeling work indicates that, at an initial dose rate of 100 Gy/h, radiolysis has a significant impact on the corrosion behavior of a canister. A full and accurate assessment of water radiolysis must await the experimental acquisition of values for important model parameters. These valuses are scheduled to be determined in Phase III.

References

1. Corrosion calculations report for the safety assessment SR-Site, *SKB TR-10-66*, 38 (2010).
2. G.Hultquist, *Corros. Sci.*, **26**, 173 (1986).
3. G. Hultquist, G. K. Chuah, and. K. L.Tan, *Corros. Sci.*, **29**, 1371 (1989).
4. P. Szakálos, G. Hultquist, and G.Wikmark, *Electrochem. SolidState Letters*, **10**, C63 (2007).
5. D. D. Macdonald and S. Sharifi-Asl, *SSM-2011:09, Swedish Radiation Safety Authority*.(2011)
6. T.K. Yeh, D. D. Macdonald, and A. T. Motta.,*Nucl. Sci. Eng*., **121**, 468-482 (1995).

I. Introduction

Sweden's KBS-3 plan, which presents a repository "concept" for the disposal of high level nuclear waste (HLNW), is predicated upon the assumption that copper, the material from which the canisters will be fabricated, will not be thermodynamically immune to corrosion, when in contact with the repository environment, even though copper is sometimes classified as being a noble metal like gold. However, if copper did exist in the immune state, corrosion could not occur, because any oxidation process of the copper is characterized by a positive change in the Gibbs energy, rather than a negative change demanded by the Second Law of Thermodynamics for a spontaneous process. Accordingly, "immunity" is a thermodynamic state that must be characterized upon the basis of thermodynamic arguments. This immunity postulate was apparently intriguing, because of the occurrence of deposits of native (metallic) copper in various geological formations throughout the World (e.g., in the upper Michigan peninsular in the USA and in Finland). Accordingly, it was reasoned that, during the anoxic period, when all of the oxygen that was present during the initial oxic period, due to exposure to air upon placement of the waste, had been consumed and the redox potential, E_h, might fall to a sufficiently low value, that copper might become thermodynamically immune and corrosion might not occur, even over geological times, provided the environment remained conducive to that condition. We now understand, from the Phase I work, that this condition can be realized only if hydrogen is present at a suitably high fugacity, if activating species, such as sulphide, are present at suitably low concentrations, and if the activity of Cu^+ is suitably high. We also understand that these conditions cannot be met in any practical repository environment, particularly with regard to the concentrations of activating species. In that case, the corrosion of copper is thermodynamically spontaneous and the safe iosolation of HLNW requires inhibiting corrosion to the extent that the waste will be safely contained over the designated storage period.

The issue of copper immunity in pure water under anoxic conditions has developed into one of considerable controversy within both the scientific and lay communities in Sweden, because direct experimentation has failed to achieve resolution. Thus, Hultquist, et. al. [1-3] have reported detection of hydrogen evolution when copper metal is exposed to deoxygenated, pure water, while other experiments appear to refute those claims [4-6]. The experiments were all carried out to the highest of scientific standards using hydrogen detection techniques that were more than adequate for the task of quantitatively detecting and measuring the gas,and each group reports internally-consistent results that, nevertheless, appear to be diametrically opposite from one group to the other. While the work reported in Refs. 1 to 6 is of great scientific interest, it is perhaps moot, when viewed in light of the environment that is present at Forsmark, the site of the initial HLNW repository in Sweden. Nevertheless, resolution of the scientific controversy underlying the experiments of Hultquist, et.al. [1-3], and those in refute, is important, because it would remove one aspect of uncertainty in the assessment of the KBS-3 plan for storing High Level Nuclear Waste (HLNW) in Sweden.

In Phase I of this study, we reported a comprehensive thermodynamic study of copper in contact with anoxic pure water and granitic groundwater of the type and composition that is expected in the Forsmark repository in Sweden. Our primary objective was to ascertain whether copper could exist in the thermodynamically immune state, when in contact with pure water under anoxic conditions, and to provide a thermodynamic basis for assessing the corrosion behavior of copper in the repository. In spite of the fact that metallic copper is known to exist for geological times in granitic, geological formations, copper is well-known to be activated from the immune state,and to corrode, by specific species that may exist in the environment. The principal activator of copper is known to be

sulphur in its various forms, including sulphide (H_2S, HS^-, S^{2-}), polysulphide (H_2S_x, HS_x^-, S_x^{2-}), some polysulphurthiosulphate ($S_xO_3^{2-}$), and polythionates ($S_xO_6^{2-}$). A comprehensive study of this aspect of copper chemistry has never been reported, and yet an understanding of this issue is surely vital for assessing whether copper is a suitable material for fabricating canisters for the disposal of HLNW. Our Phase I study identified and explored those species that activate copper; these species include sulphur-containing entities as well as other, non-sulphur species that may be present in the repository. In order to explore these issues, we have introduced new, innovative techniques, such as corrosion domain diagrams (CDDs) and Volt-Equivalent Diagrams (VEDs), as well as traditional Gibbs energy minimization algorithms, in order to display the chemical implications of copper activation and the electrochemical properties of the activating species, in a manner that allows a reader to discern the issues and follow their resolution. No new experiments were performed, but considerable analysis of the thermodynamic data for copper metal in contact with the environments of interested is reported. From this analysis, the question of copper corrosion in pure water under anoxic conditions and in HLNW repositories is readily addressed.

In Phase II of this research, the thermodynamics of the reaction of copper with a wide range of species that was explored in Phase I, has been continued. All of these species activate copper toward corrosion by giving rise to a reaction that occurs at more negative potentials than the reaction of copper with water to produce cuprous oxide (Cu_2O) or cuprous ion, namely:

$$2Cu + H_2O \rightarrow Cu_2O + H_2 \qquad \text{(I-1)}$$

and

$$Cu + H^+ \rightarrow Cu^+ + 1/2H_2 \qquad \text{(I-2)}$$

Reaction (I-2) was of special interest, because it lies at the basis of the claim by Szakálos and Hultquist [1-3] that copper corrodes when in contact with deoxygenated, pure water. This claim has caused considerable controversy in the Swedish HLNW isolation community, because it indicates that copper is not thermodynamically immune, even in oxygen-free, pure water, as had been previously assumed by many researchers in the field of corrosion. This controversy was largely resolved in Phase I, as described below.

Consider the lowest corrosion reaction in the copper/water system represented by Reaction (I-2). The change in Gibbs energy for this reaction can be written as

$$\Delta G = \Delta G^0 + 2.303 Log\left(f_{H_2}^{1/2} a_{Cu^+} / a_{H^+}\right) \qquad \text{(I-3)}$$

which, upon rearrangement yields

$$Log\left(f_{H_2}^{1/2}a_{Cu^+}\right)=\frac{\Delta G-\Delta G^0}{2.303RT}-pH \qquad \text{(I-4)}$$

where ΔG^0 is the change in standard Gibbs energy; i.e., the change in Gibbs energy when all components of the reaction are in their standard state, with the fugacity of hydrogen, f_{H_2}, and the activity of cuprous ion, a_{Cu^+}, being equal to one. At equilibrium, $\Delta G = 0$, and designating the equilibrium values of f_{H_2} and a_{Cu^+} with superscripts "e" we may write

$$f_{H_2}^{e,1/2}a_{Cu^+}^{e}=10^{-\left(\frac{\Delta G^0}{2.303RT}+pH\right)} \qquad \text{(I-5)}$$

We now define two quantities, P and P^e, as follows

$$P=f_{H_2}^{1/2}a_{Cu^+} \qquad \text{(I-6)}$$

and

$$P^e=f_{H_2}^{e,1/2}a_{Cu^+}^{e} \qquad \text{(I-7)}$$

where superscript "*e*" designates equilibrium values. From the Second Law of Thermodynamics, the condition for spontaneity of Reaction (I-2) then becomes $P < P^e$ and immunity is indicated by $P > P^e$.

The quantity P^e has been calculated for Reaction (I-2) using Equation (I-5) and is plotted as a function of pH in Figure I-1, which has been named by one of the present authors (DDM) as a "Corrosion Domain Diagram" (CDD) [5] for reasons that will become evident below. These plots divide the P versus pH domain into regions of immunity (upper region) and corrosion (lower region). These plots clearly demonstrate that whether copper is immune (thermodynamically stable) depends sensitively upon the value of P relative to P^e and hence upon the initial conditions in the system. Thus, if P is small (e.g., at Point a, Figure I-1), $P < P^e$ and the corrosion of copper is spontaneous from left to right, as written in Equation (I-2). On the other hand, if the system is located at Point b, Figure I-1, $P > P^e$ and corrosion is not possible, thermodynamically, and hence the metal is "immune". Returning now to the case described by Point a, we note that as the corrosion reaction proceeds, the concentration of Cu^+ and the fugacity of hydrogen at the interface will increase, particularly in a medium of restricted mass transport like compacted bentonite buffer, such that P will steadily increase with time until it meets the value of P^e at the corresponding temperature. At this point, the metal may be classified as being "quasi-immune"; "quasi" only because transport of Cu^+ and H_2 away from the canister surface, through the bentonite buffer, must be matched by corrosion, in order to maintain $P = P^e$ at the metal surface. Accordingly, the corrosion rate ultimately becomes controlled by the diffusion of Cu^+ and H_2 through the adjacent bentonite buffer. Thus, we conclude that, for

any system starting at a point below the P^e versus pH for the relevant temperature, copper metal is not thermodynamically immune and will corrode in the repository at a rate that is governed by the rate of transport of the reactants to, or corrosion products from, the metal surface. Of course, this rate is readily predicted by solving the relevant mass transport equations, if the diffusivities of H^+, Cu^+ and H_2 in bentonite are known. This is essentially the basis of the PEM for predicting the corrosion rate and the evolution of corrosion damage to the canister as the system evolves along the CEP, as described later in this report.

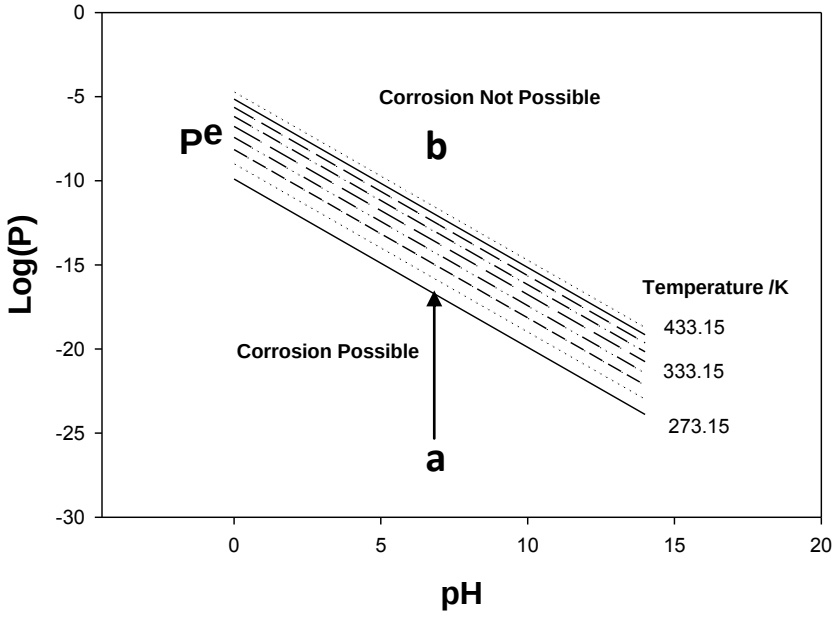

Figure I-1: Corrosion domain diagram for copper in pure water as a function of temperature.

This analysis showed that the claims by Szakálos and Hultquist [1-3] are thermodynamically viable, provided and only provided that $P < P^e$. Numerical analysis showed that this condition could only be met in exceptionally pure solutions where the concentrations of H_2 and Cu^+ were simultaneously very low.

As noted above, for any system whose initial conditions (value of P) lie above the relevant P^e versus pH line, copper is unequivocally immune and corrosion cannot occur, as it would violate the Second Law of Thermodynamics. It is evident, that the conditions for immunity may be engineered in advance by doping the bentonite with a *Cu(I)* salt and a suitable reducing agent to simulate hydrogen, such that the initial conditions lie above P^e versus *pH*. It is suggested that cuprous sulphite, Cu_2SO_3, might be a suitable material. Of course, the dopant will slowly diffuse out of the bentonite and into the external environment, but it might be sufficiently slow that the conditions of immunity may be maintained for a considerable period. Thus, in a "back-of-the-envelope" calculation, we estimate the diffusion time as

$$t = L^2 / D \quad \text{(I-7)}$$

we choose L = 10 cm (as the thickness of the bentonite buffer) and $D = 10^{-9}$ cm^2/s to yield a diffusion time of 10^{11} seconds or 316,456 years. At a time of this order, the value of P at the canister surface will have been reduced to P^e by the diffusion of the dopant (Cu_2SO_3) from the buffer (away from the canister) and corrosion will have initiated when $P = P^e$ at a rate that is determined by the transport of Cu^+ and H_2 through the bentonite buffer. It is important to note that the above calculation is only a rough estimate and that a more accurate value can be obtained by solving the mass transport equations with experimentally determined values for the diffusivities of Cu^+ and H_2. The important point is that immunity may be maintained for a sufficiently long period that the more active components of the HLNW will have decayed away and the waste will have become benign.

The analysis presented above is restricted to the corrosion of copper in contact with pure water, because it makes use of the data contained in Figure I-1. However, ground water is far from pure and a common contaminant is bisulphide ion, HS^-. This species arises from dissolution of sulphide minerals in the host rock of the repository, from dissolution of pyrite in the bentonite, and even from the decomposition of organic (plant) material. It is fair to conclude that bisulphide, and other sulphur-containing species are ubiquitous in groundwater environments at concentrations ranging up to a few parts per million (ppm), at least. It is also well-known that sulphide species, including bisulphide, activate copper by giving rise to the formation of Cu_2S at potentials that are significantly more negative than that for the formation of Cu_2O or Cu^+, thereby rendering the evolution of hydrogen via the reduction of water a viable cathodic process. Thus, in the presence of bisulphide, the lowest corrosion reaction of copper may be written as

$$2Cu + HS^- + H^+ = Cu_2S + H_2 \quad \text{(I-8)}$$

for which the change in Gibbs energy is written as Equation (I-9).

$$\Delta G = \Delta G^0 + RTLn\left(f_{H_2} / a_{HS^-} a_{H^+}\right) \quad \text{(I-9)}$$

As before, we define an equilibrium value of P as Equation (I-10).

$$P = f_{H_2} / a_{HS^-} \quad \text{(I-10)}$$

and the equilibrium value as

$$P^e = f^e_{H_2} / a^e_{HS^-} = 10^{-\left(\frac{\Delta G^0}{2.303RT} + pH\right)} \quad \text{(I-11)}$$

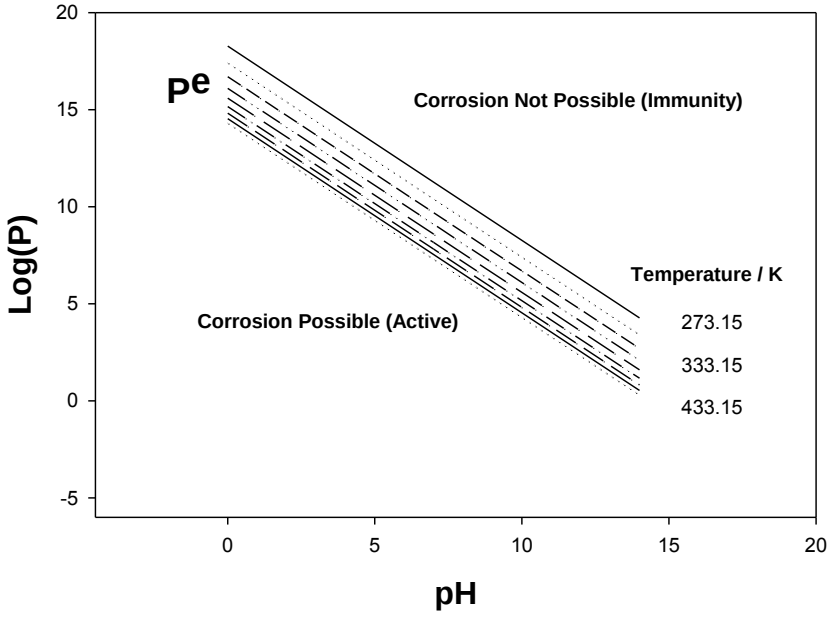

Figure I-2: Corrosion domain diagram for copper in water + HS^- as a function of temperature.

Values of P^e versus pH are plotted in Figure I-2 as a function of temperature for temperatures ranging from 0 ^oC to 160 ^oC in steps of 20 ^oC. Again, P^e versus pH divides the diagram into two regions corresponding to spontaneous corrosion (lower region) and immunity (upper region). The reader will note that the P^e values for the lines are more positive than those for the Cu – pure water case by a factor of about 10^{27}, demonstrating that immunity is much more difficult to achieve in the presence of bisulphide.

The relative ability of a species to activate copper is determined by the position of the line on the vertical axis. The higher the position of the line [more positive the value of Log(*Pe*)] dividing the "corrosion possible" and "corrosion not possible" domains, the more effective is the species in activating the metal. Thus, with regard to Figures I-1 and I-2 it is evident that bisulphide ion is a very effective activator of copper. On the other hand, if we take the case of ammonia, the CDDs for which are shown below in Figures III-9 and III-10 for the formation of $Cu(NH_3)_2^{2+}$ and $Cu(NH_3)^{2+}$, respectively, we find that the values of Log(P^e) at pH = 10 to be -23 and -27, compared with -17 in the absence of NH_3 (Figure I-1) and 7 in the case of HS^- (Figure I-2), which would argue that ammonia is not an activator. However, ammonia is well-known to cause massive corrosion of copper alloys in steam surface condensers in the thermal power industry. This is attributed to the formation of soluble complexes [$Cu(NH_3)_2^{2+}$ and $Cu(NH_3)^{2+}$], that destroy passivity, which is a kinetic phenomenon. This serves to emphasize the difficulty and pitfalls one can experience when attempting to explain kinetic processes in terms of thermodynamic concepts.

As noted above, the environment within the proposed repository is not pristine, pure water, but instead is a complex brine containing a variety of species, including halide

ions, iron oxidation products, as well as small amounts of hydrogen (determined to be about 10^{-6}M by bore-hole sampling), in addition to various sulphur-containing species. Parenthetically, we note that the concentration of H_2 of 10^{-6} M stated above is the maximum value reported [8] for many bore-hole samples, with about half of the reported concentrations being at or close to the detection limit of 10^{-8} M. Some of these species are known to activate copper by forming a reaction product at potentials that are more negative than in their absence, thereby leading to a much larger value for P^e. For example, in the case of sulphide, whence $2Cu+HS^- + H^+ \rightarrow Cu_2S + H_2$, the value of P^e rises by more than twenty-five orders of magnitude at ambient temperature for sulphide concentrations that are typical of the repository compared to the sulphide-absent case, as noted above. Since sulphide species are ubiquitous in groundwater in Sweden, and elsewhere, the controversy raging around whether copper corrodes in pure water is moot. In this study we have derived CDDs for copper in the presence of a large number of species that are known, or suspected, to exist in the repository. We show that a wide variety of sulphur-containing species activate copper, thereby destroying the immunity that has been postulated for copper in groundwater systems. For example, in addition to the sulphide species (S^{2-}, HS^-, H_2S) the polysulphides (S_x^{2-}, x = 2 – 8), polythionates ($S_xO_6^{2-}$) and thiosulphate ($S_2O_3^{2-}$) are all found to be powerful activators of copper. Interestingly, many of the polythiosulphates ($S_2O_3^{2-}$, $x \geq 3$) are found not to activate copper. The reason for this unexpected result is not yet known and may require determination of electron densities on the atoms in the ions to resolve this issue. Chloride ion, which is also ubiquitous in groundwater systems, is found to be a mild activator, but the other halide ions (F^-, Br^-, I^-) are not.

Because of their propensity to activate copper, and because some, at least, are present in the repository ground water, sulphur species were singled out for a more intensive study in Phase II. It is well-known that, except for carbon, sulphur displays the richest chemistry of any element in the periodic table. Sulphur-containing species display oxidation states ranging from -2 to +8, with a multitude of fractional oxidation states. The polysulphurspecies are generally labile with little kinetic inhibition to interconversion. We summarized this redox chemistry in Phase I in the form of volt-equivalent diagrams (VEDs), in which the equilibrium potential of the species with respect to elemental sulphur multiplied by the average oxidation state of sulphur in the species (the "volt equivalent") is plotted versus the average sulphur oxidation state for a given temperature (ranging from 25 ^oC to 125 ^oC) and pH. These diagrams provide a set of rules that determine which species react with which, and identify which species undergo disproportionation. The diagrams have been developed to match the conditions that are found in the proposed repository. The diagrams reveal that those sulphur compounds, e.g., the poly thiosulphates ($S_xO_3^{2-}$, x = 3 – 6), that are found not to activate copper, are characterized by excessively low (negative) volt-equivalent values. While this is seen to be an important factor, it is not considered to be decisive and we continue with our search for a rational electrochemical explanation as to why some of the polythiosulphates ($S_xO_3^{2-}$, x = 3 – 6) are found not to activate copper while others do ($S_2O_3^{2-}$).

Under anoxic conditions the activation of copper produces hydrogen and the relationship between the equilibrium hydrogen pressure from the reaction and the hydrogen pressure in the repository, for a given cuprous ion activity is another indicator of whether copper will corrode. Thus, if the equilibrium hydrogen pressure for a reaction is greater

than the hydrogen pressure in the repository, the reaction will proceed in the forward (hydrogen-producing and corrosion-inducing) direction, whereas if the equilibrium hydrogen pressure is less than that of the repository the reaction is spontaneous in the reverse direction. It is this latter situation that assures immunity to corrosion. Not unexpectedly, the results of this analysis are in accord with the findings from the Corrosion Domain Diagrams, and, again, the propensity of the sulphur-containing species to activate copper is demonstrated. Chloride ion is, again, found to be a weak activator in accordance with the CDDs. This work was also performed to more closely define the conditions of the Szakálos and Hultquist [1-3] experiments, which have detected the formation of hydrogen when copper is in contact with highly pure, deoxygenated water. As with the CDDs, the hydrogen pressure calculations predict that the reaction of copper with water under these conditions is only spontaneous if the hydrogen partial pressure and concentration of Cu^+ are both exceptionally low, providing further corroboration that the lack of agreement between the various sets of experiments reflects differences in the initial states of the experiment with respect to the quantity $P = [Cu^+] p_{H_2}^{1/2}$ compared to the equilibrium value, P^e.

In carrying out this analysis, it was necessary to consider the processes that might establish the hydrogen partial pressure in the repository. From a review of the geochemical literature, it appears that the hydrogen partial pressure is established by either the hydrolysis of Fayalite [$3Fe_2SiO_4 + 2H_2O \rightarrow 2Fe_3O_4 + 3SiO_2 + 2H_2$] or the Schikorr reaction [$3Fe(OH)_2 \rightarrow Fe_3O_4 + 2H_2O + H_2$], or both. In Phase I, we carried out a thermodynamic analysis of these reactions and found that the Fayalite hydrolysis reaction is, theoretically, capable of producing only a fraction of an atmosphere, while the Schikorr reaction is predicted to produce an equilibrium hydrogen pressure of the order of 1000 atm, which assumes that $Fe(OH)_2$ and the reaction product (Fe_3O_4) are both present in the system. However, if $Fe(OH)_2$ is a minor component of the rock, and recognizing that hydrogen is continually lost from the system, with the hydrogen concentration being determined by the rate of formation (Fayalite hydrolysis and/or the Schikorr reaction) and the rate of loss, due to transport through the rock to the surface, reaction with reducible species (e.g., Fe^{3+}), etc., the effective, steady-state hydrogen concentration will be much lower. Thus, the measured concentration of hydrogen from bore-hole sampling programs is of the order of 10^{-6}M -10^{-8} M, corresponding to a partial pressure of about 10^{-9} atm – 10^{-11} atm. This range is so much lower than the thermodynamic predictions that it raises the question as to whether the measured values are accurate or whether neither of the two reactions identified above actually occur in the repository. Certainly, if the Schikorr reaction controls the hydrogen pressure in geological formations, explaining the existence of native copper is straight forward, provided the concentrations of sulphur-containing species that can activate copper are suitably low. Even if Fayalite hydrolysis is the operative hydrogen-control mechanism, the existence of native copper is, again, readily explained, but it requires a correspondingly lower (by a factor of about 10^4) sulphide concentration. The discrepancy between the calculated hydrogen pressure and that sampled from bore-holes is disturbing and needs to be resolved, although it is outside of the scope of the current project. We note, however, that the geosphere is a large and exceedingly complex reservoir of

chemical reductants and that any analysis based upon only a few components is probably too simplistic ([5]).

Currently, there exist data on the chemical composition of the ground water that are the result of analyzing "grab" samples from bore holes. While this procedure is notoriously unreliable, particularly when volatile gases are involved, it does provide good measures of dissolved components, provided that precipitation does not occur during the sampling process. Frequently, solid phases will precipitate in response to the loss of volatile gases, and unless the sampling capsule is tightly sealed considerable error may ensue. Given these caveats, as well as the fact that some techniques measure the total concentration of an element (e.g., sulphur as sulphate by oxidizing all sulphur species in the system to SO_4^{2-} with a strong oxidizing agent, such as H_2O_2), we accept the analysis of the concentrations of the ionic species, because they are measured using the normally reliable method of ion chromatography. However, these anions (e.g., Cl^-, Br^-, CO_3^{2-}, etc) are generally not particularly strong activators and hence are of only secondary interest in determining the corrosion behavior of copper. Accordingly, we decided to employ a modern, sophisticated Gibbs Energy Minimization algorithm to predict the composition of the repository environment as a function of temperature and redox condition, with the latter being adjusted by changing the relative concentrations of hydrogen and oxygen in the input to the code, in order to obtain the desired output hydrogen concentration (a maximum of 10^{-6}M). After evaluating several codes, we chose GEMS, which was developed in Switzerland by Prof. Dmitrii Kulik. This code is designed specifically to model geochemical systems, contains a large database of compounds, and is in general use in the geochemical community. Prior to using the code to model the repository, we upgraded the database by adding thermodynamic data for various polysulphur species (polysulphides, polythiosulphates, and polythionates) that had been developed earlier in this program (Phase I). However, GEMS became ill-behaved when the data for $S_xO_3^{2-}$, x = 3 – 7 were added, a phenomenon that remains puzzling. Consultation with the code developer, Prof. Dmitrii Kulik at the Paul Scherer Institute in Switzerland failed to identify and isolate the problem and, accordingly, it was necessary to remove those species from the database. The reader will recall that these are the very species that, anomalously, do not activate copper. With the code in its present form, we have modeled the repository under both oxic and anoxic conditions with the greatest emphasis being placed on the latter, because the great fraction of the storage time is under anoxic conditions. The most important finding to date is that the concentrations of the polysulphur species (polysulphides, poly thiosulphates, and polythionates) under anoxic conditions are predicted to be very low, but it is still not possible, because of the uncertainty in the calculations, to ascertain with certainty whether these species will still activate copper in the repository. However, the point may be moot, because sulphide species (S^{2-}, HS^-, and H_2S) are predicted to be present in sufficient concentration to activate copper and cause the metal to corrode under simulated repository conditions.

Finally, we have initiated work to define the corrosion evolutionary path (CEP) in preparation for modeling the corrosion of the canisters in this next phase. This task of defining the CEP essentially involves predicting the redox potential (E_h), pH, and granitic groundwater composition, as defined by the variation of temperature (note that the temperature decreases roughly exponentially with time, due to radioactive decay of the short-lived isotopes, such as $^{137}Cs_{55}$ with a half-life of 30.1 years), and then applying Gibbs

energy minimization to predict speciation at selected times along the path. At each step, the CDD for copper is derived and the value of P is compared to P^e to ascertain whether copper is active or thermodynamically immune. Although the polysulphur species (e.g., HS_2^- and S_2^{2-}) are predicted to be present at very low concentrations, or are predicted to be absent altogether (e.g., polysulphur oxyanions), the concentrations of certain polysulphides (e.g., S_2^{2-}) are sufficiently high to activate copper (the activating concentration is predicted to be only 10^{-44} M for $[H_2] = 10^{-11}$ M) for activation to occur. However, an unequivocal resolution of this issue must await access to the GEMs source code, because the code apparently sets the concentration of any species with a calculated concentration of less than 10^{-20} M equal to zero. In any event, sulphide (H_2S, HS^-, and/or S^{2-}) are predicted to be present during the entire anoxic period at sufficiently high concentrations that they will activate copper. An important finding of this work is thar copper remains activated along the entire corrosion evolutionary path, due to the presence of sulphide species in the repository environment.

References

1. G. Hultquist, *Corros. Sci.*, **26**, 173 (1986).

2. G. Hultquist, G. K. Chuah, andK. L Tan, *Corros. Sci.*, **29**, 1371 (1989).

3. P. Szakálos, G. Hultquist and G. Wikmark, *Electrochem. SolidState Letters*, **10**, C63 (2007).

4. E. Mattsson, *Br. Corros. J.*, **15**, 6 (1980).

5. T. E. Eriksen, P. Ndalamba, and I. Grenthe, *Corros. Sci.*, 28, 1231 (1989).

6. B. Berskog and I. Puigdomenech, *J. Electrochem. Soc.*, **144**, 3476 (1997).

7. D. D. Macdonald and S. Sharifi-Asl, "Corrosion of Copper in Water", Proc. Workshop on Copper Corrosion and Buffer Erosion, Hotel Rica, Stockholm, Sweden, September 15 – 17, 2010, SSM Report 2011:08 (2011).

8. E-L Tullborg, J Smellie, A.Ch. Nilsson, M. J. Gimeno, V. Brüchert, J. Molinero, *SKB, TR-10-39, Svensk Kärnbränslehantering AB*, (2010)

II. Objectives of Phase II

The Phase II work, reported upon here, follows on that accomplished in Phase I, in order to provide a better and more accurate definition of the conditions and the corrosion processes that are expected to exist as the repository evolves over the planned storage period of 100,000 years. Using more advanced physico-electrochemical models, the work will also yield the corrosion potential and the corrosion rate that can be compared with that predicted by SKB in their modeling program [1]. The objectives of the Phase II work were accomplished through seven tightly coupled tasks that either expanded upon the Phase I work or introduced entirely new activities into this program, such as the development of a radiolysis/mixed potential model for the corrosion of copper in the repository. This model has been used to preliminarily explore the impact of radiolysis of water resulting from the low radiation field of γ photons (1 Gy/hr) at the canister surface.

II-1. Task 1: Continued Definition of Repository Chemistry.

This task continued to define the chemistry of the repository over wide ranges of conditions, including temperature (20^{o}C to 80^{o}C), pH (6-9), [H_2] (10^{-8} to 10^{-12} M), [Fe^{2+}], [Fe^{3+}], [O_2] (10^{-70} to 10^{-6} M), [S], [Cl^-], etc., with the ranges being chosen to more than cover those expected in the repository. This is done to identify positive and negative synergistic effects between various parameters, in order to better understand the repository chemistry. The principal tool used in this task was the Gibbs Energy Minimization code, GEMS, as employed in Phase I. In these calculations, we attempted to relax the equilibrium constraint on some species, recognizing that in the repository the concentration of a species may be established by rate processes rather than by equilibrium relationships.

II-2. Task 2: Continued Development of CDDs for Complexing Systems

In Phase I we derived CDDs for some systems that form complexes, such as $Cu/CuCl_2^-$,$Cu/Cu(HCO_3)_2^-$, $Cu/Cu(HS)_2^-$, $Cu/Cu(H_2PO_4)_2^-$, to name but a few. At the time that the diagrams were derived, we did not possess detailed information on speciation within the repository, except that from "grab samples" from Forsmark. However, by using GEMS, we are now in a position to predict the equilibrium concentrations of a multitude of anions that form complexes with copper. This is an important issue, because some complexing anions may be strong activators, rivaling the sulphides and polysulphur species, in this respect. Accordingly, in this second task, we calculated ranges for P in the repository for comparison with the P^e values already derived. This comparison has allowed us to develop a comprehensive library of activating species.

II-3. Task 3: Continued Development of the Mixed Potential Model.

Two key parameters in defining the corrosion evolutionary path are the redox potential of the environment and the corrosion potential of the copper canister. Current geochemical algorithms attempt to estimate the redox potential by using the Nernst equation; which is electrochemically incorrect, because the redox potential arises from the occurrence of a multitude of redox reactions on an inert substrate (e.g., *Pt*), not from a single reaction at equilibrium (for which the Nernst equation applies). In the system of interest, there are many redox species existing in the system, with each being involved in a redox reaction. In essence, the redox potential is a measure of the oxidizing/reducing power of the medium. If the redox potential is high, reduced species will tend to be oxidized, but if the redox potential is low, oxidized species will tend to be reduced. In the case of the "electrochemical corrosion potential" (ECP), one of the "redox reactions" is the oxidation of the substrate itself and the ECP provides a measure of the tendency for specific corrosion reactions (e.g., metal electro-dissolution, passivity) and processes (general corrosion, pitting, stress corrosion cracking, etc.) to occur. Indeed, most localized corrosion phenomena (pitting, stress corrosion cracking, etc) only occur at potentials that are above or below a critical value, so that knowledge of the ECP provides a convenient and powerful means of identifying probable damaging mechanisms. The Mixed Potential Model (MPM) developed conceptually in this work is a derivative of that previously developed by the authors for calculating the ECP of stainless steel components in the primary coolant circuits of water-cooled nuclear power reactors [2], a system in which a multitude of redox species (from the radiolysis of water) also exists. It also incorporates features of the Thin Layer Mixed Potential Model that was previouslydeveloped by two of the present authors [3] for describing the corrosion of copper canisters in a "dry" repository (Yucca Mountain) in the US [3]. The major changes that were made include: (1) It was customized for copper; (2) It incorporated a wide range of redox couples involving relevant electroactive species, including Fe^{2+}/Fe^{3+}, O_2/H_2O, H_2/H^+,Cu^{2+}/Cu^+,S_x^{2-}/S^{2-}, and other sulphur-containing species, and not just O_2/H_2O, H_2/H^+, and H_2O_2/H_2O couples that were incorporated into the reactor model [2], if they were deemed to be significant; (3) The model employed the generalized Butler-Volmer equation for describing the kinetics of the redox reactions, incorporating thermodynamic (through the equilibrium potential), kinetic (exchange current density, Tafel constants), and mass transport (limiting currents) information in the model; (4) The mass transfer limited currents were to be expressed in terms of transport through a porous medium (the bentonite buffer). This model was conceptually much more comprehensive than previously-developed models [1], which were based on a single redox reaction being irreversible in the cathodic sense and that did not consider water radiolysis. Input data for the model are currently being obtained by re-analyzing experiments reported in the literature, although, if necessary, some may be measured.

II-4. Task 4: Continued Definition of the Corrosion Evolutionary Path.

The evolution of corrosion damage must be modeled along the corrosion evolutionary path, which is defined by the variation of temperature, *pH*, [HS^-], p_{H_2}, and other independent variables that have significant impact on the corrosion rate on a canister, as the repository ages. The time dependences of pH, [HS^-], and p_{H_2} must be modeled by solving the transport equations for the transfer of H^+, HS^-, and H_2 across the bentonite layer, recognizing the existence of a source term for HS^- and S_2^{2-} in the bentonite (dissolution of FeS_2, which is iron disulphide, containing the anion, S_2^{2-}). Solution of the thermal diffusion equation yields the temperature as a function of distance from the copper surface and time. Because the diffusivities of H^+, HS^-, and H_2 are temperature-dependent, as is the rate constant for FeS_2 dissolution, the system of equations that describe the evolution of the repository and hence that indicate whether, and under what conditions, immunity may be achieved, are highly non-linear and must be solved numerically. An important goal of this task, therefore, was to predict if, and how long, the condition $P > P^e$ might be sustained as the repository ages.

II-5. Task 5: Development of a Physico-Electrochemical Model (PEM) for Canister Corrosion.

In this major task, a model was developed that describes the accumulation of corrosion damage as the canister moves along the corrosion evolutionary path. This model is a variant of the mixed potential model (MPM) developed in Task 3, but emphasizes the corrosion of copper and the transport of reactants (e.g., HS^-, H_2O) to, and products [e.g., H_2] from the metal surface. These fluxes are interrelated by the stoichiometry of the reaction. Thus, for the reaction, $2Cu + HS^- + H^+ \rightarrow Cu_2S + H_2$ the fluxes are related by $J_{HS^-} = J_{H^+}$ and $J_{HS^-} + J_{H_2} = 0$. These relations form the boundary conditions for solving the continuity equations $\frac{\partial C_i}{\partial t} = -\nabla . J_i$ for species i = 1 to K; in this case for H^+, HS^-, and H_2, in the presence of the HS^- activator, with the corrosion rate, expressed as the rate of production of Cu_2S, being equal to J_{H_2} (mol/cm^2.s). In general, the fluxes are defined as $J_i = -D_i \frac{\partial C_i}{\partial x} - z_i D_i C_i \gamma \frac{\partial \phi}{\partial x} + \bar{V} C_i$, where z_i, D_i, C_i, ϕ, $\bar{V}$, and γ are the charge, diffusivity, and concentration of the species, the electrostatic potential, flow velocity, and F/RT, respectively. A set of K such equations must be solved for K concentrations along with Poisson's equation for the potential, in order to calculate values for the K+1 unknowns in the model. The last term in the flux equation accounts for the contribution from convection. Thus, many activation reactions consume water, so that as corrosion proceeds and H_2O is consumed at the interface, water flows through the bentonite buffer towards the

canister, taking with it dissolved species (e.g., HS^-) and inhibiting the transport of corrosion products away from the surface. "Back-of-the-envelope" calculation shows that convection might represent a significant contribution to the flux and, in some cases, convection might be more important than diffusion. This contribution has not been considered in previous models [1] and the corrosion rate estimated therefrom (10 nm/year) is likely to be low. Poisson's equation is given as $\frac{\partial^2 \phi}{\partial x^2} = -\frac{F}{\varepsilon \varepsilon_0} \sum_{i=1}^{K} z_i C_i$, where F is Faraday's constant, ε, is the dielectric constant of water (78 at 25°C), and ε_0 is the permittivity of a vacuum (8.85×10^{-14} F/cm). The quantity, $\sum_{i=1}^{K} z_i C_i$, is the charge density and is responsible for the development of space charge. The above equation set was solved numerically using a MatLab software package. The output of this task is the calculated corrosion rate at any point along the Corrosion Evolutionary Path (CEP) and an estimate of the total corrosion damage (loss of thickness of the canister wall) at the end of the storage period.

II-6. Task 6: Assessment of Corrosion in the Resaturation Period.

Various estimates suggest that a period of up to 1000 years may elapse before the bentonite buffer is saturated with ground water. However, the canister may be in contact with steam if superheat exists at the canister surface; that is if the temperature is higher than the boiling temperature of the groundwater for the prevailing pressure. If this condition exists, then the canister may suffer steam corrosion. In order to assess whether this scenario is likely, it is be necessary to estimate the pressure in the repository, which is located 500 m below the surface. Even if the temperature is not higher than the boiling temperature at that pressure a steam front is expected to precede the ground water and make contact with the canister. Many of the dissolved species in the ground water (e.g., H_2, O_2) segregate into the steam phase to an extent described by the distribution coefficient. Distribution coefficients for many of the species of interest have been measured in the steam cycle industry should be employed in an analysis of this type. The goal of this task was, therefore, to define the reaction mechanisms and estimate the corrosion rate of copper during the resaturation period from data that are available in the literature. This issue has been previously considered by SKB [1], but that analysis does not appear to have considered the literature that exists on the atmospheric and steam phase corrosion of copper.

II-7. Task 7: Assessment of the Impact of Water Radiolysis

Using computer codes developed by the author for describing the radiolysis of water in water-cooled nuclear power reactors and in thin aqueous films on metal surfaces, we proposed exploring the impact of radiolysis on the corrosion of copper. Radiolysis is known to produce a myriad of reactive species, including O_2, H_2O_2, H_2, OH, O_2^-, H, OH, H^+, OH^-, O^{2-}, and others. These species can have a significant effect on the corrosion

potential, as described by the mixed potential model (MPM, Task 3) and the Physico-Electrochemical Model (PEM, Task 5) and may react with species in the groundwater to produce species that are deleterious toward copper (e.g., FeS_2→sulphides, polysulphides, and polysulphur oxyanions). This work will generally follow our previous work in the early Yucca Mountain project [3], but with updated inputs to reflect the Swedish HLNW isolation technology (γ-dose rates, temperature, groundwater composition, etc.), and will incorporate the latest radiolysis model. The principal objective will be to ascertain whether water radiolysis is a significant factor in the corrosion of copper in the Swedish granitic rock repository.

References:

1. F. King, L. Ahonen, C. Taxen, U. Vuorinen and L. Werme, *SKB, TR-01-23*, Svensk Kärnbränslehantering AB.(2001).
2. D. D. Macdonald, *Corrosion*, 48(3), 194-205 (1992).
3. D. D. Macdonald, and M. Urquidi-Macdonald, *Corrosion*, **46**(5), 380-390 (1990).

III. Phase II Accomplishments

III-1: Definition of Repository Chemistry

The equilibrium composition of the groundwater adjacent to the canister plays an important role in the stability of the copper canister in the Engineered Barrier System (EBS). Of great importance is the concentration of different sulphur species. It is known that sulphur species exist and probably form, because of dissolution of sulphide minerals in the rock or by dissolution of pyrite present in the bentonite, thereby rendering sulphur-containing species ubiquitous in the groundwater. These species can react with copper causing corrosion, thereby decreasing the life time of the canister [1]. Besides sulphur species, some other components of the groundwater, such as dissolved gases (e.g. hydrogen and carbon dioxide), chloride ion, and pyrite may also play key roles in the corrosion of copper canisters.

In order to obtain a more accurate view of the repository at equilibrium, we continued to define the chemistry of the repository over the ranges of operating conditions that had been previously indicated by using the Gibbs Energy Minimization code, GEMS, as employed in Phase I. Table (III-1) shows the concentration of the input material that has been selected for defining the chemistry of system.

Table-III-1: Input material in the anoxic condition.

Component	Concentration
$CaSO_4$	0.016(g/L)
$FeCO_3$	0.005(g/L)
$H_2(g)$	1e-10(M)
KOH	0.0018(g/L)
Na_2SO_4	0.003(g/L)
$NaCl$	0.005(g/L)
$O_2(g)$	1e-77(M)
$NH_3(a)$	1e-10(M)
$Pyrite$	100(g/L)
CuO	0.01(g/L)

In performing the Gibbs energy minimization using GEMS, we assume that the bentonite buffer is fully saturated with groundwater and that the redox condition is anoxic. Since pyrite is assumed to be the most important sulphur-containing component of the bentonite in the EBS, in our calculation, we added enough pyrite to saturate the system. The temperature range was selected based upon the temperature evolution of the canister to be in the range of 18^{o}C to 100^{o}C. Tables A-1 to A-4, in Appendix (A) show the equilibrium concentrations of the defined groundwater species as a function of temperature. In the following part, we will discuss the most important species indicated for the equilibrium condition. The reader should note that the following results are based upon the output of the

Gibbs energy minimization of the system and hence are equilibrium concentrations and hence do not incorporate any kinetic factors.

Identification of the most important species in the equilbrium condition

SO_4^{2-}

In general, sulphate is the main component in the bedrock groundwater and its origin could be from different sources, such as sulphate minerals (e.g., *$CaSO_4$*, *$BaSO_4$*) or the oxidation of sulphide species by atmospheric oxygen prior to the establishment of anoxic conditions. Sulphate can play an important role in the corrosion of copper canister in an indirect way. Thus, in the presence of sulphate reducing bacteria (*SRB*), it is possible to have the reduction of sulphate by electrons supplied by the microbe,

$$SO_4^{2-}(a) + 7H^+ + 8e^- \rightarrow HS^- + 4H_2O(l) \qquad \text{(III-1)}$$

thereby converting sulphate to additional HS^- and enhancing the corrosion rate of the canister as in form of Reaction (III-2)

$$2Cu(s) + HS^- + H^+ \rightarrow Cu_2S(s) + H_2(aq) \qquad \text{(III-2)}$$

Figure (III-1) shows the GEMS-predicted evolution of equilibrium sulphate activity as a function of canister temperature. As we can see, the activity of sulphate is predicted to be relatively high in the system and increases with decreasing temperature, as the repository ages. The reader should note that copper sulphate is highly soluble in aqueous environments and a very high concentration of sulphate ion is needed to form solid copper sulphate in the system, which seems to be not possible for the concentration level of suphate predicted for the repository ground water here.

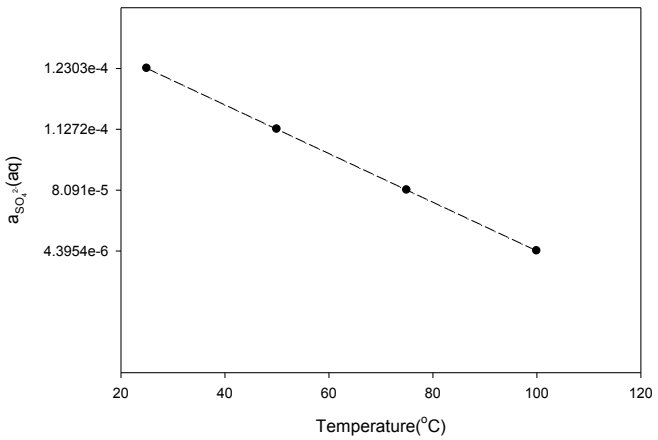

Figure-III-1: Activity of sulphate species in the simulated groundwater as a function of temperature

***Cl*⁻(aq)**

It is well known that chloride ions are also ubiquitous in the bedrock groundwater environment. Figure (III-2) shows how the simulated chloride activity in the groundwater is predicted to change with temperature. As can be seen, the chloride activity in the system is relatively low and constant at elevated temperature, corresponding to short exposure times (but still thousands of years) and is predicted to rise sharply as the temperature approaches ambient corresponding to long exposure times. The CDD's show that chloride ion is a moderate activator of copper.

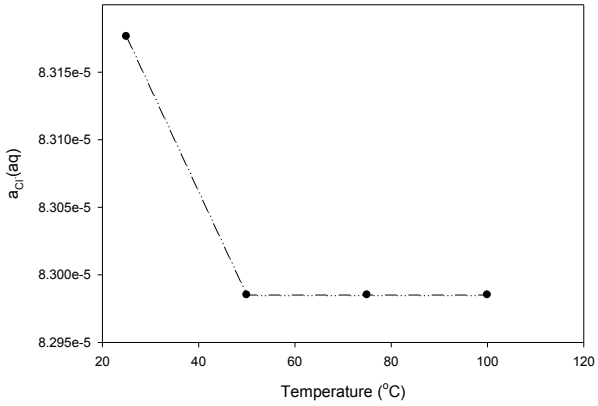

Figure-III-2: Activity of chloride ion in the simulated groundwater as a function of temperature.

Methane

The importance of dissolved methane (CH_4) in the groundwater is because of its ability to participate as a nutrient in the anaerobic reduction reaction of sulphate (SO_4^{2-}) in the presence of sulphate reducing bacteria (*SRB*)[2]. The predicted reaction is in the overall form of the following

$$CH_4(aq) + SO_4^{2-}(a) \rightarrow HCO_3^{-}(a) + HS^{-}(a) + H_2O(l) \qquad \text{(III-3)}$$

Figure (III-3) shows the calculated activity of methane as a function of temperature in the simulated groundwater composition. As can be seen, the concentration of dissolved methane gas in the system is very low, and probably does not play an important role on the reduction of sulphate.

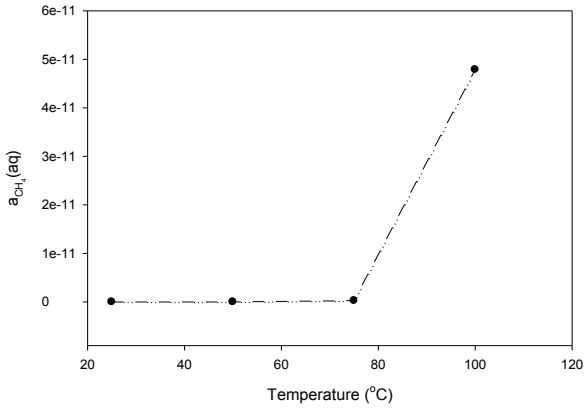

Figure-III-3: Activity of dissolved methane gas in the simulated groundwater as a function of temperature.

Hydrogen

Figure (III-4) shows the variation of the predicted activity of dissolved hydrogen in the simulated groundwater environment as a function of temperature, as calculated using Gibbs energy minimization. As we can see, the predicted concentration is in the range of 3e-12 M to 5e-8 M and increases with increasing temperature, particularly at the higher temperatures. Even with increasing the input hydrogen value in the calculation, the concentration in the equilibrium condition was very low compared to the values reported by SKB [2]. Therefore, it can be concluded that, as far as hydrogen is concerned, the condition in the repository is probably far from equilibrium.

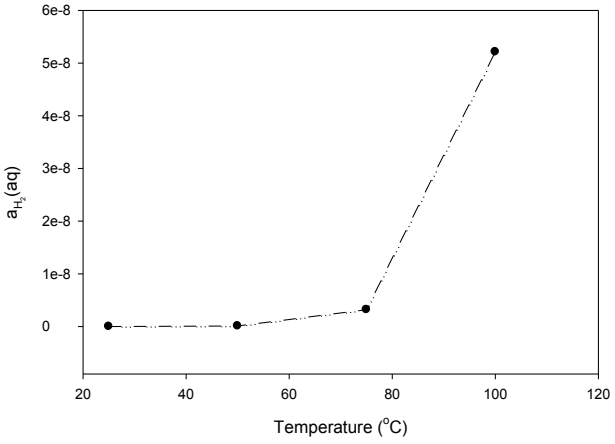

Figure-III-4: Activity of dissolved H_2 gas in the simulated groundwater as a function of temperature.

Carbon dioxide (CO_2)

Since carbon dioxide in the groundwater can provide a food source for potential bacterial activity, it is important to track its concentration in the equilibrium system. Figure (III-5) shows the evolution of dissolved carbon dioxide concentration in the simulated groundwater system as a function of temperature. As it can be seen, the concentration of dissolved CO_2 is of the order of 1e-6 M and decreases with increasing temperature.

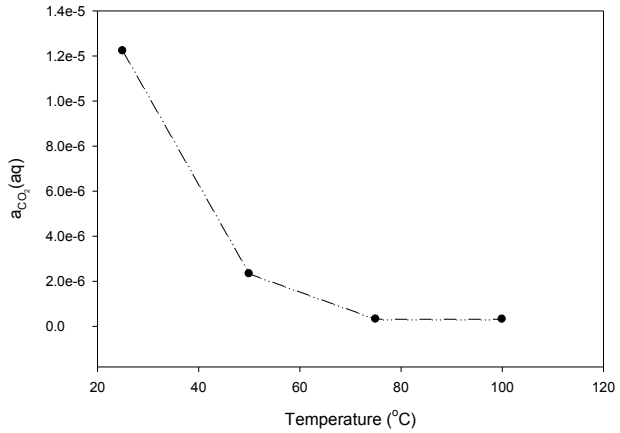

Figure-III-5: Activity of dissolved CO_2 gas in the simulated groundwater as a function of temperature.

HS^-

HS^- is the principal sulphur species in the repository that can activate copper through the following reaction

$$2Cu(s) + HS^- + H^+ \rightarrow Cu_2S(s) + H_2(aq) \qquad \text{(III-4)}$$

Figure (III-6) shows the activity of HS^-(aq) in the simulated groundwater system, as a function of temperature. It is seen that the concentration of the specie in the solution is relatively high and that the concentration is predicted to increase with increasing temperature. It should be noted that the maximum concentration of sulphide species may be controlled by the solubilities of various sulphide minerals, such as FeS and FeS_2.

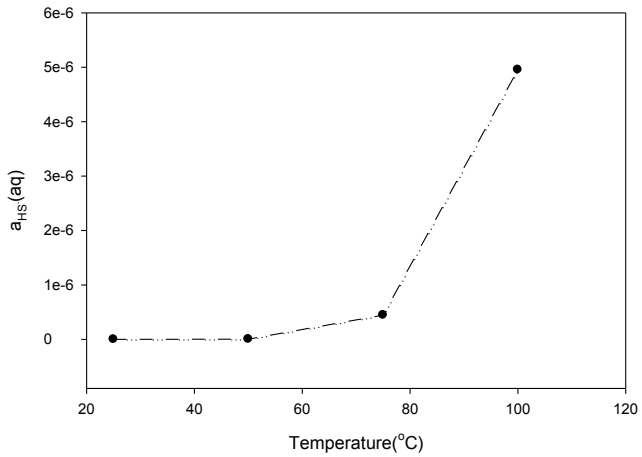

Figure-III-6: Activity of dissolved HS^- gas in the simulated groundwater as a function of temperature.

Other sulphur species

As we can see from the GEMs data tables (Appendix A), the activities of the other, available sulphur species in the system are quite low and perhaps, they will not play an important role in the corrosion reaction of copper. Although some of the sulphur species such as $HS_2O_8^-(aq)$,$HS_2O_7^-(aq)$ and HSO_4^-(aq) have higher activities compared to the rest, they are not able to donate atomic sulphur to the metal and and hence cannot activate copperactivate it.

Estimation of hydrogen concentration based on reported redox potentials

The results of the Gibbs energy minimization of the repository system have revealed that H_2/H^+ equilibrium is probably the only important redox reaction in the simulated ground water composition. Although other redox reactions possibly exist, such as Fe^{3+}/Fe^{2+}, the conditions in the repository do not appear to be sufficiently conducive for them to make a significant contribution to the redox potential. Thus, for the Fe^{3+}/Fe^{2+} case, the concentration of Fe^{3+} is so low as to be immeasurable and hence precludes a significant contribution to E_{redox}. Accordingly, it appears that the H_2/H^+ equilibrium dominates the redox properties and we will assume that it in possible to use the Nernst equation to approximate the redox potential. Therefore, we have used the reported redox potential and the pH of the system, in order to estimate the range of hydrogen concentration that exists in the system. Consider Reaction (III-5) as being the responsible redox reaction,

$$H^+ + e^- = 1/2H_2(aq) \qquad \text{(III-5)}$$

then using the Nernst equation we have,

$$E = E^0 - \frac{2.303RT}{nF}\log\left(f_{H2}^{1/2} \Big/ [H^+]\right) \quad \text{(III-6)}$$

where, E is the equilibrium potential (V), and E^0 is the standard potential, which is equal to zero for the hydrogen electrode electrode, R is the standard gas constant (=8.314 $J.K^{-1}.mol^{-1}$), T is absolute temperature (*Kelvin*), n is the number of electrons, F is Faraday's constant (=96485 $C.equiv^{-1}$), f_{H2} is fugacity of hydrogen gas and $[H^+]$ is the concentration of hydrogen in the solution. Table (III-2) shows the calculated hydrogen concentrations (Henry's law has been used to convert fugacity to concentration) in the system after 10,000 years based upon pH and E_h that is reported by SKB [3]. Rearrangement of Equation (III-6) yields

$$\log\left(f_{H_2}\right) = -\frac{2F}{2.303RT}E_h - 2pH \quad \text{(III-7)}$$

and noting Henry's law, $[H_2] = K_H f_{H_2}$, where K_H is Henry's coefficient for the dissolution of hydrogen in water, we obtain

$$\log\left(C_{H_2}\right) = -\frac{2F}{2.303RT}E_h - 2pH + \log\left(K_H\right) \quad \text{(III-8)}$$

By further noting that at 25 ^oC, $2.303RT/F$ = 0.05916 V, and that Henry's coefficient for hydrogen at the same temperature is 7.06×10^{-4} *mol/L.atm* we calculate the concentrations of hydrogen as summarized in Table III-2.

Table-III-2: Calculated hydrogen concentration based on the reported E_h/pH values at 25 ^oC.

pH	6.7	8.3	6.7	8.3
E_h (*mV*)	-150	-260	-260	-150
[H_2] (*mol/L*)	3.37×10^{-12}	1.11×10^{-11}	1.77×10^{-8}	2.13×10^{-15}

As can be seen from Table (III-2), the hydrogen concentration under all selected conditions (excluding the case of pH=6.7 and E_h=-260mV) is much lower than the values measured from grab samples, as reported by SKB [1,2]. Therefore, the reader should be aware that, in order to explain the redox potential reported by SKB, the hydrogen concentration should be lower than the values reported by SKB, and it is evident that the calculated values for hydrogen concentration ly below the detection limit reported by the SKB(2×10^{-8} (*mol/L)*) [1]. In other words, an inconsistency may exist between the reported redox potential and the measured hydrogen concentration. This inconsistency needs to be resolved. However, we note here that SKB [4] regards it necessary to consider Fe^{2+}, S^{2-}, and *Mn* and *U* species, in addition to microbial activity, when modeling the redox properties of the groundwater system, but it is also necessary to point out that there are three important factors that must be considered when assessing the contributions that given species might make to controlling the redox properties. These factors are whether the conjugate redox

species (e.g., Fe^{3+}, Fe^{2+}) are both present at finite concentration, the concentrations of these species with respect to the concentrations of other redox species, and the exchange current densities of the redox couples upon the indicating electrode surface (commonly platinum). In turn, the exchange current density depends upon the concentrations of the redox species in the bulk of the solution. An answer to whether any given species makes a significant contribution to the redox potential must be sought within the realm of electrochemical kinetics and not from thermodynamics, because the redox potential is an example of a "mixed potential" not an equilibrium potential. In the opinion of the present authors, SKB has not carried out the requisite analysis and hence their position on this matter is little more than speculation.

References:

1. E.L Tullborg, J. Smellie, A.Ch. Nilsson, M. J. Gimeno, V. Brüchert, J. Molinero,*SKB, TR-10-39, Svensk Kärnbränslehantering AB*, (2010)
2. Main Report of the SR-Can project, *SKB, TR-06-09, Svensk Kärnbränslehantering AB*, (2009).
3. F. King, C. Lilja, K. Pedersen, P.Pitkänen and P. Posiva, *SKB-TR-10-67, Svensk Kärnbränslehantering AB*, (2010).
4. Site description of Forsmark at completion of the site investigate phase, *SKB, TR-08-05 Svensk Kärnbränslehantering AB*, 319-324 (2008).

III-2: Corrosion Domain Diagrams-complexing reactions

As we described in Phase-I [1], the objective of deriving Corrosion Domain Diagrams (CDDs) was to present the consequence of the Second Law of Thermodynamic in the clearest form possible when assessing the immunity and activation of copper. In Phase I [1] we derived CDDs for systems that form complexes, such as $Cu/CuCl_2^-$, $Cu/Cu(HCO_3)_2^-$, $Cu/Cu(HS)_2^-$, $Cu/Cu(H_2PO_4)_2^-$, to name but a few. At the time that the diagrams were derived, we did not possess detailed information on speciation within the repository, except that from "grab samples" from Forsmark. However, by using GEMS, we are now in a position to predict the equilibrium concentrations of a multitude of anions that form complexes with copper. Many of these species were not reported in the grab sample analyses. This is an important issue, because some complexing anions may be strong activators, rivaling the sulphides and polysulphur species, in this respect. Accordingly, in this first part, we will calculate ranges for P in the repository for comparison with the P^e values already derived. This comparison will allow us to develop a comprehensive library of activating species. Here, we discuss the effect of some of the species on the basis of the derived corrosion domain diagram and the complete list of the diagrams/reactions is presented in Appendix B. It should be mentioned that some of the complexing species, such as sulphate, carbonate, nitrate, chloride, etc, are highly soluble in the aquous solution and therefore as a result of of the high solubility they may not able to activate the copper. The only time that it is possible to have activation by these species would seem to be when very high concentration of those species exist in the system, which seems not to be applicable to the ground water composition.

In the presence of carbonate ions (CO_3^{2-}) the corrosion of copper canister can be written is the form of

$$Cu + CO_3^{2-}(a) + 2H^+(a) = CuCO_3(a) + H_2(g) \qquad \text{(III-9)}$$

where $CuCO_3(a)$ is the dissolved cupric complex and for which the change in Gibbs energy can be written as

$$\Delta G = \Delta G^0 + 2.303RT \log(f_{H_2} \times a_{CuCO_3} / a_{CO_3^{2-}} \times a_{H^+}{}^2) \qquad \text{(III-10)}$$

Rearrangement yields,

$$\log(\frac{f_{H_2} \times a_{CuCO_3}}{a_{CO_3^{2-}}}) = \frac{\Delta G - \Delta G^0}{2.303RT} - 2pH \qquad \text{(III-11)}$$

where ΔG^0 is the change in standard Gibbs energy; i.e., the change in Gibbs energy when all components of the reaction are in their standard state, with the fugacity of hydrogen, f_{H_2}, and the activity of ionic species being equal to one. At equilibrium, $\Delta G = 0$, and designating the equilibrium values of f_{H_2} and activity of other species with superscripts "e" we may write

$$P^e = \frac{f^e{}_{H_2} \times a^e{}_{CuCO_3}}{a^e{}_{CO_3^{2-}}} = 10^{-(\frac{\Delta G^0}{2.303RT} + 2pH)} \qquad \text{(III-12)}$$

where P^e is termed the "partial equilibrium quotient". We now define the partial reaction quotients, P, for non-equilibrium conditions as follows

$$P = \frac{f_{H_2} \times a_{CuCO_3}}{a_{CO_3^{2-}}} \qquad \text{(III-13)}$$

The condition for spontaneity of reaction (III-9) then becomes $P < P^e$ and immunity is indicated by $P > P^e$.

Figure (III-7) shows the CDD for Reaction (III-9) and it can be sen that at the pH value about 7.7, the Reaction (III-9) is spontaneous, but, as we mentioned earlier, due to the high solubility of carbonate ion in the aqueous system, this specie cannot activate copper at the low carbonate ion concentration in the repository.

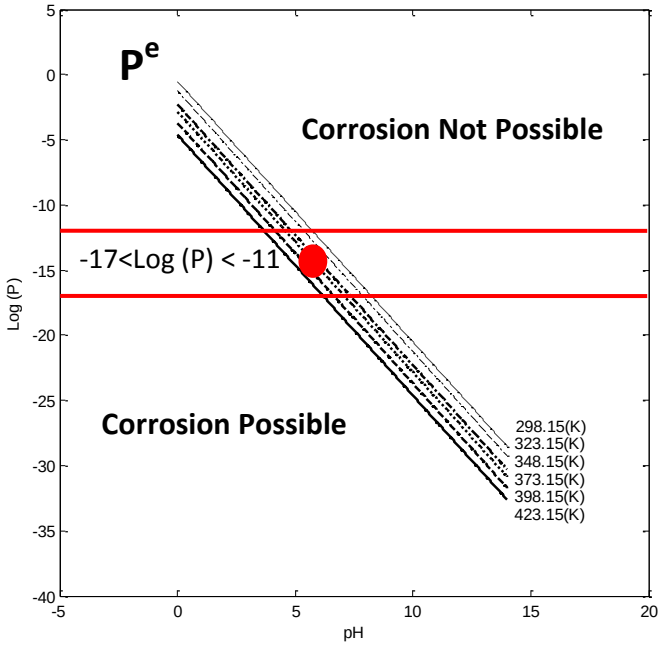

Figure-III-7: Corrosion domain diagram for copper in the presence of carbonate ions as a function of temperature (*Cu +CO₃(-2a) + 2H(+a)= CuCO₃(a) + H₂(g)*). Red circle shows the calculated Log (P) based on available measured data.

Figures (III-8) to (III-11) show CDDs for other complexing reactions that might occur in the system. As we can see, most of the species as appear to be only mild activators of copper and in some cases (e.g., ammonia) the species seem not to activate copper at all, at least thermodynamically (as reflected by a positive shift in Log(P^e). Of course, ammonia is a well-known corrodent toward copper alloys in the thermal power industry, resulting in the

extensive corrosion of copper-alloyed tubes in steam surface condensers. However, the process by which corrosion is induced by ammonia in condensers is the destruction of passivity via the formation of soluble reaction products [$Cu(NH_3)_2^{2+}$ and $Cu(NH_3)^{2+}$] not a change in immunity as reflected by a shift in Log(P^e) in the positive direction, as emphasized earlier in this report. As also noted previously, this serves to emphasize the difficulty and pitfalls one can experience when attempting to explain kinetic processes (e.g., passivity) in terms of thermodynamic concepts (e.g., immunity), Pourbaix notwithstanding.

It sould be mentioned that all of the calculated values are based upon Gibbs energy minimization of the system and the red lines in the diagrams show the ranges of the calculated values for the temperatures of interest.

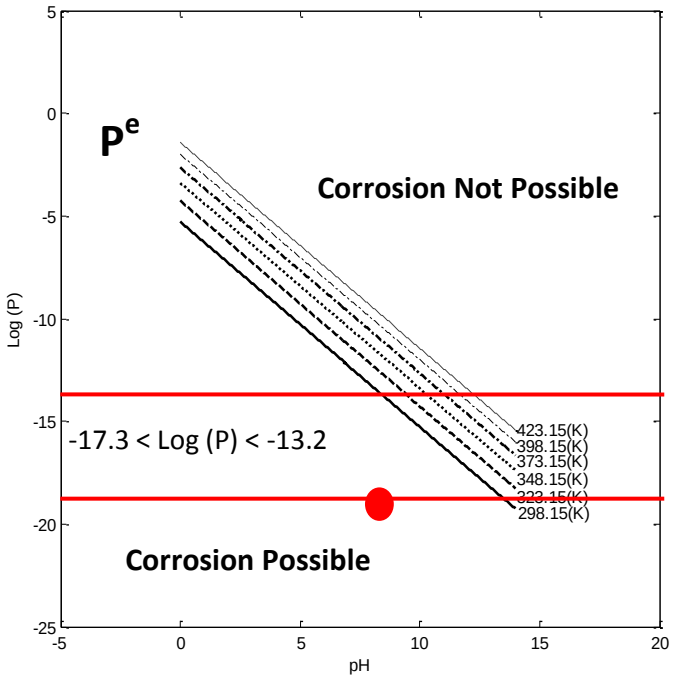

Figure-III-8: Corrosion domain diagram for copper in the presence of chloride ions as a function of temperature ($Cu + Cl(-a) + H(+a) = CuCl(a) + ½\ H_2(g)$). Red circle shows the calculated Log (P) based on available measured data.

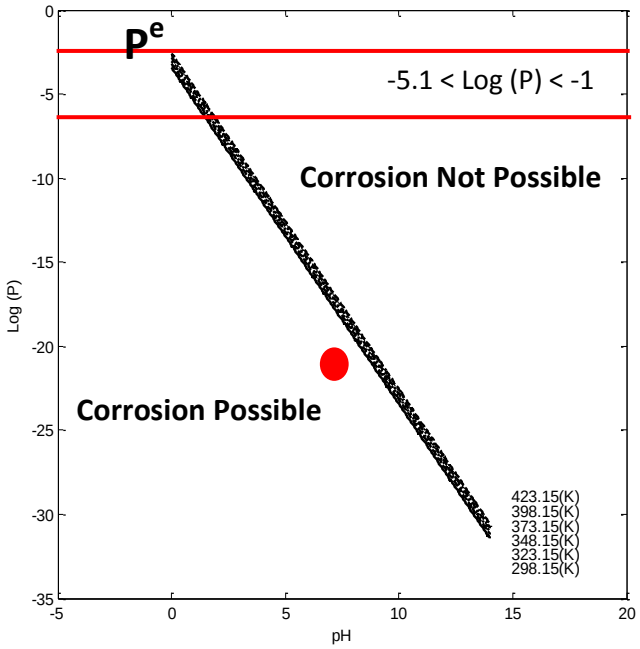

Figure-III-9: Corrosion domain diagram for copper in the presence of ammonia as a function of temperature (*$Cu + 2NH_3(a) + 2H(+a) = Cu(NH_3)_2(+2a) + H_2(g)$*). Red circle shows the calculated Log (P) based on available measured data.

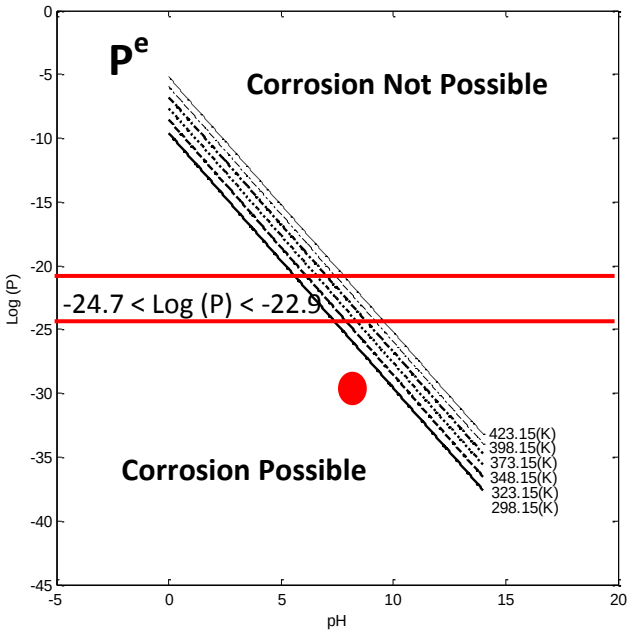

Figure-III-10: Corrosion domain diagram for copper in the presence of ammonia as a function of temperature (*Cu + NH_3(a) + 2H(+a) = Cu(NH_3)(+2a) + H_2(g))*. Red circle shows the calculated Log (P) based on available measured data.

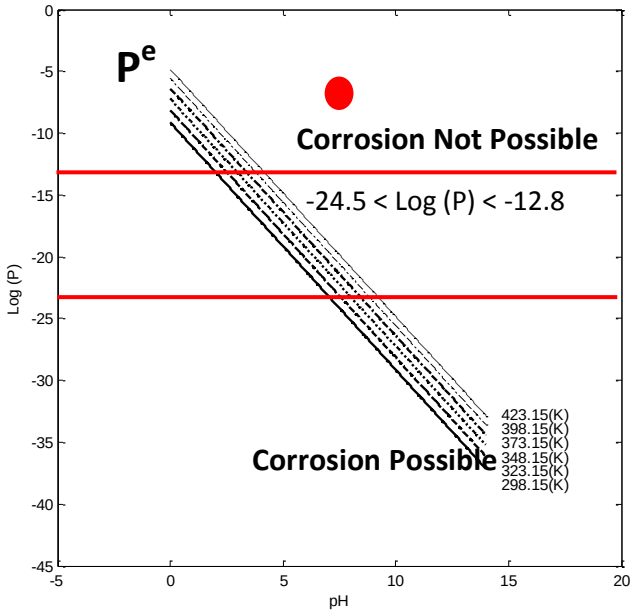

Figure-III-11: Corrosion domain diagram for copper in the presence of sulphate species as a function of temperature ($Cu + SO_4(-2a) + 2H(+a) = CuSO_4(ia) + H_2(g)$). Red circle shows the calculated Log (P) based on available measured data.

Tables (III-3) to (III-5), we summarize calculated *Log (P)* values for predicted copper corrosion in simulated groundwater in the repository. In order to develop a better understanding of whether a selected species can activate metallic copper, we also list the *Log* (P^e) value in the table. It should be noted that the calculated values are based upon the Gibbs energy minimization results for three different temperatures.

As we can see, at all temperatures, most of the available species in the system can activate copper although the activity of most of the species is very low. In some cases, e.g., ammonia ($NH_3(aq)$) based upon the calculated concentration of this species in the repository, can not activate copper thermodynamically. Interstingly, some of the polythionates family ($S_xO_6^{2-}$), with increasing the temperature, start not to activate copper. It should be mentioned that all of these calculated values are based upon the results of Gibbs energy minimization of the system purely and hence reflect thermodynamic arguments alone.

Table-III-3: Calculated *P* values for different reactions at T = 25 °C, pH=7.7

Reaction	Log (P)/Log (P^e)	Corrosion possible?
$2Cu + H_2O\ (l) = Cu_2O + H_2(g)$	-8.36/-15.63	NO
$2Cu + H_2S_2O_3(a) = Cu_2S + SO_3(-2a) + 2H(+a)$	11.99/21.54	YES
$2Cu + H_2S_2O_4(a) = Cu2S + SO_4(-2a) + 2H(+a)$	42.72/52.5	YES
$2Cu + HS_2O_3(-a) = Cu_2S + SO_3(-2a) + H(+a)$	5.83/14.45	YES
$2Cu + HS_2O_4(-a) = Cu_2S + SO_4(-2a) + H(+a)$	36.34/45.19	YES
$2Cu + S(-2a) + 2H(+a) = Cu_2S + H_2(g)$	14.5/14.39	NO
$2Cu + H_2S = Cu_2S + H_2\ (g)$	2.00/9.72	YES
$2Cu + S_2O_3(-2a) = Cu_2S + SO_3(-2a)$	N/A**	N/A
$2Cu + S_2O_4(-2a) = Cu_2S + SO_4(-2a)$	32.09/39.92	YES
$4Cu + S_2(-2a) + 2H(+a) = 2Cu_2S + H_2(g)$	14.19/27.68	YES
$4Cu + S_3O_3(-2a) = 2Cu_2S + SO_3(-2a)$	N/A	N/A
$4Cu + S_4O_6(-2a) = 2Cu_2S + SO_3(-2a) + SO_3(a)$	23.15/24.55	YES*
$6Cu + S_3(-2a) + 2H(+a) = 3Cu_2S + H_2(g)$	20.02/41.34	YES
$6Cu + S_4O_3(-2a) = 3Cu_2S + SO_3(-2a)$	N/A	N/A
$6Cu + S_5O_6(-2a) = 3Cu_2S + SO_3(-2a) + SO_3(a)$	30.37/54.16	YES
$8Cu + S_4(-2a) + 2H(+a) = 4Cu_2S + H_2\ (g)$	26.06/53.41	YES
$8Cu + S_5O_3(-2a) = 4Cu_2S + SO_3(-2a)$	N/A	N/A
$8Cu + S_6O_6(-2a) = 4Cu_2S + SO_3(-2a) + SO_3(a)$	11.29/26.56	YES
$10Cu + S_5(-2a) + 2H(+a) = 5Cu_2S + H_2\ (g)$	32.2/69.95	YES
$10Cu + S_6O_3(-2a) = 5Cu_2S + SO_3(-2a)$	N/A	N/A
$10Cu + S_7O_6(-2a) = 5Cu_2S + SO_3(-2a) + SO_3\ (a)$	9.03/34.57	YES
$12Cu + S_6(-2a) + 2H(+a) = 6Cu_2S + H_2(g)$	39.67/84.95	YES
$12Cu + S_7O_3(-2a) = 6Cu_2S + SO_3(-2a)$	N/A	N/A
$Cu + Cl(-a) + H(+a) = CuCl + 0.5H_2(g)$	-17.2/-12.97	YES
$4Cu + HS_3O_3(-a) = 2Cu_2S + SO_3(-2a) + H(+a)$	23.55/39.82	YES
$Cu + CO_3(-2a) + 2H(+a) = CuCO_3(a) + H_2(g)$	-16.2/-20.03	NO
$Cu + 2CO_3(-2a) + 2H(+a) = Cu(CO_3)_2(-2a) + H_2(g)$	-15.6/-16.6	NO
$Cu + Cl(-a) + H(+a) = CuCl(a) + ½\ H_2(g)$	-17.28/-12.97	YES
$Cu + 2Cl(-a) + 2H(+a) = CuCl_2(a) + H_2(g)$	-29.7/-26.57	YES
$Cu + 2Cl(-a) + H(+a) = CuCl_2\ (-a) + ½\ H_2(g)$	-14.31/-10.66	YES
$Cu + 3Cl(-a) + 2H(+a) = CuCl_3\ (-a) + H_2(g)$	-31.3/-19.13	YES
$Cu + 4Cl(-a) + 2H(+a) = CuCl_4\ (-2a) + H_2(g)$	-33.6/-30.81	YES
$2Cu + 4Cl(-a) + 2H(+a) = Cu_2Cl_4(-2a) + H_2(g)$	-28.2/-21.99	YES
$3Cu + 6Cl(-a) + 3H(+a) = Cu_3Cl_6(-3a) + 1.5H_2(g)$	-202.6/-193	YES
$Cu + HCO_3(-a) + 2H(+a) = Cu(HCO_3)(+a) + H_2(g)$	-24.06/-25	NO
$Cu + HPO_4(-2a) + 2H(+a) = CuHPO_4(a) + H_2(g)$	-39.19/-21.48	YES
$Cu + H_2PO_4(-a) + H(+a) = CuH_2PO_4(a) + ½\ H_2(g)$	-23.6/-14.22	YES

*: The Log P values are very close to the Log P^e values which means there is very small driving force for the corrosion reaction.

**: N/A means there is no thermodynamic information available for at least one species involved in the reaction.

Table-III-3: Calculated *P* values for different reactions at T = 25 °C, pH=7.7(cont'd)

Reaction	Log (P)/Log (P^e)	Corrosion possible?
$Cu + H_2PO_4(-a) + 2H(+a) = Cu(H_2PO_4)(+a) + H_2(g)$	-32.1/-24.44	YES
$Cu + 2HPO_4(-2a) + 2H(+a) = Cu(HPO_4)_2(-2a) + H_2(g)$	-24.7/-17.01	YES
$Cu + HPO_4(-2a) + H_2PO_4(-a) + 2H(+a) = Cu(HPO_4)(H_2PO_4)(-a) + H_2(g)$	-19.1/-19.02	YES
$Cu + HPO_4(-2a) + H_2PO_4(-a) + H(+a) = Cu(HPO_4)(H_2PO_4)(-2a) + ½ H_2(g)$	-21.1/-9.62	YES
$Cu + HS(-a) + H(+a) = Cu(HS)(a) + ½ H_2(g)$	N/A	N/A
$Cu + 2HS(-a) + H(+a) = Cu(HS)_2(-a) + ½ H_2(g)$	N/A	N/A
$Cu + NH_3(a) + 2H(+a) = Cu(NH_3)(+2a) + H_2(g)$	-24.7/-22.48	YES
$Cu + 2NH_3(a) + 2H(+a) = Cu(NH_3)_2(+2a) + H_2(g)$	0.2/-18.84	NO
$Cu + 2NH_3(a) + H(+a) = Cu(NH_3)_2(+a) + ½ H_2(g)$	12.6/-5.31	NO
$Cu + 3NH_3(a) + 2H(+a) = Cu(NH_3)_3(+2a) + H_2(g)$	24.5/-8.12	NO
$Cu + 4NH_3(a) + 2H(+a) = Cu(NH_3)_4(+2a) + H_2(g)$	48.1/-13.58	NO
$Cu + 2NO_2(-a) + 2H(+a) = Cu(NO_2)_2(a) + H_2(g)$	-26.4/-24.18	YES
$Cu + 2NO_3(-a) + 2H(+a) = Cu(NO_3)_2(ia) + H_2(g)$	-29.4/-27.21	YES
$Cu + NO_2(-a) + 2H(+a) = Cu(NO_2)(+a) + H_2(g)$	-27.1/-24.81	YES
$Cu + NO_3(-a) + 2H(+a) = Cu(NO_3)(+a) + H_2(g)$	-28.5/-26.3	YES
$Cu + 2H_2O = Cu(OH)_2(ia) + H_2(g)$	-31.8/-27.63	YES
$Cu + H_2O + H(+a) = CuOH(+a) + H_2(g)$	-30.2/-27.05	YES
$Cu + 2H_2O = Cu(OH)_2(-a) + H(+a) + ½ H_2(g)$	-22.3/-17.04	YES
$Cu + 3H_2O = Cu(OH)_3(-a) + H(+a) + H_2(g)$	-35.5/-30.39	YES
$Cu + 4H_2O = Cu(OH)_4(-2a) + 2H(+a) + H_2(g)$	-41.7/-35.59	YES
$2Cu + 2H_2O + 2H(+a) = Cu_2(OH)_2(+2a) + 2H_2(g)$	-55.1/-48.54	YES
$3Cu + 4H_2O + 2H(+a) = Cu_3(OH)_4(+2a) + 3H_2(g)$	-81.3/-70.68	YES
$2Cu + 3HS(-a) + H(+a) = Cu_2S(HS)_2(-2a) + H_2(g)$	N/A	N/A
$Cu + SO_4(-2a) + 2H(+a) = CuSO_4(ia) + H_2(g)$	-24.6/-24.55	YES
$Cu + S_2O_3(-2a) + H(+a) = Cu(S_2O_3)(-a) + ½ H_2(g)$	N/A	N/A
$2Cu + H_2S_2O_3(a) + H_2O(l) = Cu_2S + SO_4(-2a) + 2H(+a) + H_2(g)$	15.4/25.1	YES
$2Cu + H_2S_2O_4(a) + H_2(g) = Cu_2S + SO_3(-2a) + 2H(+a) + H_2O(l)$	-53.9/48.88	YES
$2Cu + HS_2O_3(-a) + H_2O(l) = Cu_2S + SO_4(-2a) + H(+a) + H_2(g)$	9.27/18.07	YES
$2Cu + HS_2O_4(-a) + H_2(g) = Cu_2S + SO_3(-2a) + H(+a) + H_2O(l)$	-47.6/41.57	YES
$2Cu + S_2O_3(-2a) + H_2O(l) = Cu_2S + SO_4(-2a) + H_2(g)$	N/A	N/A
$2Cu + S_2O_4(-2a) + H_2(g) = Cu_2S + SO_3(-2a) + H_2O(l)$	-43.3/36.3	YES
$4Cu + S_3O_3(-2a) + H_2O(l) = 2Cu_2S + SO_4(-2a) + H_2(g)$	N/A	N/A
$4Cu + S_4O_6(-2a) + H_2O(l) = 2Cu_2S + SO_4(-2a) + SO_3(a) + H_2(g)$	12.5/28.1	YES
$6Cu + S_4O_3(-2a) + H_2O(l) = 3Cu_2S + SO_4(-2a) + H_2(g)$	N/A	N/A
$6Cu + S_5O_6(-2a) + H_2O(l) = 3Cu_2S + SO_4(-2a) + SO_3(a) + H_2(g)$	33.8/57.7	YES
$8Cu + S_5O_3(-2a) + H_2O(l) = 4Cu_2S + SO_4(-2a) + H_2(g)$	N/A	N/A
$8Cu + S_6O_6(-2a) + H_2O(l) = 4Cu_2S + SO_4(-2a) + SO_3(a) + H_2(g)$	0.66/30.19	YES
$10Cu + S_6O_3(-2a) + H_2O(l) = 5Cu_2S + SO_4(-2a) + H_2(g)$	N/A	N/A
$10Cu + S_7O_6(-2a) + H_2O(l) = 5Cu_2S + SO_4(-2a) + SO_3(a) + H_2(g)$	-1.59/38.19	YES
$12Cu + S_7O_3(-2a) + H_2O(l) = 6Cu_2S + SO_4(-2a) + H_2(g)$	N/A	N/A
$4Cu + HS_3O_3(-a) + H_2O(l) = 2Cu_2S + SO_4(-2a) + H(+a) + H_2(g)$	26.9/43.44	YES

Table-III-4: Calculated P values for different reactions at T = 75 °C, pH=7.7

Reaction	Log (P)/Log (P^e)	Corrosion possible?
$2Cu + H_2O\ (l) = Cu_2O + H_2(g)$	-5.23/-12.75	NO
$2Cu + H_2S_2O_3(a) = Cu_2S + SO_3(-2a) + 2H(+a)$	14.88/19.21	YES
$2Cu + H_2S_2O_4(a) = Cu2S + SO_4(-2a) + 2H(+a)$	41.35/45.88	YES
$2Cu + HS_2O_3(-a) = Cu_2S + SO_3(-2a) + H(+a)$	7.49/12.54	YES
$2Cu + HS_2O_4(-a) = Cu_2S + SO_4(-2a) + H(+a)$	33.7/39.02	YES
$2Cu + S(-2a) + 2H(+a) = Cu_2S + H_2(g)$	8.9/11.72	YES
$2Cu + H_2S = Cu_2S + H_2\ (g)$	2.96/8.68	YES
$2Cu + S_2O_3(-2a) = Cu_2S + SO_3(-2a)$	N/A	N/A
$2Cu + S_2O_4(-2a) = Cu_2S + SO_4(-2a)$	28.09/34.01	YES
$4Cu + S_2(-2a) + 2H(+a) = 2Cu_2S + H_2(g)$	10.29/24.58	YES
$4Cu + S_3O_3(-2a) = 2Cu_2S + SO_3(-2a)$	N/A	N/A
$4Cu + S_4O_6(-2a) = 2Cu_2S + SO_3(-2a) + SO_3(a)$	25.41/19.35	NO
$6Cu + S_3(-2a) + 2H(+a) = 3Cu_2S + H_2(g)$	16.18/35.44	YES
$6Cu + S_4O_3(-2a) = 3Cu_2S + SO_3(-2a)$	N/A	N/A
$6Cu + S_5O_6(-2a) = 3Cu_2S + SO_3(-2a) + SO_3(a)$	27.96/45.81	YES
$8Cu + S_4(-2a) + 2H(+a) = 4Cu_2S + H_2\ (g)$	22.2/45.5	YES
$8Cu + S_5O_3(-2a) = 4Cu_2S + SO_3(-2a)$	N/A	N/A
$8Cu + S_6O_6(-2a) = 4Cu_2S + SO_3(-2a) + SO_3(a)$	17.1/21.23	YES
$10Cu + S_5(-2a) + 2H(+a) = 5Cu_2S + H_2\ (g)$	28.5/59.76	YES
$10Cu + S_6O_3(-2a) = 5Cu_2S + SO_3(-2a)$	N/A	N/A
$10Cu + S_7O_6(-2a) = 5Cu_2S + SO_3(-2a) + SO_3\ (a)$	16.14/28.24	YES
$12Cu + S_6(-2a) + 2H(+a) = 6Cu_2S + H_2(g)$	35.2/73	YES
$12Cu + S_7O_3(-2a) = 6Cu_2S + SO_3(-2a)$	N/A	N/A
$Cu + Cl(-a) + H(+a) = CuCl(a) + 0.5H_2(g)$	-16.3/-11.09	YES
$4Cu + HS_3O_3(-a) = 2Cu_2S + SO_3(-2a) + H(+a)$	26.68/38.74	YES
$Cu + CO_3(-2a) + 2H(+a) = CuCO_3(a) + H_2(g)$	-15.2/-18.24	YES
$Cu + 2CO_3(-2a) + 2H(+a) = Cu(CO_3)_2(-2a) + H_2(g)$	-15.32/-13.84	YES
$Cu + Cl(-a) + H(+a) = CuCl(a) + ½\ H_2(g)$	-16.38/-11.09	YES
$Cu + 2Cl(-a) + 2H(+a) = CuCl_2(a) + H_2(g)$	-30.1/-24.2	YES
$Cu + 2Cl(-a) + H(+a) = CuCl_2\ (-a) + ½\ H_2(g)$	-14.1/-9.35	YES
$Cu + 3Cl(-a) + 2H(+a) = CuCl_3\ (-a) + H_2(g)$	-31.8/-17.45	YES
$Cu + 4Cl(-a) + 2H(+a) = CuCl_4\ (-2a) + H_2(g)$	-34.7/-28.34	YES
$2Cu + 4Cl(-a) + 2H(+a) = Cu_2Cl_4(-2a) + H_2(g)$	-27.4/-19.71	YES
$3Cu + 6Cl(-a) + 3H(+a) = Cu_3Cl_6(-3a) + 1.5H_2(g)$	-179.3/-168	YES
$Cu + HCO_3(-a) + 2H(+a) = Cu(HCO_3)(+a) + H_2(g)$	-24.5/-23.03	YES
$Cu + HPO_4(-2a) + 2H(+a) = CuHPO_4(a) + H_2(g)$	-31.4/-19.61	YES
$Cu + H_2PO_4^- + H^+ = CuH_2PO_4(a) + ½\ H_2$	-18.2/-12.58	YES

Table-III-4: Calculated *P* values for different reactions at T = 75 °C, pH=7.7(cont'd)

Reaction	Log (P)/Log (P^e)	Corrosion possible?
$Cu + H_2PO_4(-a) + 2H(+a) = Cu(H_2PO_4)(+a) + H_2(g)$	-26.2/-22.96	YES
$Cu + 2HPO_4(-2a) + 2H(+a) = Cu(HPO_4)_2(-2a) + H_2(g)$	-20/-17.14	YES
$Cu + HPO_4(-2a) + H_2PO_4(-a) + 2H(+a) = Cu(HPO_4)(H_2PO_4)(-a) + H_2(g)$	-13.7/-18.7	NO
$Cu + HPO_4(-2a) + H_2PO_4(-a) + H(+a) = Cu(HPO_4)(H_2PO_4)(-2a) + ½\ H_2(g)$	-17.5/-7.99	YES
$Cu + HS(-a) + H(+a) = Cu(HS)(a) + ½\ H_2(g)$	N/A	N/A
$Cu + 2HS(-a) + H(+a) = Cu(HS)_2(-a) + ½\ H_2(g)$	N/A	N/A
$Cu + NH_3(a) + 2H(+a) = Cu(NH_3)(+2a) + H_2(g)$	-25.9/-21.38	YES
$Cu + 2NH_3(a) + 2H(+a) = Cu(NH_3)_2(+2a) + H_2(g)$	-6.9/-18.41	NO
$Cu + 2NH_3(a) + H(+a) = Cu(NH_3)_2(+a) + ½\ H_2(g)$	7.1/-5.07	NO
$Cu + 3NH_3(a) + 2H(+a) = Cu(NH_3)_3(+2a) + H_2(g)$	11.4/-8.36	NO
$Cu + 4NH_3(a) + 2H(+a) = Cu(NH_3)_4(+2a) + H_2(g)$	29.1/-14.46	NO
$Cu + 2NO_2(-a) + 2H(+a) = Cu(NO_2)_2(a) + H_2(g)$	-27.2/-22.51	YES
$Cu + 2NO_3(-a) + 2H(+a) = Cu(NO_3)_2(ia) + H_2(g)$	-30.1/-25.55	YES
$Cu + NO_2(-a) + 2H(+a) = Cu(NO_2)(+a) + H_2(g)$	-27.8/-23.1	YES
$Cu + NO_3(-a) + 2H(+a) = Cu(NO_3)(+a) + H_2(g)$	-29.3/-24.72	YES
$Cu + 2H_2O = Cu(OH)_2(ia) + H_2(g)$	-27.1/-23.66	YES
$Cu + H_2O + H(+a) = CuOH(+a) + H_2(g)$	-28.1/-24.44	YES
$Cu + 2H_2O = Cu(OH)_2(-a) + H(+a) + ½\ H_2(g)$	-18.1/-15.95	YES
$Cu + 3H_2O = Cu(OH)_3(-a) + H(+a) + H_2(g)$	-28.6/-26.3	YES
$Cu + 4H_2O = Cu(OH)_4(-2a) + 2H(+a) + H_2(g)$	-33.2/-31.72	YES
$2Cu + 2H_2O + 2H(+a) = Cu_2(OH)_2(+2a) + 2H_2(g)$	-51.2/-43.36	YES
$3Cu + 4H_2O + 2H(+a) = Cu_3(OH)_4(+2a) + 3H_2(g)$	-74.2/-63.12	YES
$2Cu + 3HS(-a) + H(+a) = Cu_2S(HS)_2(-2a) + H_2(g)$	N/A	N/A
$Cu + SO_4(-2a) + 2H(+a) = CuSO_4(ia) + H_2(g)$	-21.1/-22.64	NO
$Cu + S_2O_3(-2a) + H(+a) = Cu(S_2O_3)(-a) + ½\ H_2(g)$	N/A	N/A
$2Cu + H_2S_2O_3(a) + H_2O(l) = Cu_2S + SO_4(-2a) + 2H(+a) + H_2(g)$	18.7/23.1	YES
$2Cu + H_2S_2O_4(a) + H_2(g) = Cu_2S + SO_3(-2a) + 2H(+a) + H_2O(l)$	-53.3/41.9	YES
$2Cu + HS_2O_3(-a) + H2O(l) = Cu_2S + SO_4(-2a) + H(+a) + H_2(g)$	11.3/16.4	YES
$2Cu + HS_2O_4(-a) + H_2(g) = Cu_2S + SO_3(-2a) + H(+a) + H_2O(l)$	-45.7/33.1	YES
$2Cu + S_2O_3(-2a) + H_2O(l) = Cu_2S + SO_4(-2a) + H_2(g)$	N/A	N/A
$2Cu + S_2O_4(-2a) + H_2(g) = Cu_2S + SO_3(-2a) + H_2O(l)$	-40.1/30.1	YES
$4Cu + S_3O_3(-2a) + H_2O(l) = 2Cu_2S + SO_4(-2a) + H_2(g)$	N/A	N/A
$4Cu + S_4O_6(-2a) + H_2O(l) = 2Cu_2S + SO_4(-2a) + SO_3(a) + H_2(g)$	11.6/23.26	YES
$6Cu + S_4O_3(-2a) + H_2O(l) = 3Cu_2S + SO_4(-2a) + H_2(g)$	N/A	N/A
$6Cu + S_5O_6(-2a) + H_2O(l) = 3Cu_2S + SO_4(-2a) + SO_3(a) + H_2(g)$	31.7/49.7	YES
$8Cu + S_5O_3(-2a) + H_2O(l) = 4Cu_2S + SO_4(-2a) + H_2(g)$	N/A	N/A
$8Cu + S_6O_6(-2a) + H_2O(l) = 4Cu_2S + SO_4(-2a) + SO_3(a) + H_2(g)$	3.34/25.13	YES
$10Cu + S_6O_3(-2a) + H_2O(l) = 5Cu_2S + SO_4(-2a) + H_2(g)$	N/A	N/A
$10Cu + S_7O_6(-2a) + H_2O(l) = 5Cu_2S + SO_4(-2a) + SO_3(a) + H_2(g)$	2.38/32.14	YES
$12Cu + S_7O_3(-2a) + H_2O(l) = 6Cu_2S + SO_4(-2a) + H_2(g)$	N/A	N/A
$4Cu + HS_3O_3(-a) + H_2O(l) = 2Cu_2S + SO_4(-2a) + H(+a) + H_2(g)$	30.5/42.6	YES

Table-III-5: Calculated P values for different reactions at T = 150°C, pH=7.7

Reaction	Log (P)/Log (P^e)	Corrosion possible?
$2Cu + H_2O\ (l) = Cu_2O + H_2(g)$	-2.09/-9.75	NO
$2Cu + H_2S_2O_3(a) = Cu_2S + SO_3(-2a) + 2H(+a)$	12.63/16.22	YES
$2Cu + H_2S_2O_4(a) = Cu2S + SO_4(-2a) + 2H(+a)$	34.60/38.36	YES
$2Cu + HS_2O_3(-a) = Cu_2S + SO_3(-2a) + H(+a)$	6.45/10.16	YES
$2Cu + HS_2O_4(-a) = Cu_2S + SO_4(-2a) + H(+a)$	28.27/32.14	YES
$2Cu + S(-2a) + 2H(+a) = Cu_2S + H_2(g)$	8.00/9.36	YES
$2Cu + H_2S = Cu_2S + H_2\ (g)$	3.7/7.44	YES
$2Cu + S_2O_3(-2a) = Cu_2S + SO_3(-2a)$	N/A	N/A
$2Cu + S_2O_4(-2a) = Cu_2S + SO_4(-2a)$	23.81/27.75	YES
$4Cu + S_2(-2a) + 2H(+a) = 2Cu_2S + H_2(g)$	11.26/16.85	YES
$4Cu + S_3O_3(-2a) = 2Cu_2S + SO_3(-2a)$	-13.55/-21.88	YES
$4Cu + S_4O_6(-2a) = 2Cu_2S + SO_3(-2a) + SO_3(a)$	27.34/13.75	NO
$6Cu + S_3(-2a) + 2H(+a) = 3Cu_2S + H_2(g)$	17.15/29.87	YES
$6Cu + S_4O_3(-2a) = 3Cu_2S + SO_3(-2a)$	N/A	N/A
$6Cu + S_5O_6(-2a) = 3Cu_2S + SO_3(-2a) + SO_3(a)$	25.49/37.00	YES
$8Cu + S_4(-2a) + 2H(+a) = 4Cu_2S + H_2\ (g)$	23.2/37.86	YES
$8Cu + S_5O_3(-2a) = 4Cu_2S + SO_3(-2a)$	N/A	N/A
$8Cu + S_6O_6(-2a) = 4Cu_2S + SO_3(-2a) + SO_3(a)$	22.64/15.13	NO
$10Cu + S_5(-2a) + 2H(+a) = 5Cu_2S + H_2\ (g)$	29.42/49.78	YES
$10Cu + S_6O_3(-2a) = 5Cu_2S + SO_3(-2a)$	N/A	N/A
$10Cu + S_7O_6(-2a) = 5Cu_2S + SO_3(-2a) + SO_3\ (a)$	23/21.04	NO
$12Cu + S_6(-2a) + 2H(+a) = 6Cu_2S + H_2(g)$	36.4/61.22	YES
$12Cu + S_7O_3(-2a) = 6Cu_2S + SO_3(-2a)$	N/A	N/A
$Cu + Cl(-a) + H(+a) = CuCl + 0.5H_2(g)$	-13.2/-9.13	YES
$4Cu + HS_3O_3(-a) = 2Cu_2S + SO_3(-2a) + H(+a)$	27.3/40.05	YES
$Cu + CO_3(-2a) + 2H(+a) = CuCO_3(a) + H_2(g)$	-11.2/-15.92	YES
$Cu + 2CO_3(-2a) + 2H(+a) = Cu(CO_3)_2(-2a) + H_2(g)$	-10.8/-10.45	YES
$Cu + Cl(-a) + H(+a) = CuCl(a) + ½\ H_2(g)$	-13.2/-9.13	YES
$Cu + 2Cl(-a) + 2H(+a) = CuCl_2(a) + H_2(g)$	-25.5/-20.82	YES
$Cu + 2Cl(-a) + H(+a) = CuCl_2\ (-a) + ½\ H_2(g)$	-11.2/-8.03	YES
$Cu + 3Cl(-a) + 2H(+a) = CuCl_3\ (-a) + H_2(g)$	-27.3/-15.53	YES
$Cu + 4Cl(-a) + 2H(+a) = CuCl_4\ (-2a) + H_2(g)$	-30.4/-25.4	YES
$2Cu + 4Cl(-a) + 2H(+a) = Cu_2Cl_4(-2a) + H_2(g)$	-22.6/-17.02	YES
$3Cu + 6Cl(-a) + 3H(+a) = Cu_3Cl_6(-3a) + 1.5H_2(g)$	-148.9/-140	YES
$Cu + HCO_3(-a) + 2H(+a) = Cu(HCO_3)(+a) + H_2(g)$	-21.4/-20.61	YES
$Cu + HPO_4(-2a) + 2H(+a) = CuHPO_4(a) + H_2(g)$	-21.7/-17.18	YES
$Cu + H_2PO_4(-a) + H(+a) = CuH_2PO_4(a) + ½\ H_2(g)$	-11.54/-10.82	YES

Table-III-5: Calculated *P* values for different reactions at T = 150°C, pH=7.7(cont'd)

Reaction	Log (P)/Log (P^e)	Corrosion possible?
$Cu + H_2PO_4(-a) + 2H(+a) = Cu(H_2PO_4)(+a) + H_2(g)$	-18.4/-21.01	NO
$Cu + 2HPO_4(-2a) + 2H(+a) = Cu(HPO_4)_2(-2a) + H_2(g)$	-13.3/-18.35	No
$Cu + HPO_4(-2a) + H_2PO_4(-a) + 2H(+a) = Cu(HPO_4)(H_2PO_4)(-a) + H_2(g)$	-7/-19.04	NO
$Cu + HPO_4(-2a) + H_2PO_4(-a) + H(+a) = Cu(HPO_4)(H_2PO_4)(-2a) + ½\ H_2(g)$	-12.1/-5.46	YES
$Cu + HS(-a) + H(+a) = Cu(HS)(a) + ½\ H_2(g)$	N/A	N/A
$Cu + 2HS(-a) + H(+a) = Cu(HS)_2(-a) + ½\ H_2(g)$	N/A	N/A
$Cu + NH_3(a) + 2H(+a) = Cu(NH_3)(+2a) + H_2(g)$	-23/-20.02	YES
$Cu + 2NH_3(a) + 2H(+a) = Cu(NH_3)_2(+2a) + H_2(g)$	-5.03/-17.98	NO
$Cu + 2NH_3(a) + H(+a) = Cu(NH_3)_2(+a) + ½\ H_2(g)$	8.2/-5.04	NO
$Cu + 3NH_3(a) + 2H(+a) = Cu(NH_3)_3(+2a) + H_2(g)$	12.2/-8.88	NO
$Cu + 4NH_3(a) + 2H(+a) = Cu(NH_3)_4(+2a) + H_2(g)$	28.7/-15.88	NO
$Cu + 2NO_2(-a) + 2H(+a) = Cu(NO_2)_2(a) + H_2(g)$	-23.9/-19.92	YES
$Cu + 2NO_3(-a) + 2H(+a) = Cu(NO_3)_2(ia) + H_2(g)$	-26.5/-23.72	YES
$Cu + NO_2(-a) + 2H(+a) = Cu(NO_2)(+a) + H_2(g)$	-24.3/-21.02	YES
$Cu + NO_3(-a) + 2H(+a) = Cu(NO_3)(+a) + H_2(g)$	-25.9/-22.65	YES
$Cu + 2H_2O = Cu(OH)_2(ia) + H_2(g)$	-23.2/-19.06	YES
$Cu + H_2O + H(+a) = CuOH(+a) + H_2(g)$	-23.8/-21.39	YES
$Cu + 2H_2O = Cu(OH)_2(-a) + H(+a) + ½\ H_2(g)$	-17/-16.77	YES
$Cu + 3H_2O = Cu(OH)_3(-a) + H(+a) + H_2(g)$	-25/-23.25	YES
$Cu + 4H_2O = Cu(OH)_4(-2a) + 2H(+a) + H_2(g)$	-30.3/-29.93	YES
$2Cu + 2H_2O + 2H(+a) = Cu_2(OH)_2(+2a) + 2H_2(g)$	-44.1/-37.76	YES
$3Cu + 4H_2O + 2H(+a) = Cu_3(OH)_4(+2a) + 3H_2(g)$	-64.5/-55.18	YES
$2Cu + 3HS(-a) + H(+a) = Cu_2S(HS)_2(-2a) + H_2(g)$	N/A	N/A
$Cu + SO_4(-2a) + 2H(+a) = CuSO_4(ia) + H_2(g)$	-12.8/-20.24	NO
$Cu + S_2O_3(-2a) + H(+a) = Cu(S_2O_3)(-a) + ½\ H_2(g)$	N/A	N/A
$2Cu + H_2S_2O_3(a) + H_2O(l) = Cu_2S + SO_4(-2a) + 2H(+a) + H_2(g)$	16.2/20.38	YES
$2Cu + H_2S_2O_4(a) + H_2(g) = Cu_2S + SO_3(-2a) + 2H(+a) + H_2O(l)$	-57.3/34.2	YES
$2Cu + HS_2O_3(-a) + H2O(l) = Cu_2S + SO_4(-2a) + H(+a) + H_2(g)$	10.6/14.32	YES
$2Cu + HS_2O_4(-a) + H_2(g) = Cu_2S + SO_3(-2a) + H(+a) + H_2O(l)$	-51.1/27.98	YES
$2Cu + S_2O_3(-2a) + H_2O(l) = Cu_2S + SO_4(-2a) + H_2(g)$	N/A	N/A
$2Cu + S_2O_4(-2a) + H_2(g) = Cu_2S + SO_3(-2a) + H_2O(l)$	-46.5/23.59	YES
$4Cu + S_3O_3(-2a) + H_2O(l) = 2Cu_2S + SO_4(-2a) + H_2(g)$	N/A	N/A
$4Cu + S_4O_6(-2a) + H_2O(l) = 2Cu_2S + SO_4(-2a) + SO_3(a) + H_2(g)$	10.7/17.91	YES
$6Cu + S_4O_3(-2a) + H_2O(l) = 3Cu_2S + SO_4(-2a) + H_2(g)$	N/A	N/A
$6Cu + S_5O_6(-2a) + H_2O(l) = 3Cu_2S + SO_4(-2a) + SO_3(a) + H_2(g)$	29.6/41.1	YES
$8Cu + S_5O_3(-2a) + H_2O(l) = 4Cu_2S + SO_4(-2a) + H_2(g)$	N/A	N/A
$8Cu + S_6O_6(-2a) + H_2O(l) = 4Cu_2S + SO_4(-2a) + SO_3(a) + H_2(g)$	6.1/19.2	YES
$10Cu + S_6O_3(-2a) + H_2O(l) = 5Cu_2S + SO_4(-2a) + H_2(g)$	N/A	N/A
$10Cu + S_7O_6(-2a) + H_2O(l) = 5Cu_2S + SO_4(-2a) + SO_3(a) + H_2(g)$	6.36/25.2	YES
$12Cu + S_7O_3(-2a) + H_2O(l) = 6Cu_2S + SO_4(-2a) + H_2(g)$	N/A	N/A
$4Cu + HS_3O_3(-a) + H_2O(l) = 2Cu_2S + SO_4(-2a) + H(+a) + H_2(g)$	31.4/44.2	YES

References:

1. D. D. Macdonald and S. Sharifi-Asl, *SSM-2011:09, Swedish Radiation Safety Authority* (2011).

III-3: Continued Development of the Mixed Potential Model.

*One of the four pillars of c*orrosion science is the conservation of charge (CoC), a natural law, which states that charge must be conserved in a system or if charge of one sign is created an equal amount of charge of the opposite sign must also be created. For an electrochemical interface, the CoC implies that the sum of the partial currents on a surface must be equal to zero. Violation of this principle, would lead to a macroscopic separation of charge and Poisson's equation predicts that that would be accompanied by a powerful electrostatic restoring force that would lead to charge recombination. Thus, consider a metal surface upon which a variety of redox reactions occur, with each being represented by

$$R \xleftrightarrow{k_{R/O}} O + ze^{-} \qquad \text{(III-14)}$$

Suppose that each reaction, for whatever reason, occurs uniformly upon a specific area, A_i. The CoC then states that

$$\sum_{i=1}^{N} A_i i_{R/o,i} = 0 \qquad \text{(III-15)}$$

where $i_{R/O}$ is the (uniform) current density for the redox reaction. Because the rate and the direction of Reaction (III-14) is potential dependent, the potential that the metal will adopt is such that some of the N redox rections will proceed in the forward (oxidation) direction while others will proceed in the reverse (reduction) direction, so that Equation (III-15) holds. This relationship defines the "redox potential" [1]. Now, suppose that one of the reactions involves oxidation of the substrate and occurs uniformly upon an area A_a. Equation (III-15) is modified accordingly to read:

$$A_a i_a + \sum_{i=1}^{N} A_i i_{R/o,i} = 0 \qquad \text{(III-16)}$$

where i_a is the anodic current density for the oxidation of the metal. The potential at which this condition is satisfied in known as the "electrochemical corrosion potential (ECP)" [2]. Thus, the difference between the two cases is the occurrence of the metal oxidation reaction. If the metal is inert over the potential range of interest (e.g., *Pt* and *Au*) at potentials well below that at which the oxygen equilibrium occurs, then i_a is zero and Equation (III-16) collapses into Equation (III-15). Thus, the redox potential is <u>always</u> measured on an inert substrate, whereas the corrosion potential is always measured upon the (reactive) metal of interest. It is important that these definitions and the differences between them be recognized, as the redox potential is often calculated using the Nernst equation, particularly in the geochemical literature. This is valid only when a single redox couple exists in the system and it is at equilibrium, as discussed above. In that case, the potential is more correctly referred to as an equilibrium potential. For example, in the proposed Swedish

repository under anoxic conditions, the concentration of H_2 is 2×10^{-8} M (close to the detection limit) [13] and that of H^+ at ambient temperature is $10^{-7.5}$M [3] with the result that the hydrogen electrode reaction (*HER*), $2H^+ + 2e^- = H_2$ dominate the redox properties and the redox potential may be reasonably estimated using the Nernst equation for the *HER*. However, this is not the case for the oxic period, when oxygen is present or when O_2 and H_2O_2 are produced by the radiolysis of water. In this instance, two additional reactions must be considered; the oxygen electrode reaction (*OER*, $O_2 + 4H^+ + 4e- = 2H_2O$) and the hydrogen peroxide electrode reaction (*HPER*, $H_2O_2 + 2H^+ 2e^- = 2H_2O$), which along with the *HER* gives three redox reactions in the system. No simple, Nernst-like equation exists for estimating the redox potential of the corrosion potential, as is evident from the literature [1, 2].

We now suppose that the redox and metal dissolution reactions occur uniformly across the entire surface, in which case Equations (III-15) and (III-16) become

$$\sum_{i=1}^{N} i_{R/o,i} = 0 \qquad \text{(III-17)}$$

and

$$i_a + \sum_{i=1}^{N} i_{R/o,i} = 0 \qquad \text{(III-18)}$$

That is, the CoC reduces to being that the sums of the current densities at the surfaces must be zero.

Cathodic Processes

The current density for a redox reaction occurring in contact with a bulk electrolyte under well-defined hydrodynamic and mass transport conditions is conveniently described by the generalized Butler-Volmer equation:

$$i_{R/O,i} = \frac{e^{\eta_i / b_{a,i}} - e^{-\eta_i / b_{c,i}}}{\frac{1}{i_{0,R/O,i}} + \frac{e^{\eta_i / b_{a,i}}}{i_{l,f,R/O,i}} - \frac{e^{-\eta_i / b_{c,i}}}{i_{l,r,R/O,i}}} \qquad \text{(III-19)}$$

where $i_{0,R/O,i}$ is the exchange current density (the current at the equilibrium potential, $E^e_{R/O},i$, as given by the Nernst equation in terms of the local activities of the redox species, $i_{l,f,R/O,i}$ and $i_{l,r,R/O,i}$ are the limiting current densities for Reaction (III-14) in the forward and reverse directions, respectively, $\eta = E - E^e_{R/O,i}$ and $b_{a,i}$ and $b_{c,i}$ are the anodic and cathodic Tafel constants. One equation of the form of Equation (III-19) is required for each redox couple in the system, including:

$$1/2H_2 + OH^- \Leftrightarrow H_2O + e^- \quad \text{(III-20}$$

$$4OH^- \Leftrightarrow O_2 + 2H_2O + 4e^- \quad \text{(III-21)}$$

$$2OH^- \Leftrightarrow H_2O_2 + 2e^- \quad \text{(III-22)}$$

$$Fe^{2+} \Leftrightarrow Fe^{3+} + e^- \quad \text{(III-23)}$$

$$Cu^+ \Leftrightarrow Cu^{2+} + e^- \quad \text{(III-24)}$$

$$xS^{2-} \Leftrightarrow S_x^{2-} + 2(x-1)e^- \quad \text{(III-25)}$$

for example. A general principle, established in our prediction of corrosion potentials in water-cooled nuclear reactors, is that the contribution that any species makes to establishing the redox potential or the corrosion potential is proportional to its concentration. This is, because at very low concentrations, the rates of the cathodic partial reactions are controlled by the rates of mass transport of the species to the metal surface. This rate is proportional to the species concentrations. We list the concentrations of the species that are reported by KBS-3 to exist in the repository in Table III-6. Of the species listed only Fe^{2+}, HS^-, and possibly NO_3^- have redox properties (i.e., they can participate in reduction/oxidation reactions, but their conjugate species are often present at only very low concentration [3]. Our Gibbs Energy Minimization (GEMs) studies reported in Phase I of this project indicate that many more species exist, at least as indicated thermodynamically, but, generally, the species are at very low concentrations and are judged as being unimportant in establishing the redox potential or the corrosion potential. Note that the "E_h" value listed in Table III-6 is actually the redox potential that has been estimated using the Nernst equation, with the tacit assumption that only a single redox couple exists in the system. Thus, from this analysis, we conclude that the only important redox reactions are Reactions (III-20) - (III-22) and possibly Reactions (III-23) – (III-25) above. In the absence of radiolysis, and under anoxic conditions, only Reactions (III-20) and (III-23) – (III-25) are considered to be significant and then Reactions (III-23) – (III-25) are considered as being only marginally so. Another set of chemical speciation data for the Forsmark repository are listed in Table (III-7). The data between the two tables are nor entirely in agreement, probably reflecting an inherent difficulty in measuring the data as well as an inherent variability in the properties of the system.

Table III-6: Concentrations of species in and properties of the groundwater environment in the proposed Forsmark HLNW repository in Sweden [3].

Constituent		At closure	After resaturation (<100y after closure)	10,000 years into the future
pH		6-8	7.0-7.9	7-9
E_h	mV	0 to -400	-200 to -250	-200 to -300
Na^+	mg/L mol/L	300-2,000 $(1.3\text{-}8.7).10^{-2}$	1,700-275 $(7.4\text{-}1.2).10^{-2}$	100-1,000 $(0.4\text{-}4.3).10^{-2}$
K^+	mg/L mol/L	2-13 $(0.5\text{-}3.3).10^{-4}$	13-2 $(3.3\text{-}0.5).10^{-4}$	2-10 $(0.5\text{-}2.6).10^{-4}$
Ca^{2+}	mg/L mol/L	150-1,650 $(0.4\text{-}4.1).10^{-2}$	1,650-142 $(4.1\text{-}0.4).10^{-2}$	20-1,000 $(0.05\text{-}2.5).10^{-2}$
Mg^{2+}	mg/L mol/L	17-110 $(0.7\text{-}4.5).10^{-3}$	110-17 $(4.5\text{-}0.7).10^{-3}$	4-100 $(0.2\text{-}4.1).10^{-3}$
HCO_3^-	mg/L mol/L	50-300 $(0.8\text{-}4.9).10^{-3}$	47-278 $(0.8\text{-}4.6).10^{-3}$	20-40 $(0.3\text{-}0.7).10^{-3}$
Cl^-	mg/L mol/L	500-5,000 $(0.1\text{-}1.4).10^{-1}$	5,500-555 $(1.6\text{-}0.2).10^{-1}$	200-5,000 $(0.06\text{-}1.4).10^{-1}$
SO_4^{2-}	mg/L mol/L	40-400 $(0.4\text{-}4.2).10^{-3}$	370-49 $(3.9\text{-}0.5).10^{-3}$	1-400 $(0.01\text{-}4.2).10^{-3}$
HS^-	mg/L mol/L	0-10 $(0\text{-}0.3).10^{-3}$	<0.01-0 $<0.3.10^{-6}\text{-}0$	0-1 $(0\text{-}0.3).10^{-4}$

Table III-7: Concentrations of chemical species in the Forsmark repository [3].

Constituent		At closure, infiltration into unsaturated bentonite	After closure and saturation (up to 100 years)	10,000 years into the future
pH		6-8	7-8	7-9
Redox	mV	Oxic to -400	-150 to -308	-200 to -300
DIC[a)]	mol/L	$(0.1\text{-}16.4).10^{-3}$	$(0.5\text{-}10).10^{-3}$	$(0.1\text{-}7).10^{-3}$
Cl-	mol/L	$(0.1\text{-}6.2).10^{-1}$	$(0.2\text{-}1.6).10^{-1}$	$(0.06\text{-}4.2).10^{-1}$
Na^+	mol/L	$(0.1\text{-}2.8).10^{-1}$	$(0.02\text{-}9.1).10^{-2}$	$(0.04\text{-}2.2).10^{-1}$
Ca^{2+}	mol/L	$(0.03\text{-}1.5).10^{-1}$	$(0.03\text{-}0.2).10^{-1}$	$(0.005\text{-}1.0).10^{-1}$
Mg^{2+}	mol/L	$(0.4\text{-}1.0).10^{-2}$	$(0.4\text{-}1.0).10^{-2}$	$(0.004\text{-}1.0).10^{-2}$
K^+	mol/L	$(1.3\text{-}7.7).10^{-4}$	$(1.3\text{-}7.7).10^{-4}$	$(0.5\text{-}5.1).10^{-4}$
SO_4^{2-}	mol/L	$(0\text{-}6.3).10^{-3}$	$(0\text{-}5.8).10^{-3}$	$(0\text{-}5.2).10^{-3}$
HS^-	mol/L	$(0\text{-}3.0).10^{-4}$	$(0\text{-}3.0).10^{-4}$	$(0\text{-}0.9).10^{-4}$
NH_4^+	mol/L	$< 5.5.10^{-6}$, if marine $< 1.7.10^{-4}$	$(0.03\text{-}1.7).10^{-4}$	$< 0.6.10^{-4}$
$CH_4(g)$	mol/L	$< 4.5.10^{-6}$, If saline $< 2.7.10^{-2}$	$0.4.10^{-2}$	$(0.004\text{-}17.9).10^{-3}$
$H_2(g)$	mol/L	$< 2.2.10^{-5}$, if saline $< 8.9.10^{-4}$	$< 4.4.10^{-6}$	$< 2.2.10^{-5}$
DOC[b)]	mol/L of C	$< 1.7.10^{-4}$	$< 8.3.10^{-4}$	$< 1.7.10^{-4}$

a) dissolved inorganic carbon
b) dissolved organic carbon

From the experimental data that are available [4] and from our chemistry modeling of the repository environment using Gibbs Energy Minimization (GEMS) we conclude that during the oxic period the two most important redox species present in the system are oxygen and hydrogen, although some polysulphur species are judged to be significant. Under anoxic conditions, the only species at significant concentration is found to be hydrogen, with all iron existing in the ferrous state and hence incapable of oxidizing copper.

In any event, no kinetic data could be found for the oxygen electrode reaction (*OER*) and the hydrogen electrode reaction (*HER*) or for any redox reactions involving the polysulphur species on copper in the presence of sulphide. Likewise, we could find no data for the reduction of hydrogen peroxide on copper in the presence of sulphide, although work on modeling the corrosion potential in the cores of nuclear reactors [2], where H_2O_2 is generated radiolytically from the radiolysis of water, as it is in the case of the isolation of HLNW being modeled here, it is possible to assume the kinetic constants (exchange current density, transfer coefficients) for the *OER*, but to use the equilibrium potential calculated for the hydrogen peroxide electrode reaction, with satisfactory results [2]. The presence of sulphide is important, since the corrosion domain diagrams (e.g. Figure III-2) and the Pourbaix diagrams predict that a film of Cu_2S will form on the metal surface at potentials that are much more negative than those at which the oxide, Cu_2O, forms. Accordingly, the exchange current densities are expected to be considerably altered by the presence of the cuprous sulphide film, compared with the bare surface case in the absence of sulphide or on an oxide-covered surface. This is, because the Cu_2S film will impose a barrier to the quantum mechanical tunneling of charge carriers across the interface, thereby reducing the exchange current density and modifying the transfer coefficients and hence the Tafel constants. These data must be measured experimentally before a full analysis of the electrochemical and corrosion behaviors of copper in sulphide-containing aqueous environments can be made. We have proposed to make these measurements in a Phase III of the present program. We should note that data are available for the kinetics of the *OER* and *HER* on copper in the absence of sulphide [5] and these data could be employed in modeling the electrochemistry of copper in sulphide-free environments.

Anodic Reaction

The anodic processes that occur on copper in pure, deoxygenated water is a matter of considerable controversy, with Hultquist et.al. [6-8] claiming that copper corrodes under these conditions while others insist that the metal is immune, as indicated above. This controversy was resolved in Phase I of this report, where we demonstrated that both positions could be correct depending upon the initial conditions, as shown in Figure I-1. Thus, if the initial value of $P = p_{H_2}^{1/2} / \left[Cu^+\right]$ lies below the equilibrium value (P_e) calculated for the reaction, $Cu + H^+ = Cu^+ + 1/2H_2$ copper will corrode, because the Gibbs energy change (ΔG) is negative, as reported by Hultquist, et.al. [6-8], but if $P > P^e$, corrosion cannot occur, because ΔG is positive and hence the metal is immune. In the presence of sulphide, copper corrodes unequivocally under all practical conditions, because of the formation of Cu_2S at a potential that is much more negative than those for Cu/Cu^+ and Cu/Cu_2O. The potential of the Cu/Cu_2S reaction is sufficiently negative that the hydrogen evolution reaction, Reaction (III-20), is thermodynamically viable, according to the criterion derived from the Second Law of Thermodynamics, which states that for a corrosion process to be viable then $E_a^e < E_{corr} < E_c^e$ where E_a^e and E_c^e are the equilibrium potentials for the partial anodic and cathodic processes, respectively, and E_{corr} is the corrosion potential. It is evident, therefore, that the partial anodic reaction of interest is

$$2Cu + HS^- \rightarrow Cu_2S + H^+ + 2e^- \text{ or}$$

$$Cu + 1/2HS^- \rightarrow CuS_{1/2} + 1/2H^+ + e^- \quad \text{(III-26)}$$

The Point Defect Model representation of the formation of Cu_2S on copper in sulphide-containing environments is depicted as [9,10]:

Metal | Barrier Layer, Cu_2S | Solution/Precipitated Outer Layer

(1) $Cu + V_{Cu}^{1'} \xrightarrow{k_1} Cu_{Cu} + v_{Cu} + e^-$

(2) $Cu \xrightarrow{k_2} Cu_i^+ + v_{Cu} + e^-$

(3) $Cu \xrightarrow{k_3} Cu_{Cu} + \frac{1}{2}V_S^{\bullet\bullet} + e^-$

(4) $Cu_{Cu} \xrightarrow{k_4} Cu_s^+ + V_{Cu}^{1'}$

(5) $Cu_i^+ \xrightarrow{k_5} Cu_s^+$

(6) $V_S^{\bullet\bullet} + HS^- \xrightarrow{k_6} S_S + H^+$

(7) $CuS_{1/2} + \frac{1}{2}H^+ \xrightarrow{k_7} Cu^+ + \frac{1}{2}HS^-$

Figure III-12: Point Defect Model representation of the formation of Cu_2S on copper. Note that the Cu^+ cations that are transmitted through the barrier layer via cation vacancy movement through Reactions (1) and (4) and as interstitials via Reactions (2) and (5) will react with additional HS^- to form the precipitated, outer later with the overall stoichiometry being described by Reaction (III-26).

The rate constants for these reactions have been derived using the method of partial charges and the expressions are summarized in Tables III-8 and III-9 [9,10].

Table III-8: Rate constants $k_i = k_i^0 e^{a_i V} e^{b_i L} e^{c_i pH}$ for the interfacial defect generation and annihilation reactions employed in the Point Defect Model. Note that for the formation of Cu_2S on copper, χ = 1 and Γ =1.

Reaction	a_i (V^{-1})	b_i (cm^{-1})	c_i
(1) $Cu + V_{Cu}^{1'} \xrightarrow{k_1} Cu_{Cu} + v_{Cu} + e'$	$\alpha_1(1-\alpha)\gamma$	$-\alpha_1\varepsilon\gamma$	$-\alpha_1\beta\gamma$
(2) $Cu \xrightarrow{k_2} Cu_i^+ + v_{Cu} + e'$	$\alpha_2(1-\alpha)\gamma$	$-\alpha_2\varepsilon\gamma$	$-\alpha_2\beta\gamma$
(3) $Cu \xrightarrow{k_3} Cu_{Cu} + \frac{1}{2}V_S^{\cdot\cdot} + e'$	$\alpha_3(1-\alpha)\gamma$	$-\alpha_3\varepsilon\gamma$	$-\alpha_3\beta\gamma$
(4) $Cu_{Cu} \xrightarrow{k_4} Cu_s^+ + V_{Cu}^{1'}$	$\alpha_4\alpha\Gamma\gamma$		$\alpha_4\beta\gamma$
(5) $Cu_i^+ \xrightarrow{k_5} Cu_s^+$	$\alpha_5\alpha\gamma$		$\alpha_5\beta\gamma$
(6) $V_S^{\cdot\cdot} + HS^- \xrightarrow{k_6} S_S + H^+$	$2\alpha_6\alpha\gamma$		$2\alpha_6\beta\gamma$
(7) $CuS_{1/2} + \frac{1}{2}H^+ \xrightarrow{k_7} Cu^+ + \frac{1}{2}HS^-$	0		0

Table III-9: Definition of the standard rate constants for the interfacial defect generation and annihilation reactions employed in the Point Defect Model. Note that the base rate constant for the i^{th} reaction is designated k_i^{00}. Note that for the formation of Cu_2S on copper, χ = 1 and Γ =1.

Reaction	k_i^0
(1) $Cu + V_{Cu}^{1'} \xrightarrow{k_1} Cu_{Cu} + v_{Cu} + e'$	$k_1^{00} e^{-\alpha_1 \gamma \phi_{f/s}^0} e^{\frac{-E_{a,1}}{RT}\left(\frac{1}{T}-\frac{1}{T_0}\right)}$
(2) $Cu \xrightarrow{k_2} Cu_i^+ + v_{Cu} + e'$	$k_2^{00} e^{-\alpha_2 \gamma \phi_{f/s}^0} e^{\frac{-E_{a,2}}{RT}\left(\frac{1}{T}-\frac{1}{T_0}\right)}$
(3) $Cu \xrightarrow{k_3} Cu_{Cu} + \frac{1}{2}V_S^{\cdot\cdot} + e'$	$k_3^{00} e^{-\alpha_3 \gamma \phi_{f/s}^0} e^{\frac{-E_{a,3}}{RT}\left(\frac{1}{T}-\frac{1}{T_0}\right)}$
(4) $Cu_{Cu} \xrightarrow{k_4} Cu_s^+ + V_{Cu}^{1'}$	$k_4^{00} e^{\alpha_4 \gamma \phi_{f/s}^0} e^{\frac{-E_{a,4}}{RT}\left(\frac{1}{T}-\frac{1}{T_0}\right)}$
(5) $Cu_i^+ \xrightarrow{k_5} Cu_s^+$	$k_6^{00} e^{\alpha_5 \gamma \phi_{f/s}^0} e^{\frac{-E_{a,5}}{RT}\left(\frac{1}{T}-\frac{1}{T_0}\right)}$
(6) $V_S^{\cdot\cdot} + HS^- \xrightarrow{k_6} S_S + H^+$	$k_6^{00} e^{2\alpha_6 \gamma \phi_{f/s}^0} e^{\frac{-E_{a,6}}{RT}\left(\frac{1}{T}-\frac{1}{T_0}\right)}$
(7) $CuS_{1/2} + \frac{1}{2}H^+ \xrightarrow{k_7} Cu^+ + \frac{1}{2}HS^-$	$k_7^{00} e^{\frac{-E_{a,7}}{RT}\left(\frac{1}{T}-\frac{1}{T_0}\right)}$

As noted elsewhere [9,10], the rate of change of the barrier layer thickness for a barrier layer that forms irreversibly on a metal or alloy surface can be expressed as

$$\frac{dL}{dt} = \Omega k_3^0 e^{a_3 V} e^{b_3 L} e^{c_3 pH} - \Omega k_7^0 (C_{H^+} / C_{H^+}^0)^n e^{a_7 V} e^{c_7 pH} \qquad \text{(III-27)}$$

where $a_3 = \alpha_3(1-\alpha)\gamma$, $a_7 = 0$, $b_3 = -\alpha_3\varepsilon\gamma$, $c_3 = -\alpha_3\beta\gamma$, and $c_7 = 0$ (Table III-8). In these expressions, Ω is the mole volume of the barrier layer (Cu_2S) per cation, ε is the electric field strength within the barrier layer (postulated to be a constant and independent of the applied voltage in the steady state, because of the buffering action of Esaki tunneling [9,10]), k_i^0 and α_i are the standard rate constant and transfer coefficient, respectively, for the appropriate reactions depicted in Figure III-8 [i.e., Reactions (3) and (7)], α is the polarizability of the barrier layer/solution (outer layer) interface, (i.e., the dependence of the voltage drop across the interface, $\phi_{f/s}$, on the applied voltage, *V*), β is the dependence of $\phi_{f/s}$on *pH* (assumed to be linear), γ = *F/RT*, C_{H^+} is the concentration of hydrogen ion, $C_{H^+}^0$ is the standard state concentration, and *n* is the kinetic order of the barrier layer dissolution reaction with respect to H^+. Note that the rate of the dissolution reaction is voltage-dependent only if the oxidation state of copper in the barrier layer were different from the oxidation state of copper in the solution. Under anoxic conditions, the oxidation state of copper in both phases is +1. Thus, the rate of dissolution is voltage-independent.

By setting the left side of Equation (III-27) equal to zero, the steady state thickness of the barrier layer, L_{ss}, is readily derived as

$$L_{ss} = \left[\frac{1-\alpha}{\varepsilon}\right]V + \left[\frac{2.303n}{\alpha_3\varepsilon\gamma} - \frac{\beta}{\varepsilon}\right]pH + \frac{1}{\alpha_3\varepsilon\gamma}ln\left(\frac{k_3^0}{k_7^0}\right) \qquad \text{(III-28)}$$

where the parameters are as previously defined. Note that in deriving these expressions, the convention has been adopted that, for the rate of barrier layer dissolution, C_{H^+} and $C_{H^+}^0$ have units of mol/L. Thus, the standard states for the dissolution reaction [second term on the right side of Equation (III-27)] and for the pH are both 1.0 mol/l. The introduction of a standard state into the dissolution rate renders the units of k_7^0 independent of the kinetic order, *n*, without altering the numerical value of the rate.

The steady state passive current density is readily derived [9,10] as

$$I_{ss} = F\left[k_2^0 e^{a_2V} e^{b_2L_{ss}} e^{c_2pH} + k_4^0 e^{a_4V} e^{c_4pH} + k_7^0 e^{a_7V} e^{c_7pH} \cdot (C_{H^+}/C_{H^+}^0)^n\right] \qquad \text{(III-29)}$$

where the first, second, and third terms arise from the generation and transport of cation interstitials, cation vacancies, and oxygen vacancies, respectively, with the term due to the latter being expressed in terms of the rate of dissolution of the barrier layer [9,10]. This expression is derived in part by noting that the fluxes of a given defect at the two defects under steady-state conditions are equal; in this way the expression of the current can be formulated so as to avoid the defect concentrations at the interfaces. It is Equation (III-29) that must be inserted into Equation (III-18) for the quantity i_a.

Because metal interstitials and oxygen vacancies are electron donors and recognizing that the barrier later is a highly-doped, defect semi-conductor the barrier layer will display n-type conductivity if either interstitials and/or oxygen vacancies (sulphur vacancies, in the case of a Cu_2S film) are the dominant defects in the system. On the other hand, if the cation vacancy, which is an electron acceptor, dominates, the film will display p-type conductivity. With regard to Equation (III-29), n-type conductivity would imply that the second or third terms dominate the current, in which case the expression for the passive current density can be reduced to

$$I_{ss} = F\left[k_2^0 e^{a_2 V} e^{b_2 L_{ss}} e^{c_2 pH} + k_7^0 e^{a_7 V} e^{c_7 pH} \cdot (C_{H^+} / C_{H^+}^0)^n\right] \qquad \text{(III-30)}$$

Noting that $a_7 = 0$ and that $a_2 V + b_2 L_{ss} = 0$, the passive current is predicted to be

$$I_{ss} = F\left[k_2^0 e^{c_2 pH} + k_7^0 e^{c_7 pH} \cdot (C_{H^+} / C_{H^+}^0)^n\right] \qquad \text{(III-31)}$$

which is voltage-independent.. On the other hand, if the film is p-type then cation vacancies dominate and the expression for the passive current density reduces to

$$I_{ss} = F\left[k_4^0 e^{a_4 V} e^{c_4 pH} + k_7^0 e^{c_7 pH} \cdot (C_{H^+} / C_{H^+}^0)^n\right] \qquad \text{(III-32)}$$

which corresponds to Tafel's law if the first term dominates.

The electronic type of the Cu_2S passive film does not appear to have been determined, even though is a straight forward matter to do so, using Mott-Schottky analysis [9,10]. If the film was found to be n-type the passive current density, which would be incorporated into Equation (III-18) would have the form

$$i_a = A \qquad \text{(III-33)}$$

where $A = F\left[k_2^0 e^{c_2 pH} + k_7^0 e^{c_7 pH} \cdot (C_{H^+} / C_{H^+}^0)^n\right]$ is a constant, but if it is found to be p-type the functional form would be:

$$i_a = A e^{a_4 V} + B \qquad \text{(III-34)}$$

where $A = Fk_4^0 e^{c_4 pH}$ and $B = Fk_7^0 e^{c_7 pH} \cdot (C_{H^+} / C_{H^+}^0)^n$. Substituting these expressions into Equation (III-18) and assuming, as a first approximation, that under anoxic conditions the only important cathodic partial reaction is hydrogen evolution via water reduction, we obtain the following:

$$A - \frac{e^{\left(V - E_{HER}^e\right)/b_{a,i}} - e^{-\left(V - E_{HER}^e\right)/b_{c,i}}}{\frac{1}{i_{0,R/O,i}} + \frac{e^{\left(V - E_{HER}^e\right)/b_{a,i}}}{i_{l,f,R/O,i}} - \frac{e^{-\left(V - E_{HER}^e\right)/b_{c,i}}}{i_{l,r,R/O,i}}} = 0 \quad \text{(n-type)} \qquad \text{(III-35)}$$

and

$$Ae^{a_4 V} + B - \frac{e^{\left(V - E_{HER}^e\right)/b_{a,i}} - e^{-\left(V - E_{HER}^e\right)/b_{c,i}}}{\frac{1}{i_{0,R/O,i}} + \frac{e^{\left(V - E_{HER}^e\right)/b_{a,i}}}{i_{l,f,R/O,i}} - \frac{e^{-\left(V - E_{HER}^e\right)/b_{c,i}}}{i_{l,r,R/O,i}}} = 0 \qquad \text{(p-type)} \quad \text{(III-36)}$$

for the n-type and p-type cases, respectively.

These equations can be solved iteratively to yield $V = E_{corr}$. Once E_{corr} is obtained, it may be substituted back into the anodic term to calculate the corrosion current density. In the case of an n-type passive film, i_{corr} is simply equal to A and is voltage-independent, whereas, in the p-type case, the corrosion current density depends exponentially upon E_{corr} and is given by $i_{corr} = Ae^{a_4 E_{corr}} + B$. Thus, in the case of an n-type film, the corrosion potential does not need to be accurately known, because the passive current density is independent of potential, but it does need to be accurately known in the case of a p-type film. It should be noted that the expressions for the partial anodic current densities correspond to the Generation II PDM [11], which postulates that the passive film comprises a single barrier layer and that the precipitated outer layer presents little impediment to current flow across the interface and/or the cathodic partial reactions occur at the barrier layer/outer layer (solution) interface (i.e., it is assumed that the cathode is not remote so that the passive current need not pass through the outer layer in order to be annihilated by the cathodic processes). If the local cathode were "remote", then it would be necessary to take into account the IR potential drop across the porous outer layer [12].

A search of the literature reveals few data that can be used in solving Equations (III-35) and (III-36) for the corrosion potential and the corrosion current density directly. It is for this reason, and because these models were superceded by the Physico-Electrochemical Model (PEM) described below, that we did not carry out any scoping calculations using "guesstimated" model parameter values. In this regard, it should be noted that these models are "stand alone" models, in that they are not coupled to the transport of species (HS^-, H^+, H_2, O_2, H_2O_2) through the buffer and the radiolytic generation of species (H_2, O_2, and H_2O_2 as a function of distance away from the canister surface or the reaction of these species with HS^- within the near-field, buffer environment. These limitations do not exist with the PEM and we concluded that the PEM would provide for superior simulation

of canister corrosion than could be obtained from the MPM. Nevertheless, an advanced version of the PEM currently under consideration makes use of the Point Defect Model (PDM) description of the anodic process that occurs at the metal surface.

This issue is best illustrated with reference to the Generalized Butler-Volmer equation, which is contained in the formulation of the MPM for a passive metal with an n-type passive film in contact with a solution containing a single redox couple R/O as described by Equation (III-36), which for convenience is repeated here:

$$Ae^{a_4 V} + B - \frac{e^{\left(V - E^e_{HER}\right)/ b_{a,i}} - e^{-\left(V - E^e_{HER}\right)/ b_{c,i}}}{\frac{1}{i_{0,R/O,i}} + \frac{e^{\left(V - E^e_{HER}\right)/ b_{a,i}}}{i_{l,f,R/O,i}} - \frac{e^{-\left(V - E^e_{HER}\right)/ b_{c,i}}}{i_{l,r,R/O,i}}} = 0 \qquad \text{(III-36)}$$

The third term of this equation describes the kinetics of the partial cathodic process (\hydrogen evolution via the reduction of water in the case of anoxic conditions). In this equation, E is the potential, E^e_{HER} is the equilibrium potential of the redox couple, $i_{0,R/O,i}$ is the exchange current density, $b_{a,i}$ is the anodic Tafel Constant, $b_{c,i}$ is the cathodic Tafel constant, and $i_{l,f,R/O,i}$ and $i_{l,r,R/O,i}$ are the limiting current densities in the forward and reverse directions of the redox reaction ($R = O + ne^-$,), respectively. In the formulation of the generalized Butler-Volmer equation, these latter two quantities (the limiting current densities for the forward and reverse directions of *R/O*) are assumed to be constants, corresponding to the mass-transfer limited transport of *R* and *O* to the metal surface in a time-invariant mass transport field. This model is appropriate for systems where the mass-transfer limited currents assume steady state values rapidly (order of seconds) upon changing the hydrodynamic and hence mass-transfer field, as occurs in the case of a freely-flowing fluid. Thus, the diffusional relaxation time in this case is very short, as estimated by the expression, $t \sim L_D^2/D$, where L_D is the diffusion layer thickness and D is the diffusivity of the species being transported to the metal surface. For mass transport to surfaces in contact with bulk solutions with no mass transfer restrictions, L_D ~ 0.001 cm and D ~ 10^{-5} cm^2/s, giving a diffusional relaxation time of 0.1 s. In the case of restricted mass transport through 10-cm of compacted bentonite layer, however, L_D = 10 cm and D ~ 10^{-9} cm^2/s giving a relaxation time of the order of 10^{11} s (3,175 years). Accordingly, transport through the buffer dominates the supply of species to the metal surface and the rate of supply evolves very slowly with time. Accordingly, the limiting currents in Equation (III-36) cannot be regarded as being constants, so that the generalized Butler-Volmer equation, Equation (III-19). does not provide a good decription of the cathodic partial processes, because it is not possible to assume that the kinetics of the surface reactions are coupled to a fast mass transfer process. Instead, it is evident that the exceedingly slow mass transfer process through the buffer is strongly coupled to the surface reactions and that the mass transfer step is rate-controlling regardless of the potential and that the supply of species to the surface evolves very slowly with time. It is for this reason that the MPM, as described

above, was discarded in favor of the Physico-Electrochemical Model (PEM) that is described in Section (III-5) below.

As in the case of the cathodic partial reactions, no kinetic data could be found for the Point Defect Model representation of the anodic oxidation copper in the presence of sulphide, as described above. Also, no PDM data could be found for the anodic oxidation of copper in the absence of sulphide ion, where cuprous oxide is expected to form. Accordingly, the full implementation of the theory for estimating the corrosion potential, in particular, is not possible at this time. We have proposed to make these measurements in a Phase III of the present program. We should note that the measurement of the values for the PDM parameters involves optimizing the expression for the impedance developed from the PDM on experimental electrochemical impedance spectroscopy (EIS) data. We have developed these techniques to a high degree of sophistication in our work on the corrosion of carbon steel overpack in contact with simulated concrete pore water, as part of Belgium's program on the isolation of HLNW, but they have never been applied to the formation of sulphide films on copper or on any other metal, to the authors' knowledge.

References:

1. D. D. Macdonald, A. C. Scott, and P. Wentrcek.,*J. Electrochem., Soc.*, **128**, 250-257 (1981).
2. D. D. Macdonald,. *Corrosion*, **48**(3), 194-205 (1992).
3. "Final Storage of spent Nuclear fuel-KBS-3, Part 3: Barriers", *SKB, Svensk Kärnbränslehantering AB*, (1983).
4. D. D. Macdonald and S. Sharifi-Asl,*SSM-2011:09, Swedish Radiation Safety Authority* (2011).
5. G. Kear, B. D. Barker, and F. C. Walsh,*Corros. Sci.*, **46**, 109 (2004).
6. G. Hultquist, *Corros. Sci.*, **26**, 173 (1986).
7. G. Hultquist, G. K. Chuah, and. K. L. Tan, *Corros. Sci.*, **29**, 1371 (1989).
8. P. Szakálos, G. Hultquist, and G. Wikmark, *Electrochem. SolidState Letters*, **10**, C63 (2007).
9. D. D. Macdonald,*J. Electrochem. Soc*., **139**(12), 3434-3449 (1992).
10. D. D. Macdonald, *Pure Appl. Chem*., **71**, 951-986 (1999).
11. D. D. Macdonald,, *Electrochimica. Acta*, **56** 1761 (2011).
12. D. D. Macdonald and G. R. Engelhardt,ECS Trans., **28**(24), 123 (2010).
13. E-L Tullborg, J Smellie, A.Ch. Nilsson, M. J. Gimeno, V. Brüchert, J. Molinero, *SKB, TR-10-39, Svensk Kärnbränslehantering AB*, (2010)

III-4: Continued Definition of the Corrosion Evolutionary Path

The evolution of corrosion damage must be modeled along the corrosion evolutionary path, which is defined by the variation of temperature, *pH*, sulphur species activity (concentration), p_{H_2}, and other independent variables that have a significant impact on the damage accumulation rate as the repository ages. The time dependences of *pH*, sulphur species activity (concentration), and p_{H_2} must be modeled by solving the transport equations for the transfer of H^+, sulphur species, and H_2 across the bentonite layer, recognizing the existence of a source term for sulphur species in the bentonite (dissolution of FeS_2, which is iron disulphide, containing the anion, S_2^{2-}). As shown elsewhere, S_2^{2-} is a strong activator of copper, but it further dissoctiates into $S + S^{2-}$ (or HS^-). Solution of the thermal diffusion equation yields the temperature as a function of distance from the copper surface and time, as shown in Figure III-21 [1]. Because the diffusivities of H^+, sulphur species, and H_2 are temperature-dependent, as is the rate constant for FeS_2 dissolution, the system of equations that will describe the evolution of the repository and hence that will indicate whether, and under what conditions, the activation of copper may occur, will be highly non-linear and must be solved numerically. In Phase I of the current work, we showed the evoloution of the pH and hydrogen gas fugacity in the system, as a function of time and temperature. The goal of this task is to assess which of the sulphur species play the most important role in the activating the copper canister as the system evolves along the corrosion evolutionary path (CEP) [2]. The result of this task will lead us to pick the most deleterious sulphur species in the system and conduct experimental work in the presence of it in future work.

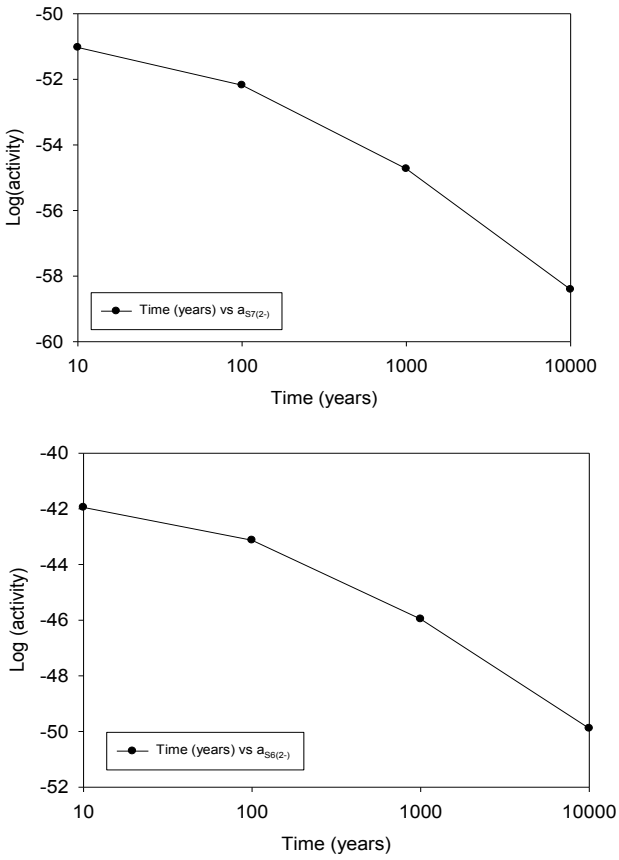

Figure III-13: Activity of dissolved Sulphur species in the simulated groundwater as a function of time, S_7^{2-}(top) and S_6^{2-}(bottom).

In this part, we selected some of the sulphur species predicted to be present in the vicinity of the copper canister and derived their activities as a function of time. Figures III-13 to III-19 show the calculated activities of polysulphur species in the simulated groundwater as a function of time. The reader should note that all of the calculated activities are based upon the Gibbs energy minimization of the system using GEMS software [2]. The calculations have been performed for anoxic conditions and reflect the change in temperature along the CEP.

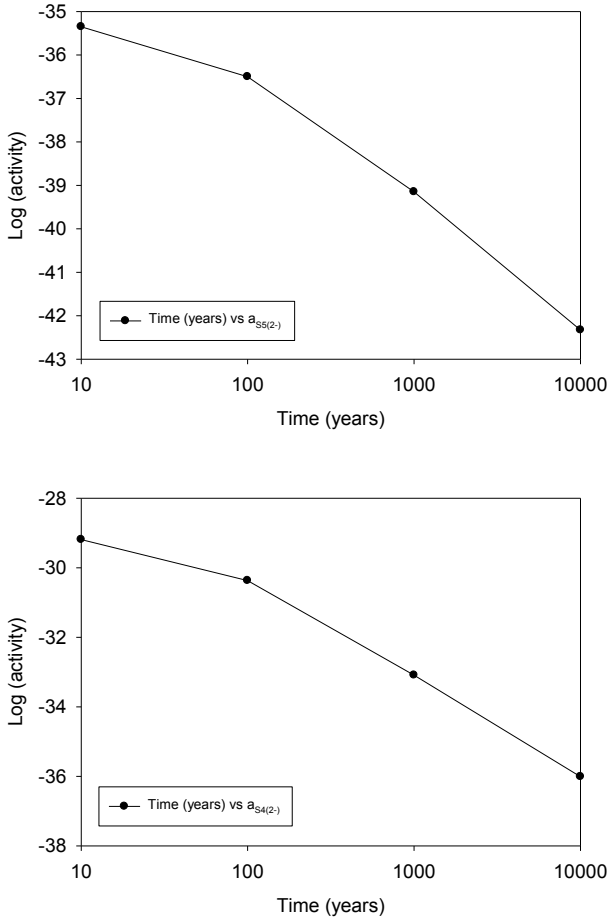

Figure III-14: Activity of dissolved Sulphur species in the simulated groundwater as a function of time, S_5^{2-}(top) and S_4^{2-}(bottom).

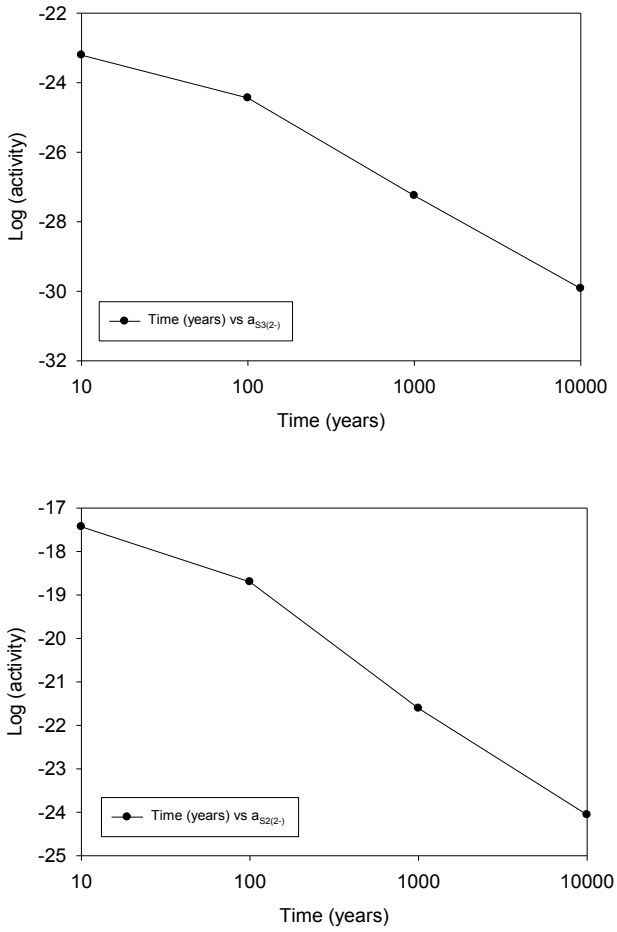

Figure III-15: Activity of dissolved Sulphur species in the simulated groundwater as a function of time, S_3^{2-}(top) and S_2^{2-}(bottom).

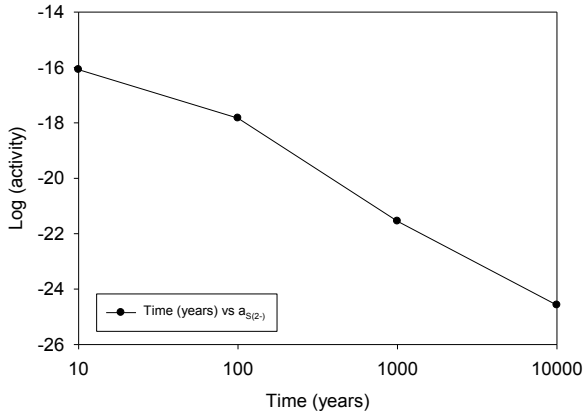

Figure III-16: Activity of dissolved Sulphur species in the simulated groundwater as a function of time, S^{2-}.

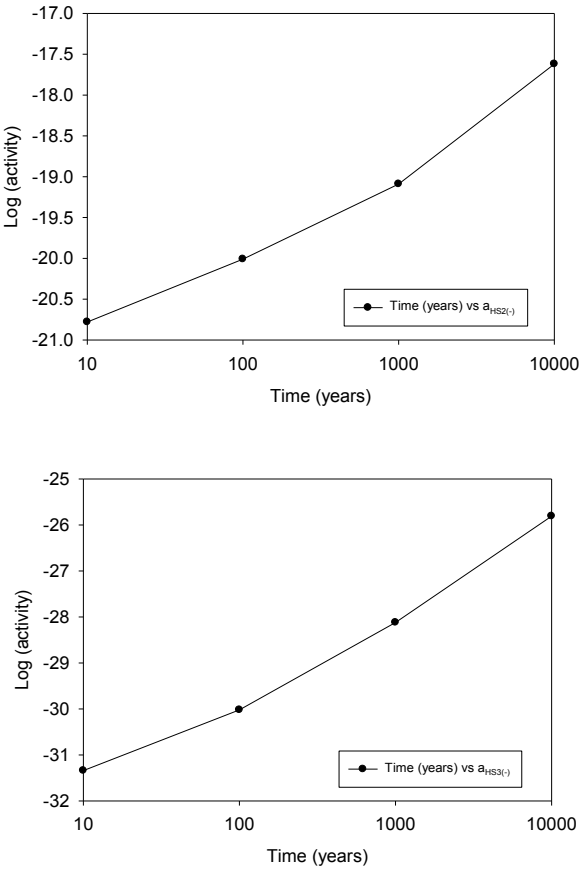

Figure III-17: Activity of dissolved Sulphur species in the simulated groundwater as a function of time, HS_2^-(top) and HS_3^-(bottom).

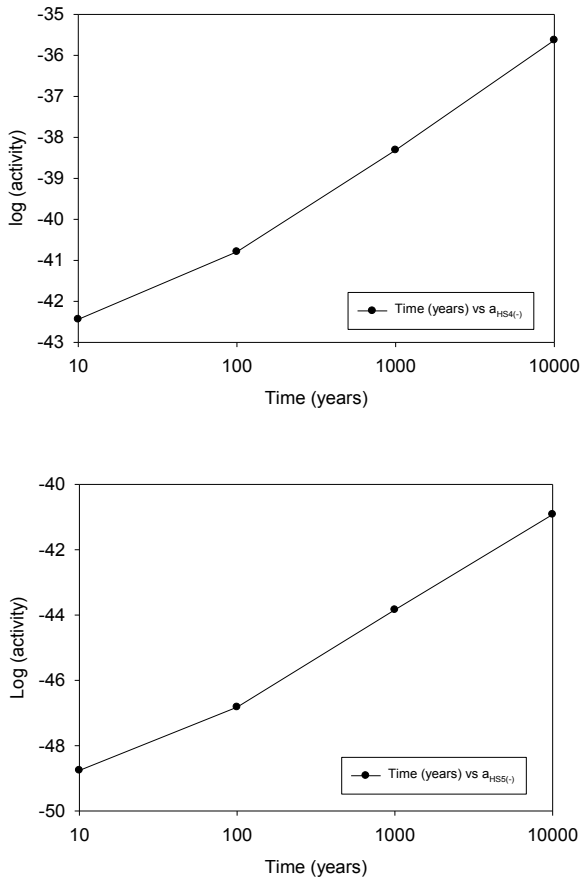

Figure III-18: Activity of dissolved Sulphur species in the simulated groundwater as a function of time, HS_4^-(top) and HS_5^-(bottom).

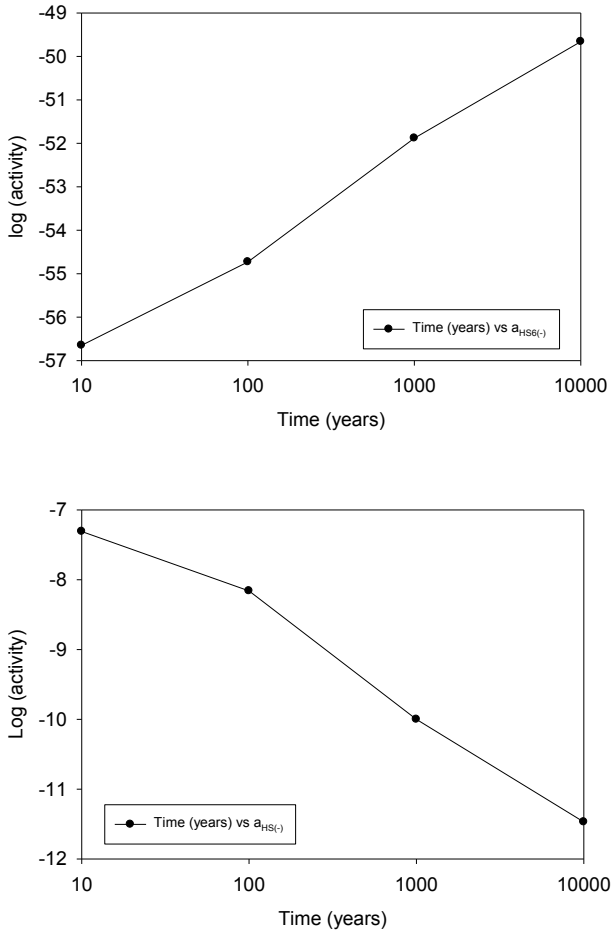

Figure III-19: Activity of dissolved Sulphur species in the simulated groundwater as a function of time, HS_6^-(top) and HS^-(bottom).

Initial calculations showed that the concentrations (activities) of the polysulphur oxyanions under anoxic conditions are predicted to be exceedingly low compared to the polysulphide species and HS^- and for this reason the polysulphur oxyanions were not included in the analysis.

As can be seen from Figures III-13 to III-19, the activities of some of the polysulphides decrease with increasing time and some vice versa. The most important finding of this work is recognizing that HS^-(aq) has the highest concentration of all sulphur-containing species in the system. It is clear that the HS^-(aq) concentration in the simulated ground water is much higher than the rest of the available species and its activity is predicted to decrease with time, but not to the extent that it ceases to be the dominant species. Although our previous work on the Corrosion Domain Diagrams (CDDs) revealed that all of the sulphide and polysulphide species can activate the copper canister thermodynamically, it is important to note that, from a kinitec point of view, it is the rate of

supply of atomic sulphur to the canister surface that governs the rate of corrosion. Noting that the Nernst-Planck equations are linear in concentration, we therefore conclude that the kinetic propensity for activation also depends upon the concentration. We further conclude that the most important, practical acivators of copper in the repository is HS^-, followed distantly by S_2^{2-}, S_3^{2-}, S_4^{2-} and their protonated forms, HS_x^- Therefore, we opine that for the future study of copper corrosion, both the anodic dissolution of metallic copper and cathodic evolution of hydrogen or the reduction of oxygen, should be studied in the presence of bisulphide [HS^-(aq)] ion in order to accurately represent the repository system. Finally, it is important to note that, in performing these calculations, we have not considered micrbiological sources of sulphide and other sulphur-containing species. It is possible that sulphate-reducing bacteria acting upon sulfate rock under anoxic conditions might represent an important source of sulphur-containing species, but we know of no definitive data that demonstrate that to be the case.

Finally, Table III-10 presents a comparison between the calculated and measured concentration of some of the most important species that have been predicted to be present in the ground water at the Forsmark site. As can be seen, there is some discrepency between the calculated and measured data, especially in the case of S^{2-} and CH_4 (aq), where the difference is remarkable. As we mentioned earlier, one reason for this discrepancy is that the GEMS results describe the system under the equilibrium conditions and does not considering non-equilibrium conditions that are best described in terms of reaction kinetics. However, for some of the species, we can see relatively good agreement between the calculated and measured values.

Table III-10: comparison of concentarton of species calculated by GEMs and measured from boreholes by SKB [3,4]

Constituent		**GEM SELEKTOR*** **(25°C-100°C)**	**Measured form Boreholes at Forsmark site[3,4]**
S^{2-}	*mol/L*	$10^{-22.8}$ to $10^{-11.99}$	10^{-7} to 10^{-4}
SO_4^{2-}	*mol/L*	$10^{-3.91}$ to$10^{-5.35}$	0 to 6×10^{-3}
Cl^-	*mol/L*	$10^{-4.081}$	2.7×10^{-3} to 194×10^{-3}
HCO_3^-	*mol/L*	$10^{-4.5}$ to $10^{-4.4}$	10^{-4} to 4.8×10^{-3}
$H_2(aq)$	*mol/L*	$10^{-11.52}$ to $10^{-7.28}$	10^{-8} to 10^{-3}
$CO_2(aq)$	*mol/L*	$10^{-4.91}$ to $10^{-6.5}$	10^{-6} to 10^{-3}
$CH_4(aq)$	*mol/L*	$10^{-17.07}$ to $10^{-10.32}$	10^{-7} to 10^{-3}

*The software that have been used for Gibbs energy minimization

In closing, we conclude that the most important independent variables that need to be included in defining the corrosion evolutionary path for the repository are: Temperature,

pH, [HS^-], and H_2. The hydrogen concentration is important, because hydrogen is principally responsible for the development anoxic conditions. In this regard, the presence of hydrogen drives the redox potential in the negative direction ensuring that the concentrations of the polysulphur oxyanions and to a lesser extent the polysulphide species will be low. Because bisulphide ion, HS^-, cannot be reduced, its acivity (concentration) is unaffected by the presence of hydrogen. In other words, "anoxic" conditions reflect just not the absence of oxygen, but also the presence of hydrogen.

References

1. "Final Storage of spent Nuclear fuel-KBS-3, Part 3: Barriers", *SKB, Svensk Kärnbränslehantering AB*, (1983)
2. D. D. Macdonald and S. Sharifi-Asl, *SSM-2011:09, Swedish Radiation Safety Authority* (2011)
3. E-L Tullborg, J Smellie, A.Ch. Nilsson, M. J. Gimeno, V. Brüchert, J. Molinero, *SKB, TR-10-39, Svensk Kärnbränslehantering AB*, (2010)
4. F. King, C. Lilja, K. Pedersen, P.Pitkänen and P. Posiva, *SKB-TR-10-67, Svensk Kärnbränslehantering AB*, (2010)

III-5: Development of a Physico-Electrochemical Model for Canister Corrosion.

In Phase II of this rese*a*rch program, upon which this report is written, mixed potential models (MPMs) [1,2] were initially developed to predict the redox potential of the environment and the corrosion potential and corrosion rate (expressed as the corrosion current density) of copper canisters contained in the granitic rock repository being developed in Sweden for the disposal of high level nuclear waste (HLNW). These models were designed to provide estimates of E_{redox}, E_{corr}, and i_{corr} as the system evolves along the corrosion evolutionary path. Comparison of E_{redox} and E_{corr} with critical potentials for various localized corrosion processes, such as pitting corrosion, stress corrosion cracking, and crevice corrosion, is expected to indicate whether any of these localized corrosion processes are likely to occur in the repository. Integration of the corrosion current density and use of Faraday's law yield the weight loss of copper and the dimensional change of the canister due to corrosion. The models that were initially developed are known technically as "Mixed Potential Models (MPMs)", which stem from the author's work [1,2] on modeling the heat transport circuits of boiling water (nuclear) reactors (BWRs), where they have been spectacularly successful in describing the electrochemical properties and corrosion behaviors of stainless steels in the primary coolant circuits [3].

However, upon completion of the mathematical frameworks of the models, it became apparent that the Physico-Electrochemical Model (PEM) being developed in a parallel task (see below) would also yield the results of interest and would do so in a physically more-realistic manner. This is so, because the MPMs were designed as "stand alone" models that were not coupled to the mass transport processes occurring in the bentonite buffer or to the radiolysis of water, both of which have potentially large impacts of the electrochemical and corrosion behaviors of the system. Instead the MPMs postulated that the cathodic processes could be adequately described by the generalized Butler-Volmer equation (Equation III-17) [1,2] that incorporates a mass transfer relaxation time that is very short compared with the time over which the repository evolves and short compared with the diffusional relaxation time for diffusion of species across the buffer. The diffusion of species in the buffer was judged to be so slow that "diffusion limited" currents for the cathodic depolarizer reaction (H_2O/H_2) and anodic dissolution of copper (as reflected by the transport of HS^-) may never be realized and hence it calls into question the very veracity of the Butler-Volmer equation in this application. In other words, the transport processes in the compacted bentonite buffer are envisaged to be so slow that they cause the diffusion profiles for any given species to change very slowly, such that constant limiting currents for the forward and reverse directions of the redox reactions may never be realized. For this reason, it was decided to abandon the MPM approach and focus our efforts on the PEM, as noted previously in this report. Furthermore, it was apparent that few data are available in the literature from which values for important model parameters (e.g., exchange current densities and transfer coefficients) could be obtained, but we must point out that the situation in the case of the PEM, in this regard, is hardly any better. Although the corrosion of copper in sulphide-containing, aqueous media has been studied extensively, it is still not known whether the Cu_2S passive film on a copper surface is a p- or n-type semiconductor or

what the dominant defect is within the film. (We suspect that the film is n-type and that the principal defect is the *Cu(I)* interstitial, but we will not know for sure until the proposed Phase III work is underway). Furthermore, a complete dearth exists with regards to the kinetics of the HER, the OER, and the HPER on copper in sulphide-containing media, and we do not even know whether Cu_2S passive films can exist in the presence of low concentrations of O_2 and H_2O_2, as produced by water radiolysis, for example. These are but a few of the issues that need to be addressed in Phase III over the next two years.

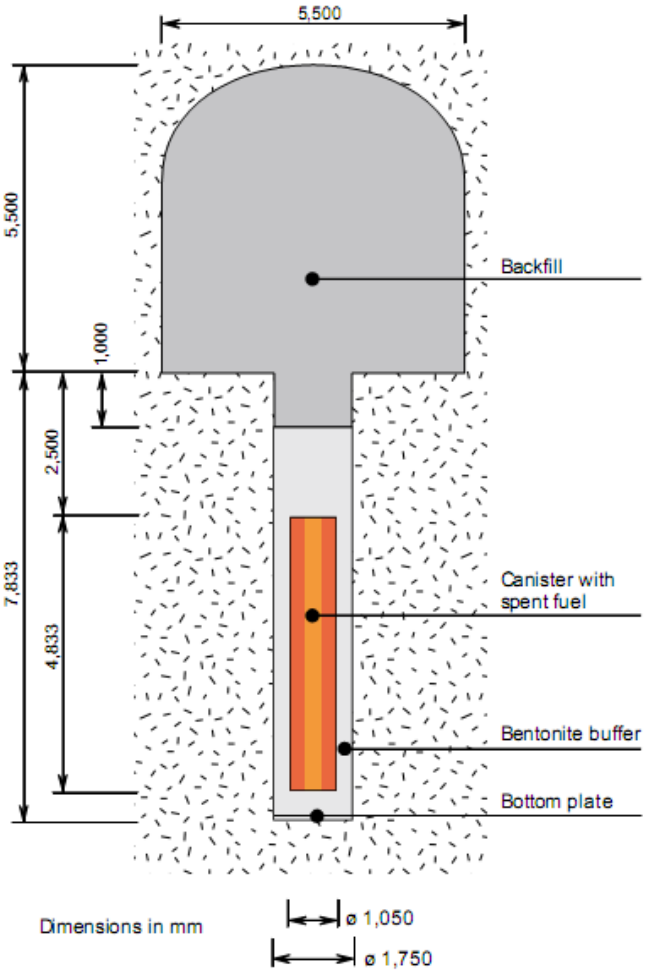

Figure III-20: Schematic of canister emplaced concentrically with the bentonite buffer located in a cylindrical hole in the floor of a tunnel in the repository [4].

The model developed in this task is based upon the cylindrical symmetry of the canister shown schematically in Figure III-20. End effects are ignored. Briefly, the model assumes that the cylindrical canister is embedded in a cylinder of bentonite buffer, which, in turn, is contained in a cylindrical hole in crystalline rock. It is assumed that the buffer is not initially fully saturated with ground water and that at zero time; a radiation field of γ-

photons is switched-on. The initial dose rate at the canister surface is assumed to be 1 Gy/hr (0.0278 rad/s). The resulting radiolysis of the water in the buffer generates H_2, O_2, and H_2O_2 as the primary products. Other radiolysis products, such as H, OH, O_2^-, O, $e(aq)^-$, and so forth, are ignored, because previous modeling of the radiolysis of water [3] shows that their concentrations are so small that they have negligible impact on the balance of partial currents at the metal interface and hence on the calculated corrosion potential and corrosion current density. The dose rate and the temperature are assumed to decay exponentially with distance away from the canister surface. The concentrations of chemical species in the far-field at the buffer-rock interface are assumed to be fixed at the groundwater values.

Because of the radiolytic production of O_2, H_2O_2, and H_2 within the buffer, the three following cathodic partial reactions are considered in the model:

$$H_2 + 2OH^- \xleftrightarrow{k_2, k_{-2}} 2H_2O + 2e^- \quad \text{(III-37)}$$

$$4OH^- \xleftarrow{k_{-3}} O_2 + 2H_2O + 4e^- \quad \text{(III-38)}$$

$$2OH^- \xleftarrow{k_{-4}} H_2O_2 + 2e^- \quad \text{(III-39)}$$

These reactions are written in the oxidation sense, because of the convention adopted here of the current being defined as positive for an oxidation reaction and negative for the reverse, reduction reaction. The reactions are also written in their alkaline solution form, because the environment has a pH of between 8 and 9. The anodic partial reaction is written as:

$$2Cu + HS^- + OH^- \xrightarrow{k_1} Cu_2S + H_2O + 2e^- \quad \text{(III-40)}$$

Reaction (III-38), (III-39), and (III-40) are assumed to be irreversible, as indicated by the arrows, whereas Reaction (III-37) is considered to be reversible, necessitating consideration of the kinetics of the reactions in the forward and reverse directions. Four other reactions are considered in the model; the reaction of bisulphide ion with O_2 and H_2O_2, viz:

$$HS^- + O_2 \xrightarrow{k_5} SP_1 \quad \text{(III-41)}$$

and

$$HS^- + H_2O_2 \xrightarrow{k_6} SP_2 \quad \text{(III-42)}$$

and the recombination of hydrogen with oxygen and hydrogen peroxide, as follows:

$$2H_2 + O_2 \xrightarrow{k_7} 2H_2O \quad \text{(III-43)}$$

and

$$H_2 + H_2O_2 \xrightarrow{k_8} 2H_2O \quad \text{(III-44)}$$

where SP_1 and SP_2 are unspecified bisulphide oxidation products that may or may not be inert toward copper. For example, if these products were sulphite (SO_3^{2-}) or sulphate (SO_4^{2-}), they are considered to be ineffective in activating copper [5], but if the products were polysulphides, elemental sulphur, or polythionates, then they could diffuse to the copper surface and activate copper in much the same way as does bisulphide ion. This is essentially an autocatalytic, "shuttle mechanism", whereby the energy contained in the oxidizing radiolysis products is transferred to the corrosion of copper via sulphide oxidation products. In the present model, we assume that Reactions (III-41) and (III-42) proceed to the *S(IV)* and *S(VI)* oxidation states to produce inert oxidation products (sulphite and sulphate). Thus, autocatalysis is ignored in the present analysis.

The condition for the conservation of charge at the copper/buffer interface is given as:

$$i_1 + i_2 + i_3 + i_4 = 0 \qquad \text{(III-45)}$$

where i_1, i_2, i_3, and i_4 are the partial currents due to Reactions (III-40), (III-37), (III-38), and (III-39), respectively. These currents are given in terms of electrochemical reaction rate theory as;

$$i_1 = 2Fk_1^0 e^{a_1 E} C_{HS^-}^s C_{OH^-}^s \qquad \text{(III-46)}$$

$$i_2 = Fk_2^0 e^{a_2 E} C_{H_2}^s \left(C_{OH^-}^s\right)^2 - Fk_{-2}^0 e^{-b_2 E} \qquad \text{(III-47)}$$

$$i_3 = -4Fk_{-3}^0 e^{-b_3 E} C_{O_2}^s \qquad \text{(III-48)}$$

and

$$i_4 = -2Fk_{-4}^0 e^{-b_4 E} C_{H_2O_2}^s \qquad \text{(III-49)}$$

where it is assumed that Reactions (III-38) and (III-39) occur irreversibly in the reduction sense (reverse directions as written, as indicated by the arrows), while Reaction (III-40) is assumed to occur irreversibly in the forward direction, as written. Reaction (III-37) is treated as being reversible, because of the presence of molecular hydrogen in the repository [4] and because the calculated equilibrium potential lies within the range expected for the corrosion potential. Thus, if the corrosion potential is found to be more positive than the equilibrium potential for Reaction (III-37) the oxidation of hydrogen becomes spontaneous and contributes to the total anodic partial current at the interface. On the other hand, if the corrosion potential is found to be more negative than the equilibrium potential for Reaction (III-37), the reduction of water and the concomitant evolution of hydrogen become spontaneous and contribute to the total cathodic partial current at the interface.

In order to proceed, it is necessary to calculate the concentrations of HS^-, O_2, H_2, OH^-, and H_2O_2 at the surface of the canister, as a function of time. We do that by assuming that the transport of these species within the buffer can be described by writing the Nernst-Planck equations as given below:

$$\vec{J}_i = -D_i \frac{\partial C_i}{\partial r} + z_i u_i F E_r c_i + v c_i \qquad \text{(III-50)}$$

Or, on taking into account that $E = -\frac{\partial \varphi}{\partial r}$

$$\vec{J}_i = -D_i \frac{\partial C_i}{\partial r} - z_i u_i F c_i \frac{\partial \varphi}{\partial r} + v c_i \qquad \text{(III-51)}$$

If the Nernst –Einstein relation, $D_i = u_i RT$, where u_i is the mobility, holds, we have

$$\vec{J}_i = -D_i \frac{\partial C_i}{\partial r} - \frac{z_i D_i F c_i}{RT} \frac{\partial \varphi}{\partial r} + v c_i \qquad \text{(III-52)}$$

The equations of mass balance (the "continuity" equation) for all species are then:

$$\frac{\partial C_i}{\partial t} = D_i \left[\frac{1}{r} \frac{\partial}{\partial r} \left(r \frac{\partial C_i}{\partial r} \right) \right] + \frac{z_i D_i F}{RT} \left[\frac{1}{r} \frac{\partial}{\partial r} \left(r \frac{\partial \varphi}{\partial r} \right) \right] - \frac{1}{r} \frac{\partial}{\partial r} (rCv) \qquad \text{(III-53)}$$

or

$$\frac{\partial C_i}{\partial t} = D_i \left[\frac{\partial^2 C_i}{\partial r^2} + \frac{1}{r} \frac{\partial C_i}{\partial r} \right] + \frac{z_i D_i F}{RT} \left[\frac{\partial^2 \varphi}{\partial r^2} + \frac{1}{r} \frac{\partial \varphi}{\partial r} \right] - v \frac{\partial C_i}{\partial r} - \frac{C_i}{r} \frac{\partial}{\partial r} (rv) \qquad \text{(III-54)}$$

where v is the velocity vector for the flow of water toward the surface and "*i*" indexes the species involved (H_2, O_2, H_2O_2, OH^-, HS^-). In the case of an incompressible fluid, $\frac{\partial}{\partial r}(rv) = 0$, and we have

$$\frac{\partial C_i}{\partial t} + v \frac{\partial C_i}{\partial r} = D_i \left[\frac{\partial^2 C_i}{\partial r^2} + \frac{1}{r} \frac{\partial C_i}{\partial r} \right] + \frac{z_i D_i F}{RT} \left[\frac{\partial^2 \varphi}{\partial r^2} + \frac{1}{r} \frac{\partial \varphi}{\partial r} \right] \qquad \text{(III-55)}$$

or

$$\frac{\partial C_i}{\partial t} = D_i\left[\frac{\partial^2 C_i}{\partial r^2} + \frac{1}{r}\frac{\partial C_i}{\partial r}\right] + \frac{z_i D_i F}{RT}\left[\frac{\partial^2 \varphi}{\partial r^2} + \frac{1}{r}\frac{\partial \varphi}{\partial r}\right] - v\frac{\partial C_i}{\partial r} \qquad \text{(III-56)}$$

and

$$\frac{\partial C_i}{\partial t} = D_i\frac{\partial^2 C_i}{\partial r^2} + \frac{z_i D_i F}{RT}\left(\frac{\partial^2 \varphi}{\partial r^2}\right) + \frac{z_i D_i F}{RT}\left(\frac{1}{r}\frac{\partial \varphi}{\partial r}\right) - \left(v - \frac{D_i}{r}\right)\frac{\partial C_i}{\partial r} \qquad \text{(III-57)}$$

These equations must be applied to predict the movement of the species, HS^-, H_2, O_2, H_2O_2, OH^-, and H^+ to or from the canister surface, recognizing that the species may be generated radiolytically or chemically at some point away from the surface, because of the presence of ionizing radiation or chemical reactions. For the first five species, we write:

$$\frac{\partial C_{HS^-}}{\partial t} = D_{HS^-}\frac{\partial^2 C_{HS^-}}{\partial r^2} - \frac{D_{HS^-}F}{RT}\left(\frac{\partial^2 \varphi}{\partial r^2}\right) - \frac{D_{HS^-}F}{RT}\left(\frac{1}{r}\frac{\partial \varphi}{\partial r}\right) - \left(v - \frac{D_i}{r}\right)\frac{\partial C_{HS^-}}{\partial r}$$
$$- k_5 C_{HS^-} C_{O_2} - k_6 C_{HS^-} C_{H_2O_2} \qquad \text{(III-58)}$$

$$\frac{\partial C_{H_2}}{\partial t} = D_{H_2}\frac{\partial^2 C_{H_2}}{\partial r^2} - \left(v - \frac{D_{H_2}}{r}\right)\frac{\partial C_{H_2}}{\partial r} + \left(\frac{\partial C_{H_2}}{\partial t}\right)_{rad} \qquad \text{(III-59)}$$
$$- k_7 C_{H_2} C_{O_2} - k_8 C_{H_2} C_{H_2O_2}$$

$$\frac{\partial C_{O_2}}{\partial t} = D_{O_2}\frac{\partial^2 C_{O_2}}{\partial r^2} - \left(v - \frac{D_{H_2}}{r}\right)\frac{\partial C_{O_2}}{\partial r} + \left(\frac{\partial C_{O_2}}{\partial t}\right)_{rad} - k_7 C_{H_2} C_{O_2} \qquad \text{(III-60)}$$

$$\frac{\partial C_{H_2O_2}}{\partial t} = D_{H_2O_2}\frac{\partial^2 C_{H_2O_2}}{\partial r^2} - \left(v - \frac{D_{H_2}}{r}\right)\frac{\partial C_{H_2O_2}}{\partial r} + \left(\frac{\partial C_{H_2O_2}}{\partial t}\right)_{rad} - k_8 C_{H_2} C_{H_2O_2} \qquad \text{(III-61)}$$

and

$$\frac{\partial C_{OH^-}}{\partial t} = D_{OH^-}\frac{\partial^2 C_{OH^-}}{\partial r^2} - \frac{D_{OH^-}F}{RT}\left(\frac{\partial^2 \varphi}{\partial r^2}\right) - \frac{D_{OH^-}F}{RT}\left(\frac{1}{r}\frac{\partial \varphi}{\partial r}\right) - \left(v - \frac{D_i}{r}\right)\frac{\partial C_{OH^-}}{\partial r} + \left(\frac{\partial C_{OH^-}}{\partial t}\right)_{rad} \quad \text{(III-62)}$$

For calculating the concentration of hydrogen ion (H^+) we invoke the autoprotolysis of water and write:

$$C_{H^+} = K_W / 10^6 C_{OH^-} \quad \text{(III-63)}$$

where the concentrations have units of mol/cm^3.

These six coupled, non-linear, second order partial differential equations must be solved simultaneously to determine the species concentrations as a function of distance, $r > r_c$, and time, $t > 0$. Developing solutions to these equations first requires specification of the initial ($t = 0$) and boundary ($t > 0$; $r = r_c$; $r = r_b$), where r_c and r_b are the canister radius and the buffer radius, respectively.

Initial conditions ($t = 0$, $r_c < r < r_b$):

The initial conditions correspond to those that exist prior to the initiation of radiolysis and corrosion of the canister and can be written as: $C_{HS^-} = C^b_{HS^-}$, $C_{H_2} = C^b_{H_2}$, $C_{O_2} = C^b_{O_2}$, $C_{H_2O_2} = 0$, $C_{OH^-} = 10^{-(pK_W - pH) - 3}$ (mol/cm^3), where $pK_w = -\log(K_W)$ and K_W is the ionic product of liquid water, which is expressed as:

$$K_w = 10^{[-(4466.2/T - 5.941 + 0.016638T)]} \quad \text{(III-64)}$$

T is the Kelvin temperature. It is assumed that the initial state corresponds to the end of the resaturation period when the bentonite buffer is fully inundated with repository water and the bentonite is fully hydrated.

Boundary Condition ($t > 0$, $r = r_c$):

The boundary conditions at the canister surface are expressed in terms of the fluxes as

$$J_{HS^-} = -D_{HS^-}\frac{\partial C_{HS^-}}{\partial r} + \frac{F}{RT}D_{HS^-}C_{HS^-}\frac{d\phi}{dx} + vC_{HS^-} = -k_1^0 e^{a_1 E} C^s_{HS^-} C^s_{OH^-} = -\frac{i_1}{2F} \quad \text{(III-65)}$$

$$J_{H_2} = -D_{H_2}\frac{\partial C_{H_2}}{\partial r} + vC_{H_2} = k_{-2}^0 e^{-b_2 E} - k_2^0 e^{a_2 E} C_{H_2}^s \left(C_{OH-}^s\right)^2 = \frac{i_2}{F} \qquad \text{(III-66)}$$

$$J_{O_2} = -D_{O_2}\frac{\partial C_{O_2}}{\partial r} + vC_{O_2} = -k_{-3}^0 e^{-b_3 E} C_{O_2}^s = \frac{i_3}{4F} \qquad \text{(III-67)}$$

$$J_{H_2O_2} = -D_{H_2O_2}\frac{\partial C_{H_2O_2}}{\partial r} + vC_{H_2O_2} = -k_{-4}^0 e^{-b_4 E} C_{H_2O_2}^s = \frac{i_4}{2F} \qquad \text{(III-68)}$$

$$J_{OH^-} = -D_{OH^-}\frac{\partial C_{OH^-}}{\partial r} + \frac{F}{RT}D_{OH^-}C_{OH^-}\frac{d\phi}{dx} + vC_{OH^-} = -k_1^0 e^{a_1 E} C_{HS^-}^s C_{OH^-}^s$$
$$- k_2^0 e^{a_2 E} C_{HS^-}^s \left(C_{OH^-}^s\right)^2 + 2k_{-2}^0 e^{-b_2 E} + 4k_{-3}^0 e^{-b_3 E} C_{O_2}^s + 2k_{-4}^0 e^{-b_4 E} C_{H_2O_2}^s = J_{HS^-} + 2J_{H_2}$$
$$- 4J_{O_2} - 2J_{H_2O_2}$$

(III-69)

and

$$i_1 + i_2 + i_3 + i_4 = 0 \qquad \text{(III-70)}$$

Note that $i_1 > 0, i_2 > 0$ or $< 0, i_3 < 0,$ and $i_4 < 0$, with the sign of i_2 depending upon the relative values of the equilibrium potential for Reaction (III-37) and the corrosion potential. Further note that, according to the Point Defect Model (PDM) [6,7], i_1 has the form of Equation (III-46) with a_1 = 0 for a n-type passive film or with $a_1 > 0$ for a p-type passive film. As noted above, the electronic character of the Cu_2S film that forms on copper under repository conditions has yet to be determined and the experiments required to resolve these issues are scheduled to be performed in Phase III.

Boundary Condition ($r = r_b$):

This boundary condition corresponds to the physico-chemical conditions that exist at the buffer/rock interface.

$C_{HS^-} = C_{HS^-}^b$, $C_{H_2} = C_{H_2}^b$, $C_{O_2} = C_{O_2}^b$, $C_{H_2O_2} = 0$, $C_{OH^-} = 10^{-(pK_W - pH) - 3}$ (mol/cm^3),

where pK_w = -log(K_W) and K_W is the ionic product of liquid water, as given by Equation (III-64). It is assumed that a source of HS^- exists in the rock that maintains the concentration of this species constant at the buffer/rock boundary. It has been reported that the bentonite contains FeS_2, which, by virtue of dissolution and dissociation, will also act as a source of HS^- as follows: $FeS_2 + H^+ \rightarrow Fe^{2+} + S + HS^-$. This reaction has not yet been incorporated into the present model, due to a lack of data for the kinetics, but it is easily included once the required data are on hand. The net effect of including the reaction in the

model will be to significantly increase the supply of HS^- to the copper surface, by an amount depending upon the value of the rate constant for pyrite dissolution. We should note that sufficient HS^- is present in the groundwater to activate copper, so that the inclusion of the pyrite dissolution reaction does not impact whether activation of copper will occur, but it will impact the rate of copper dissolution for at least as the supply of FeS_2 lasts in the near-field environment (buffer).

Radiolysis of Water

The radiolytic production of species *i* is calculated from the equation

$$\left(\frac{\partial C_i}{\partial t}\right) = \frac{G_{i,\gamma}\Gamma_\gamma}{100 N_V} \qquad \text{(III-71)}$$

with $i \equiv H_2, O_2, H_2O_2$, and $G_{i,\gamma}$, Γ_γ, and N_V are the radiolytic yield (# of particles/100 eV of energy absorbed) of Species "*i*" for γ irradiation, the dose rate (eV/cm^3.s) of γ photons absorbed, and Avogadro's number (N_V = 6.023 x 10^{23} molecules/mol), respectively. The dose rate is presumed to decay exponentially with distance from the canister surface as:

$$\Gamma_\gamma = \Gamma_\gamma^0 e^{-\mu(r-r_c)} \qquad (r \geq r_c) \qquad \text{(III-72)}$$

where μ is the absorption coefficient with dimensions of L^{-1}. Thus, it is evident from Equations (III-71) and (III-72) that the rate of radiolytic production of H_2, O_2, and H_2O_2also decays exponentially with distance from the canister surface. Finally, the dose rate at the surface of the canister decreases with the radioactive decay of the principal γ-emitting component(s) of the waste. In the case of Swedish HLNW, the principal γ-emitting component(s) of the waste is $^{137}Cs_{55}$ which has a half-life of 30.17 years, decaying to $^{137}Ba_{56}$ by β emission and subsequent emission of a γ-photon (1.176 MeV) from the excited state. Since radioactive decay is a first-order kinetic process, the dose rate at the canister surface is readily expressed as

$$\Gamma_\gamma^0 = \Gamma_\gamma^{00} e^{-\alpha t} \qquad \text{(III-73)}$$

where Γ_γ^{00} is the initial dose rate at the canister surface and α is the decay constant ($a = 0.693 / t_{1/2}$ = 0.023 yr^{-1}). Thus, the final expression for the dose rate at any distance from the canister surface and at any time after placement of the waste is:

$$\Gamma_\gamma = \Gamma_\gamma^{00} e^{-0.693 t / t_{1/2}} e^{-\mu(r-r_c)} \qquad \text{(III-74)}$$

The value for μ was taken to be 10 cm^{-1}, which is typical for the absorption of γ-photons by water and concrete.

Temperature

Since the decay of the radioactive waste produces heat, and because many of the parameters in the model are temperature-dependent, it is necessary to predict the decay in the temperature as a function of time and distance away from the canister. The variation of the temperature with time and distance from the canister surface has been modeled by SKB [4] and the data are plotted in Figure III-21. We represent the temperature as an empirical polynomial of the form

$$T(j,i) = ((\log_{10}(t(j)))^2) * ((rr_1(1) * x_2(i)^2 + rr_1(2) * x_2(i) + rr_1(3))) + ((\log_{10}(t(j)))) * (rr_2(1) * x_2(i)^2 + rr_2(2) * x_2(i) + rr_2(3)) + (rr_3(1) * x_2(i)^2 + rr_3(2) * x_2(i) + rr_3(3)) + 273.15 \quad \text{(III-75)}$$

where index *j* indicates time and index *i* indicates distance. The coefficients in this equation are summarized in Table III-9.

Table III-11: Parameters used in Equation (III-75) in interpolating temperature as a function of time and distance.

Parameter	**Canister surface**	**Edge of disposal hole**	**Rock between tunnels**
ab	0.4565	-0.8110	55.3945
ac	-1.0796	-6.4962	82.0913
rr_1	-5.3406	7.9219	-3.3939
rr_2	-48.7301	72.2830	-27.6126
rr_3	228.8299	-339.4310	181.2509

The constants given in Table III-11(*ab, ac, rr1, rr2, rr3*) are coefficients obtained by fitting polynomials of order 2 to the 3 experimental curves given in Figure III-21. The polynomials are of the form $ab(1)*\log10(T)^2 + ab(2) * \log10(T) + ab(3)$ and are of similar form for the *ac* coefficients. Those 6 coefficients (3 for *ab* and 3 for *ac*) at the distances at which temperature is given in Figure III-21 were fitted to a second 2nd order polynomial and rr_1, rr_2, and rr_3 were obtained. Accordingly, the rr_1, rr_2, and rr_3 coefficients are functions of $\log_{10}(T)$ and *x*. The rr_1, rr_2, and rr_3 coefficients are used to reconstruct the curves shown in Figure III-21 and hence to interpolate temperature values as a function of distance and time, in order to simulate the system at 17 temporal and spatial points (see below). A good approximation of the temperature versus time between the canister and the host rock is obtained by using the obtained equation.

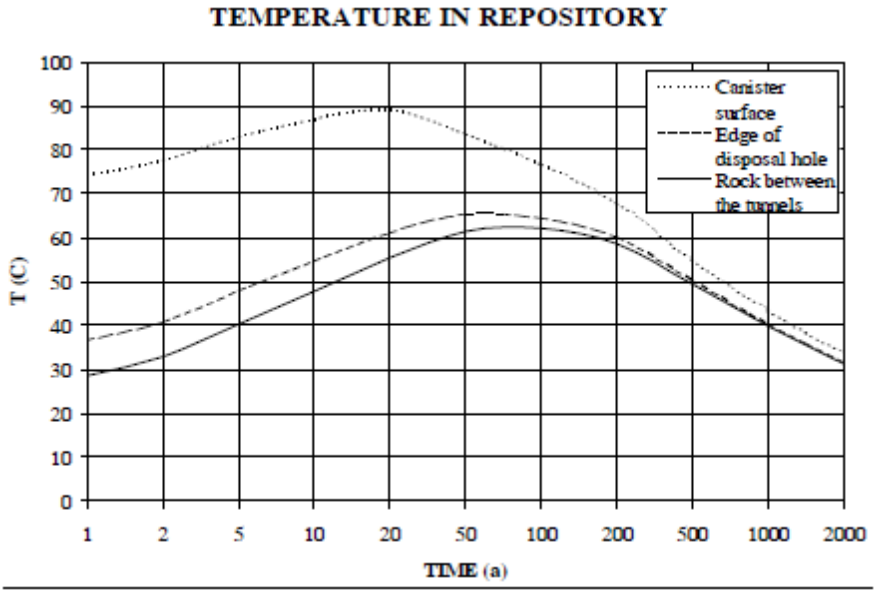

Figure III-21: Predicted variation of temperature with time at the canister surface (r_c), edge of the disposal hole (r_b), and rock between the tunnels. After King, et. al. [4].

Potential Distribution

Because of the high ionic strength compared with the concentrations of H^+, HS^- and OH^-, (10^{-8}, $0.9x10^{-4}$, and 10^{-6} M, respectively, as given in Table III-12), and because all other species of interest (H_2, O_2, H_2O_2) are uncharged, migration can be ignored, under the "indifferent electrolyte" condition of electrochemistry. Accordingly, it is unnecessary to solve for the electrical potential distribution in the near-field environment, which significantly simplifies the mass transport problem.

Table III-12: Chemical composition of the groundwater at repository depth in the forsmark-North Uppland area estimated within the SR-Can project. The concentrations are given both in mg/L and mol/L (M). Those parameters considered important for corrosion of the cinster are high-lighted in bold font. Nitrogen compounds (ammonium and nitrite) were not evaluated as part of the SR-Can project.[4]

Constituent		At closure	After resaturation (< 100y after closure)	10,000 years into the future
pH		**6–9**	**7.1–8.7**	**6.7–8.3**
Eh	**mV**	**0 to –280**	**–190 to –280**	**–150 to –260**
Na^+	mg/L	90–3,750	90–3,750	65–2,860
	M	$(4–163)\cdot10^{-3}$	$(4–163)\cdot10^{-3}$	$(3–124)\cdot10^{-3}$
K^+	mg/L	1–136	1 –136	6–104
	M	$(0.3–35)\cdot10^{-4}$	$(0.3–35)\cdot10^{-4}$	$(2–27)\cdot10^{-4}$
Ca^{2+}	mg/L	58–1,900	58–1,900	56–1,580
	M	$(1.4–47)\cdot10^{-3}$	$(1.4–47)\cdot10^{-3}$	$(1.4–39)\cdot10^{-3}$
Mg^{2+}	mg/L	0.1–460	0.1–460	12–345
	M	$(0.01–19)\cdot10^{-3}$	$(0.01–19)\cdot10^{-3}$	$(0.5–14)\cdot10^{-3}$
HCO^{3-}	mg/L	5–290	5–290	19–290
	M	$(0.1–4.8)\cdot10^{-3}$	$(0.1–4.8)\cdot10^{-3}$	$(0.3–5)\cdot10^{-3}$
Cl^-	**mg/L**	**95–6,900**	**95–6,900**	**16–5,500**
	M	**$(2.7–194)\cdot10^{-3}$**	**$(2.7–194)\cdot10^{-3}$**	**$(0.3–154)\cdot10^{-3}$**
SO_4^{2-}	mg/L	19–900	19–900	19–690
	M	$(0.2–9.4)\cdot10^{-3}$	$(0.2–9.4)\cdot10^{-3}$	$(0.2–7.2)\cdot10^{-3}$
HS^-	**mg/L**	**0–0.3**	**0–0.30**	**0–0.23**
	M	**$0–10^{-5}$**	**$0–10^{-5}$**	**$0–10^{-5}$**

Convection of Water Through the Buffer

Finally, we note that water is consumed at the copper surface via (the reverse of Reaction (III-37), which is the cathodic partial reaction occurring in the system under anoxic conditions. The rate of consumption of water per centimeter squared can be expressed as:

$$\frac{dm_{H_2O}}{dt} = \left(i_{-2} - i_2\right)/F \qquad \text{(III-76)}$$

and the volume of water consumed per unit time per centimeter squared of the copper surface is written as

$$\frac{dV_{H_2O}}{dt} = \Omega_{H_2O}\frac{dm_{H_2O}}{dt} = \Omega_{H_2O}\left(i_{-2} - i_2\right)/F \qquad \text{(III-77)}$$

where Ω_{H_2O} is the molar volume of water (18.016 cm^3/mol at 25 ^oC). The water is envisioned to flow through the porous bentonite buffer, in which case the velocity of the water (in cm/s) being transported to the copper surface becomes:

$$v = \frac{dV_{H_2O}}{dt} / \varepsilon = \Omega_{H_2O} \frac{dm_{H_2O}}{dt} / \varepsilon = \Omega_{H_2O} \left(i_{-2} - i_2\right) / \varepsilon F \qquad \text{(III-78)}$$

where ε is the porosity of the bentonite buffer. As a "back-of-the-envelope" calculation, we select $\left(i_{-2} - i_2\right)$ = 10^{-9} A/cm^2, ε = 0.001, Ω_{H_2O} = 20, and F =10^5 C/equiv to yield the flow velocity as $2x10^{-10}$ cm/s. This is a very low number ($2x10^{-3}$ nm/s), but the relevance of convective transport must be judged in comparison with diffusional transport by calculating the respective fluxes, which are given by: $J_{conv,i} = vC_i$ and $J_{diff,i} = -D_i\left(\partial C_i / \partial r\right)$. From Table III-12, it is evident that the concentrations of HS^-, H^+, and OH^- are of the order of $<10^{-5}$, 10^{-6} to 10^{-9}, and 10^{-8} to10^{-5}mol/cm^3. Thus, the convective fluxes become: $2x10^{-17}$, $2x10^{-21}$, and $2x10^{-19}$ mol/cm^2.s, respectively. In terms of current densities, the corresponding contributions of the convective fluxes will be $FJ_{conv,i}$ or $2x10^{-12}$, $2x10^{-16}$, and $2x10^{-14}$ A/cm^2. These are orders of magnitude smaller than the expected corrosion current density, so that convection may be ignored in calculating the fluxes of the cathodic depolarizers.

Final Model Equations

From the above analysis, we conclude that a viable model for canister corrosion should considered diffusional transport to the canister surface, but that migration and convection can be ignored, because of the high background concentration of indifferent electrolyte and the low rate of water consumption at the canister surface, even under anoxic conditions, respectively. Accordingly, the equations of the model become:

$$\frac{\partial C_{HS^-}}{\partial t} = D_{HS^-} \frac{\partial^2 C_{HS^-}}{\partial r^2} + \frac{D_{HS^-}}{r} \frac{\partial C_{HS^-}}{\partial r} - k_5 C_{HS^-} C_{O_2} - k_6 C_{HS^-} C_{H_2O_2} \qquad \text{(III-79)}$$

$$\frac{\partial C_{H_2}}{\partial t} = D_{H_2} \frac{\partial^2 C_{H_2}}{\partial r^2} + \frac{D_{H_2}}{r} \frac{\partial C_{H_2}}{\partial r} + \left(\frac{\partial C_{H_2}}{\partial t}\right)_{rad} - k_7 C_{H_2} C_{O_2} - k_8 C_{H_2} C_{H_2O_2} \qquad \text{(III-80)}$$

$$\frac{\partial C_{O_2}}{\partial t} = D_{O_2} \frac{\partial^2 C_{O_2}}{\partial r^2} + \frac{D_{O_2}}{r} \frac{\partial C_{O_2}}{\partial r} + \left(\frac{\partial C_{O_2}}{\partial t}\right)_{rad} - k_7 C_{H_2} C_{O_2} \qquad \text{(III-81)}$$

$$\frac{\partial C_{H_2O_2}}{\partial t} = D_{H_2O_2}\frac{\partial^2 C_{H_2O_2}}{\partial r^2} + \frac{D_{H_2}}{r}\frac{\partial C_{H_2O_2}}{\partial r} + \left(\frac{\partial C_{H_2O_2}}{\partial t}\right)_{rad} - k_8 C_{H_2} C_{H_2O_2} \quad \text{(III-82)}$$

and

$$\frac{\partial C_{OH^-}}{\partial t} = D_{OH^-}\frac{\partial^2 C_{OH^-}}{\partial r^2} + \frac{D_{OH^-}}{r}\frac{\partial C_{OH^-}}{\partial r} + \left(\frac{\partial C_{OH^-}}{\partial t}\right)_{rad} \quad \text{(III-83)}$$

For calculating the concentration of hydrogen ion (H^+), we invoke the autoprotolysis of water and write:

$$C_{H^+} = K_W / 10^6 C_{OH^-} \quad \text{(III-84)}$$

where the concentrations of H^+ and OH^- are given in units of mol/cm3. These six coupled, non-linear, second order partial differential equations must be solved simultaneously to determine the species concentrations as a function of distance, $r > r_c$, and time, $t > 0$. Developing solutions to these equations first requires specification of the initial ($t = 0$) and boundary ($t > 0$; $r = r_c$; $r = r_b$), where r_c and r_b are the canister radius and the buffer radius, respectively.

Final Initial and Boundary Conditions

Initial conditions ($t = 0$, $r_c < r < r_b$):

The initial conditions correspond to those that exist throughout the buffer prior to the initiation of radiolysis and reaction at the canister surface and can be written as:

$C_{HS^-} = C^b_{HS^-}$, $C_{H_2} = C^b_{H_2}$, $C_{O_2} = C^b_{O_2}$, $C_{H_2O_2} = 0$, $C_{OH^-} = 10^{-(pK_W - pH) - 3}$ (mol/cm^3), where pK_w = -log(K_W) and K_W is the ionic product of liquid water, which is expressed as:

$$K_w = 10^{[-(4466.2/T - 5.941 + 0.016638T)]} \quad \text{(III-85)}$$

where T is the Kelvin temperature.

Boundary Condition ($t > 0$, $r = r_c$):

The revised boundary conditions at the canister surface are expressed in terms of the fluxes as

$$J_{HS^-} = -D_{HS^-}\frac{\partial C_{HS^-}}{\partial r} = -k_1^0 e^{a_1 E} C_{HS^-}^s C_{OH^-}^s = -\frac{i_1}{2F} \quad \text{(III-86)}$$

$$J_{H_2} = -D_{H_2}\frac{\partial C_{H_2}}{\partial r} = k_{-2}^0 e^{-b_2 E} - k_2^0 e^{a_2 E} C_{H_2}^s \left(C_{OH-}^s\right)^2 = \frac{i_2}{F} \quad \text{(III-87)}$$

$$J_{O_2} = -D_{O_2}\frac{\partial C_{O_2}}{\partial r} = -k_{-3}^0 e^{-b_3 E} C_{O_2}^s = \frac{i_3}{4F} \quad \text{(III-88)}$$

$$J_{H_2O_2} = -D_{H_2O_2}\frac{\partial C_{H_2O_2}}{\partial r} = -k_{-4}^0 e^{-b_4 E} C_{H_2O_2}^s = \frac{i_4}{2F} \quad \text{(III-89)}$$

$$J_{OH^-} = -D_{OH^-}\frac{\partial C_{OH^-}}{\partial r} + \frac{F}{RT} D_{OH^-} C_{OH^-}\frac{d\phi}{dx} + \nu C_{OH^-} = -k_1^0 e^{a_1 E} C_{HS^-}^s C_{OH^-}^s$$
$$- k_2^0 e^{a_2 E} C_{HS^-}^s \left(C_{OH^-}^s\right)^2 + 2k_{-2}^0 e^{-b_2 E} + 4k_{-3}^0 e^{-b_3 E} C_{O_2}^s + 2k_{-4}^0 e^{-b_4 E} C_{H_2O_2}^s = J_{HS^-} + 2J_{H_2}$$
$$- 4J_{O_2} - 2J_{H_2O_2} \quad \text{(III-90)}$$

and

$$i_1 + i_2 + i_3 + i_4 = 0 \quad \text{(III-91)}$$

Note that $i_1 > 0, i_2 > 0$ or $< 0, i_3 < 0,$ and $i_4 < 0$, with the sign of i_2 depending upon the relative values of the equilibrium potential for Reaction (III-37) and the corrosion potential.

Boundary Condition ($r = r_b$):

The revised boundary conditions for the buffer/rock interface are now written as:

$C_{HS^-} = C_{HS^-}^b$, $C_{H_2} = C_{H_2}^b$, $C_{O_2} = C_{O_2}^b$, $C_{H_2O_2} = 0$, $C_{OH^-} = 10^{-(pK_W - pH)-3}$ (mol/cm^3), where pK_w = -log(K_W) and K_W is the ionic product of liquid water, as given by Equation (III-64).

As in the case of the cathodic partial reactions and the anodic oxidation of copper in the presence of sulphide ion, as noted above, no kinetic data could be found for the Point Defect Model representation of the anodic oxidation copper in the presence of sulphide, as described above. Also, no PDM data could be found for the anodic oxidation of copper in the absence of sulphide ion, where cuprous oxide is expected to form. Accordingly, the full implementation of the theory for estimating the corrosion potential and the corrosion rate, and hence the accumulated corrosion damage, is not possible at this time. We are scheduled to make these measurements in a Phase III of the present program. We should note that the measurement of the values for the PDM parameters involves optimizing of the expression for the impedance developed from the PDM on experimental electrochemical impedance spectroscopy (EIS) data, as described above for estimating the corrosion potential. We have developed these techniques to a high degree of sophistication in our work on the corrosion of carbon steel overpack in contact with simulated concrete pore water as part of Belgium's program on the isolation of HLNW, but they have never been applied to the formation of sulphide films on copper or on any other metal. As indicated above, we will use "guesstimated" parameter values to carry out illustrative calculations. However, the results should not be taken to represent what exists in the repository, for that calculation will require parameter values determined for the formation of cuprous sulphide films.

Model Algorithm

We solved the coupled partial differential equations using MATLAB. We used a built-in program that solves initial-boundary value problems for systems comprising parabolic and elliptic partial differential equations (PDEs) in one dimension and as a function of time. The ordinary differential equations (ODEs) resulting from discretization in space are integrated to obtain approximate solutions at times specified in the time vector ("t-span"). The function returns values of the solution on a distance-time mesh provided by the users. We chose to provide a mesh describing the bentonite buffer with distance between the canister surface and the bed rock specified as being the "x-span" (x-vector) and a similar mesh for the variation of the concentrations of the different species involved in the reactions and diffusing through the bentonite for different times. Details of the algorithm can be obtained from the literature [8-14].

We choose to work in cylindrical coordinates; accordingly, only the radial distance is plotted when describing the spatial distribution of species within the buffer. Accordingly, we plot the species concentration versus radial distance and time, the corrosion potential at the canister surface as a function of time, and the integrated loss of metal by the canister also as a function of time. The plotting independent variables are time -which for the present, illustrative calculations was chosen to be between 0 and 2000 years- and distance between the canister surface and bed rock (0 – 10 cm). There is symmetry on the angle between zero and 2π degrees at each radial distance; accordingly, it is not necessary to plot the variation of the angle around the canister as an independent parameter.

Parameterizing Functions are called by Function in the MATLAB program and the Mathematics Documentation explains how to provide additional parameters to the functions.

The defaults of the optimization parameter obtained by leaving off the input argument options will generally be satisfactory. Accordingly, default Optimization parameters were used in the solving the set of partial differential equations.

The function used performs the time integration with an ODE solver that selects both the time and the steps in the numerical formula dynamically. The elements of the *t*-mesh merely specify the time from initial exposure at which one wants to simulate the system and the cost depends weakly on the length of *t*-vector. The 17 temporal points between 10^{-8} year to 2000 years are given in the following vector ("*t*-scan")

t = [0.00000001, 0.0000001, 0.000001, 0.0001, 0.01, 0.1, 1, 2, 5, 10, 20, 50, 100, 200, 500, 1000, 2000], where the values are in years.

Likewise, the x-mesh specifies the 17 spatial points between the canister surface and the buffer/rock interface at which the specie concentrations and corrosion potential, and hence corrosion rate are calculated. These points are specified in the vector x_2 below

x = [0.01, 0.03, 0.06, 0.1, 0.15, 0.2, 0.25, 0.3, 0.35, 0.4, 0.45, 0.5, 0.6, 0.7, 0.8, 0.9, 1].*(r_b-r_c)+r_c. The values of *x* are in centimeters.

Generally, it is best to use closely spaced mesh points where the solution changes rapidly, because the functions used in MATLAB do not select the vector size or spatial steps automatically. Failing to choose appropriate vector lengths leads to a lack of convergence. The cost in computational time depends strongly on the length of the *x*-vector. It is not always necessary to use a fine mesh near the coordinate singularity that may appear when seeking a solution and upon inversion of the matrices. The time integration is done with the MATLAB function "ode15s", which exploits the capabilities of the code for solving the differential-algebraic equations that arise when elliptic equations are employed, using Jacobians with a specified sparsity pattern. After discretization, elliptic equations give rise to algebraic equations. If the elements of the initial conditions vector that correspond to elliptic equations are not "consistent" with the discretization, the function tries to adjust them before beginning the time integration. For this reason, the solution returned for the initial time may have a discretization error comparable to that at any other time. If the mesh is sufficiently fine, the algorithm can find consistent initial conditions close to the given ones.

The corrosion potential is needed to solve for the species concentrations and vice verse. Accordingly, an external loop is created to solve for the vector Corrosion Potential as a function of time. The external function uses a different MATLAB function that is equivalent to a function for finding the roots of an equation.

The nonlinear equations that need to be solved are used in the function Fun; which is a function that accepts a vector x and returns a vector *F*. The nonlinear equations are evaluated at *x*. The function Fun computes values at time *t* and distance *x* in the spatial mesh. If the user-defined values for *x* and *F* are matrices, they are converted into vectors using linear indexing. If the Jacobian can also be computed it is done so using 'Jacobian'. If

it is not convenient to compute the Jacobian matrix, *J*, in Fun when the structure is unknown; instead, the Jacob Pattern can be set to be a dense matrix and a full finite-difference approximation is computed in each interaction (this is the default if Jacob Pattern is not set). This can be very expensive for large problems, so it is usually worth the effort to determine the sparsity structure.

Table III-13: Model parameter values employed in the illustrative calculation of corrosion potential and corrosion rate for copper canisters in a Swedish HLNW repository and for the prediction of specie concentrations in the bentonite buffer.

Parameter	Value	Parameter	Value	Parameter	Value
D_{HS^-}	7×10^{-8} cm^2/s	k_6^0	1×10^{-5}	$C_{HS^-}^b$	1×10^{-7} mol/cm^3
D_{H_2}	6×10^{-8} cm^2/s			$C_{H_2}^b$	2×10^{-8} mol/cm^3
D_{O_2}	5×10^{-8} cm^2/s	k_7^o	1×10^{-6}	$C_{O_2}^b$	0 mol/cm^3
$D_{H_2O_2}$	3×10^{-8} cm^2/s	k_8^o	1×10^{-6}	$C_{H_2O_2}^b$	0 mol/cm^3
D_{OH^-}	7×10^{-8} cm^2/s	k_5^o	1×10^{-4}	$C_{OH^-}^b$	$10^{-(pK_w-pH)}/1000$ mol/cm^3
k_1^0	8×10^{-1}	a_1	0.9 V^{-1}		
k_2^0	1×10^{-2}	a_2	0.9V^{-1}		
k_{-2}^0	1×10^{-17}	b_2	0.99 V^{-1}		
k_{-3}^0	1×10^{-9}	b_3	0.99 V^{-1}		
k_{-4}^0	1×10^{-11}	b_4	0.99V^{-1}		
G_{H_2}	0.45 No/100eV	Γ_γ	1 , 10, 100 Gy/hr	$E_{a,5}$	4×10^3 J/mol
G_{O_2}	0.40 No/100eV	F	96,487 C/equiv	$E_{a,6}$	4×10^3 J/mol
$G_{H_2O_2}$	0.72 No/100eV	R	8.314 J/K.mol	$E_{a,7}$	4×10^3 J/mol
G_{OH^-}	0.10 No/100eV	N_v	6.023×10^{23} molecules/mol	$E_{a,8}$	4×10^3 J/mol

Dose Rate = 0.0278 rad/s (1 Gy/h)

Little information exists in the literature on the rate and other constants for the various reactions in PEM. In order to test the algorithm, using as the computational criterion the convergence of the corrosion potential on the distance values and times chosen in the *x*- and *t*-vectors (17 points on each), the set of parameters listed in Table III-13 below were chosen. These parameter values are also considered to be realistic, but we stress that

they are not based on experiment and hence should not be expected to yield physically realistic results. We note that for the present purposes of testing the algorithm, the exact vales of the model parameters is not important, and that some of the values reported in Table III-13 may be significantly different from those reported in various SKB reports. Also, the radius of the canister measured from the axis was taken as 40-cm and the radius of the bore-hole was set at 75-cm, again measured from the axis of the canister. The actual values, conveyed to the authors by SSM, are 52.5-cm and 92.5-cm, respectively. The actual values will be used in the final simulations carried out in Phase III.

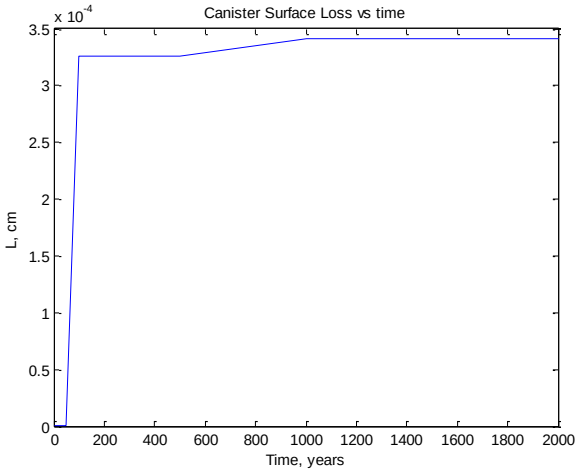

Figure III-22: Plot of calculated loss of copper over a 2000 year period for an initial γ-dose rate of 1 Gy/h (0.0278 rad/s).

In performing the simulations, the equations were solved for seventeen times within the total exposure time of 2000 years and at 17 locations for $r_c < r < r_b$. The times were selected, because they resulted in good convergence of the solutions for the concentrations of the various species and the potential. In those cases, where the convergence was relatively poor, the uncertainty in the calculated dependent variable is indicated by the error bar for that case. This is illustrated in Figure III-23 for the calculated corrosion potential. The convergence may be greatly improved by increasing the number of iterations, but only at the cost of increased computational time. Note that each curve (L, E) or surface concentrations are specified at 17 spatial points or 17x17 spatial x temporal points, respectively.

Because of the lack of a viable, experimentally-determined set of values for various model parameters, the full use of the model developed in this work must await the experimental determination of requisite parameters. However, as noted above, it was necessary to test the algorithm and to determine the general nature of the predictions that the model can yield. To do this, we have assembled a set of "guesstimated" parameter values in Table III-13, which are used here for evaluation of the algorithm only. *No credence must be placed in the predictions, until experimentally-determined parameter values are available.*

These values are expected to be measured in a two-year, Phase III program beginning in 2012. We therefore proceed to test the algorithm upon this basis and we refrain from making any predictions that might impact repository performance.

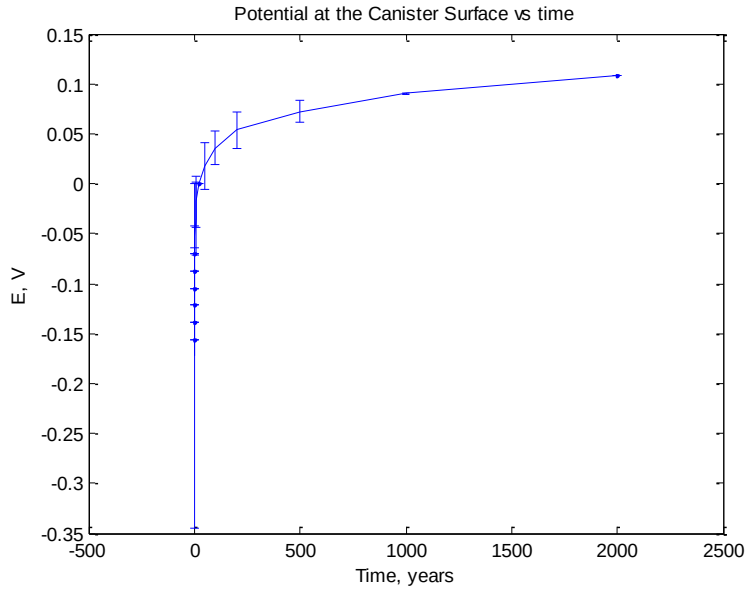

Figure III-23: Plot of calculated corrosion potential of copper over a 2000 year period for an initial γ-dose rate of 1 Gy/h (0.0278 rad/s).

The predicted loss of copper over the 2000 year exposure under base-case conditions [γ-dose rate of 0.0278 rad/s (1 Gy/h)] is shown in Figure III-22. The loss of metal is predicted to occur sharply at short times, as the sulphide ion and cathodic depolarizers in the local environment (immediately adjacent to the canister surface), some of which are produced by the radiolysis of water when the dose rate is highest (i.e., at short times), are consumed. Thereafter, the loss of metal is controlled by the transport of HS^- through the entire bentonite buffer and the rate of metal loss drops to a low value. Note that the bisulphide ion is also postulated to be consumed by reaction with the radiolysis products (O_2 and H_2O_2) at rates that depend upon the distance away from the canister surface.

With regard to the electrochemical corrosion potential (*ECP*, Figure III-23), the corrosion potential is predicted to rise sharply over the first 200 years and then drift in the positive direction more slowly thereafter. This positive shift with time is attributed to the falling temperature at the canister surface (see Figure III-21) and possibly due to the build up of oxidizing radiolysis products, most notably O_2 and H_2O_2. We note that the *ECP* lies within the range of 0.1 V_{she} to -0,35 V_{she}, which covers the range that is indicated for the redox potential in Table III-12(E_h = 0 to -0.45 V_{she}). However, we caution the reader that the *ECP* and the redox potential are entirely different quantities, and that their comparison must be made with considerable caution. Generally speaking, the *ECP* is more positive than E_{redox}, everything else being the same, because of the existence of a positive partial anodic current from dissolution of the substrate that is not present in the establishment of E_{redox}.

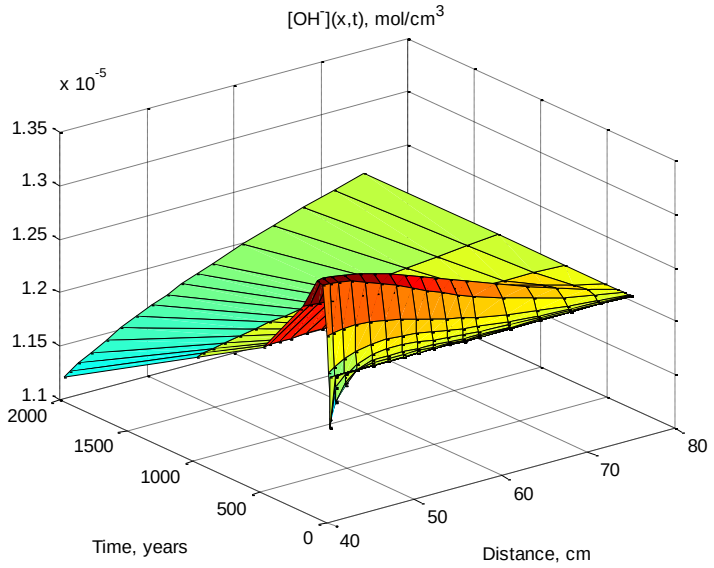

Figure III-24: Plot of calculated concentration of OH^- over a 2000 year period for an initial γ-dose rate of 1 Gy/h (0.0278 rad/s), as a function of radial distance from the canister surface, and time.

In Figure III-24 is plotted the concentration of OH^- as a function of distance from the canister surface and as a function of time. We see that the concentration of OH^- is initially depressed by the reaction of Cu with HS^-, which produces H^+, but then the reduction of water and oxygen [Reactions (III-37) and (III-38), respectively] produce hydroxide, leading to the peak in the concentration of this species that is shown at short times in Figure III-25. From then on, as the supply of OH^- becomes diffusion-limited, the concentration decreases with time

Figures III-25 and III-26 show the predicted distributions of H_2O_2 and O_2, respectively, as a function of distance and time. Since both species are radiolysis products and both are cathodic depolarizers in the corrosion process, they are expected to behave similarly. Indeed this is found to be the case, as seen from comparing the two figures. Thus, the concentrations of both species, which are very low or zero at the beginning of the anoxic period, increase due to their generation by the radiolysis of water, pass through a maximum and then decrease as the radiolytic generation dies off and the species react as cathodic depolarizers at the copper surface and with bisulphide ion in the buffer. Eventually, after 1000 years, the concentrations of both species are predicted to be essentially zero corresponding to a truly "anoxic" environment.

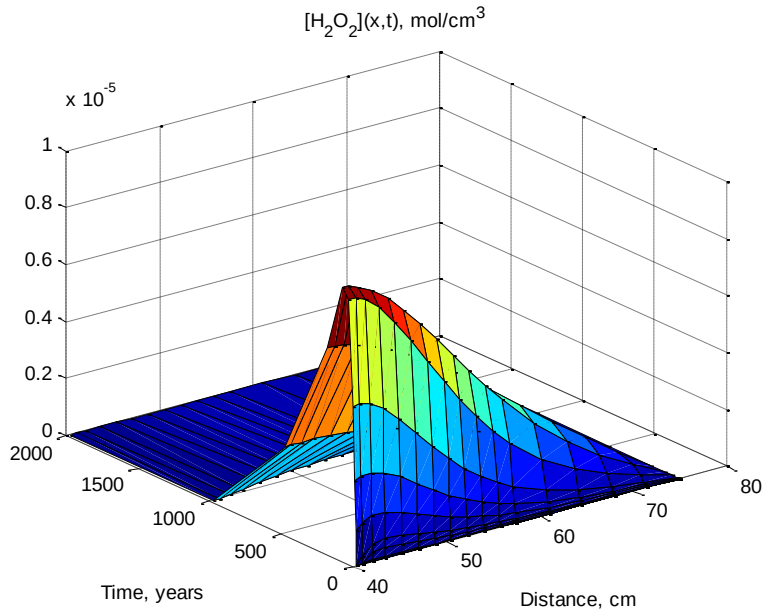

Figure III-25: Plot of calculated concentration of H_2O_2 over a 2000 year period for an initial γ-dose rate of 1 Gy/h (0.0278 rad/s), as a function of radial distance from the canister surface, and time.

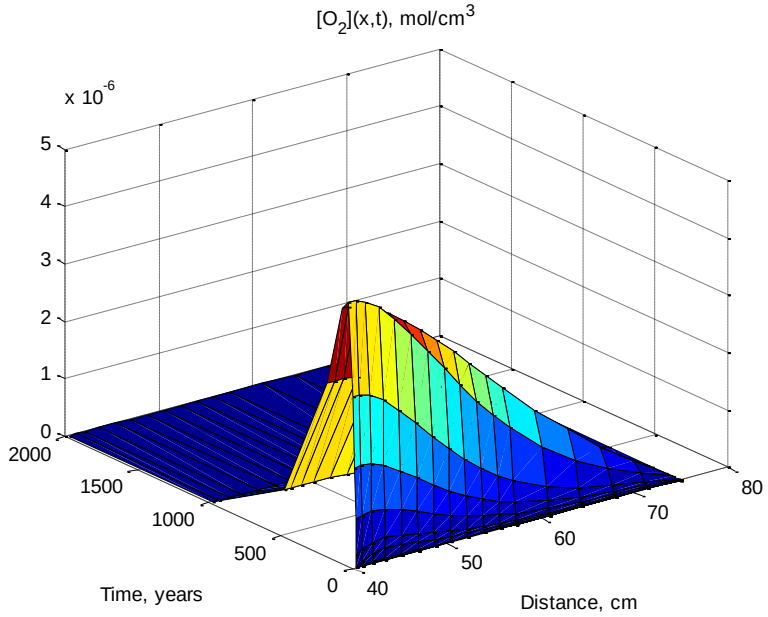

Figure III-26: Plot of calculated concentration of O_2 over a 2000 year period for an initial γ-dose rate of 1 Gy/h (0.0278 rad/s), as a function of radial distance from the canister surface, and time.

The variation of hydrogen as a function of distance and time is shown in Figure III-27. Hydrogen is produced by the corrosion reaction via the reduction of water and by radiolysis. The calculations show that the distribution is such that the hydrogen concentration peaks shortly after closure and from then on diffuses away from the canister into the repository. However, after about 1000 years, the production of hydrogen is predicted to become very low as the result of the corrosion rate becoming low and the reaction with radiolytically-produced O_2 and H_2O_2 continues, albeit at a much reduced rate due to the decay in the γ-dose rate.

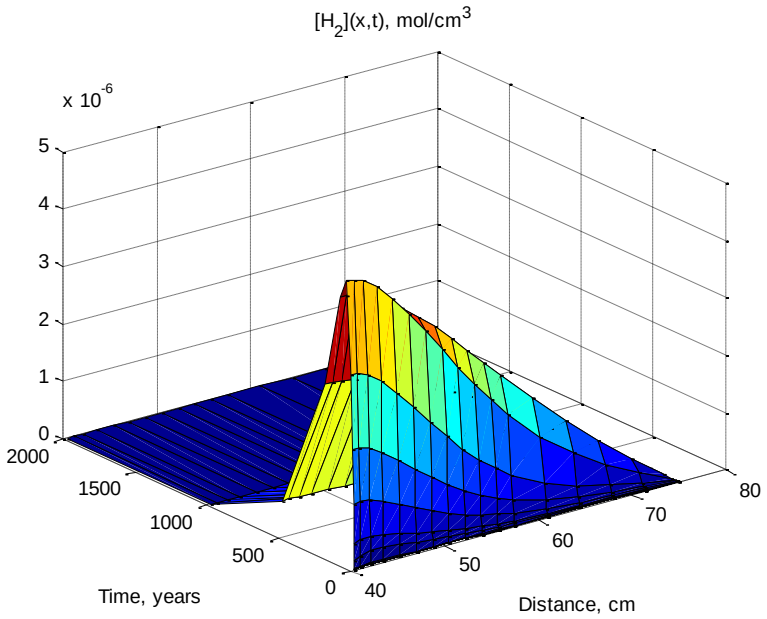

Figure III-27: Plot of calculated concentration of H_2 over a 2000 year period for an initial γ-dose rate of 1 Gy/h (0.0278 rad/s), as a function of radial distance from the canister surface, and time.

Finally, the concentration of HS^- in the near-field environment (the bentonite buffer), as a function of time and distance from the canister surface is plotted in Figure III-28. The concentration profile is determined by four effects: (1) consumption of HS^- at the copper interface; (2) diffusion of HS^- from the bulk through the bentonite buffer; (3) supply of HS^- from pyrite in the buffer (not considered); and (4), reaction of HS^- with the radiolysis products, O_2 and H_2O_2. Thus, initially, the HS^- concentration decreases sharply as the bisulphide ion in the near-field environment reacts with copper, resulting in the surface concentration of this species being depressed to zero for the remaining times. This sets up a diffusion regime in the bentonite buffer, which is coupled with the consumption of bisulphide by O_2 and H_2O_2 over relatively short times (<300 years). At longer times, the diffusional transport of HS^- toward the canister surface is still evident, but for times greater than ca 100 years, the simulation predicts that HS^- may be transported away from the canister, which is difficult to reconcile with physical reality. We must note that, at this time,

little O_2 and H_2O_2 is being produced by radiolysis (because the dose rate has decayed essentially to zero), but residual amounts of these species that were produced by radiolysis at earlier times, and which cannot be consumed at the copper surface (because of the reduction in the corrosion rate), diffuse outward and react with HS^-, thereby reducing its concentration and hence producing the predicted profile, but, of course, the concentration should not be elevated above the far-field value. We also note that at longer times, the time steps become large and it may be that the predicted decrease in bisulfide concentration at long times and large radial distance is simply a computational artifact of too large a time step for efficient convergence, which is a common problem in calculations of this type. This issue is currently being explored.

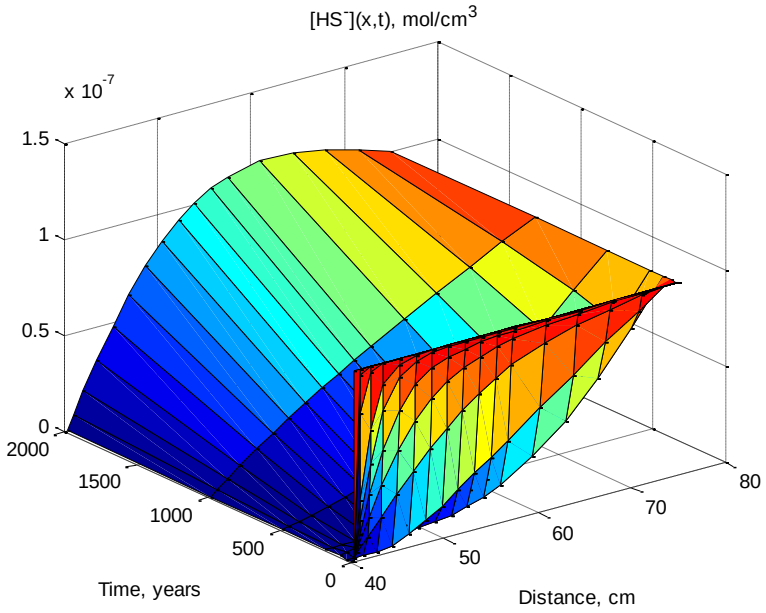

Figure III-28: Plot of calculated concentration of HS^- over a 2000 year period for an initial γ-dose rate of 1 Gy/h (0.0278 rad/s), as a function of radial distance from the canister surface, and time.

In summary, we have developed a Physico-Electrochemical Model (PEM) that realistically describes the transport processes that occur in the bentonite buffer, the electrochemical processes that occur at the canister surface (including the oxidation of copper to form Cu_2S), the reaction of HS^- with O_2 and H_2O_2, which may be present naturally (e.g., O_2 after closure) or are produced by the radiolysis of water (O_2, H_2O_2), and the radiolysis of water resulting from the decay of radionuclides, such as $^{137}Cs_{55}$, which gives rise to an exponentially decreasing γ-dose rate with time at the canister surface. Because of the lack of data for various model parameters, we are unable, at present, to simulate the actual repository. Instead, we have used "guesstimated" parameter values to perform scoping calculations and to test the algorithm. The scoping calculations show that the PEM is capable of yielding physically-reasonable results, but that the convergence of the code is a significant issue, because of the formation of ill-conditioned matrices upon matrix inversion.

We have proposed an extension of the current program into a two-year, Phase III phase, with the specific purpose of measuring important PEM parameter values, calibrating the radiolysis model on experimental water radiolysis data and sophisticated radiolysis models that we have previously developed for describing water radiolysis in Boiling Water (Nuclear) Reactors, and using the improved PEM to simulate the corrosion of copper canisters in the proposed Swedish HLNW repository.

References:

1. D. D. Macdonald, A. C. Scott, and P. Wentrcek, *J. Electrochem., Soc.*,128, 250-257 (1981).
2. D. D. Macdonald,*Corrosion*, 48(3), 194-205 (1992).
3. D. D. Macdonald, Iouri Balachov, and George Engelhardt,*Power Plant Chemistry*, 1(1), 9–16 (1999).
4. F. King, C. Lilja, K. Pedersen, P.Pitkänen and P. Posiva, *SKB-TR-10-67, Svensk Kärnbränslehantering AB,* (2010).
5. D. D. Macdonald and Samin Sharifiasl, *Report No. 2011-09, SSM, Stockholm, Sweden*, (2011).
6. D. D. Macdonald,*J. Electrochem. Soc*., 139(12), 3434-3449 (1992).
7. D. D. Macdonald, *Pure Appl. Chem*., **71**, 951 (1999).
8. T.F. Coleman, and Y. Li ,*SIAM Journal on Optimization*, Vol. 6, pp. 418-445, (1996).
9. T.F. Coleman, and Y. Li, *Mathematical Programming*, Vol. 67, Number 2, pp. 189-224, (1994).
10. J. E. Jr. Dennis, , *State of the Art in Numerical Analysis*, ed. D. Jacobs, Academic Press, pp. 269-312.(1977)
11. K. Levenberg, *Quarterly Applied Mathematics 2*, pp. 164-168, (1944).
12. D. Marquardt, *SIAM Journal Applied Mathematics*, Vol. 11, pp. 431-441, (1963).
13. J. J. Moré, *Numerical Analysis, ed. G. A. Watson, Lecture Notes in Mathematics 630, Springer Verlag*, pp. 105-116, (1977).
14. J. J. Moré, B. S. Garbow, and K. E. Hillstrom, *Argonne National Laboratory*, Rept. ANL-80-74, (1980).
15. M. J. D. Powell, *Numerical Methods for Nonlinear Algebraic Equations, P. Rabinowitz, ed*., *Ch.7*, (1970).

III-6: Assessment of Corrosion in the Resaturation Period

It is known that, due to the heat generated by the spent nuclear fuel, the surface of canister will have a temperature that is higher than the surrounding environment (see Figure III-21). It is expected that this temperature will be about 74 ^{o}C, when canister is exposed to the air and around 90 ^{o}C after emplacement in the repository. Therefore, two types of corrosion should be considered during this period; corrosion by steam that advances ahead of the water front through the bentonite buffer and, once resaturation is complete corrosion by liquid water, both under oxic conditions.

The atmospheric corrosion of copper has been extensively studied [1]. It has been shown that copper patinas are the most likely corrosion products of such a reaction [2]. Trace amounts of pollutants, including the acid gases (CO_2, SO_2, and SO_3) in the atmosphere play an important role in the formation of patinas. Besides pollutants, the relative humidity of the environment is also vital in establishing the form and mechanism of corrosion. King et al [3] have reviewed the atmospheric corrosion of copper with respect to the repository environment and have investigated the effect of environment pollutants and humidity [3]. It has been noted that, because the relative humidity of the environment could vary with distance through the buffer and with time, so could the corrosivity. It has also been argued that, when the relative humidity exceeds a critical value, the corrosion rate will increase sharply. The actual effect of relative humidity is related to the thickness of a condensed water layer on the surface of the copper canister, which permits the resuction of the cathodic depolarizer, most notably oxygen under the expected, initial oxic conditions. When this layer approaches three-four monolayer, its behavior is postulated to become similar to that of bulk water that may contain all of the dissolved pollutants (including HS^-, if present in the steam phase), thereby becoming even more aggressive. The temperature at the canister surface prior to disposal is estimated to be around 74^{o}C and therefore the corrosion rate is expected to be higher than that at ambient temperature by a factor of about 100. However, there is a severe lack of information in the literature on the experimental measurement of the atmospheric corrosion rate of copper canister in the relevant temperature range and under relevant chemical conditions. King et al [3], in a report published by SKB, estimated the rate of corrosion, based upon the measured rates at ambient temperature by Rice et al. [4], and the value was expected to be in the range of 60 to 270 nm per year. It is not clear if bisulphide plays a significant role, because this factor was not investigated.

The situation with respect to canister corrosion after emplacement in the repository is expected to be different. As a result of the higher temperature at the canister surface of an emplaced canister after 20 years of storage (i.e.. 90^{o}C, Figure III-21), the moisture that forms in the bentonite buffer ahead (toward the canister) of the liquid water front, will be redistributed and it is predicted that, the relative humidity (RH) adjacent to the canister will be greater 50%; this RH is less than 100 % presumably due to temperature gradient in the buffer [3]. This is significantly greater that the RH at ambient temperature and is probably sufficient to attack the canister electrochemically by forming a thin, electrolyte film on the copper surface that can support electrochemical reactions [3]. All-in-all, the work of King et al. [3] suggests that the corrosive attack in this period (e.g. first 100 years) will be in the

form of general corrosion with a negligible effect on the lifetime of the copper canister. Thus, it is predicted [3] that the canister temperature will be sufficiently high to evaporate adjacent groundwater and to bath the canister in steam. If this condition exists, then the canister may suffer low pressure steam corrosion, rather than aqueous-phase corrosion. In order to assess whether this scenario is likely, it will be necessary to estimate the hydrostatic pressure in the repository, which is located 500m below the surface. In an effort to understand the corrosion mechanism of copper in contact with low pressure steam we performed an extensive literature survey. Unfortunately, we were unable to locate any information about the steam corrosion of pure copper that had not already been reviewed by King, et. al. [3]. Therefore, in the opinion of the authors, a significant need exists to measure the corrosion rate of copper in contact with steam under conditions that accurately simulate the conditions that exist in the repository, including the use of an internally heated, cylindrical copper specimen and a bentonite buffer, in order to accurately simulate the emplaced canister in the repository.

References

1. H. Leidheiser, *John Wiley & Sons, Inc*., New York (1974).
2. I.T.E.Fonseca et al., *Corrosion Science*, 46, 547–561(2004).
3. F. King, L. Ahonen, C. Taxen, U. Vuorinen and L. Werme,, *SKB, TR-01-23, Svensk Kärnbränslehantering AB*, (2001).
4. D. W. Rice, P. Peterson, E. B. Rigby, P. B. P. Phipps, R. J. Cappell, and R. Tremoureux, *J. Electrochem, Soc.: ELECTROCHEMICAL SCIENCE AND TECHNOLOGY*,(1981).

III-7: Assessment of the Impact of Water Radiolysis

Because the canister contains radioactive isotopes (e.g., $^{137}Cs_{55}$, $^{137}Ba_{56}$) and because many of these isotopes decay by beta emission to form excited nuclei of elements one place higher in atomic number, which then emit γ photons, the near-field environment (bentonite buffer) is exposed to ionizing radiation, resulting in the radiolysis of water. This process produces a myriad of radiolysis products including O_2, H_2, H_2O_2, $e(aq)^-$, OH, O_2^-, O^{2-}, HO_2^-, H^+, OH^-, and others. Modeling of the radiolysis of water in the coolant circuits of water-cooled nuclear reactors [1-4] shows that only three species need be considered in predicting the corrosion behavior of the structural materials; O_2, H_2, and H_2O_2. This is because the contribution that any given species can make to the total cathodic partial current, which is instrumental in determining the corrosion potential and hence the corrosion rate, is proportional to its concentration [1,2] and it is found that the concentrations of all radiolysis species, except O_2, H_2, and H_2O_2 are negligible [4]. In the present work on exploring the impact of radiolysis on the corrosion behavior of the copper canister in the repository environment, we have used arbitrary values for various model parameters, so that the results should not be taken to represent the corrosion behavior of the canisters, but are simply used to illustrate the operation of the algorithm. The simulations were carried out for initial γ-dose rates at the canister surface of 1 Gy/h (0.0278 rad/s), 10 Gy/h (0.278 rad/s), and 100 Gy/h (2.78 rad/s). Plots for the 1 Gy/h case are shown in Figures III-22 to III-28, and for the parameter values displayed in Table III-13. These dose rates are very low, much lower than those that exist in the core of a Boiling Water Nuclear Reactor (BWR), for example, where dose rates from γ-photons are typically $>10^5$ rad/s [4]. Accordingly, the rate of production of radiolysis products is expected to be proportionally lower, as is generally borne out by the modeling studies reported here. However, our reactor models may be used to simulate the HLNW canister case, by running the reactor code at very low reactor power levels, such that the dose rate in the reactor core matches that at the canister surface (0.0278 rad/s = 1 Gy/h). This is the approach that we will adopt, together with using low dose rate experimental data for water radiolysis from the University of Notre Dame, in Phase III. The objective will be to determine rate constants for the reaction of $H_2 + O_2$ and $H_2 + H_2O_2$, such that the experimentally observed or calculated concentrations of O_2 and H_2O_2, respectively, match in the two systems (BWR core and HLNW canister) at comparable dose rates (0.1 – 100 Gy/h).

At this point, it is necessary to note that we have not invoked any the "full models" for the radiolysis of water [1-4], because considerable controversy exists as to the fundamental veracity of the models. These models normally comprise 34 to 56 "elementary" reactions between prompt radiolysis products (i.e., those species that form at femto-second time scales upon the absorption of the γ- photon) and those that are produced at longer times via chemical reaction. However, the radiolytic yields (the "G" values) that are employed in these models (the number of particles produced per 100 eV of energy absorbed from the interaction of the γ- photons with water) are generally measured under quasi-steadystate conditions, where the reactions have already occurred. Accordingly, a quasi-steady-state model in which the G-values simply describe the number of species produced over long term radiolysis coupled to reactions between these species appears to be more appropriate, and it is this type of model that is adopted in this analysis.

The temporal and spatial variations of each of the dependent variables, metal loss (L), corrosion potential (E), [OH^-], [H_2O_2], [O_2], [H_2], and [HS^-] vary with time and distance from the canister surface as described above and also with the initial γ-dose rate at the canister surface are displayed graphically in Figures III-22 to III-42. The impact of dose rate on the metal loss and the corrosion potential is summarized in Table III-14. It is seen that, even with using the "guesstimated" parameter values summarized in Table III-13, realistic concentrations are predicted, except for that for hydrogen peroxide, which is several orders of magnitude too high. However, at this stage, no attempt has been made to calibrate the model against experiment, as this will have to await the acquisition of the appropriate experimental data. As shown in Table III-14, the model in its present form predicts a loss of metal of 3.4×10^{-4} cm over 2000 years for dose rates of 1 and 10 G/h, corresponding to 1.7 nm/y. At the highest dose rate, the average corrosion rate is predicted to be 100 nm/y. The value for the lowest dose rates is considered to be too low by about a factor of 10 but the value for the highest dose rate is considered to be realistic. Of great importance is the prediction that the corrosion rate is insensitive to dose rate at the prevailing initial dose rate of the canister. Accordingly, we would conclude, if this finding holds up, when experimentally-determined model parameter values are employed, that the radiolysis of water has little impact on the corrosion behavior of the canister. However, the simulations reported to date predict that the corrosion potential shifts sharply in the positive direction with increasing time, which we attrivute primarily to falling temperature. Thus, in Figure III-23, the ECP is predicted to be elevated by almost 0.5 V and it is possible that such a change could induce various forms of localized corrosion (e.g., pitting and crevice corrosion), if the potential was displaced above the critical potentials for these forms of attack. However, the critical potentials for localized corrosion processes are commonly found to also be strongly temperature-dependent, such that the critical potentials also shift strongly in the positive direction with falling temperature. A careful assessment of the potential for localized corrosion is therefore warranted.

Finally, we note that the calculated corrosion potential varies with time in response to changes in the concentrations of the redox species and generally fall within the range expected and observed for corer in contact with sulphide-containing, slightly alkaline solution (-0.5 to 0.1 V_{she}), depending upon the temperature and the concentrations of [H_2O_2], [O_2], [H_2], and [HS^-]. For example, it is well-known that increasing temperature normally displaces the corrosion potential in the negative direction as does increasing concentration of HS^- and H_2. On the other hand, increasing concentration of O_2 or H_2O_2 has the effect of displacing the corrosion potential in the positive direction, so that the potential that is observed is the result of a delicate balance between several factors.

Table III-14: Impact of initial γ-dose rate at the canister surface on the metal loss, *L*, and the corrosion potential, *E*.

Dose Rate (Gy/h)	Metal Loss (cm)	E (mVshe)
1	3.4×10^{-4}	-0.35 to 0.1
10	3.4×10^{-4}	-0.2 to -0.5
100	0.02	-0.1 to 0.1

Dose Rate = 0.278 rad/s (10 Gy/hr)

We now explore the impact of the higher **γ**-dose rate of 10 Gy/h (0.278 rad/s). The results are displayed in Figures III-29 to III-35. The reader will note the large error bars on the data plotted in Figure III-30, signifying poor convergence of the algorithm for that case. As noted elsewhere, the convergence can be improved, and hence the error can be reduced by increasing the number of iterations, but only at a significant cost in computational time. However, in some cases, it was found that convergence could not be improved no matter what run time was imposed. This is not an unusual occurrence in solving coupled, non-linear equations and in Phase III of this program it will be necessary to address the convergence problem by further modifying the algorithm. We have determined that the error does not arise from corresponding uncertainties in the calculated concentrations, but has been traced to the inversion of matrices in solving the problem, resulting in ill-conditioned matrices. Our approach to improving conversion, which is on-going, will focus of more efficient and accurate matrix inversion techniques.

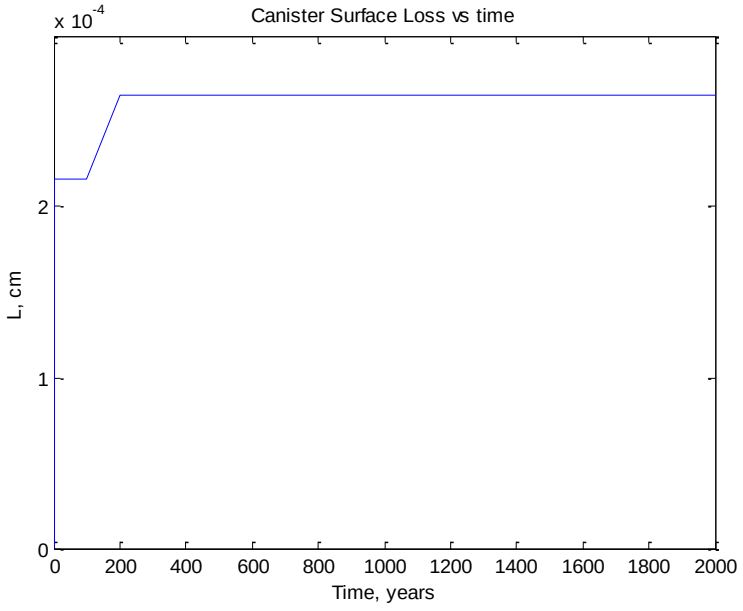

Figure III-29: Plot of calculated loss of copper over a 2000 year period for an initial γ-dose rate at the canister surface of 10 Gy/h (0.278 rad/s).

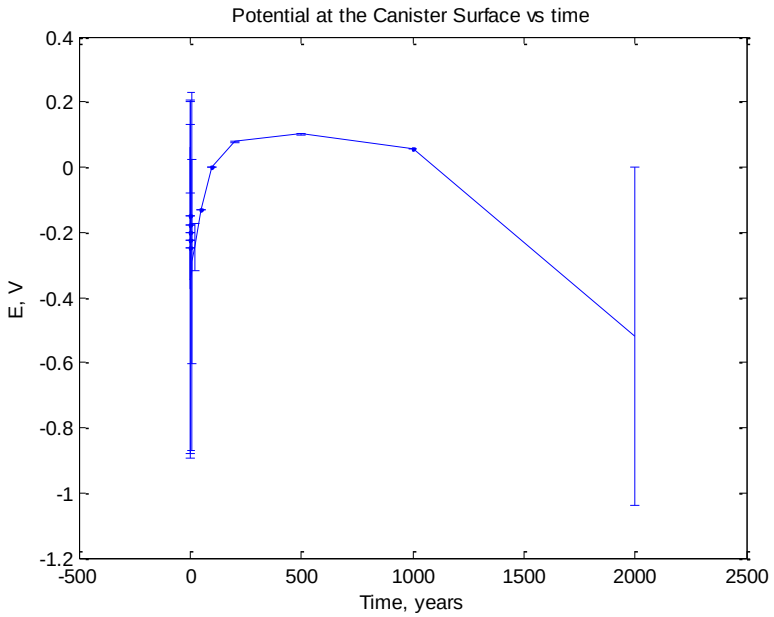

Figure III-30: Plot of calculated corrosion potential of copper over a 2000 year period for an initial γ-dose rate at the canister surface of 10 Gy/h (0.278 rad/s).

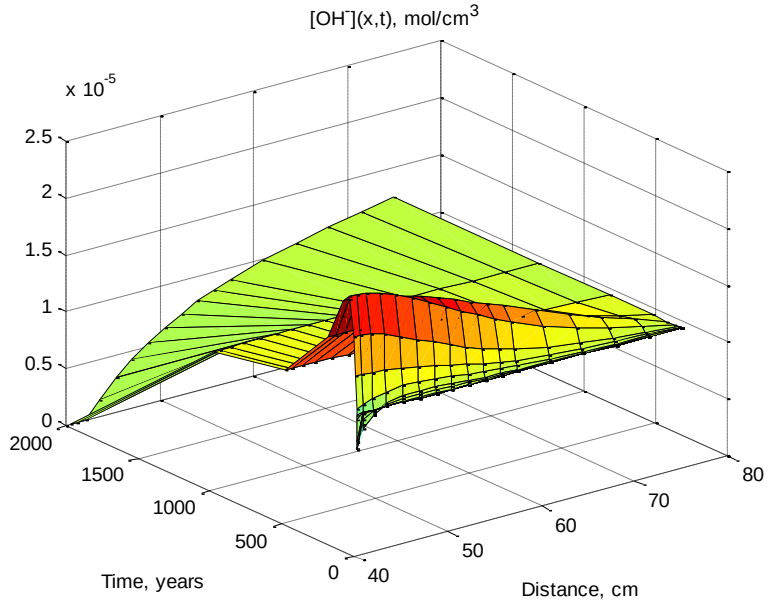

Figure III-31: Plot of calculated concentration of OH^- over a 2000 year period for an initial γ-dose rate at the canister surface of 10 Gy/h (0.278 rad/s), as a function of radial distance from the canister surface and time.

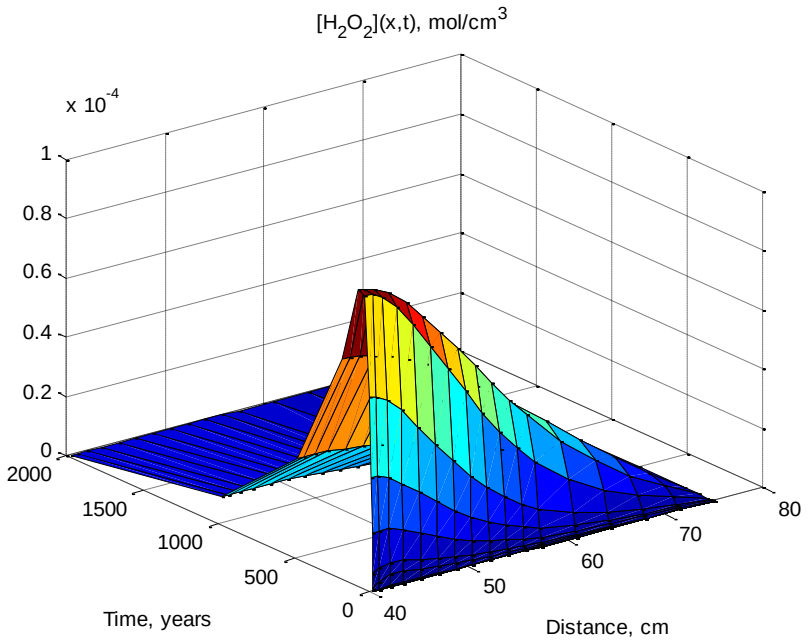

Figure III-32: Plot of calculated concentration of H_2O_2 over a 2000 year period for an initial γ-dose rate at the canister surface of 10 Gy/h (0.278 rad/s), as a function of radial distance from the canister surface and time.

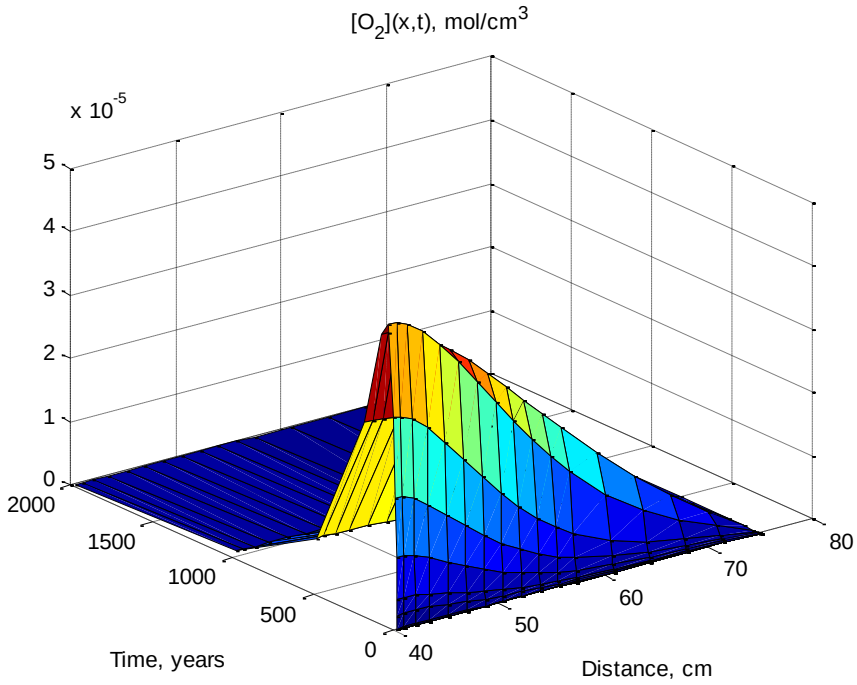

Figure III-33: Plot of calculated concentration of O_2 over a 2000 year period for an initial γ-dose rate of 10 Gy/h (0.278 rad/s), as a function of radial distance from the canister surface, and time.

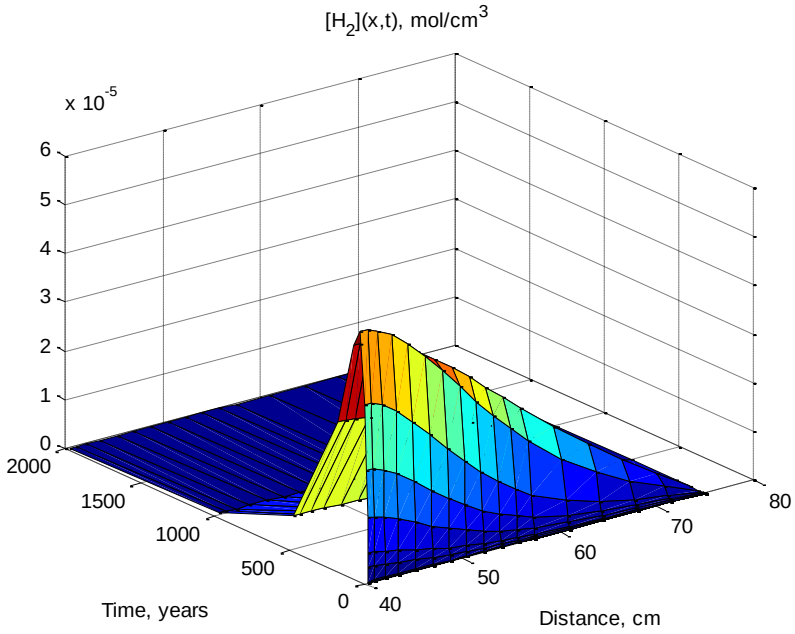

Figure III-34: Plot of calculated concentration of H_2 over a 2000 year period for an initial γ-dose rate at the canister surface of 10 Gy/h (0.278 rad/s), as a function of radial distance from the canister surface and time.

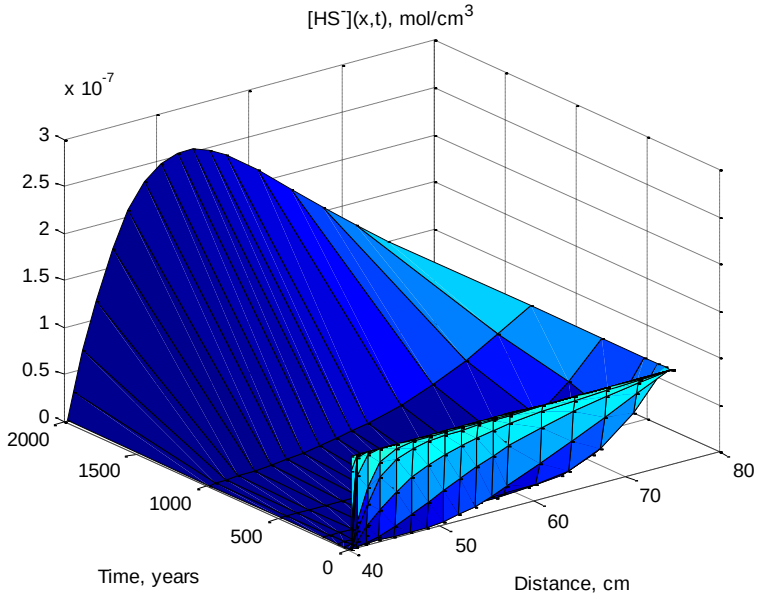

Figure III-35: Plot of calculated concentration of HS^- over a 2000 year period for an initial γ-dose rate at the canister surface of 10 Gy/h (0.278 rad/s), as a function of radial distance from the canister surface and time.

Dose rate: 2.78 rad/s (100 Gy/hr)

In this final set of calculations, we simulate the canister corrosion behavior at an initial γ-dose rate at the canister surface of 100 Gy/h, which is a factor of 100 higher than that estimated to exist at a canister surface in the actual repository.

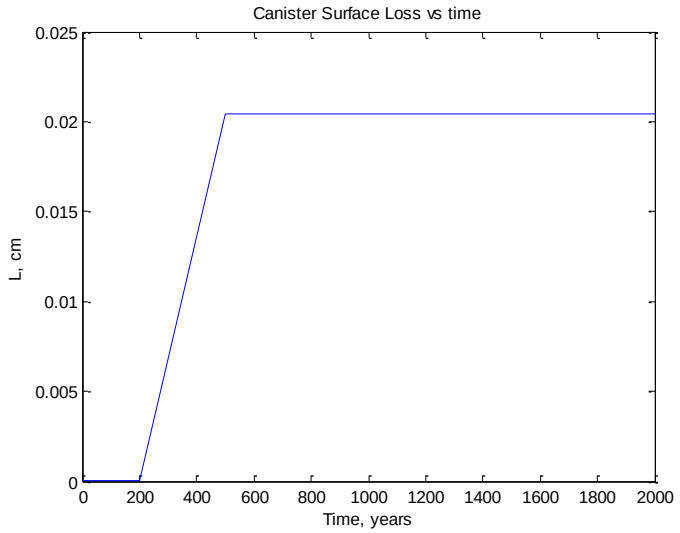

Figure III-36: Plot of calculated loss of copper over a 2000 year period for an initial γ-dose rate at the canister surface of 100 Gy/h (2.78 rad/s).

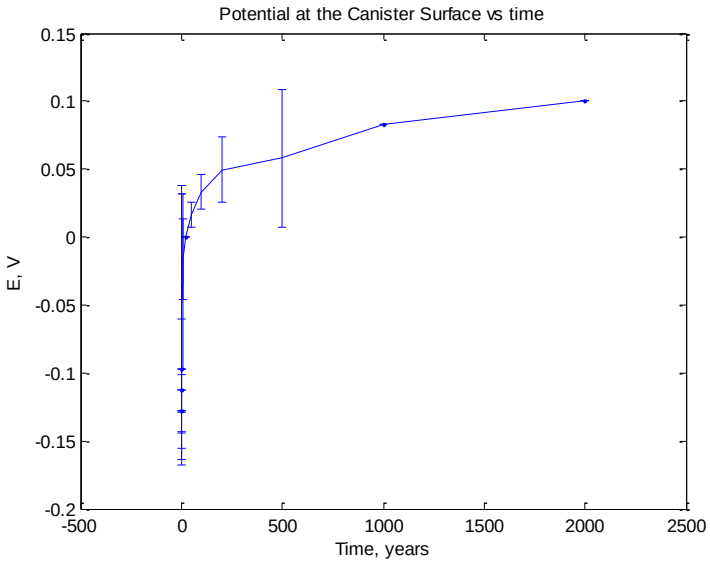

Figure III-37: Plot of calculated corrosion potential of copper over a 2000 year period for an initial γ-dose rate at the canister surface of 100 Gy/h (2.78 rad/s).

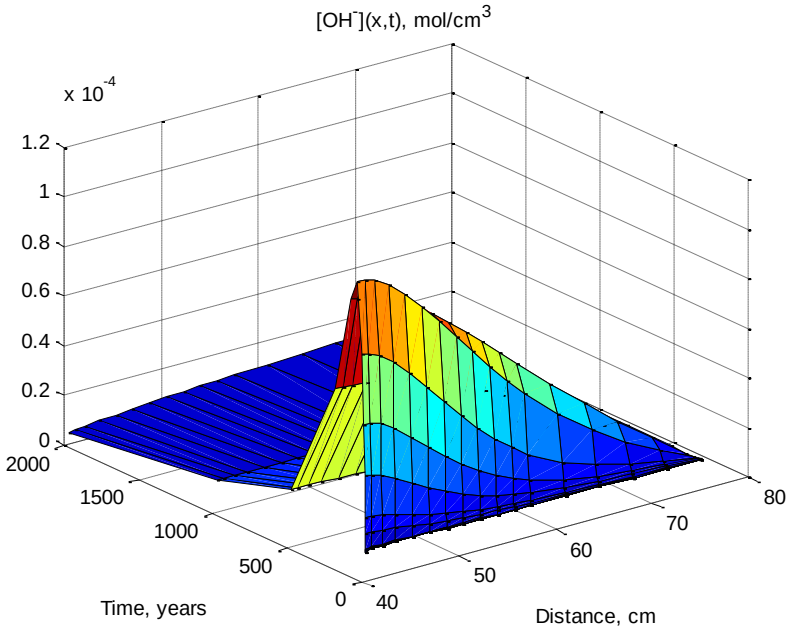

Figure III-38: Plot of calculated concentration of OH^- over a 2000 year period for an initial γ-dose rate at the canister surface of 100 Gy/h (2.78 rad/s), as a function of radial distance from the canister surface and time.

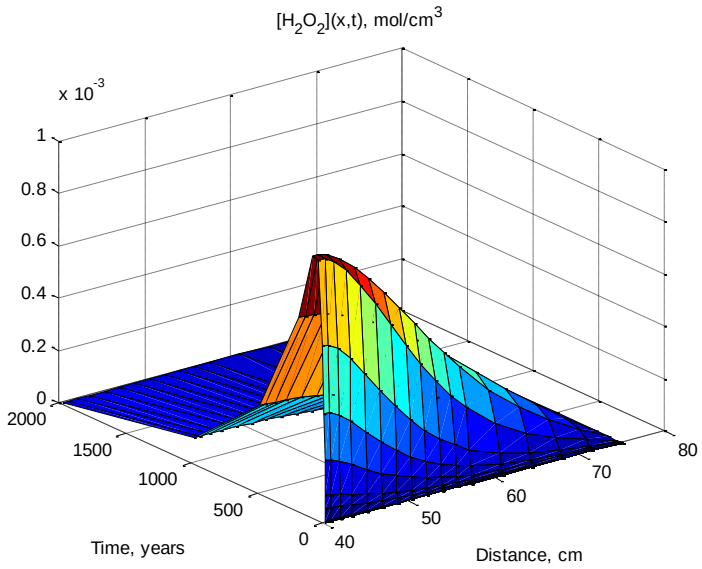

Figure III-39: Plot of calculated concentration of H_2O_2 over a 2000 year period for an initial γ-dose rate at the canister surface of 100 Gy/h (2.78 rad/s), as a function of radial distance from the canister surface and time.

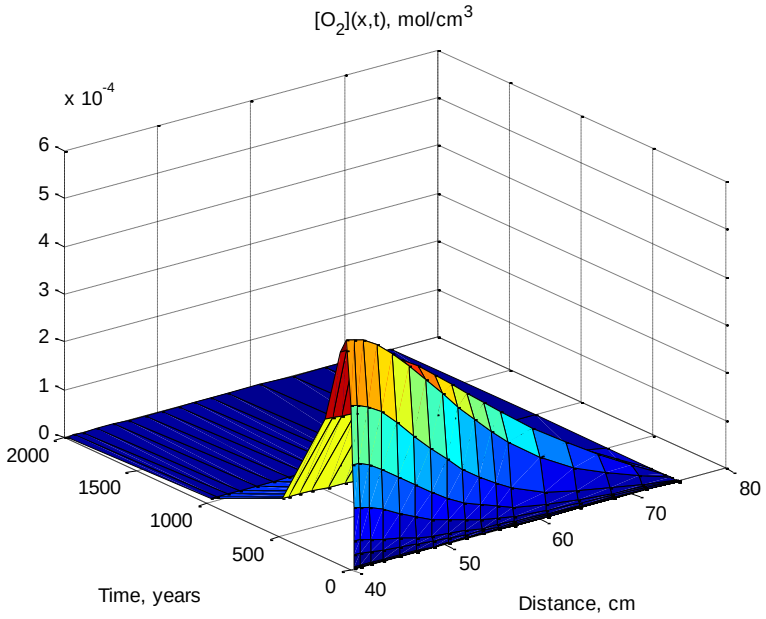

Figure III-40: Plot of calculated concentration of O_2 over a 2000 year period for an initial γ-dose rate at the canister surface of 100 Gy/h (2.78 rad/s), as a function of radial distance from the canister surface and time.

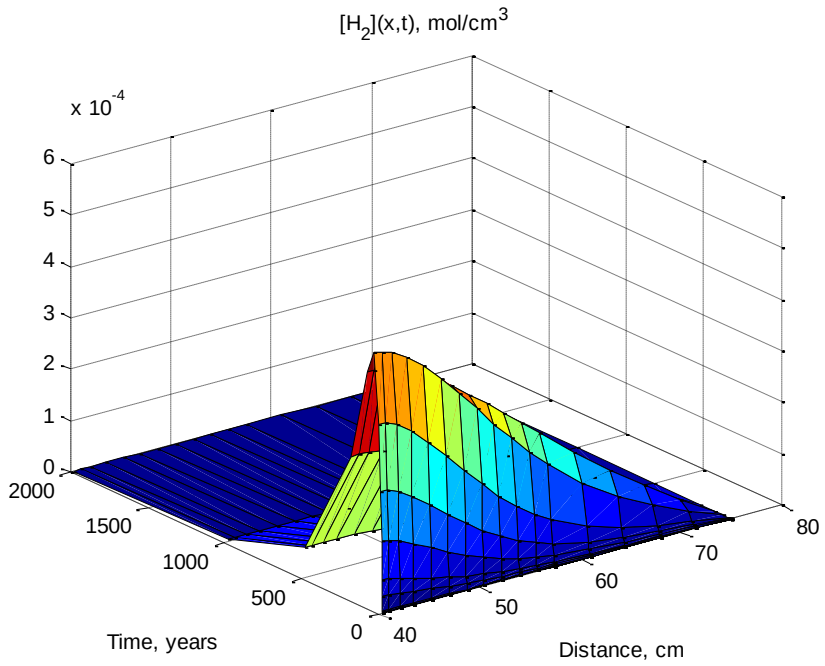

Figure III-41: Plot of calculated concentration of H_2 over a 2000 year period for an initial γ-dose rate at the canister surface of 100 Gy/h (2.78 rad/s), as a function of radial distance from the canister surface and time.

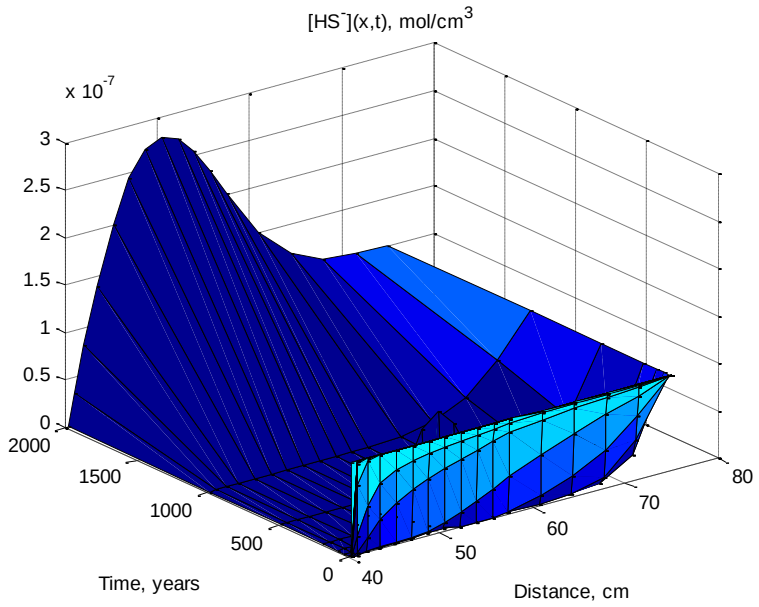

Figure III-42: Plot of calculated concentration of HS^- over a 2000 year period for an initial γ-dose rate at the canister surface of 100 Gy/h (2.78 rad/s), as a function of radial distance from the canister surface and time.

In closing, we emphasize that the Physico-Electrochemical Model ((PEM) suggests that the radiolysis of water at the expected initial γ-dose rate of 1 Gy/h (0.0278 rad/s) will not play a significant role in determining the corrosion behavior, including total metal loss over the storage period, of a copper canister in the proposed Swedish HLNW repository. However, this tentative conclusion is made without the PEM being calibrated for the radiolysis of water and without experimentally-determined values being available for important model parameters. These values must be measured experimentally and the radiolysis model contained within the PEM must be calibrated against low γ-dose rate radiolysis data (concentrations of O_2, H_2, and H_2O_2 as a function of time) and/or against BWR radiolysis codes for low power (low dose-rate) operation that we have developed previously.

References:

1. D. D. Macdonald, A. C. Scott, and P. Wentrcek, *J. Electrochem., Soc*., **128**, 250-257 (1981).
2. D. D. Macdonald,*Corrosion*, **48**(3), 194-205 (1992).

3. D. D. Macdonald, Iouri Balachov, and George Engelhardt, *Power Plant Chemistry*, **1(1)**, 9–16 (1999).
4. T.K. Yeh, D.D. Macdonald, and A. T. Motta, *Nucl. Sci. Eng.*, **121**, 468-482 (1995).

IV. Summary and Conclusions

The work reported here has resulted in a number of important conclusions that have a bearing on the behavior of copper in a Forsmark-type repository. These conclusions are as follows:

Continued Development of CDDs for Complexing Systems

- Following our work in Phase I, the thermodynamic properties of copper are expressed in corrosion domain diagrams (CDDs) as plots of P^e versus *pH*, where P^e is the partial quotient of the reaction at equilibrium. For any other value of the reaction quotient, *P*, where $P \neq P^e$, the system is not at equilibrium and, provided that $P < P^e$, the composition (as described by *P*) will change such that $P \rightarrow P^e$.
- Corrosion is spontaneous only for $P < P^e$. Cu is immune to corrosion for $P > P^e$.
- Certain species commonly found in ground water, e.g. HS^-, polysulphides, and certain polysulphur oxyanions are deleterious by (thermodynamically) activating copper and hence denying the metal thermodynamic immunity. Activation results from the formation of a Cu_2S phase on the metal at a potential that is much more negative than that for the formation of Cu_2O oe Cu^+, such that the evolution of hydrogen from water becomes a viable cathodic reaction.
- The thermodynamic conditions for the corrosion of copper in water have been defined with emphasis on complexing systems. Species that form complexes with *Cu(I)* and *Cu(II)* activate copper thermodynamically. These species include the halides, carbonate ion, and phosphate ion. It should be emphasized that the activation depends on the pH and temperature of the system.
- Some polythiosulphates, notably, $S_xO_3^{2-}$, x = 3 – 7, are found not to activate copper, for reasons that are not yet completely understood. These species tend to possess very negative volt equivalencies and to have low, positive average sulphur oxidation states.
- All polysulphides are predicted to activate copper.
- Some members of the polythionates family ($S_xO_6^{2-}$) become unable to activate copper with increasing temperature.

Continued Definition of Repository Chemistry

- In order to explore the composition of granitic groundwater, we decided to employ a modern, sophisticated Gibbs energy minimization algorithm to predict the composition of the repository environment, as a function of temperature and redox condition, with the latter being adjusted by changing the relative concentrations of hydrogen and oxygen in the input to the code.
- After evaluating several codes, we chose GEMS, which was developed in Switzerland by Prof. Dmitri Kulik. This code is designed specifically to model geochemical systems, contains a large database of compounds, and is in general use in the geochemical community.
- Prior to using the code to model the repository, we upgraded the database by adding thermodynamic data for various polysulphur species (polysulphides, poly thiosulphates, and polythionates) that had been developed earlier in this program (Phase I). However, the code became ill-behaved when the data for $S_xO_3^{2-}$, $x = 3 – 7$ were added. Consultation with the code developer, Prof. Dmitrii Kulik at Paul Scherer Institute in Switzerland, failed to identify and isolate the problem and,

accordingly, it was necessary to remove those species from the database. The reader will recall that these are the very species that, anomalously, are predicted not activate copper.

- With the code in its present form, we have modeled the repository under both oxic and anoxic conditions with the greatest emphasis being placed on the latter, because the great fraction of the storage time is under anoxic conditions. The most important finding to date is that the concentrations of many, but not all, polysulphur species (polysulphides, poly thiosulphates, and polythionates) under anoxic conditions are predicted to be very low, but it is still not possible, because of the uncertainty in the calculations, to ascertain with certainty whether these species will activate copper in the repository. However, the point may be moot, because the lower sulphide species (S^{2-}, HS^{-}, H_2S, HS_2^{2-}, and S_2^{2-}) are predicted to be present in sufficient concentration to activate copper and cause the metal to corrode under simulated repository conditions over the lifetime of the repository.
- The activity of sulphate ions in the system is predicted to be relatively high (10^{-4} to 10^{-6}) and decreasing with increasing the system temperature.Sulphate does not activate copper, because it cannot donate atomic sulphur to the metal surface.
- Chloride ion activity is also relatively high in the system and is predicted to decrease with increasing the temperature.
- The activity of methane (CH_4) in the repository is not so high as to be able to play a role in the reduction of sulphate.
- The activity of dissolved hydrogen gas under simulated repository condition is in the range of $3x10^{-12}$ M to $5x10^{-8}$M and is predicted to increase with increasing temperature. Its activity is far below the measured concentration; therefore, it could be concluded that the system real condition (as indicated by [H_2] determined by "grab" samples) is not in the equilibrium state, which seems to be reasonable.
- Bisulphide (HS^{-}) activity in the system is higher than other sulphur species (excluding SO_4^{2-}) and is predicted to activate copper canister. Its activity increases with increasing temperature.

Continued Development of Mixed Potential Model

- During Phase II, we developed the theoretical basis of the Mixed Potential Models (MPMs) for estimating the redox potential of the repository environment and for calculating the corrosion potential of the copper canister as the system evolves along the corrosion evolutionary path.
- While the model was developed, it became superceded by the Physico-Electrochemical Model (PEM) for canister corrosion and our work on the MPMs was rolled into the development of the latter (see below).

Continued Definition of the Corrosion Evolutionary Path

- We initiated work to define the corrosion evolutionary path (CEP)in Phase I, in preparation for modeling the corrosion of the canisters in Phase II of this study. This task essentially involved predicting the redox potential (E_h), *pH*, and granitic groundwater composition as defined by the variation of temperature as a function of time (note that the temperature decreases roughly exponentially due to radioactive decay of the short-lived isotopes), and by then applying Gibbs energy minimization to predict speciation at selected times along the path.
- At each step, the CDD for copper was derived and the value of *P*was compared to P^e to ascertain whether copper is active or thermodynamically immune. Although

the polysulphur species are predicted to be present at very low concentration (e.g., HS_2^- and S_2^{2-}), the CDDs indicate that certain species need be present at only miniscule concentrations (10^{-44} M) for activation to occur.

- In any event, sulphur species are predicted to be present during the entire anoxic period and are predicted to be able to thermodynamically activate copper. However, the concentration of all of the sulphur species, except HS^-, are predicted to be solow that they probably do not significantly impact the corrosion rate, because their fluxes to the metal surface are correspondingly small.
- Among all of the sulphur-containing species, bisulphide ion (HS^-(aq)) have the highest concentration in the entire anoxic period and it is predicted to dominate the kinetic of corrosion reaction in the system.

Development of a Physico-Electrochemical Model for Canister Corrosion

- A comprehensive physico-electrochemical model for canister corrosion over the repository horizon of 100,000 years has been developed. The model considered the three modes of specie transport (diffusion, migration, and convection), incorporates water radiolysis, evolving temperature from the decay of radionuclides in the waste, and electrochemical kinetics. The model is deterministic, because the predictions are constrained by the two relevant natural laws; the conservation of charge and Faraday's Law (equivalence of mass and charge).
- The model also recognizes the reaction between water radiolysis products (O_2, H_2O_2) and bisulphide ion (HS^-), with HS^- being converted to other sulphur species that are non activating (e.g., SO_3^{2-} and SO_4^{2-}).
- Using "guesstimates" of the various model parameters, it is shown that the model predicts specie concentrations, metal loss, and the corrosion potential that are considered to be eminently reasonable, except for the concentration of hydrogen peroxide, which is considered to be too high. However, this issue is expected to be resolved once radiolytic aspects of the model are calibrated against the highly successful codes that we have previously developed for modeling the radiolysis of water in water-cooled nuclear reactors, particularly Boiling Water Reactors (BWRs), albeit at much lower dose rates. We will also employ the extensive data that have been obtained at the Radiation Laboratory at the University of Notre Dame in South Bend, Indiana for the low dose rate radiolysis of water by γ-photons. These activities are scheduled for Phase III.
- Despite the paucity of data for the model parameters, the predicted loss of metal from a canister is estimated be 1.7 nm/y to 100 nm/y, depending upon the dose rate, when averaged over a two thousand year period, with most of the loss occurring at short times when oxic conditions prevail and when the concentration of HS^- asdjacent to the metal surface is high and hence the flux is large.

Assessment of Corrosion in the Resaturation Period

- The atmospheric corrosion of copper has been extensively studied by others and the results of this work are described in the scientific literature. It has shown that copper patinas are most likely tcorrosion products of the atmospheric corrosion of copper in contact with low pressure steam.

- It has known that the canister temperature will be high enough to evaporate adjacent groundwater and hence the canister will be in contact with steam for much of the resaturation period. If this condition exists, then the canister will suffer low pressure steam corrosion, which is a form of atmospheric corrosion. In order to assess whether this scenario is likely, it will be necessary to estimate the pressure in the repository, which is located 500m below the surface and to investigate the phenomenon experimentally.
- There is lack of information about the steam corrosion of pure copper in the available literature. Therefore, some experimental needs to be performed, in order to address the corrosion mechanism and rate of copper canister corrosion in contact with steam.

Assessment of the impact of Water Radiolysis

- Using "guesstimated" values for important model parameters, the physico-electrochemical model developed in this Phase II work suggests that at an initial γ-dose rate of 1 Gy/h, radiolysis is not a significant factor in determining the corrosion behavior of the canisters.
- This same modeling work indicates that an at initial dose rate of 100 Gy/h, radiolysis has a significant impact on the corrosion behavior of a canister.A full and accurate assessment of the impact of water radiolysis must await the experimental acquisition of values for important model parameters. These values are scheduled to be determined in Phase III.

Appendix A, Gibbs energy minimization results

Temperature = 25°C

State variables:
P(bar) = 1 T= 25 (°C) = 298.15 (K) V(cm^3) = 1022.9068
Mass(kg) = 1.1000358 Min. potential (moles): $G(x)$ = -5369.23023

Aqueous phase:
I(molal)= 0.0006503 pH= 6.742 p_e= -2.535 E_h(V)= -0.1497

Table A-1: Parameters of Dependent Components at 25°C

Species name	Log activity	Species name	Log activity
$Ca(CO_3)(aq)$	-8.875	Cu^{+2}	-20.69
$Ca(HCO_3)^+$	-7.407	$Cu_2(OH)_2^{+2}$	-38.27
$Ca(SO_4)(aq)$	-5.6	$Cu_3(OH)_4^{+2}$	-56.25
Ca^{+2}	-3.99	$CuCl^+$	-24.37
$CaOH^+$	-10.03	$CuCl_2(aq)$	-29.54
$Cu(NH_3)^{+2}$	-32.99	$CuCl_3^-$	-35.22
$Cu(NH_3)_2(OH)_2(aq)$	-51.02	$CuCl_4^{-2}$	-41.61
$Cu(NH_3)_2^+$	-16.41	CuO_2^{-2}	-35.14
$Cu(NH_3)_2^{+2}$	-24.67	CuO_2H^-	-28.03
$Cu(NH_3)_3(OH)^+$	-19.54	$CuO(aq)$	-22.02
$Cu(NH_3)_3^{+2}$	-16.97	$CuOH^+$	-21.88
$Cu(NH_3)_4^{+2}$	-10.05	$Fe(CO_3)(aq)$	-9.402
$Cu_2Cl_4^{-2}$	-36.25	$Fe(HCO_3)^+$	-8.195
$Cu_3Cl_6^{-3}$	-214.6	$Fe(HSO_4)^+$	-13.26
$Cu(HCO_3)^+$	-20.22	$Fe(SO_4)(aq)$	-7.333
$Cu(OH)_2^-$	-18.14	Fe^{+2}	-5.672
$Cu(OH)(aq)$	-20.25	$FeCl^+$	-9.613
Cu^+	-15.43	$FeCl_2(aq)$	-22
$CuCl_2^-$	-18.29	FeO_2H^-	-14.65
$CuCl_3^{-2}$	-21.97	$FeO(aq)$	-12.59
$CuCl(aq)$	-17.18	$FeOH^+$	-8.43
$Cu(CO_3)_2^{-2}$	-23.51	$Fe(HSO_4)^{+2}$	-27.41
$Cu(NO_2)^+$	-85.47	$Fe(SO_4)^+$	-21.1
$Cu(NO_2)_2(aq)$	-151.6	$Fe(SO_4)^{2-}$	-23.67
$Cu(NO_3)^+$	-106.3	Fe^{+3}	-21.23
$Cu(NO_3)_2(aq)$	-193.3	$Fe_2(OH)_2^{+4}$	-31.92
$Cu(OH)_2(aq)$	-23.47	$Fe_3(OH)_4^{+5}$	-43.01
$Cu(OH)_3^-$	-27.19	$FeCl^{+2}$	-23.83
$Cu(OH)_4^{-2}$	-33.36	$FeCl_2^+$	-27.26

Table A-1: Parameters of Dependent Components-Cont'd

Species name	Log activity	Species name	Log activity
$FeCl_3(aq)$	-32.34	$N_2(aq)$	-20.52
FeO^+	-13.41	$O_2(aq)$	-69.16
FeO_2^-	-15.86	$H_2O_2(aq)$	-51.21
$FeO_2H(aq)$	-13.56	HO_2^-	-56.15
$FeOH^{+2}$	-16.67	$HS_7O_3^-$	-64.45
$K(SO_4)^-$	-7.567	$HS_6O_3^-$	-57.58
K^+	-4.507	$HS_5O_3^-$	-53.33
$KOH(aq)$	-12.22	$HS_4O_3^-$	-45.11
$Na(CO_3)^-$	-10.75	$HS_3O_3^-$	-39.27
$Na(HCO_3)(aq)$	-8.679	$S_7O_6^{-2}$	-24.75
$Na(SO_4)^-$	-7.117	$S_6O_6^{-2}$	-27.01
Na^+	-3.906	$H_2S_2O_3(aq)$	-27.71
$NaOH(aq)$	-11.34	$HS_2O_3^-$	-21.55
$CO(aq)$	-18.38	$S_5O_6^{-2}$	-60.16
$CO_2(aq)$	-4.913	$S_4O_6^{-2}$	-38.87
CO_3^{-2}	-8.109	$H_2S_2O_4(aq)$	-46.63
HCO_3^-	-4.523	$HS_2O_4^-$	-40.25
$CH_4(aq)$	-17.07	$S_2O_4^{-2}$	-36
CN^-	-42.6	$S_3O_6^{-2}$	-46.46
$HCN(aq)$	-40.1	$HS_2O_5^-$	-5.769
OCN^-	-28.47	HSO_3^-	-15.24
SCN^-	-35.49	$S_2O_5^{-2}$	-35.79
ClO^-	-53.77	$SO_2(aq)$	-20.37
$HClO(aq)$	-52.96	SO_3^{-2}	-15.72
ClO_2^-	-96.36	$HS_2O_6^-$	-26.02
$HClO_2(aq)$	-101.1	$S_2O_6^{-2}$	-38.14
ClO_3^-	-125.1	$HS_2O_7^-$	-6.739
ClO_4^-	-158.1	HSO_4^-	-8.665
Cl^-	-4.08	$S_2O_7^{-2}$	-101.2
$HCl(aq)$	-11.53	$SO_3(aq)$	-14.07
$H_2(aq)$	-11.52	SO_4^{-2}	-3.91
$H_2N_2O_2(aq)$	-98.33	$HS_2O_8^-$	-15.85
$HN_2O_2^-$	-98.63	$S_2O_8^{-2}$	-78.39
$N_2O_2^{-2}$	-102.9	HSO_5^-	-62.53
$HNO_2(aq)$	-70.28	S_8^{-2}	-64.95
NO_2^-	-66.76	S_7^{-2}	-56.7
$HNO_3(aq)$	-94.16	HS_6^-	-50.08
NO_3^-	-86.12	S_6^{-2}	-48.04
$N_2H_5^+$	-55.35	HS_5^-	-41.55
$N_2H_6^{+2}$	-63.12	HS_4^-	-36.15
$NH_3(aq)$	-16.62	HS_3^-	-26.18
NH_4^+	-14.12	S_2^{-2}	-22.56

Table A-1: Parameters of Dependent Components-Cont'd

Species name	Log activity	Species name	Concentration(moles)
S_3^{-2}	-28.39	*Calcite(s)*	0
S_4^{-2}	-34.43	*Gypsum(s)*	0
S_5^{-2}	-40.7	*Chalcopyrite(s)*	0
HS_2^-	-17.71	*Cuprite(s)*	0
$H_2S(aq)$	-10.37	*Chalcocite(s)*	3.14285e-005
HS^-	-10.62	*Covellite(s)*	0
S^{-2}	-22.88	*Fe-carbonate(s)*	0
OH^-	-7.257	*Magnetite(s)*	0
H^+	-6.742	*Goethite(s)*	5.94097e-005
$H_2O(aq)$	-4.20E-06	*Pyrite(s)*	0.833
$CO_2(g)$	-3.446	*Pyrrhotite(s)*	0
$CH_4(g)$	-14.22	*Troilite(s)*	0
$H_2(g)$	-8.414	*Melanterite(s)*	0
$O_2(g)$	-66.28	*Sulphur(s)*	0
$H_2O(g)$	-4.20E-06		

*Concentration is given for aqueous species in mol/(kgH_2O), for other species - in the mole fraction scale.

Temperature = 50°C

State variables
P(bar) = 1 T = 50 (°C) = 323.15 (K) V(cm^3) = 1032.1627
Mass(kg) = 1.1000358 Min. potential (moles): $G(x)$ = -4991.98176

Aqueous phase:
I(molal)= 0.000631 pH= 7.504 p_e= -3.819 E_h(V)= -0.2444

Table A-2: Parameters of Dependent Components at 50°C

Species name	Log activity	Species name	Log activity
$Ca(CO_3)(aq)$	-7.584	Cu^{+2}	-22.41
$Ca(HCO_3)^+$	-7.23	$Cu_2(OH)_2^{+2}$	-39.23
$Ca(SO_4)(aq)$	-5.553	$Cu_3(OH)_4^{+2}$	-57.01
Ca^{+2}	-3.993	$CuCl^+$	-26.03
$CaOH^+$	-8.227	$CuCl_2(aq)$	-31.18
$Cu(NH_3)^{+2}$	-32.29	$CuCl_3^-$	-36.99
$Cu(NH_3)_2(OH)_2(aq)$	-45.24	$CuCl_4^{-2}$	-43.67
$Cu(NH_3)_2^+$	-14.44	CuO_2^{-2}	-31.22
$Cu(NH_3)_2^{+2}$	-24.21	CuO_2H^-	-25.53
$Cu(NH_3)_3(OH)^+$	-18.1	$CuO(aq)$	-21.18
$Cu(NH_3)_3^{+2}$	-16.75	$CuOH^+$	-22.21
$Cu(NH_3)_4^{+2}$	-10.05	$Fe(CO_3)(aq)$	-10.29
$Cu_2Cl_4^{-2}$	-37.19	$Fe(HCO_3)^+$	-10.21
$Cu_3Cl_6^{-3}$	-204.2	$Fe(HSO_4)^+$	-15.82
$Cu(HCO_3)^+$	-21.71	$Fe(SO_4)(aq)$	-9.248
$Cu(OH)_2^-$	-16.78	Fe^{+2}	-7.689

$Cu(OH)(aq)$	-18.23	$FeCl^{+}$	-11.58
Cu^{+}	-15.5	$FeCl_2(aq)$	-22.63
$CuCl_2^{-}$	-18.89	FeO_2H^{-}	-12.52
$CuCl_3^{-2}$	-22.86	$FeO(aq)$	-11.54
$CuCl(aq)$	-17.43	$FeOH^{+}$	-8.972
$Cu(CO_3)_2^{-2}$	-22.62	$Fe(HSO_4)^{+2}$	-31.4
$Cu(NO_2)^{+}$	-81.1	$Fe(SO_4)^{+}$	-23.87
$Cu(NO_2)_2(aq)$	-141.1	$Fe(SO_4)^{2-}$	-26.48
$Cu(NO_3)^{+}$	-101	Fe^{+3}	-24.22
$Cu(NO_3)_2(aq)$	-180.9	$Fe_2(OH)_2^{+4}$	-35.62
$Cu(OH)_2(aq)$	-22.53	$Fe_3(OH)_4^{+5}$	-48.14
$Cu(OH)_3^{-}$	-25.16	$FeCl^{+2}$	-26.73
$Cu(OH)_4^{-2}$	-30.53	$FeCl_2^{+}$	-30.18

Table A-2: Parameters of Dependent Components-Cont'd

Species name	**Log activity**	**Species name**	**Log activity**
$FeCl_3(aq)$	-35.39	$N_2(aq)$	-17.68
FeO^{+}	-13.82	$O_2(aq)$	-64.71
FeO_2^{-}	-13.45	$H_2O_2(aq)$	-47.65
$FeO_2H(aq)$	-12.43	HO_2^{-}	-51.44
$FeOH^{+2}$	-18.33	$HS_7O_3^{-}$	-65.76
$K(SO_4)^{-}$	-7.532	$HS_6O_3^{-}$	-58.8
K^{+}	-4.507	$HS_5O_3^{-}$	-54.21
$KOH(aq)$	-10.62	$HS_4O_3^{-}$	-45.66
$Na(CO_3)^{-}$	-9.988	$HS_3O_3^{-}$	-39.36
$Na(HCO_3)(aq)$	-8.521	$S_7O_6^{-2}$	-26.65
$Na(SO_4)^{-}$	-7.081	$S_6O_6^{-2}$	-28.27
Na^{+}	-3.907	$H_2S_2O_3(aq)$	-27.62
$NaOH(aq)$	-9.844	$HS_2O_3^{-}$	-20.92
$CO(aq)$	-17.42	$S_5O_6^{-2}$	-58.93
$CO_2(aq)$	-5.633	$S_4O_6^{-2}$	-38.33
CO_3^{-2}	-7.069	$H_2S_2O_4(aq)$	-45.66
HCO_3^{-}	-4.404	$HS_2O_4^{-}$	-38.75
$CH_4(aq)$	-14.8	$S_2O_4^{-2}$	-33.83
CN^{-}	-37.27	$S_3O_6^{-2}$	-45.25
$HCN(aq)$	-36.09	$HS_2O_5^{-}$	-8.348
OCN^{-}	-24.87	HSO_3^{-}	-14.47
SCN^{-}	-31.09	$S_2O_5^{-2}$	-34.27
ClO^{-}	-50.67	$SO_2(aq)$	-20.06
$HClO(aq)$	-50.78	SO_3^{-2}	-14.35
ClO_2^{-}	-90.41	$HS_2O_6^{-}$	-19.8
$HClO_2(aq)$	-95.71	$S_2O_6^{-2}$	-37.04
ClO_3^{-}	-117.4	$HS_2O_7^{-}$	-5.189
ClO_4^{-}	-148.5	HSO_4^{-}	-9.143
Cl^{-}	-4.081	$S_2O_7^{-2}$	-95.58
$HCl(aq)$	-12.38	$SO_3(aq)$	-15.71
$H_2(aq)$	-9.975	SO_4^{-2}	-3.948
$H_2N_2O_2(aq)$	-89.97	$HS_2O_8^{-}$	-12.06

$HN_2O_2^-$	-89.28	$S_2O_8^{-2}$	-75.07
$N_2O_2^{-2}$	-92.43	HSO_5^-	-59.16
$HNO_2(aq)$	-65.05	S_8^{-2}	-60.91
NO_2^-	-60.6	S_7^{-2}	-52.83
$HNO_3(aq)$	-87.59	HS_6^-	-52.63
NO_3^-	-79.04	S_6^{-2}	-43.8
$N_2H_5^+$	-50.1	HS_5^-	-44.54
$N_2H_6^{+2}$	-58.76	HS_4^-	-38.69
$NH_3(aq)$	-13.87	HS_3^-	-28.17
NH_4^+	-12.84	S_2^{-2}	-18.94

Table A-2: Parameters of Dependent Components-Cont'd

Species name	Log activity	Species name	Concentration(moles)
S_3^{-2}	-24.74	*Calcite(s)*	0
S_4^{-2}	-30.75	*Gypsum(s)*	0
S_5^{-2}	-36.95	*Chalcopyrite(s)*	0
HS_2^-	-18.66	*Cuprite(s)*	0
$H_2S(aq)$	-9.222	*Chalcocite(s)*	3.14e-5
HS^-	-8.441	*Covellite(s)*	0
S^{-2}	-18.47	*Fe-carbonate(s)*	0
OH^-	-5.771	*Magnetite(s)*	0
H^+	-7.504	*Goethite(s)*	6.12e-5
$H_2O(aq)$	-4.14E-06	*Pyrite(s)*	0.833
$CO_2(g)$	-3.922	*Pyrrhotite(s)*	0
$CH_4(g)$	-11.81	*Troilite(s)*	0
$H_2(g)$	-6.836	*Melanterite(s)*	0
$O_2(g)$	-61.69	*Sulphur(s)*	0
$H_2O(g)$	-4.14E-06		

*Concentration is given for aqueous species in mol/(kgH_2O), for other species - in the mole fraction scale.

Temperature = 75°C

State variables:
P(bar) = 1 T = 75 (°C) = 348.15 (K) V(cm^3) = 1046.0971
Mass(kg) = 1.1000358 Min. potential (moles): $G(x)$ = -4671.74553

Aqueous phase:
I(molal) = 0.0005945 pH = 8.404 p_e = -5.224 E_h(V) = -0.3601

Table A-3: Parameters of Dependent Components at 75°C

Species name	Log activity	Species name	Log activity
$Ca(CO_3)(aq)$	-6.338	Cu^{+2}	-24.43
$Ca(HCO_3)^+$	-7.101	$Cu_2(OH)_2^{+2}$	-40.78
$Ca(SO_4)(aq)$	-5.577	$Cu_3(OH)_4^{+2}$	-58.58
Ca^{+2}	-3.997	$CuCl^+$	-27.94
$CaOH^+$	-6.449	$CuCl_2(aq)$	-33.03

$Cu(NH_3)^{+2}$	-31.83	$CuCl_3^-$	-38.9
$Cu(NH_3)_2(OH)_2(aq)$	-39.62	$CuCl_4^{-2}$	-45.8
$Cu(NH_3)_2^+$	-12.55	CuO_2^{-2}	-27.54
$Cu(NH_3)_2^{+2}$	-23.91	CuO_2H^-	-23.28
$Cu(NH_3)_3(OH)^+$	-16.75	$CuO(aq)$	-20.54
$Cu(NH_3)_3^{+2}$	-16.63	$CuOH^+$	-22.81
$Cu(NH_3)_4^{+2}$	-10.1	$Fe(CO_3)(aq)$	-11.32
$Cu_2Cl_4^{-2}$	-38.51	$Fe(HCO_3)^+$	-12.36
$Cu_3Cl_6^{-3}$	-196	$Fe(HSO_4)^+$	-18.63
$Cu(HCO_3)^+$	-23.74	$Fe(SO_4)(aq)$	-11.35
$Cu(OH)_2^-$	-15.46	Fe^{+2}	-9.817
$Cu(OH)(aq)$	-16.55	$FeCl^+$	-13.6
Cu^+	-15.81	$FeCl_2(aq)$	-23.47
$CuCl_2^-$	-19.57	FeO_2H^-	-10.37
$CuCl_3^{-2}$	-23.74	$FeO(aq)$	-10.55
$CuCl(aq)$	-17.85	$FeOH^+$	-9.587
$Cu(CO_3)_2^{-2}$	-22.27	$Fe(HSO_4)^{+2}$	-35.7
$Cu(NO_2)^+$	-77.67	$Fe(SO_4)^+$	-27.03
$Cu(NO_2)_2(aq)$	-132.2	$Fe(SO_4)^{2-}$	-29.74
$Cu(NO_3)^+$	-96.99	Fe^{+3}	-27.5
$Cu(NO_3)_2(aq)$	-170.6	$Fe_2(OH)_2^{+4}$	-39.73
$Cu(OH)_2(aq)$	-21.9	$Fe_3(OH)_4^{+5}$	-53.69
$Cu(OH)_3^-$	-23.39	$FeCl^{+2}$	-29.89
$Cu(OH)_4^{-2}$	-27.89	$FeCl_2^+$	-33.25

Table A-3: Parameters of Dependent Components-Cont'd

Species name	Log activity	Species name	Log activity
$FeCl_3(aq)$	-38.52	$N_2(aq)$	-14.72
FeO^+	-14.45	$O_2(aq)$	-61.11
FeO_2^-	-11.19	$H_2O_2(aq)$	-44.73
$FeO_2H(aq)$	-11.53	HO_2^-	-47.34
$FeOH^{+2}$	-20.24	$HS_7O_3^-$	-67.76
$K(SO_4)^-$	-7.565	$HS_6O_3^-$	-60.57
K^+	-4.507	$HS_5O_3^-$	-55.58
$KOH(aq)$	-9.048	$HS_4O_3^-$	-46.65
$Na(CO_3)^-$	-9.203	$HS_3O_3^-$	-39.84
$Na(HCO_3)(aq)$	-8.436	$S_7O_6^{-2}$	-29.3
$Na(SO_4)^-$	-7.12	$S_6O_6^{-2}$	-30.26
Na^+	-3.907	$H_2S_2O_3(aq)$	-28.04
$NaOH(aq)$	-8.347	$HS_2O_3^-$	-20.65
$CO(aq)$	-16.72	$S_5O_6^{-2}$	-58.71
$CO_2(aq)$	-6.501	$S_4O_6^{-2}$	-38.57
CO_3^{-2}	-6.088	$H_2S_2O_4(aq)$	-45.45
HCO_3^-	-4.397	$HS_2O_4^-$	-37.86
$CH_4(aq)$	-12.6	$S_2O_4^{-2}$	-32.19

CN^-	-32.23	$S_3O_6^{-2}$	-44.81
$HCN(aq)$	-32.37	$HS_2O_5^-$	-11.06
OCN^-	-21.45	HSO_3^-	-13.97
SCN^-	-26.95	$S_2O_5^{-2}$	-33.32
ClO^-	-48.15	$SO_2(aq)$	-20.14
$HClO(aq)$	-49.26	SO_3^{-2}	-13.16
ClO_2^-	-85.58	$HS_2O_6^-$	-15.1
$HClO_2(aq)$	-91.53	$S_2O_6^{-2}$	-36.59
ClO_3^-	-111.1	$HS_2O_7^-$	-4.622
ClO_4^-	-140.7	HSO_4^-	-9.843
Cl^-	-4.081	$S_2O_7^{-2}$	-91.29
$HCl(aq)$	-13.28	$SO_3(aq)$	-17.59
$H_2(aq)$	-8.495	SO_4^{-2}	-4.092
$H_2N_2O_2(aq)$	-82.46	$HS_2O_8^-$	-9.791
$HN_2O_2^-$	-80.72	$S_2O_8^{-2}$	-72.96
$N_2O_2^{-2}$	-82.74	HSO_5^-	-56.66
$HNO_2(aq)$	-60.56	S_8^{-2}	-57.76
NO_2^-	-55.08	S_7^{-2}	-49.68
$HNO_3(aq)$	-82.07	HS_6^-	-55.37
NO_3^-	-72.87	S_6^{-2}	-40.48
$N_2H_5^+$	-45.16	HS_5^-	-47.36
$N_2H_6^{+2}$	-54.82	HS_4^-	-41.02
$NH_3(aq)$	-11.1	HS_3^-	-29.91
NH_4^+	-11.58	S_2^{-2}	-15.53

Table A-3: Parameters of Dependent Components-Cont'd

Species name	**Log activity**	**Species name**	**Concentration(moles)**
S_3^{-2}	-21.42	*Calcite(s)*	0
S_4^{-2}	-27.49	*Gypsum(s)*	0
S_5^{-2}	-33.76	*Chalcopyrite(s)*	0
HS_2^-	-19.41	*Cuprite(s)*	0
$H_2S(aq)$	-8.191	*Chalcocite(s)*	3.14e-5
HS^-	-6.352	*Covellite(s)*	0
S^{-2}	-14.22	*Fe-carbonate(s)*	0
OH^-	-4.303	*Magnetite(s)*	0
H^+	-8.404	*Goethite(s)*	6.14e-5
$H_2O(aq)$	-4.39E-06	*Pyrite(s)*	0.833
$CO_2(g)$	-4.631	*Pyrrhotite(s)*	0
$CH_4(g)$	-9.543	*Troilite(s)*	0
$H_2(g)$	-5.363	*Melanterite(s)*	0
$O_2(g)$	-58.03	*Sulphur(s)*	0
$H_2O(g)$	-4.39E-06		

*Concentration is given for aqueous species in mol/(kgH_2O), for other species - in the mole fraction scale.

Temperature = 100°C

State variables:
P(bar) = 3 T = 100 (°C) = 373.15 (K) V(cm^3) = 1063.6275
Mass(kg) = 1.1000358 Min. potential (moles): $G(x)$ = -4396.81029

Aqueous phase:
I(molal) = 0.0005093 pH = 8.493 p_e = -5.697 E_h(V) = -0.421

Table A-4: Parameters of Dependent Components at 100°C

Species name	Log activity	Species name	Log activity
$Ca(CO_3)(aq)$	-5.966	Cu^{+2}	-24.74
$Ca(HCO_3)^+$	-6.943	$Cu_2(OH)_2^{+2}$	-40.69
$Ca(SO_4)(aq)$	-6.693	$Cu_3(OH)_4^{+2}$	-58.51
Ca^{+2}	-3.997	$CuCl^+$	-28.1
$CaOH^+$	-5.604	$CuCl_2(aq)$	-33.08
$Cu(NH_3)^{+2}$	-31.59	$CuCl_3^-$	-38.96
$Cu(NH_3)_2(OH)_2(aq)$	-37.99	$CuCl_4^{-2}$	-46.02
$Cu(NH_3)_2^+$	-11.78	CuO_2^{-2}	-25.74
$Cu(NH_3)_2^{+2}$	-23.8	CuO_2H^-	-22
$Cu(NH_3)_3(OH)^+$	-16.43	$CuO(aq)$	-19.94
$Cu(NH_3)_3^{+2}$	-16.65	$CuOH^+$	-22.58
$Cu(NH_3)_4^{+2}$	-10.25	$Fe(CO_3)(aq)$	-11.56
$Cu_2Cl_4^{-2}$	-38.23	$Fe(HCO_3)^+$	-12.82
$Cu_3Cl_6^{-3}$	-186.8	$Fe(HSO_4)^+$	-20.02
$Cu(HCO_3)^+$	-24.14	$Fe(SO_4)(aq)$	-12.92
$Cu(OH)_2^-$	-15.07	Fe^{+2}	-10.3
$Cu(OH)(aq)$	-15.11	$FeCl^+$	-13.93
Cu^+	-15.35	$FeCl_2(aq)$	-22.75
$CuCl_2^-$	-19.36	FeO_2H^-	-9.23
$CuCl_3^{-2}$	-23.67	$FeO(aq)$	-9.73
$CuCl(aq)$	-17.46	$FeOH^+$	-9.449
$Cu(CO_3)_2^{-2}$	-22.06	$Fe(HSO_4)^{+2}$	-37.64
$Cu(NO_2)^+$	-75.32	$Fe(SO_4)^+$	-28.77
$Cu(NO_2)_2(aq)$	-127.2	$Fe(SO_4)^{2-}$	-32.67
$Cu(NO_3)^+$	-94	Fe^{+3}	-28.25
$Cu(NO_3)_2(aq)$	-164.2	$Fe_2(OH)_2^{+4}$	-40.48
$Cu(OH)_2(aq)$	-21.36	$Fe_3(OH)_4^{+5}$	-54.98
$Cu(OH)_3^-$	-22.62	$FeCl^{+2}$	-30.48
$Cu(OH)_4^{-2}$	-27.09	$FeCl_2^+$	-33.69

Table A-4: Parameters of Dependent Components-Cont'd

Species name	Log activity	Species name	Log activity
$FeCl_3(aq)$	-38.97	$N_2(aq)$	-15.07
FeO^+	-14.31	$O_2(aq)$	-57.77
FeO_2^-	-9.969	$H_2O_2(aq)$	-42.14
$FeO_2H(aq)$	-10.8	HO_2^-	-44.45

$FeOH^{+2}$	-20.49	$HS_7O_3^-$	-69.69
$K(SO_4)^-$	-8.693	$HS_6O_3^-$	-62.33
K^+	-4.507	$HS_5O_3^-$	-57.06
$KOH(aq)$	-8.407	$HS_4O_3^-$	-47.83
$Na(CO_3)^-$	-9.245	$HS_3O_3^-$	-40.66
$Na(HCO_3)(aq)$	-8.344	$S_7O_6^{-2}$	-32.2
$Na(SO_4)^-$	-8.26	$S_6O_6^{-2}$	-32.65
Na^+	-3.907	$H_2S_2O_3(aq)$	-28.12
$NaOH(aq)$	-7.77	$HS_2O_3^-$	-20.84
$CO(aq)$	-15.44	$S_5O_6^{-2}$	-59.25
$CO_2(aq)$	-6.506	$S_4O_6^{-2}$	-39.57
CO_3^{-2}	-5.995	$H_2S_2O_4(aq)$	-44.89
HCO_3^-	-4.406	$HS_2O_4^-$	-37.43
$CH_4(aq)$	-10.32	$S_2O_4^{-2}$	-31.85
CN^-	-29.57	$S_3O_6^{-2}$	-45.28
$HCN(aq)$	-30.11	$HS_2O_5^-$	-13.62
OCN^-	-20.1	HSO_3^-	-14.02
SCN^-	-25.01	$S_2O_5^{-2}$	-33.5
ClO^-	-45.88	$SO_2(aq)$	-19.95
$HClO(aq)$	-47.12	SO_3^{-2}	-13.37
ClO_2^-	-81.2	$HS_2O_6^-$	-11.16
$HClO_2(aq)$	-86.99	$S_2O_6^{-2}$	-37.1
ClO_3^-	-105.5	$HS_2O_7^-$	-4.173
ClO_4^-	-133.6	HSO_4^-	-10.84
Cl^-	-4.081	$S_2O_7^{-2}$	-88.32
$HCl(aq)$	-13.32	$SO_3(aq)$	-18.86
$H_2(aq)$	-7.283	SO_4^{-2}	-5.357
$H_2N_2O_2(aq)$	-78.81	$HS_2O_8^-$	-7.853
$HN_2O_2^-$	-76.87	$S_2O_8^{-2}$	-71.84
$N_2O_2^{-2}$	-78.67	HSO_5^-	-54.79
$HNO_2(aq)$	-58	S_8^{-2}	-56.11
NO_2^-	-52.36	S_7^{-2}	-48.05
$HNO_3(aq)$	-78.54	HS_6^-	-58.4
NO_3^-	-69.49	S_6^{-2}	-38.96
$N_2H_5^+$	-43.32	HS_5^-	-50.38
$N_2H_6^{+2}$	-53.18	HS_4^-	-43.67
$NH_3(aq)$	-10.31	HS_3^-	-32.11
NH_4^+	-11.41	S_2^{-2}	-14.02

Table A-4: Parameters of Dependent Components-Cont'd

Species name	**Log activity**	**Species name**	**Concentration(moles)**
S_3^{-2}	-19.92	*Gypsum(s)*	0
S_4^{-2}	-26	*Chalcopyrite(s)*	0
S_5^{-2}	-32.26	*Cuprite(s)*	0
HS_2^-	-20.81	*Chalcocite(s)*	0
$H_2S(aq)$	-7.314	*Covellite(s)*	3.14e-5
HS^-	-5.305	*Fe-carbonate(s)*	0
S^{-2}	-11.99	*Magnetite(s)*	0
OH^-	-3.765	*Goethite(s)*	0

H^+	-8.493	*Pyrite(s)*	6.39e-5
$H_2O(aq)$	-5.09E-06	*Pyrrhotite(s)*	0.833
$CO_2(g)$	-4.536	*Troilite(s)*	0
$CH_4(g)$	-7.256	*Melanterite(s)*	0
$H_2(g)$	-4.184	*Sulphur(s)*	0
$O_2(g)$	-54.68	*Gypsum(s)*	0
$H_2O(g)$	0.4771		

*Concentration is given for aqueous species in mol/(kgH_2O), for other species - in the mole fraction scale.

Appendix B, Corrosion Domain Diagrams

1) $Cu + CO_3^{2-} + 2H^+ = CuCO_3(a) + H_2$

$$\log\left(\frac{p_{H2} \times a_{CuCO3}}{a_{CO3(2-)}}\right) = \frac{-\Delta G^0}{2.303RT} - 2pH$$

298.15: **log (p) = -4.63-2pH**

323.15: **log (p) = -3.70-2pH**

348.15: **log (p) = -2.84-2pH**

373.15: **log (p) = -2.30-2pH**

398.15: l**og (p) = -1.26-2pH;** 423.15: **log (p) = -0.52-2pH**

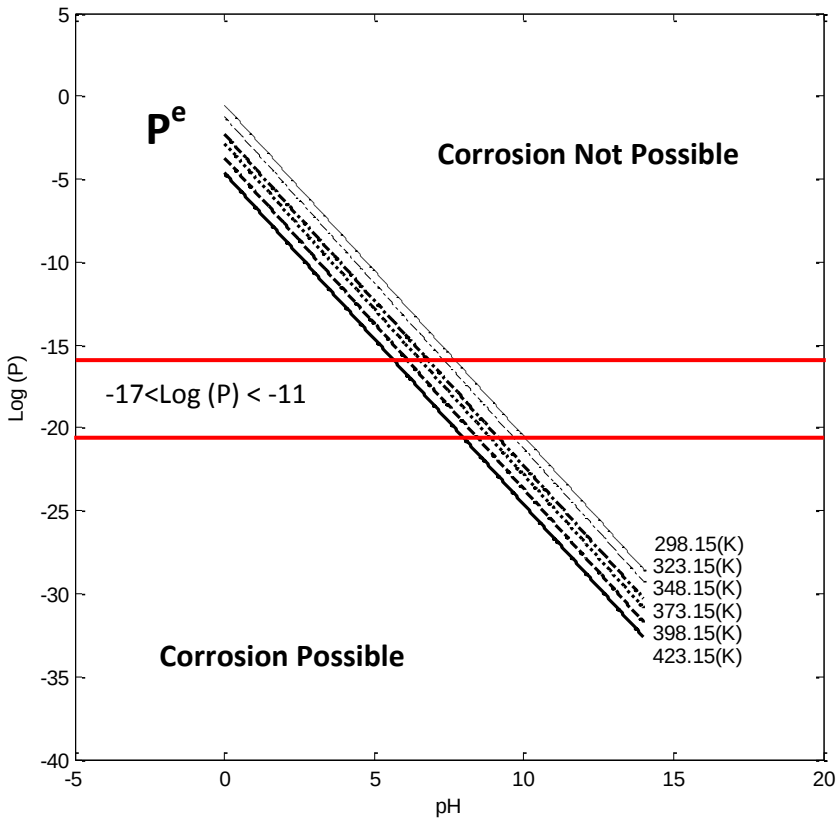

2) $Cu + 2CO_3^{2-} + 2H^+ = Cu(CO_3)_2^{-2}(a) + H_2$

$$\log\left(\frac{p_{H2} \times a_{Cu(CO3)2(-2)}}{a^2_{CO3(-2)}}\right) = \frac{-\Delta G^0}{2.303RT} - 2pH$$

298.15: **log (p) = -1.20-2pH**

323.15: **log (p) = 0.24-2pH**

348.15: **log (p) = 1.56-2pH**

373.15: **log (p) = 2.77-2pH**

398.15: **log (p) = 3.89-2pH**

423.15: **log (p) = 4.95-2pH**

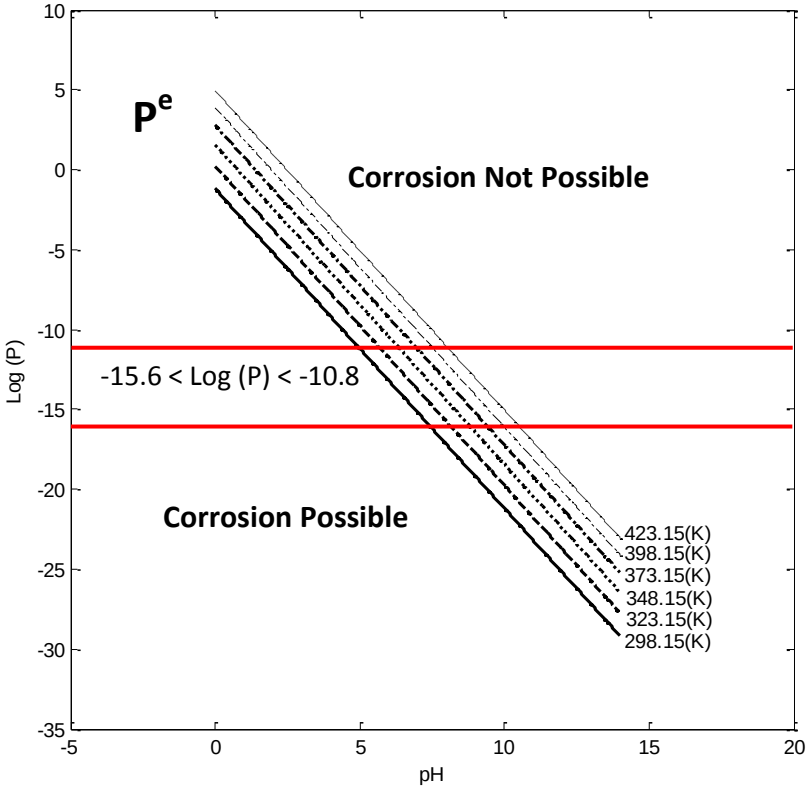

3) $Cu + Cl^- + H^+ = CuCl\ (a) + ½\ H_2$

$$\log\left(\frac{p_{H2}^{0.5} \times a_{CuCl}}{a_{Cl(-)}}\right) = \frac{-\Delta G^0}{2.303RT} - pH$$

298.15: **log (p) = -5.27-pH**

323.15: **log (p) = -4.26-pH**

348.15: **log (p) = -3.39-pH**

373.15: **log (p) = -2.65-pH**

398.15: **log (p) = -2.00-pH**

423.15: **log (p) = -1.43-pH**

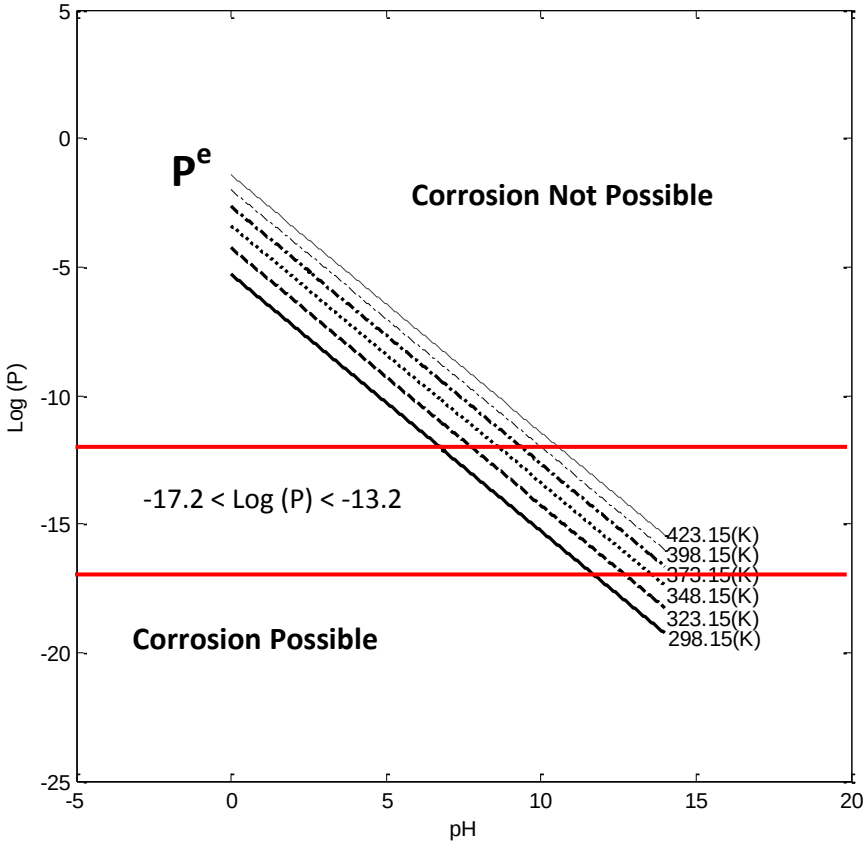

4) $Cu + 2Cl^- + 2H^+ = CuCl_2(a) + H_2$

$$\log\left(\frac{p_{H2} \times a_{CuCl2}}{a_{Cl(-)}^2}\right) = \frac{-\Delta G^0}{2.303RT} - 2pH$$

298.15: **log (p) = -11.17-2pH**

323.15: **log (p) = -9.99-2pH**

348.15: **log (p) = -8.82-2pH**

373.15: **log (p) = -7.68-2pH**

398.15: **log (p) = -6.54-2pH**

423.15: **log (p) = -5.42-2pH**

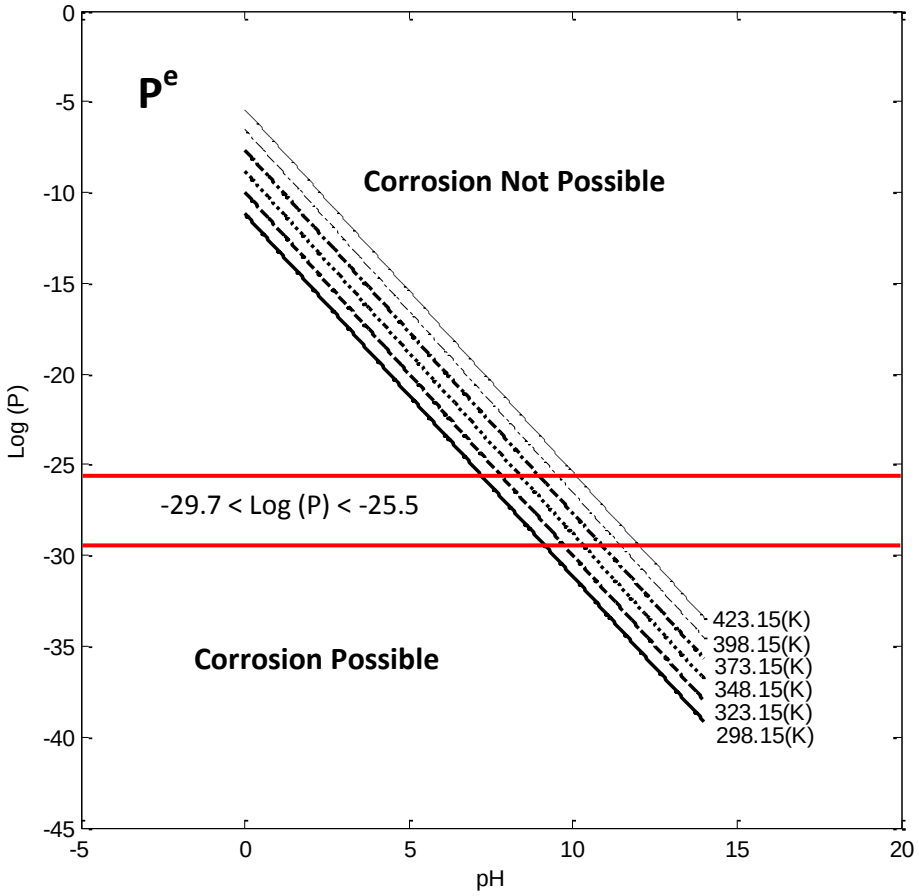

5) $Cu + 2Cl^- + H^+ = CuCl_2^-(a) + ½\ H_2$

$$\log\left(\frac{p_{H2}^{0.5} \times a_{CuCl2(-)}}{a_{Cl(-)}^2}\right) = \frac{-\Delta G^0}{2.303RT} - pH$$

298.15: **log (p) = -2.96-pH**

323.15: **log (p) = -2.25-pH**

348.15: **log (p) = -1.65-pH**

373.15: **log (p) = -1.14-pH**

398.15: **log (p) = -0.70-pH**

423.15: **log (p) = -0.33-pH**

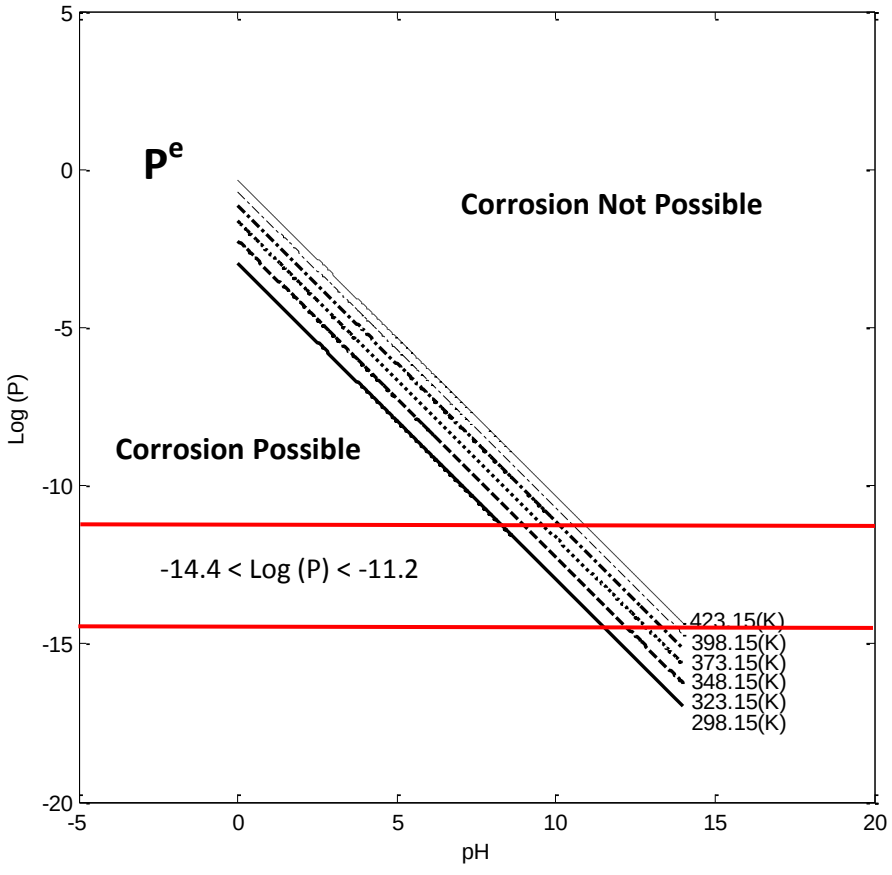

6) $Cu + 3Cl^- + 2H^+ = CuCl_3^-(a) + H_2$

$$\log\left(\frac{p_{H2} \times a_{CuCl3(-)}}{a_{Cl(-)}^3}\right) = \frac{-\Delta G^0}{2.303RT} - 2pH$$

298.15: **log (p) = -3.73-2pH**

323.15: **log (p) = -2.84-2pH**

348.15: **log (p) = -2.05-2pH**

373.15: **log (p) = -1.35-2pH**

398.15: **log (p) = -0.71-2pH**

423.15: **log (p) = -0.13-2pH**

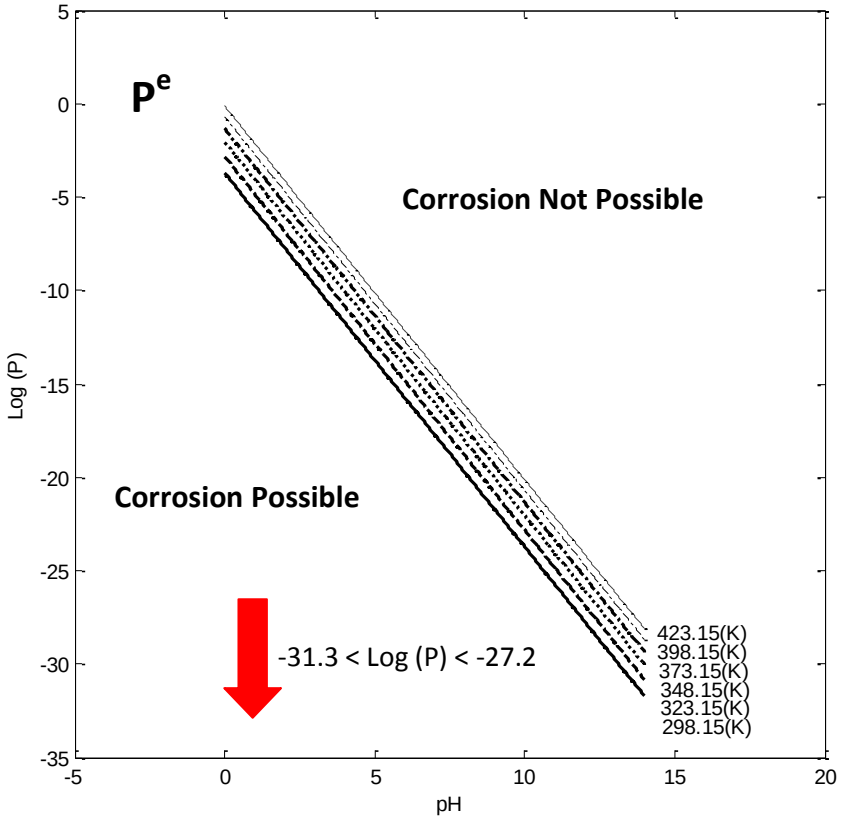

7) $Cu + 4Cl^- + 2H^+ = CuCl_4^{-2}(a) + H_2$

$$\log\left(\frac{p_{H2} \times a_{CuCl4(-2)}}{a^4_{Cl(-)}}\right) = \frac{-\Delta G^0}{2.303RT} - 2pH$$

298.15: **log (p) = -15.41-2pH**

323.15: **log (p) = -14.11-2pH**

348.15: **log (p) = -12.94-2pH**

373.15: **log (p) = -11.88-2pH**

398.15: **log (p) = -10.91-2pH**

423.15: **log (p) = -10.00-2pH**

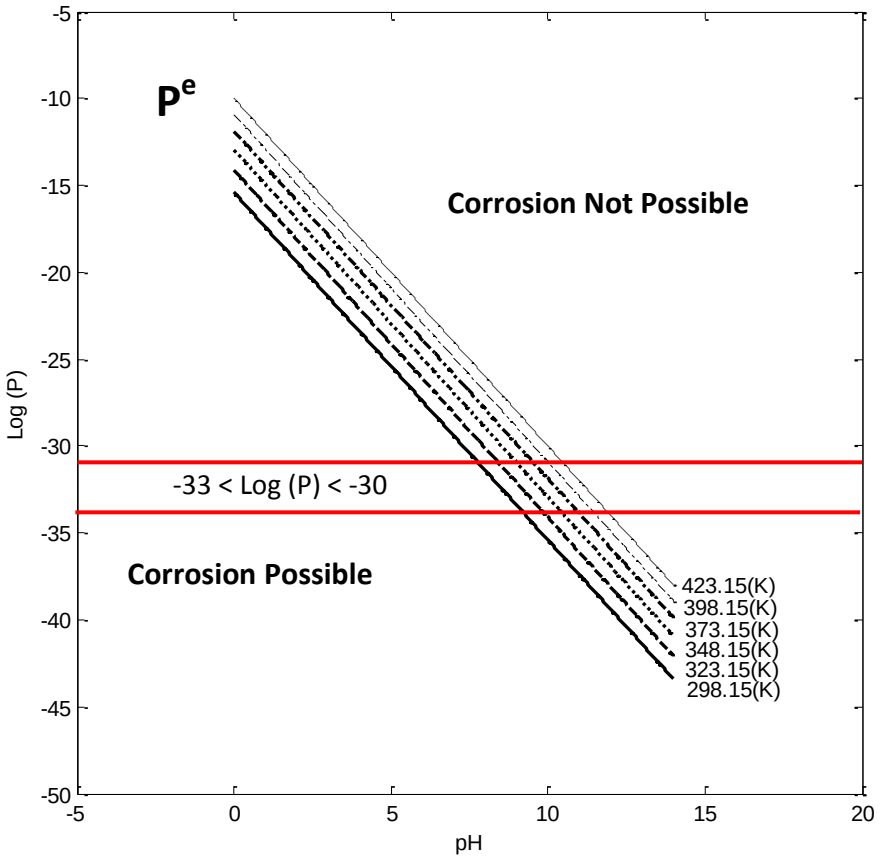

8) $2Cu + 4Cl^- + 2H^+ = Cu_2Cl_4^{-2}(a) + H_2$

$$\log\left(\frac{p_{H2} \times a_{Cu2Cl4(-2)}}{a^4_{Cl(-)}}\right) = \frac{-\Delta G^0}{2.303RT} - 2pH$$

298.15: **log (p) = -6.59-2pH**

323.15: **log (p) = -5.39-2pH**

348.15: **log (p) = -4.31-2pH**

373.15: **log (p) = -3.34-2pH**

398.15: **log (p) = -2.45-2pH**

423.15: **log (p) = -1.62-2pH**

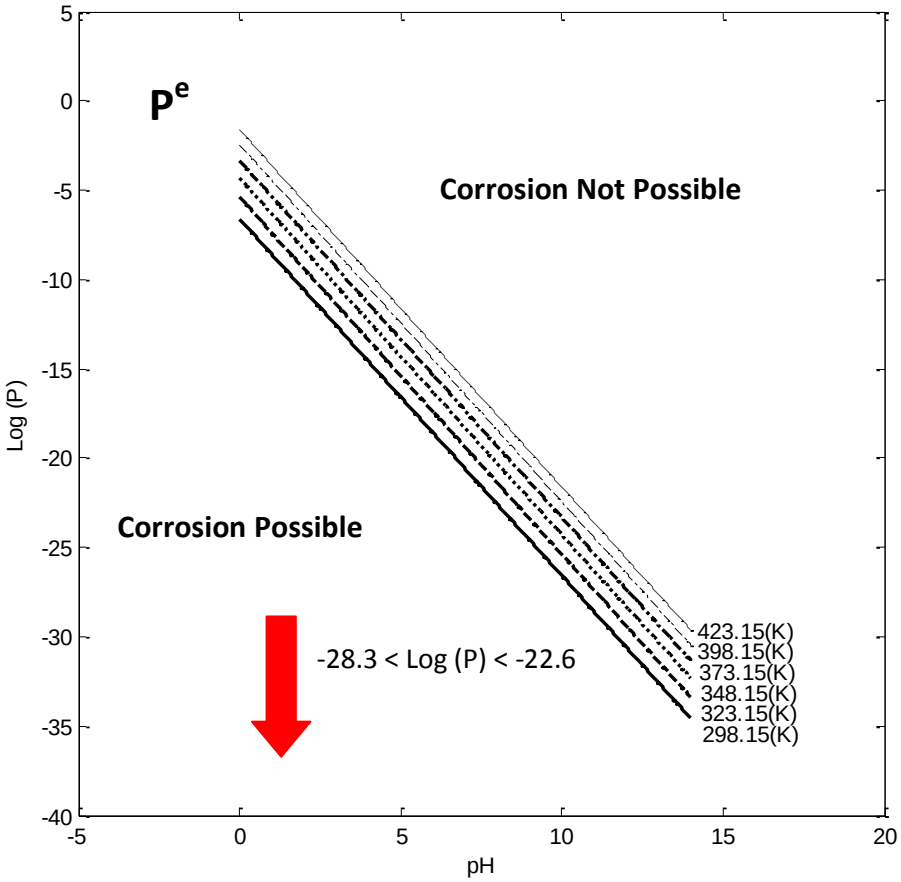

9) $3Cu + 6Cl^- + 3H^+ = Cu_3Cl_6^{-3}(a) + 1.5H_2$

$$\log\left(\frac{p_{H2}^{1.5} \times a_{Cu3Cl6(-3)}}{a_{Cl(-)}^{6}}\right) = \frac{-\Delta G^0}{2.303RT} - 3pH$$

298.15: **log (p) = -170.11-3pH**

323.15: **log (p) = -156.46-3pH**

348.15: **log (p) = -144.65-3pH**

373.15: **log (p) = -134.33-3pH**

398.15: **log (p) = -125.22-3pH**

423.15: **log (p) = -117.08-3pH**

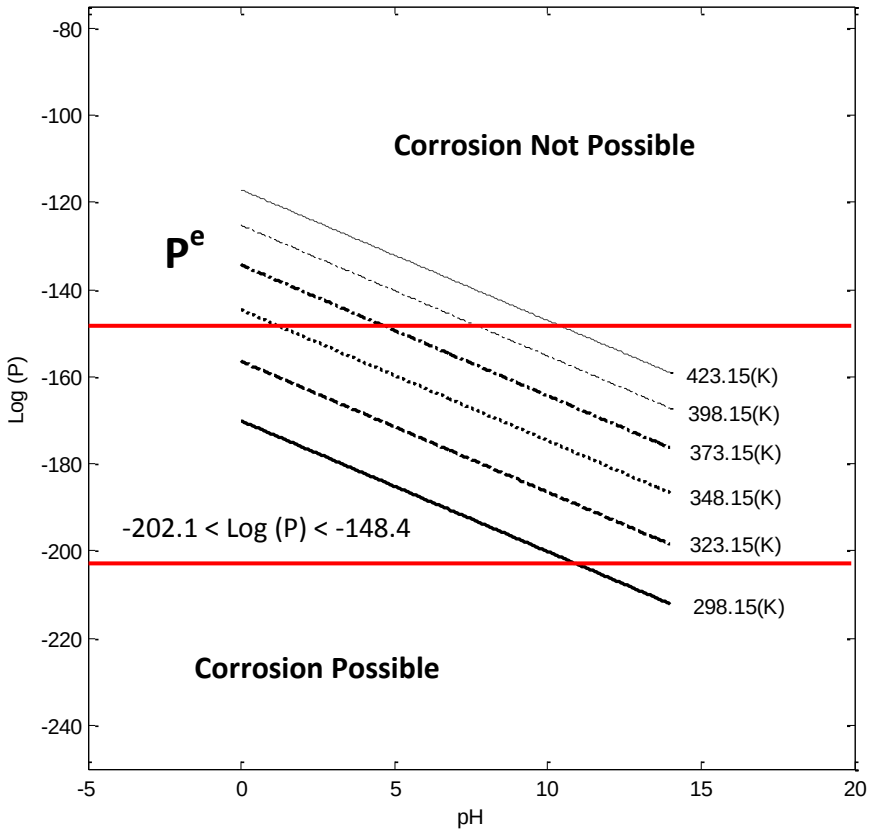

10) $Cu + HCO_3^- + 2H^+ = Cu(HCO_3)^+ (a) + H_2$

$$\log\left(\frac{p_{H2} \times a_{Cu(HCO3)(+)}}{a_{HCO3(-)}}\right) = \frac{-\Delta G^0}{2.303RT} - 2pH$$

298.15: **log (p) = -9.60-2pH**

323.15: **log (p) = -8.56-2pH**

348.15: **log (p) = -7.63-2pH**

373.15: **log (p) = -6.76-2pH**

398.15: **log (p) = -5.96-2pH**

423.15: **log (p) = -5.21-2pH**

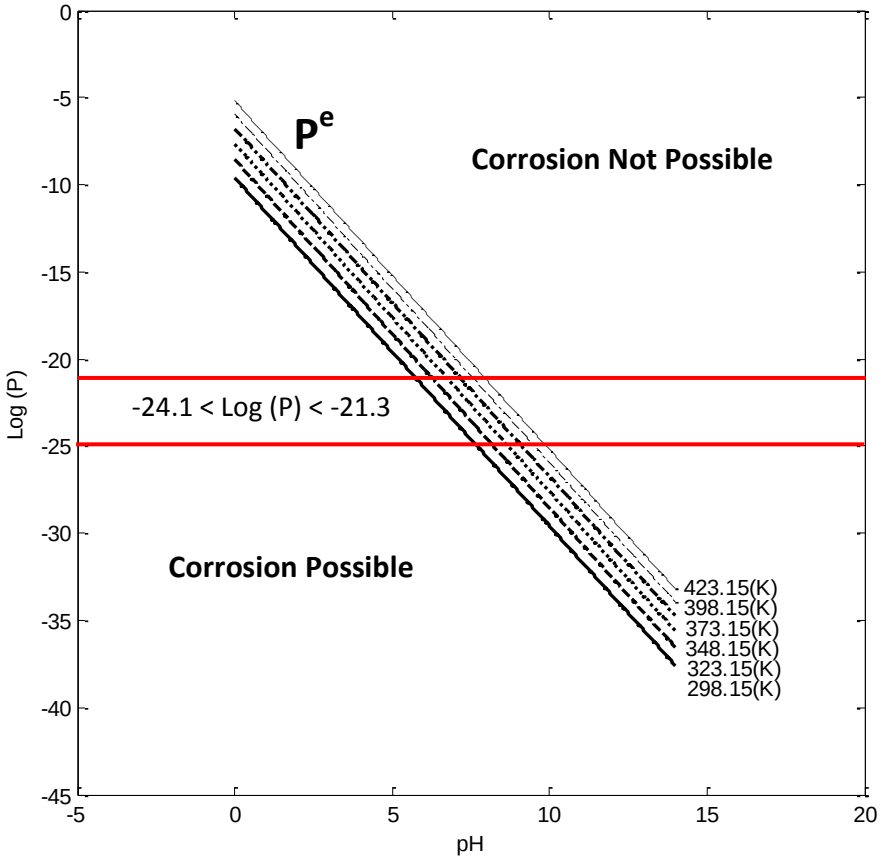

11) $Cu + HPO_4^{2-} + 2H^+ = CuHPO_4(a) + H_2$

$$\log\left(\frac{p_{H2} \times a_{CuHPO4}}{a_{HPO4(-2)}}\right) = \frac{-\Delta G^0}{2.303RT} - 2pH$$

298.15: **log (p) = -6.08-2pH**

323.15: **log (p) = -5.12-2pH**

348.15: **log (p) = -4.21-2pH**

373.15: **log (p) = -3.36-2pH**

398.15: **log (p) = -2.56-2pH**

423.15: **log (p) = -1.78-2pH**

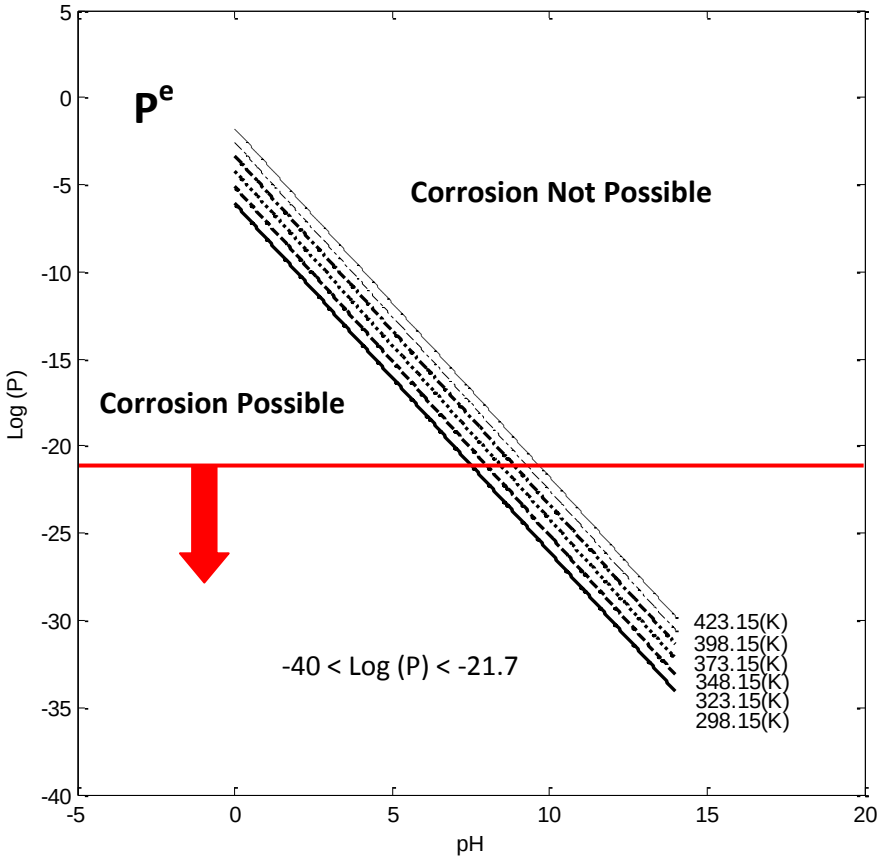

12) $Cu + H_2PO_4^- + H^+ = CuH_2PO_4(a) + ½\ H_2$

$$\log\left(\frac{p_{H2}^{0.5} \times a_{CuH2PO4}}{a_{H2PO4(-)}}\right) = \frac{-\Delta G^0}{2.303RT} - pH$$

298.15: **log (p) = -6.52-pH**

323.15: **log (p) = -5.64-pH**

348.15: **log (p) = -4.88-pH**

373.15: **log (p) = -4.23-pH**

398.15: **log (p) = -3.64-pH**

423.15: **log (p) = -3.12-pH**

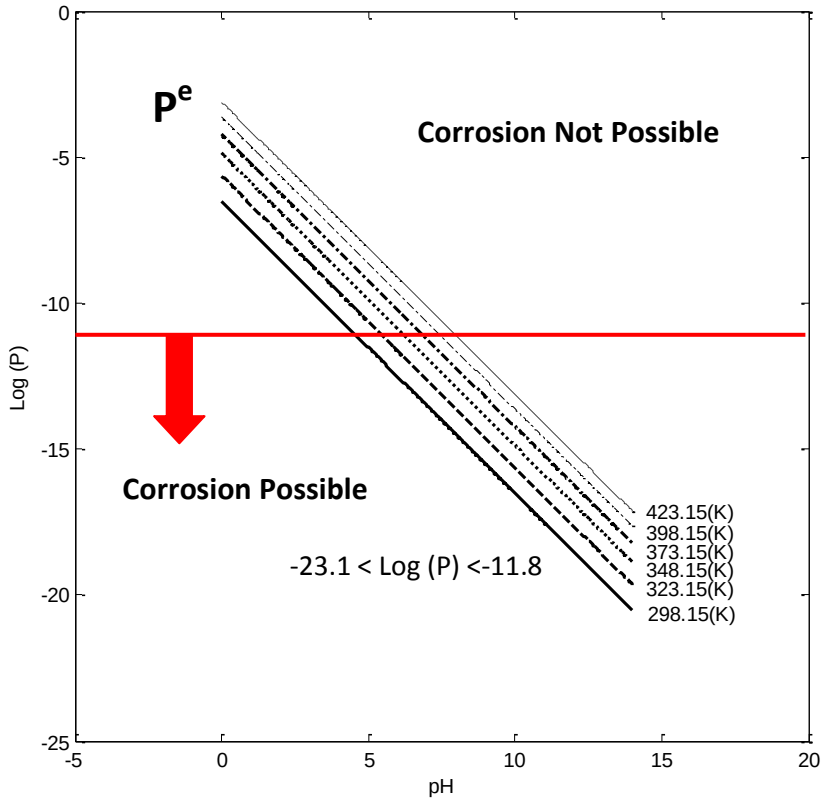

13) $Cu + H_2PO_4^- + 2H^+ = Cu(H_2PO_4)^+ (a) + H_2$

$$\log\left(\frac{p_{H2} \times a_{Cu(H2PO4)(+)}}{a_{H2PO4(-)}}\right) = \frac{-\Delta G^0}{2.303RT} - 2pH$$

298.15: **log (p) = -9.04-2pH**

323.15: **log (p) = -8.27-2pH**

348.15: **log (p) = -7.56-2pH**

373.15: **log (p) = -6.88-2pH**

398.15: **log (p) = -6.23-2pH**

423.15: **log (p) = -5.61-2pH**

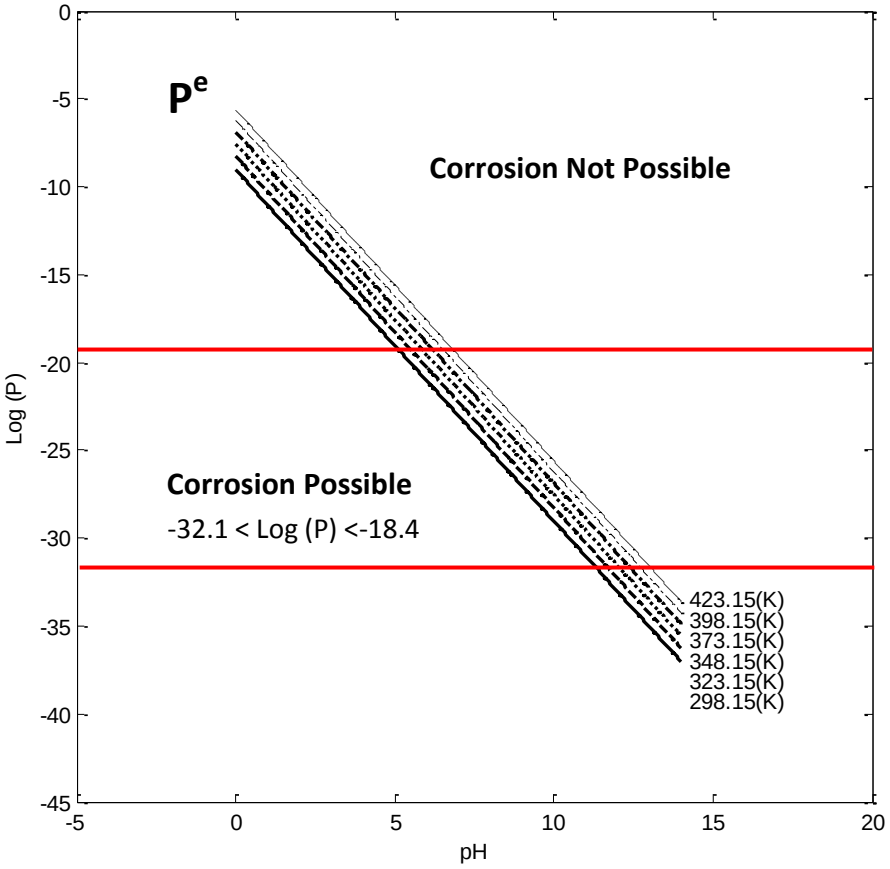

14) $Cu + 2HPO_4^{2-} + 2H^+ = Cu(HPO_4)_2^{-2}(a) + H_2$

$$\log\left(\frac{p_{H2} \times a_{Cu(HPO4)2(-2)}}{a^2_{HPO4(-2)}}\right) = \frac{-\Delta G^0}{2.303RT} - 2pH$$

298.15: **log (p) = -1.61-2pH**

323.15: **log (p) = -1.59-2pH**

348.15: **log (p) = -1.74-2pH**

373.15: **log (p) = -2.04-2pH**

398.15: **log (p) = -2.45-2pH**

423.15: **log (p) = -2.95-2pH**

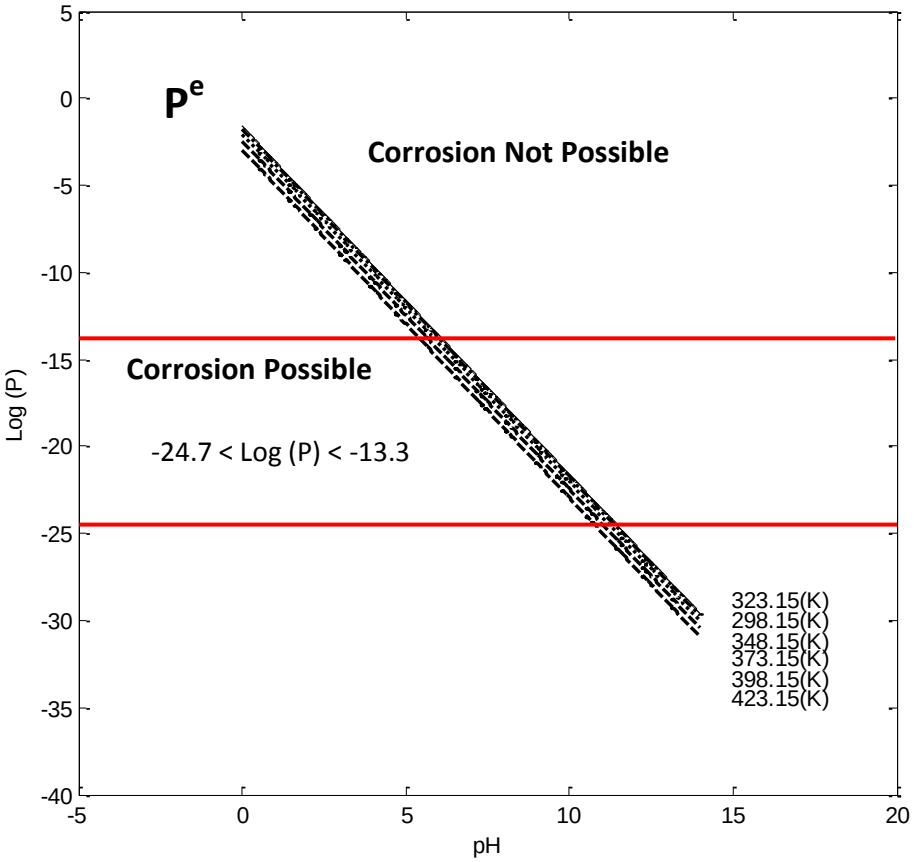

15) $Cu + HPO_4^{2-} + H_2PO_4^- + 2H^+ = Cu(HPO_4)(H_2PO_4)^-(a) + H_2$

$$\log\left(\frac{p_{H2} \times a_{Cu(HPO4)(H2PO4)(-)}}{a_{HPO4(-2)} \times a_{H2PO4(-)}}\right) = \frac{-\Delta G^0}{2.303RT} - 2pH$$

298.15: **log (p) = -3.62-2pH**

323.15: **log (p) = -3.39-2pH**

348.15: **log (p) = -3.30-2pH**

373.15: **log (p) = -3.33-2pH**

398.15: **log (p) = -3.45-2pH**

423.15: **log (p) = -3.64-2pH**

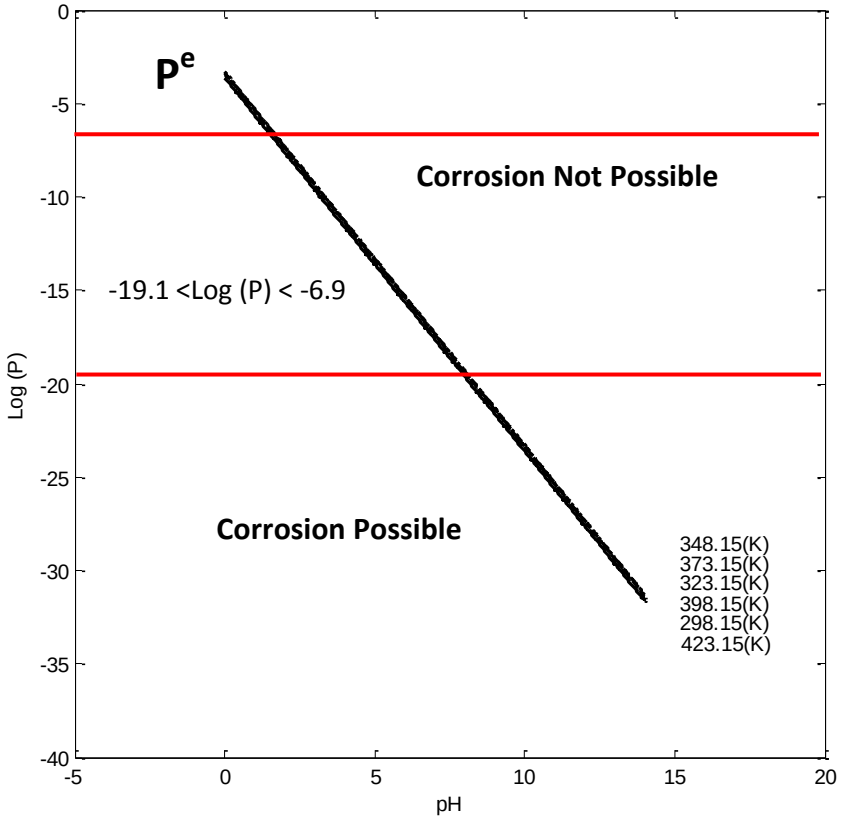

16) $Cu + HPO_4^{2-} + H_2PO_4^- + H^+ = Cu(HPO_4)(H_2PO_4)^{-2}\ (a) + ½\ H_2$

$$\log\left(\frac{p_{H2}^{0.5} \times a_{Cu(HPO4)(H2PO4)(-2)}}{a_{HPO4(-2)} \times a_{H2PO4(-)}}\right) = \frac{-\Delta G^0}{2.303RT} - pH$$

298.15: **log (p) = -1.92-pH**

323.15: **log (p) = -1.11-pH**

348.15: **log (p) = -0.29-pH**

373.15: **log (p) = 0.54-pH**

398.15: **log (p) = 1.38-pH**

423.15: **log (p) = 2.24-pH**

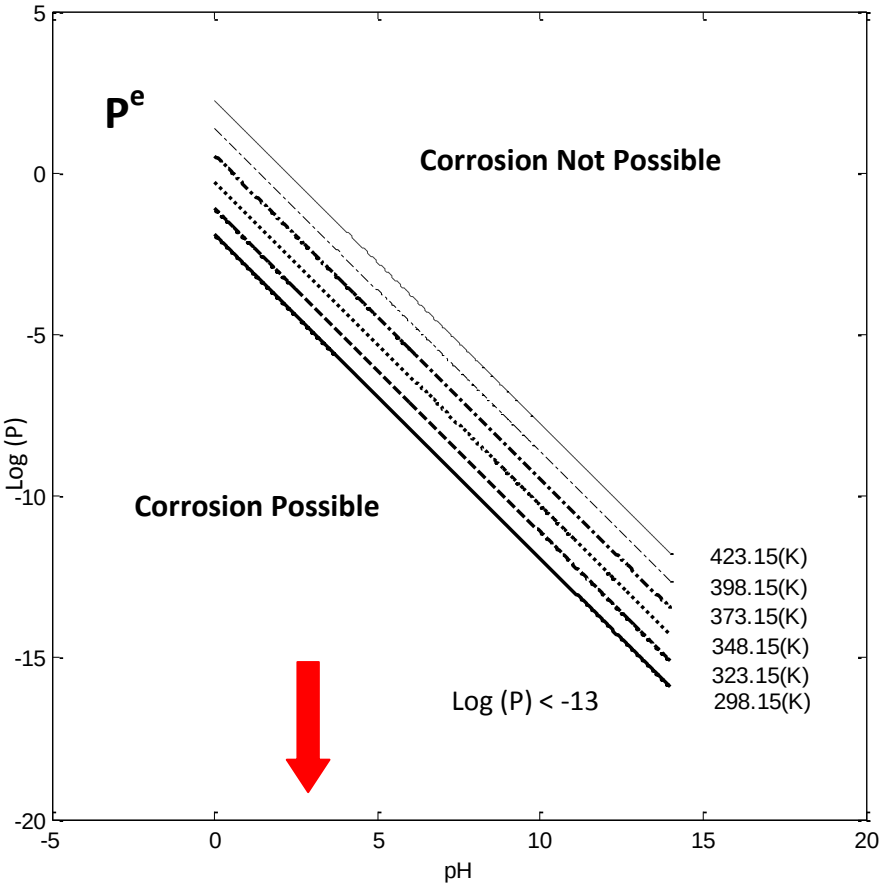

17) $Cu + NH3(a) + 2H^{+} = Cu(NH_3)^{+2}(a) + H_2$

$$\log\left(\frac{p_{H2} \times a_{Cu(NH3)(+2)}}{a_{NH3}}\right) = \frac{-\Delta G^0}{2.303RT} - 2pH$$

298.15: **log (p) = -7.08-2pH**

323.15: **log (p) = -6.51-2pH**

348.15: **log (p) = -5.98-2pH**

373.15: **log (p) = -5.50-2pH**

398.15: **log (p) = -5.05-2pH**

423.15: **log (p) = -4.62-2pH**

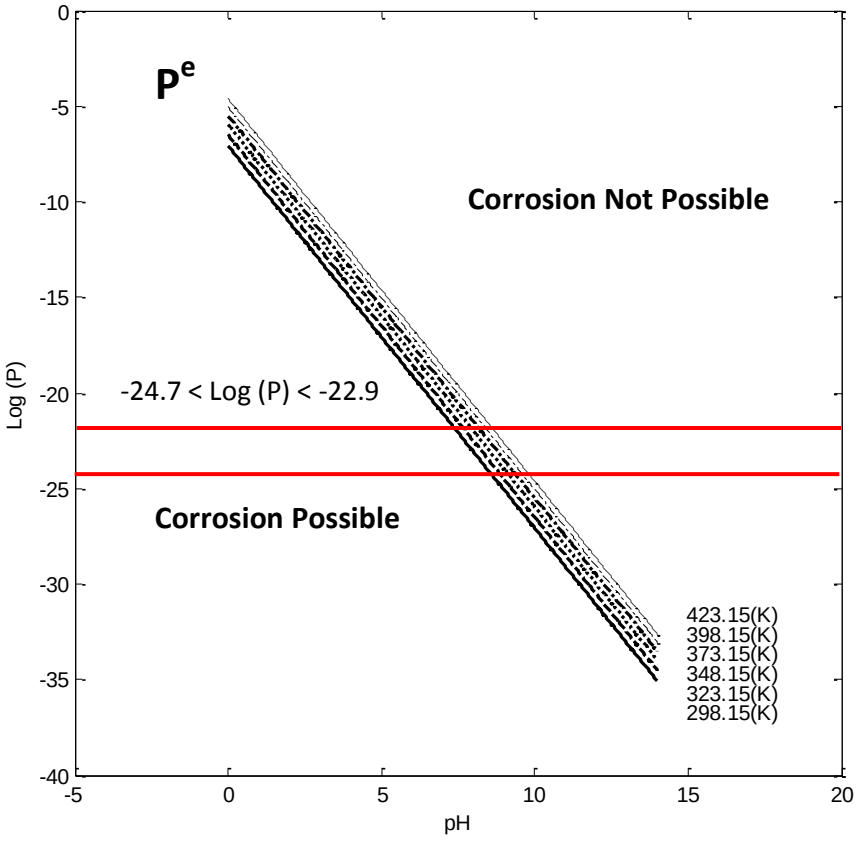

18) $Cu + 2NH_3 + 2H^+ = Cu(NH_3)_2^{+2}(a) + H_2$

$$\log\left(\frac{p_{H2} \times a_{Cu(NH3)2(+2)}}{a_{NH3}^2}\right) = \frac{-\Delta G^0}{2.303RT} - 2pH$$

298.15: **log (p) = -3.44-2pH**

323.15: **log (p) = -3.20-2pH**

348.15: **log (p) = -3.01-2pH**

373.15: **log (p) = -2.84-2pH**

398.15: **log (p) = -2.70-2pH**

423.15: **log (p) = -2.58-2pH**

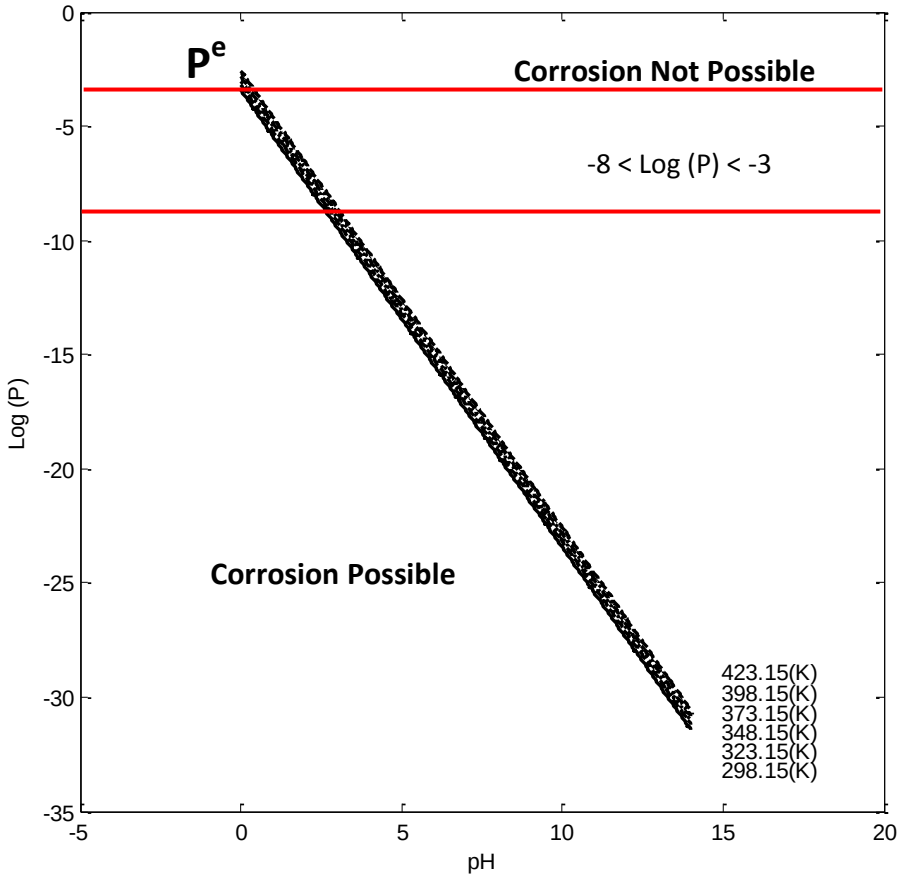

19) $Cu + 2NH_3 + H^+ = Cu(NH_3)_2^+ (a) + ½ H_2$

$$\log\left(\frac{p_{H2}^{0.5} \times a_{Cu(NH3)2(+)}}{a_{NH3}^2}\right) = \frac{-\Delta G^0}{2.303RT} - pH$$

298.15: **log (p) = 2.39-pH**

323.15: **log (p) = 2.54-pH**

348.15: **log (p) = 2.63-pH**

373.15: **log (p) = 2.68-pH**

398.15: **log (p) = 2.67-pH**

423.15: **log (p) = 2.66-pH**

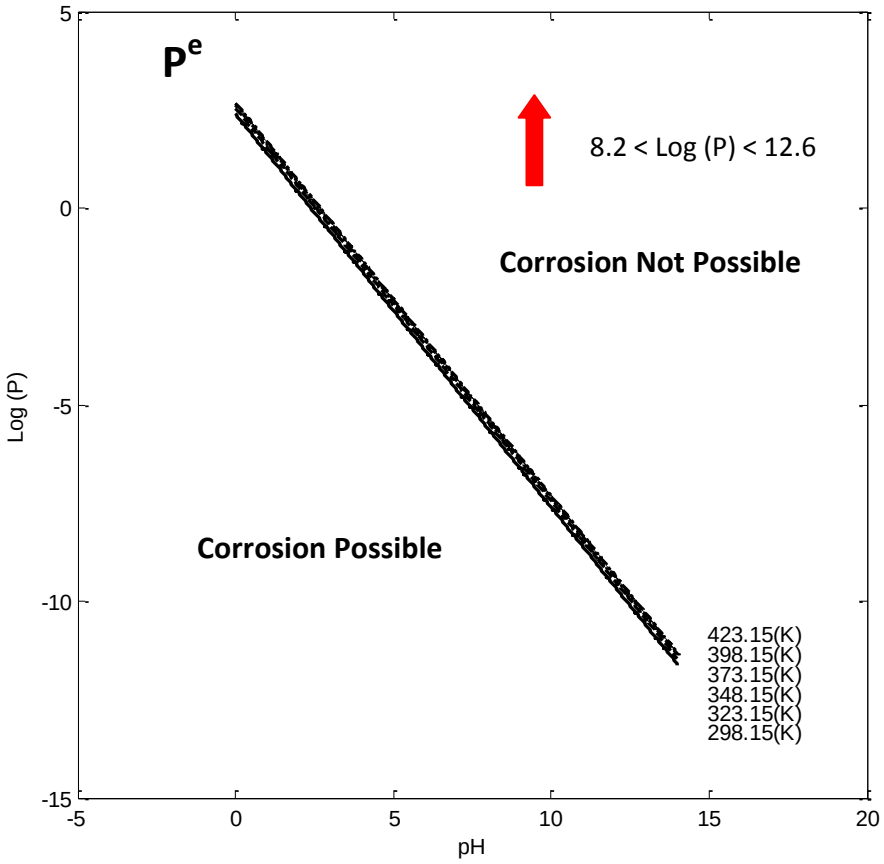

20) $Cu + 3NH_3 + 2H^+ = Cu(NH_3)_3^{+2}(a) + H_2$

$$\log\left(\frac{p_{H2} \times a_{Cu(NH3)3(+2)}}{a_{NH3}^3}\right) = \frac{-\Delta G^0}{2.303RT} - 2pH$$

298.15: **log (p) = -0.42-pH**

323.15: **log (p) = -0.52-pH**

348.15: **log (p) = -0.66-pH**

373.15: **log (p) = -0.82-pH**

398.15: **log (p) = -1.00-pH**

423.15: **log (p) = -1.18-pH**

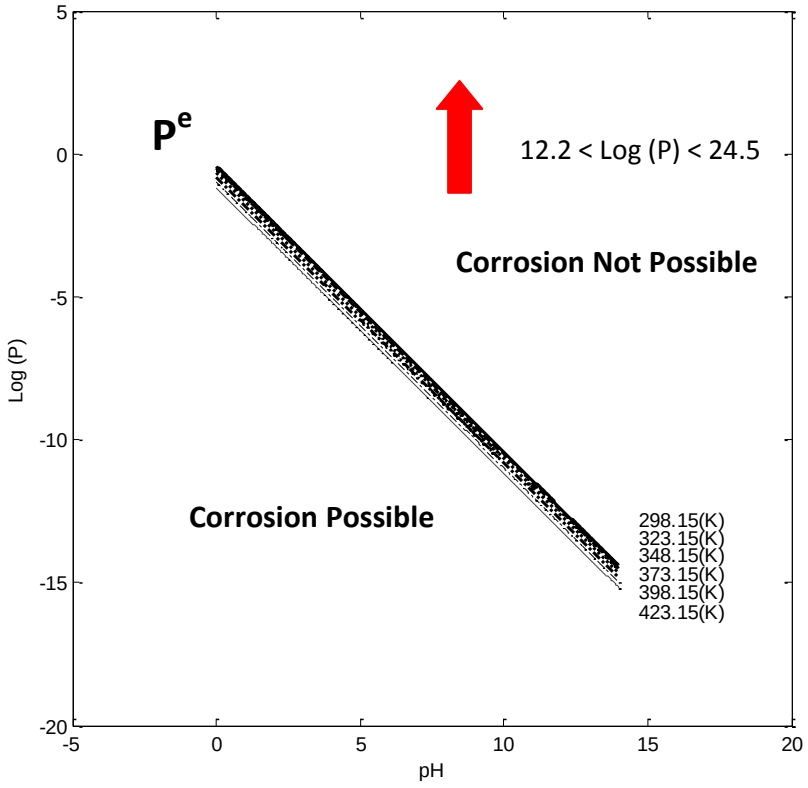

21) $Cu + 4NH_3 + 2H^+ = Cu(NH_3)_4^{+2}\ (a) + H_2$

$$\log\left(\frac{p_{H2} \times a_{Cu(NH3)4(+2)}}{a_{NH3}^4}\right) = \frac{-\Delta G^0}{2.303RT} - 2pH$$

298.15: **log (p) = 1.82-2pH**

323.15: **log (p) = 1.39-2pH**

348.15: **log (p) = 0.94-2pH**

373.15: **log (p) = 0.47-2pH**

398.15: **log (p) = 0.00-2pH**

423.15: **log (p) = -0.48-2pH**

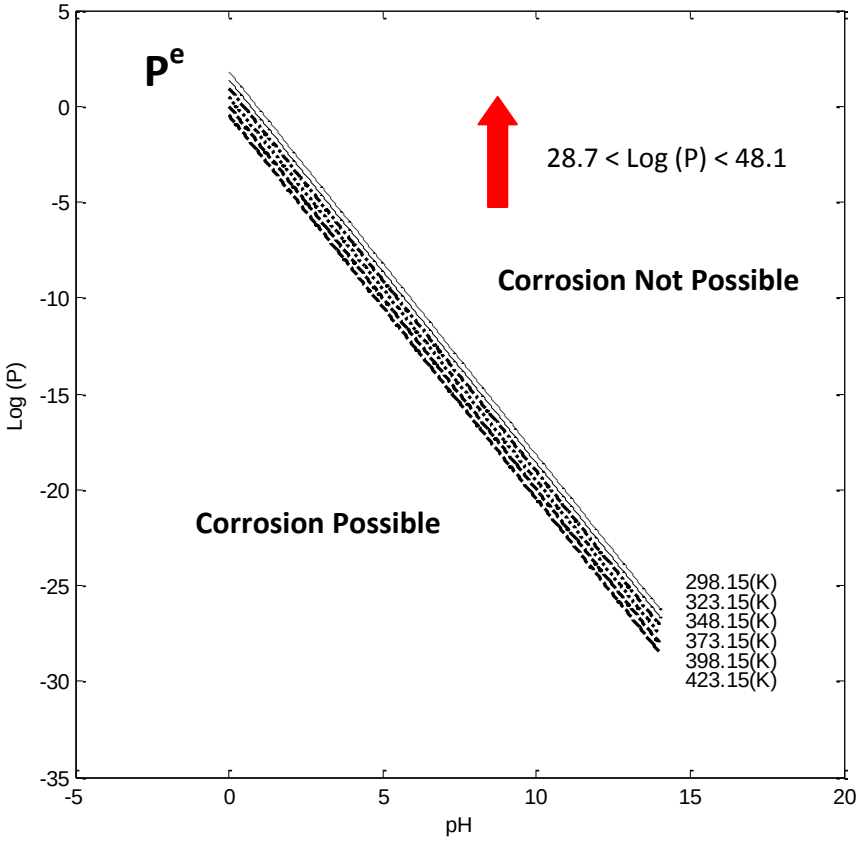

22) $Cu + 2NO_2^- + 2H^+ = Cu(NO_2)_2(a) + H_2$

$$\log\left(\frac{p_{H2} \times a_{Cu(NO2)2}}{a^2_{NO2(-)}}\right) = \frac{-\Delta G^0}{2.303RT} - 2pH$$

298.15: **log (p) = -8.78-2pH**

323.15: **log (p) = -7.95-2pH**

348.15: **log (p) = -7.11-2pH**

373.15: **log (p) = -6.25-2pH**

398.15: **log (p) = -5.39-2pH**

423.15: **log (p) = -4.52-2pH**

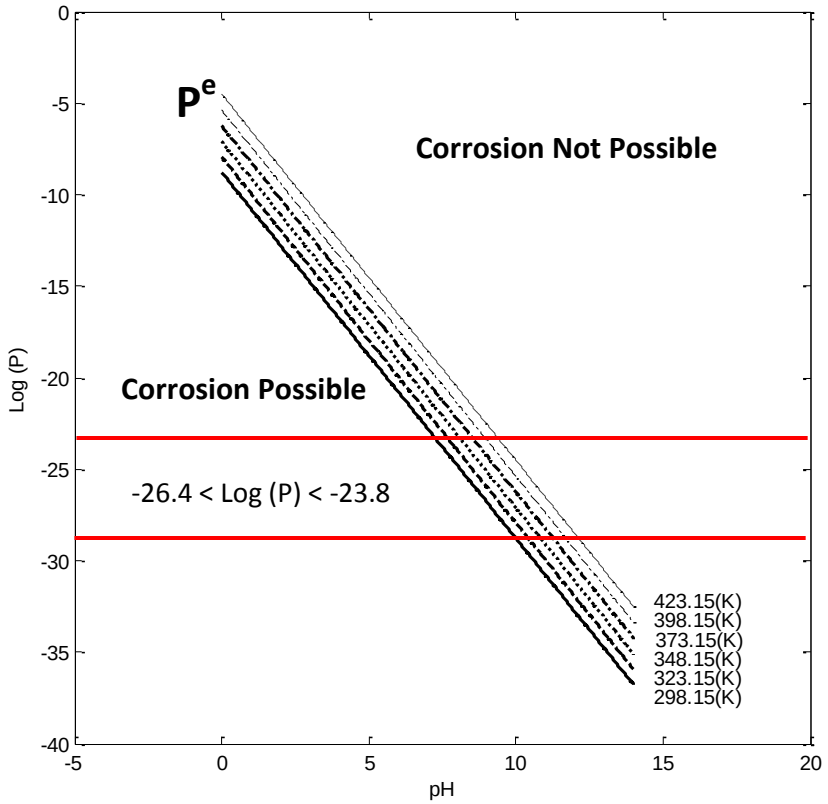

23) $Cu + 2NO_3^- + 2H^+ = Cu(NO_3)_2(ia) + H_2$

$$\log\left(\frac{p_{H2} \times a_{Cu(NO3)2}}{a^2_{NO3(-)}}\right) = \frac{-\Delta G^0}{2.303RT} - 2pH$$

298.15: **log (p) = -11.81-2pH**

323.15: **log (p) = -10.93-2pH**

348.15: **log (p) = -10.15-2pH**

373.15: **log (p) = -9.48-2pH**

398.15: **log (p) = -8.87-2pH;** 423.15: **log (p) = -8.32-2pH**

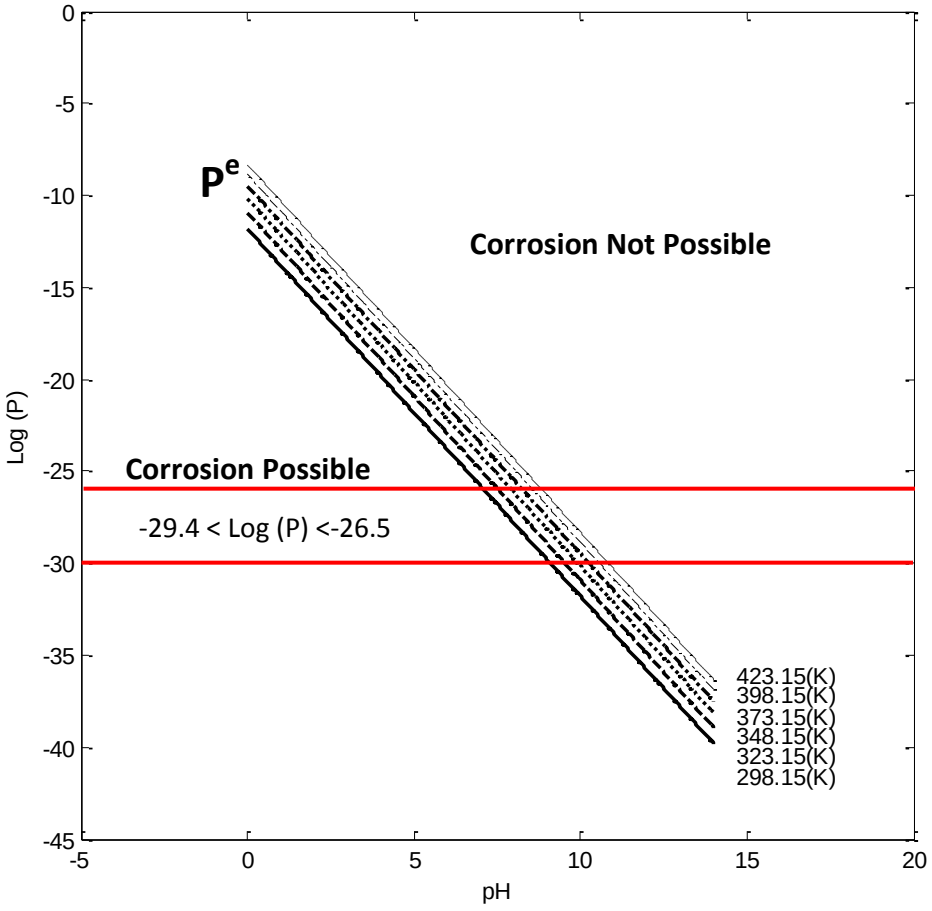

24) $Cu + NO_2^- + 2H^+ = Cu(NO_2)^+(a) + H_2$

$$\log\left(\frac{p_{H2} \times a_{Cu(NO2)(+)}}{a_{NO2(-)}}\right) = \frac{-\Delta G^0}{2.303RT} - 2pH$$

298.15: **log (p) = -9.41-2pH**

323.15: **log (p) = -8.57-2pH**

348.15: **log (p) = -7.77-2pH**

373.15: **log (p) = -7.02-2pH**

398.15: **log (p) = -6.31-2pH**

423.15: **log (p) = -5.62-2pH**

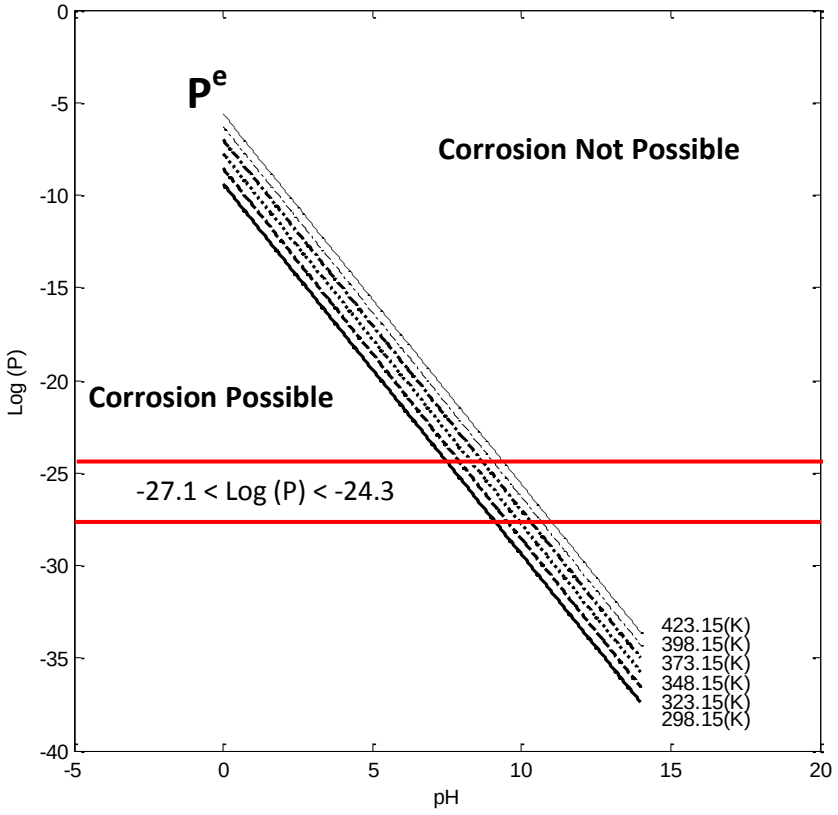

25) $Cu + NO_3^- + 2H^+ = Cu(NO_3)^+(a) + H_2$

$$\log\left(\frac{p_{H2} \times a_{Cu(NO3)(+)}}{a_{NO3(-)}}\right) = \frac{-\Delta G^0}{2.303RT} - 2pH$$

298.15: **log (p) = -10.90-2pH**

323.15: **log (p) = -10.08-2pH**

348.15: **log (p) = -9.32-2pH**

373.15: **log (p) = -8.59-2pH**

398.15: **log (p) = -7.91-2pH**

423.15: **log (p) = -7.25-2pH**

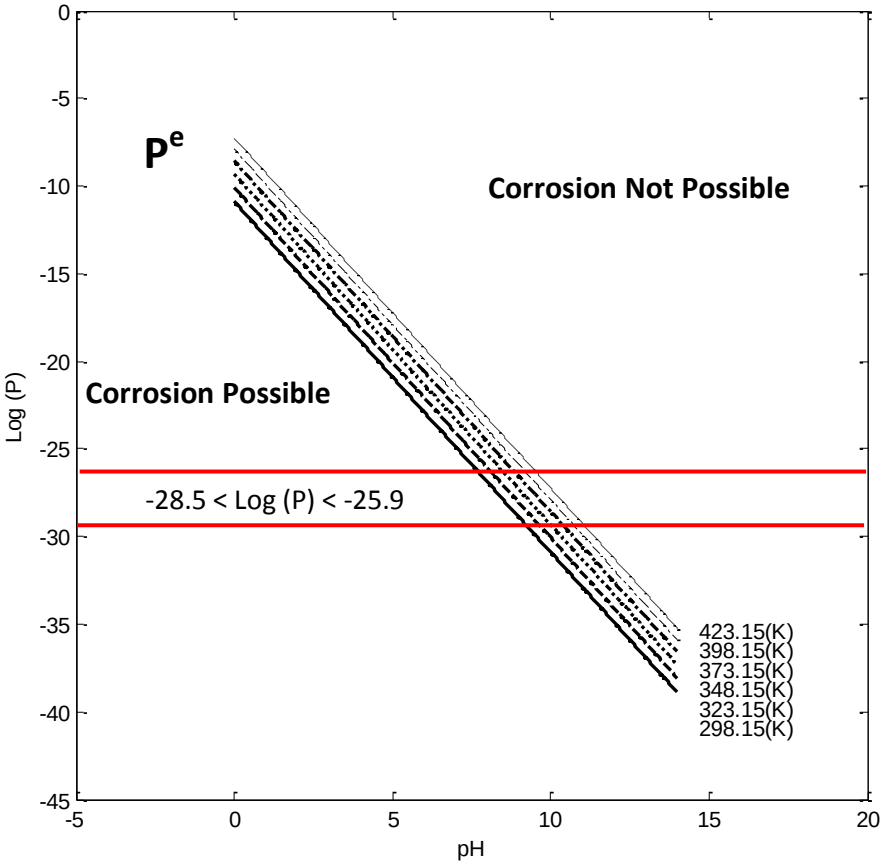

26) $Cu + 2H_2O = Cu(OH)_2(ia) + H_2$

$$\log\left(\frac{p_{H2} \times a_{Cu(OH)2}}{a_{H2O}^2}\right) = \frac{-\Delta G^0}{2.303RT}$$

298.15: **log (p) = -27.63**

323.15: **log (p) = -25.53**

348.15: **log (p) = -23.66**

373.15: **log (p) = -21.99**

398.15: **log (p) = -20.47**

423.15: **log (p) = -19.06**

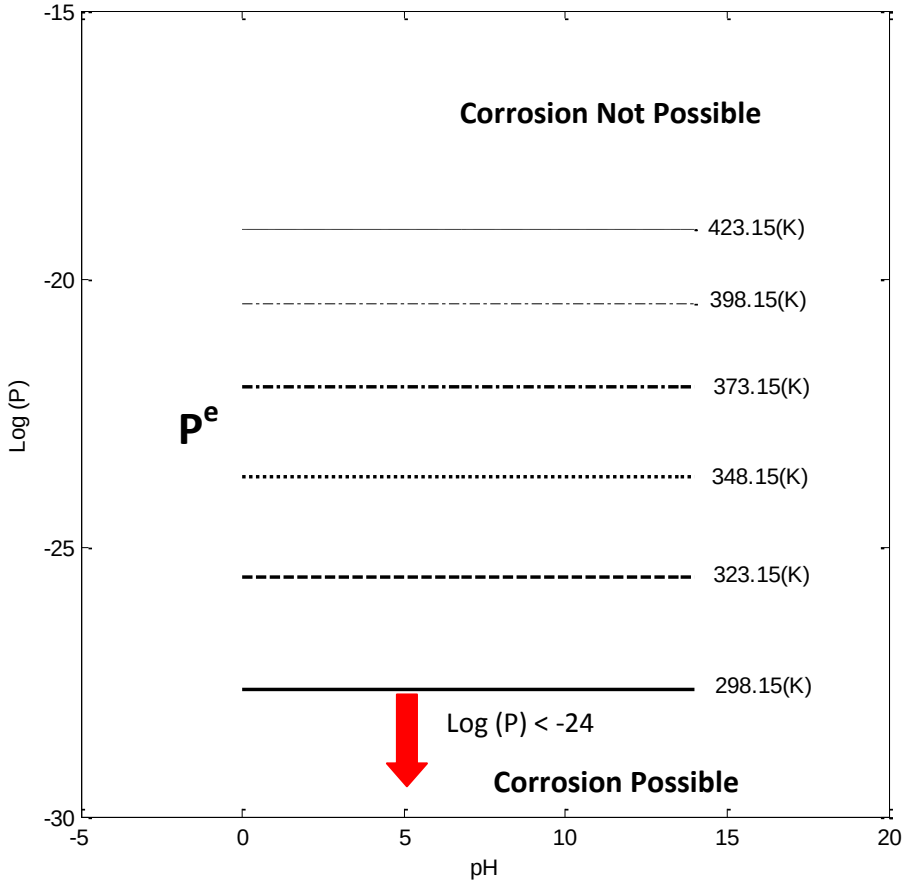

27) $Cu + H_2O + H^+ = CuOH^+ (a) + H_2$

$$\log(\frac{p_{H2} \times a_{Cu(OH)(+)}}{a_{H2O}}) = \frac{-\Delta G^0}{2.303RT} - pH$$

298.15: **log (p) = -19.35-pH**

323.15: **log (p) = -17.97-pH**

348.15: **log (p) = -16.74-pH**

373.15: **log (p) = -15.63-pH**

398.15: **log (p) = -14.62-pH**

423.15: **log (p) = -13.69-pH**

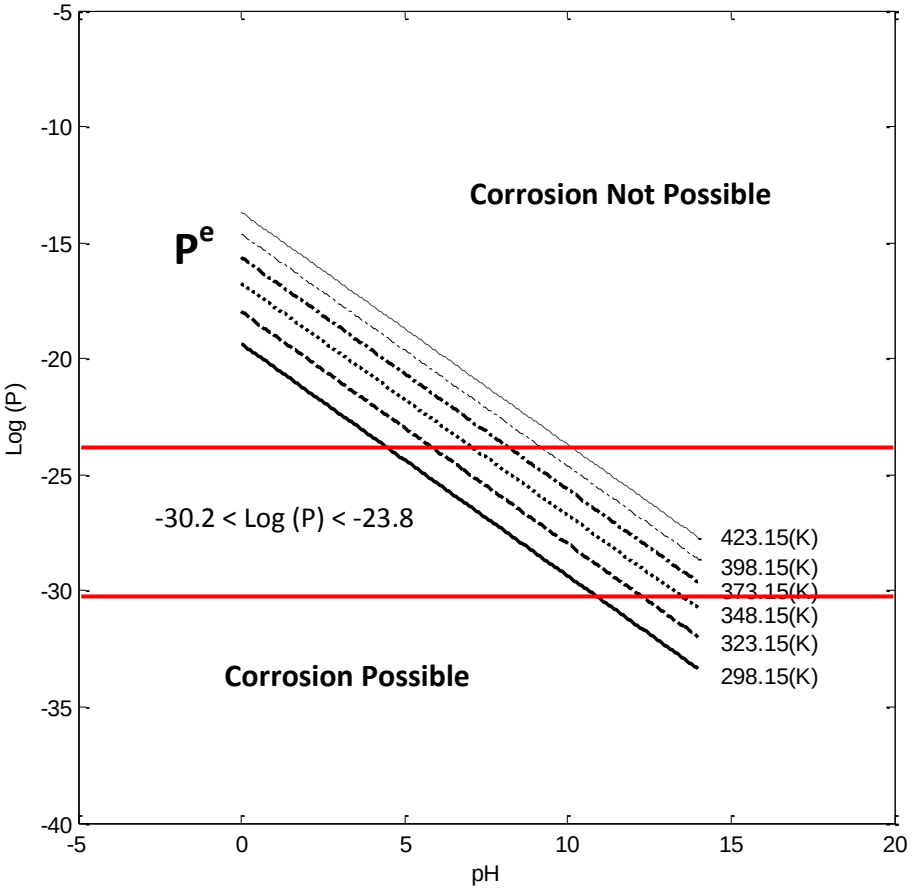

28) $Cu + 2H_2O = Cu(OH)_2^-(a) + H^+ + ½\ H_2$

$$\log\left(\frac{p_{H2}^{0.5} \times a_{Cu(OH)2(-)}}{a_{H2O}^2}\right) = \frac{-\Delta G^0}{2.303RT} + pH$$

298.15: **log (p) = -24.74+pH**

323.15: **log (p) = -23.98+pH**

348.15: **log (p) = -23.65+pH**

373.15: **log (p) = -23.67+pH**

398.15: **log (p) = -23.96+pH**

423.15: **log (p) = -24.47+pH**

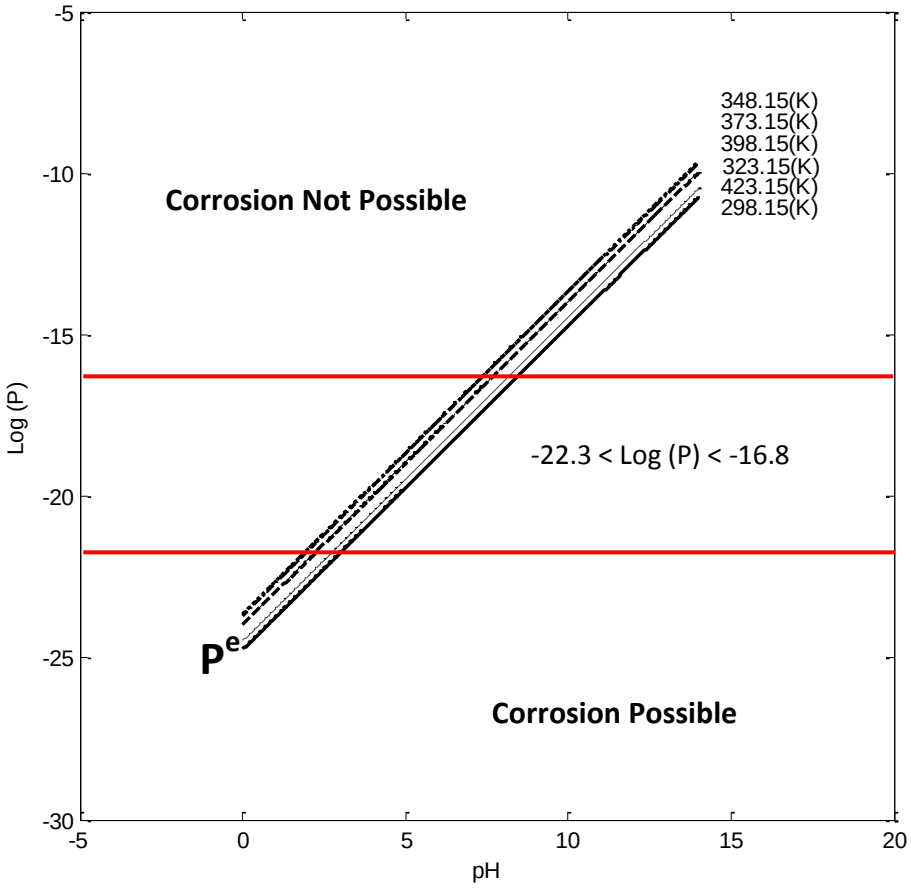

29) $Cu + 3H_2O = Cu(OH)_3^-(a) + H^+ + H_2$

$$\log\left(\frac{p_{H2} \times a_{Cu(OH)3(-)}}{a_{H2O}^3}\right) = \frac{-\Delta G^0}{2.303RT} + pH$$

298.15: **log (p) = -38.09+pH**

323.15: **log (p) = -35.77+pH**

348.15: **log (p) = -34.00+pH**

373.15: **log (p) = -32.66+pH**

398.15: **log (p) = -31.66+pH;** 423.15: **log (p) = -30.95+pH**

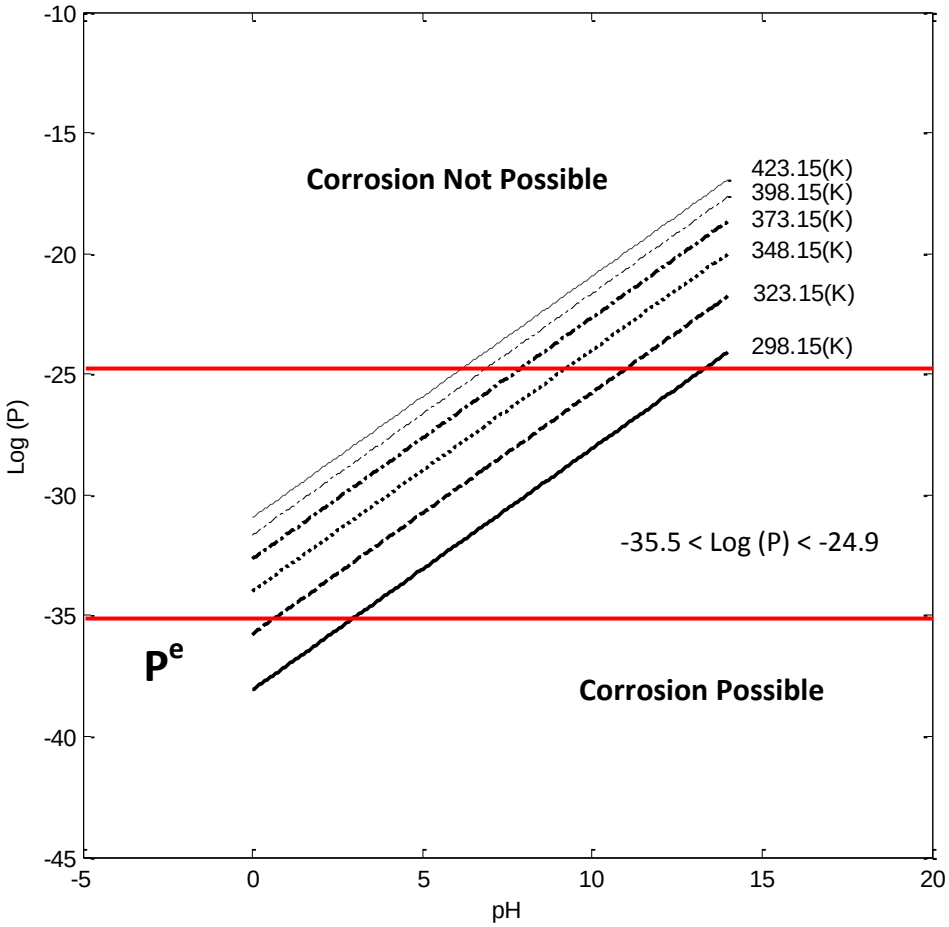

30) $Cu + 4H_2O = Cu(OH)_4^{-2}(a) + 2H^+ + H_2$

$$\log\left(\frac{p_{H2} \times a_{Cu(OH)4(-2)}}{a_{H2O}^4}\right) = \frac{-\Delta G^0}{2.303RT} + 2pH$$

298.15: **log (p) = -50.99+2pH**

323.15: **log (p) = -48.70+2pH**

348.15: **log (p) = -47.12+2pH**

373.15: **log (p) = -46.10+2pH**

398.15: **log (p) = -45.53+2pH**

423.15: **log (p) = -45.33+2pH**

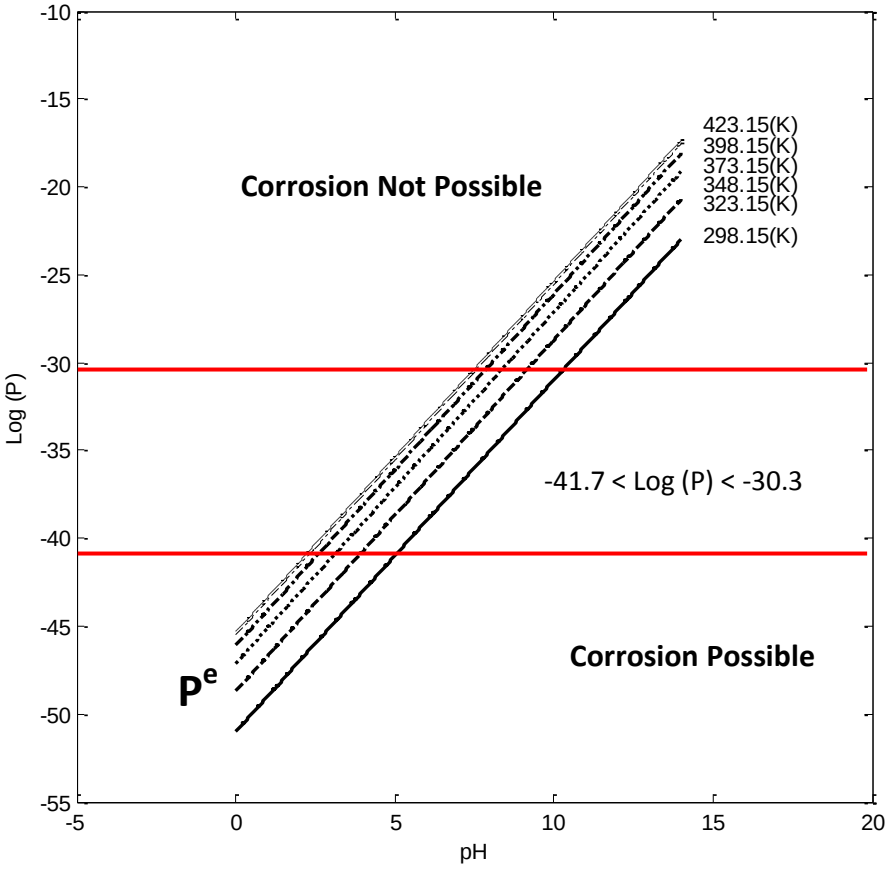

31) $2Cu + 2H_2O + 2H^+ = Cu_2(OH)_2^{+2}(a) + 2H_2$

$$\log\left(\frac{p_{H2}^2 \times a_{Cu2(OH)2(+2)}}{a_{H2O}^2}\right) = \frac{-\Delta G^0}{2.303RT} - 2pH$$

298.15: **log (p) = -33.14-2pH**

323.15: **log (p) = -30.36-2pH**

348.15: **log (p) = -27.96-2pH**

373.15: **log (p) = -25.86-2pH**

398.15: **log (p) = -24.01-2pH**

423.15: **log (p) = -22.36-2pH**

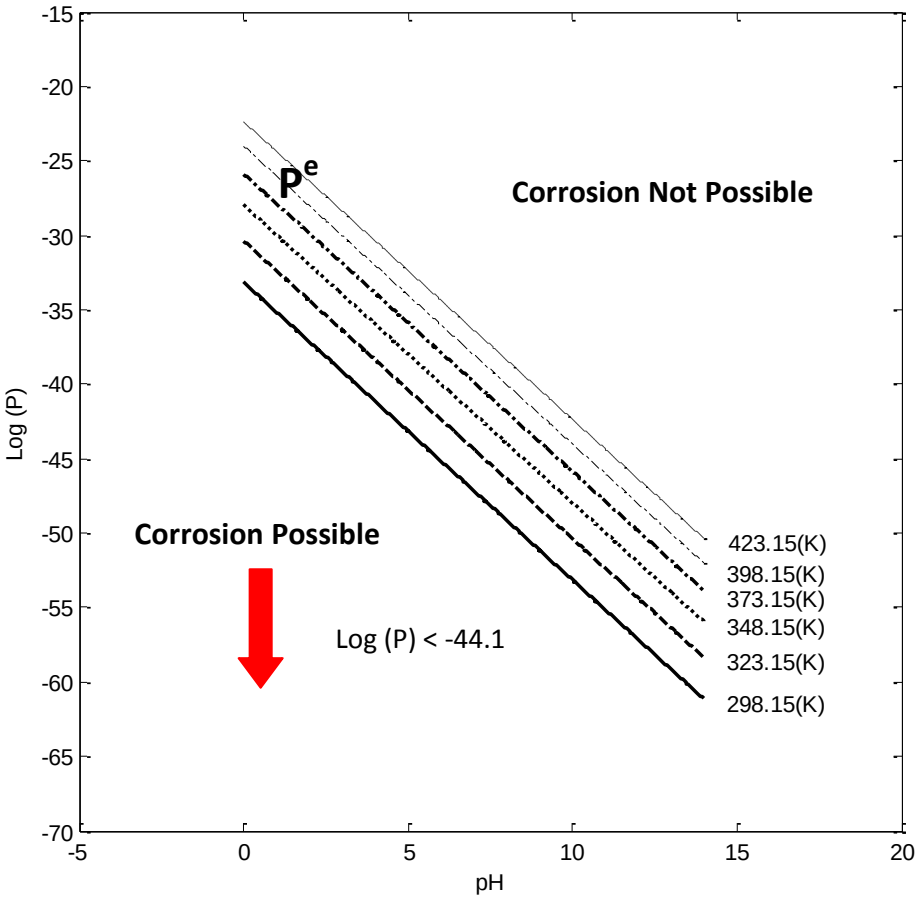

32) $3Cu + 4H_2O + 2H^+ = Cu_3(OH)_4{}^{+2}(a) + 3H_2$

$$\log\left(\frac{p_{H2}^3 \times a_{Cu3(OH)4(+2)}}{a_{H2O}^4}\right) = \frac{-\Delta G^0}{2.303RT} - 2pH$$

298.15: **log (p) = -55.28-2pH**

323.15: **log (p) = -51.20-2pH**

348.15: **log (p) = -47.72-2pH**

373.15: **log (p) = -44.72-2pH**

398.15: **log (p) = -42.09-2pH**

423.15: **log (p) = -39.78-2pH**

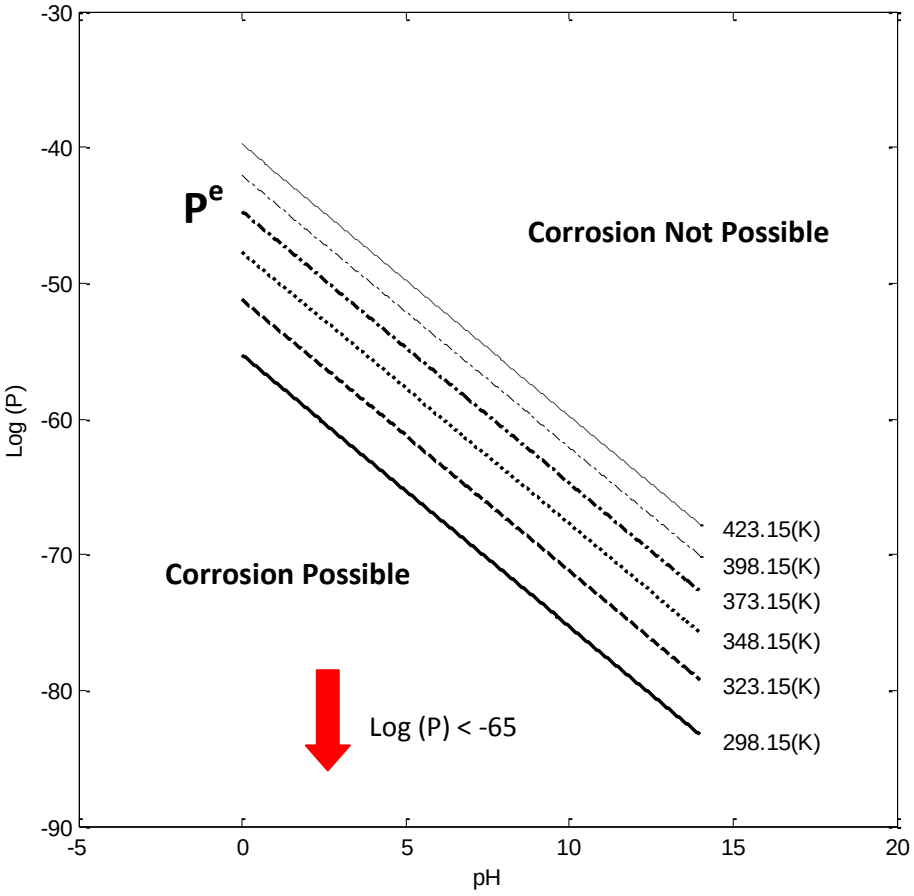

33) $Cu + SO_4^{2-} + 2H^+ = CuSO_4(ia) + H_2$

$$\log\left(\frac{p_{H2} \times a_{CuSO4}}{a_{SO4(2-)}}\right) = \frac{-\Delta G^0}{2.303RT} - 2pH$$

298.15: **log (p) = -9.15-2pH**

323.15: **log (p) = -8.15-2pH**

348.15: **log (p) = -7.24-2pH**

373.15: **log (p) = -6.39-2pH**

398.15: **log (p) = -5.59-2pH**

423.15: **log (p) = -4.84-2pH**

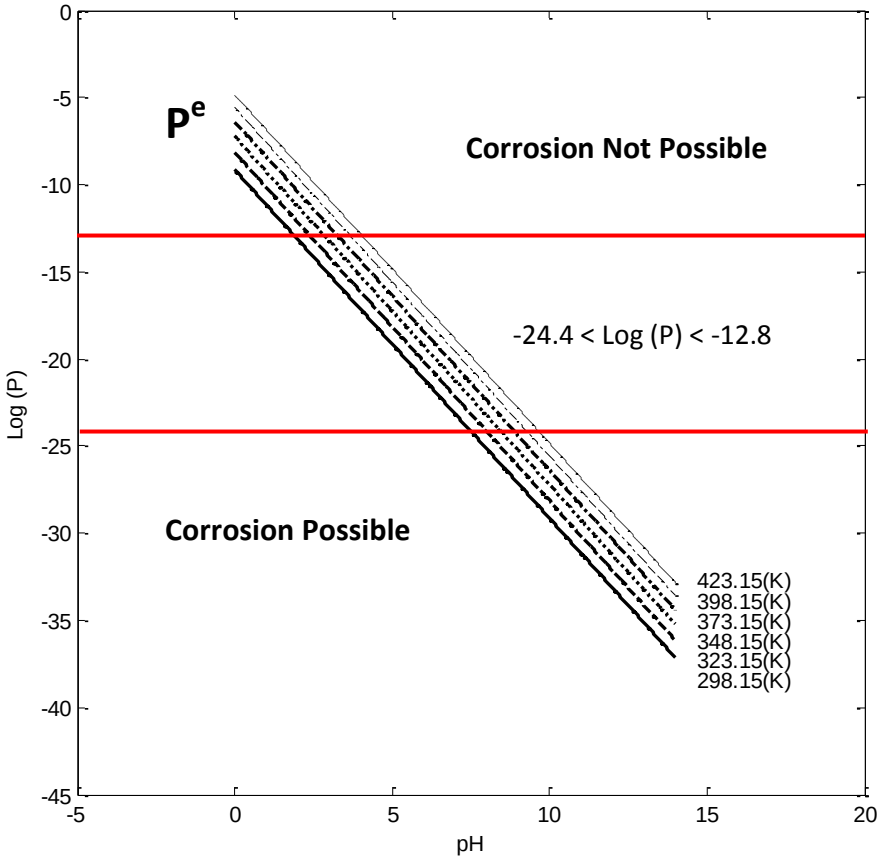

2012:11

The Swedish Radiation Safety Authority has a comprehensive responsibility to ensure that society is safe from the effects of radiation. The Authority works to achieve radiation safety in a number of areas: nuclear power, medical care as well as commercial products and services. The Authority also works to achieve protection from natural radiation and to increase the level of radiation safety internationally.

The Swedish Radiation Safety Authority works proactively and preventively to protect people and the environment from the harmful effects of radiation, now and in the future. The Authority issues regulations and supervises compliance, while also supporting research, providing training and information, and issuing advice. Often, activities involving radiation require licences issued by the Authority. The Swedish Radiation Safety Authority maintains emergency preparedness around the clock with the aim of limiting the aftermath of radiation accidents and the unintentional spreading of radioactive substances. The Authority participates in international co-operation in order to promote radiation safety and finances projects aiming to raise the level of radiation safety in certain Eastern European countries.

The Authority reports to the Ministry of the Environment and has around 270 employees with competencies in the fields of engineering, natural and behavioural sciences, law, economics and communications. We have received quality, environmental and working environment certification.

Strålsäkerhetsmyndigheten
Swedish Radiation Safety Authority

SE-171 16 Stockholm
Solna strandväg 96

Tel: +46 8 799 40 00
Fax: +46 8 799 40 10

E-mail: registrator@ssm.se
Web: stralsakerhetsmyndigheten.se